

2013

An experimental and computational investigation of rotating flexible shaft system dynamics in rotary drilling assemblies for down hole drilling vibration mitigation

Richard Duff

Louisiana State University and Agricultural and Mechanical College, richardduff@gmail.com

Follow this and additional works at: https://digitalcommons.lsu.edu/gradschool_dissertations



Part of the [Petroleum Engineering Commons](#)

Recommended Citation

Duff, Richard, "An experimental and computational investigation of rotating flexible shaft system dynamics in rotary drilling assemblies for down hole drilling vibration mitigation" (2013). *LSU Doctoral Dissertations*. 1734.
https://digitalcommons.lsu.edu/gradschool_dissertations/1734

This Dissertation is brought to you for free and open access by the Graduate School at LSU Digital Commons. It has been accepted for inclusion in LSU Doctoral Dissertations by an authorized graduate school editor of LSU Digital Commons. For more information, please contact gradetd@lsu.edu.

AN EXPERIMENTAL AND COMPUTATIONAL INVESTIGATION OF ROTATING
FLEXIBLE SHAFT SYSTEM DYNAMICS IN ROTARY DRILLING ASSEMBLIES FOR DOWN
HOLE DRILLING VIBRATION MITIGATION.

A Dissertation

Submitted to the Graduate Faculty of the
Louisiana State University and
Agricultural and Mechanical College
in partial fulfillment of the
requirements for the degree of
Doctor of Philosophy

in

The Craft and Hawkins Department of Petroleum Engineering

by

Richard Duff

B.S., University of Missouri at Rolla, 2002

M.S., University of Missouri at Rolla, 2004

August 2013

ACKNOWLEDGEMENTS

I would like to thank LSU and the Craft & Hawkins Department of Petroleum Engineering for the opportunity to study.

and my wife Stacy ... for everything.

TABLE OF CONTENTS

ACKNOWLEDGEMENTS	ii
TABLE OF CONTENTS.....	iii
TABLE OF TABLES	v
TABLE OF FIGURES.....	vi
ABSTRACT.....	x
CHAPTER 1. INTRODUCTION.....	1
1.1 General Description.....	1
1.2 Current Practice Limitations	1
1.3 Problem Statement	2
1.4 Hypotheses.....	2
CHAPTER 2. LITERATURE REVIEW	3
2.1 Stick-Slip and Whirl.....	3
2.2 Mechanisms	3
CHAPTER 3. METHODS.....	8
3.1 Hypothesis Testing Objectives.....	8
3.2 Model Scaling Requirements from Dimensionless Analysis	9
3.3 New Model Origins	10
3.4 Using Acceleration and Gyroscope Measurement to Measure BHA dynamics.....	10
3.5 Physical Model Data Collection.....	13
3.6 Prestress Numerical Modal Analysis for Rotor Dynamic Behaviors in Ansys(TM)	14
CHAPTER 4. RESULTS.....	20
4.1 Screening Measurement 1: Long Period Stick-slip Behavior	20
4.2 Screening Measurement 2: Axial Load Variation.....	21
4.3 Experiment 3: Buckling Deflection.....	24
4.4 Results from the Physical Experiments	24
4.4.1 Buckling Deflection Calculation	24
4.4.2 Buckling Deflection Experiments.....	24
4.4.3 Axial Load Boundary During Rotation Analysis	25
4.4.4 Video Stills.....	29
4.4.5 Vibration Response Surface Experiments	32
4.5 Results from the Numerical Experiments	46
4.5.1 Numerical Simulation of Buckling	46
4.5.2 Numerical Simulation of Vibration Mode.....	46
CHAPTER 5. DISCUSSIONS.....	51
5.1 Prestress Modal Simulation and Experimental Results on the Response Surface	51
5.2 Discussion of Mitigation Method.....	55
CHAPTER 6. CONCLUSIONS.....	60
6.1 Evaluating Hypotheses	60
6.2 Mitigation Method Findings	61

6.3	Measurement and Diagnoses	61
6.4	Effects of BHA Geometry	61
CHAPTER 7. FUTURE DIRECTIONS		63
BIBLIOGRAPHY		64
APPENDIX I: ADDITIONAL PROCEDURES AND EQUIPMENT SETTINGS.....		69
APPENDIX II: ACCELERATION MEASUREMENTS CALCULATION SYSTEMS		78
APPENDIX III: PHYSICAL MODEL DEVELOPMENT.....		91
APPENDIX IV: ANSYS™ MODELING OF EXPERIMENTAL SYSTEM.....		107
APPENDIX V: ADDITIONAL RESULTS.....		116
APPENDIX VI: ANSYS™ REPORTS.....		121
VITA		174

TABLE OF TABLES

Table 1. The Campbell Diagram Output Table	18
Table 2. Axial Load Boundary Summary	30
Table 3. Buckling Results for Euler, Wu and Numerical Simulation.....	46
Table 4. Vibration Mitigation Table for Stick-slip and Whirl	55
Table 5. Drill Collar System Properties.....	93
Table 6. Values used for Buckling Calculation.....	110
Table 7. Buckling Calculation Results	110
Table 8. Torsional Vibration Modeled vs. Rotation Speed.....	117

TABLE OF FIGURES

Figure 1. “Rolling Log” experiment.	5
Figure 2. Dual rotating disc connected by stem experiment. (redrawn from Mihajlovic 2004)	5
Figure 3. Rotor model. (redrawn from Wauer 1982).....	6
Figure 4. BHA sketches. (redrawn from Jansen 1993).....	6
Figure 5. Shaft and annular constraint with axial load force and rotation labels.	11
Figure 6. Sensor location inside cross section	12
Figure 7. Shaft configurations used in testing presented in the ‘Stability Approach’	14
Figure 8. This figure shows the “prestress” solution method	16
Figure 9. An example of premesh geometry.....	16
Figure 10. The meshed model is shown for the simulation geometry.....	17
Figure 11. A deformed and stressed model result example.	17
Figure 12. Campbell diagram results showing the modes	18
Figure 13. Diagram of extracting critical speed results from Campbell diagrams.	19
Figure 14. Stick-slip event. 80 second window of a long period stick-slip event	20
Figure 15. Stick-slip event. 80 second window of a long period stick-slip event	21
Figure 16. Stick slip event. Six second window of a long period stick-slip event:	22
Figure 17. Six second window of a long period stick-slip event: radial and tangential acceleration.	22
Figure 18. The observed cycle of the “long period” stick-slip event	22
Figure 19. RPM, force, and lateral accelerations for a 40 second window.....	23
Figure 20. RPM, force, and lateral accelerations for a 6 second window.....	23
Figure 21. Cycle of axial load variation.	23
Figure 22. Shaft (A) buckled within 0.25 lbs.....	25
Figure 23. Shaft (B) buckled more than 0.25 lbs.	26
Figure 24. Shaft (C) buckled near the calculated value of 1.73lbs.....	27
Figure 25. Shaft (D) was different from the other shafts.	27

Figure 26. Shaft A axial load boundary.	28
Figure 27. Shaft B axial load boundary	28
Figure 28. Shaft C axial load boundary.	29
Figure 29. Shaft D axial load boundary	30
Figure 30. Video stills depicting forward synchronous whirl, Part 1	31
Figure 31. Video stills depicting forward synchronous whirl continued, Part 2	32
Figure 32. Clockwise rotation filmed with the annual constraint removed showing forward whirl	33
Figure 33. Clockwise rotation filmed with the annual constraint removed showing backward whirl.....	35
Figure 34. Shaft A torsional vibration response surface.	36
Figure 35. Shaft B torsional vibration response surface.	36
Figure 36. Shaft C torsional vibration response surface.	37
Figure 37. Shaft D torsional vibration response surface.....	37
Figure 38. Shaft A vibration separation response surface	38
Figure 39. Shaft B vibration separation response surface.....	39
Figure 40. Shaft C vibration separation response surface.....	40
Figure 41. Shaft D vibration separation response surface	41
Figure 42. Shaft A stick-slip index response surface	42
Figure 43. Shaft B stick-slip index response surface.....	43
Figure 44. Shaft C stick-slip index response surface.....	43
Figure 45. Shaft D stick-slip index response surface	44
Figure 46. Summary image showing the average torsional acceleration.....	45
Figure 47. A screen capture of the graphical representation of the buckling simulation.....	47
Figure 48. A screen capture of the graphical representation of the buckling simulation.....	47
Figure 49. Shaft A modal results.....	48
Figure 50. Shaft B modal results	49
Figure 51. Shaft C modal results.	49

Figure 52. Shaft D modal results.....	50
Figure 53. Modal results overlay for shafts A, B, C, D.	50
Figure 54. Shaft A torsional vibration response surface with modal simulation results.....	51
Figure 55. Shaft B torsional vibration response surface with modal simulation results.....	52
Figure 56. Shaft C torsional vibration response surface with modal simulation results.....	53
Figure 57. Shaft D torsional vibration response surface with modal simulation results.....	54
Figure 58. Pinned dimensionless slick-slip screening test.....	55
Figure 59. Stick-slip index response surface with Stick-slip mitigation.....	56
Figure 60. Shaft D torsional vibration surface with whirl response mitigation.	57
Figure 61. The image suggested by the Anadrill method	58
Figure 62. Comparison of the “Sperry-Sun” method to the stick-slip index.	59
Figure 63. Motor RPM control scheme used in preliminary testing.	72
Figure 64. Wiring diagram for 0.5 HP inverter-duty AC motor attached to a 0.5 HP AC drive.....	73
Figure 65. Sensor location inside cross section.....	74
Figure 66. A cross section representing modifications made the lower shaft receiver in the test fixture...	75
Figure 67. The recorded vibration from a single location.....	76
Figure 68. The stick-slip index in this case, dimensionless stick-slip pattern.....	76
Figure 69. Depiction of potential positions for the sensor in a shaft, showing the origin, R and R_s	78
Figure 70. Non-uniform rotation, non-uniform rotation with lateral motion and two non-uniform motion paths.....	79
Figure 71. Unit vectors u_r and u_θ for the polar non-uniform rotating reference frame.	79
Figure 72. Unit vectors e_θ and e_r are linearly independent, for the Polar curvilinear reference frame.	80
Figure 73. Acceleration of a rotating point in non-uniform circular motion.	81
Figure 74. The center of the rotating shaft rotating (orbiting) about an average center of rotation.	82
Figure 75. The sensor position in the rotating shaft.	82
Figure 76. An amalgamation of Figure 74, Figure 75	83

Figure 77. The components of the complex number z , depicted on a Cartesian plane.....	84
Figure 78. The components of the complex number z substituted.....	85
Figure 79. Simple harmonic function.	88
Figure 80. Saw tooth function.....	89
Figure 81. Plots depicting the response of the radial component of acceleration	89
Figure 82. Scale factor's convergence.....	94
Figure 83. Torsional pendulum shaft.....	95
Figure 84. Free body diagram for solution to friction force calculation.	98
Figure 85. Rotation speed vs. acceleration comparison.....	117
Figure 86. Shaft A torsional vibration and stick-slip.....	118
Figure 87. Shaft D torsional vibration and stick-slip.....	119
Figure 88. Shaft C torsional vibration and stick-slip.....	119

ABSTRACT

Rotary drilling system vibration has long been associated with damaging the bit, the bottom hole assembly (BHA) and drill string. Vibration has been traditionally measured in the bottom hole assembly, and been closely associated with the resonant behaviors.

This research study proposes an improved physical laboratory model to explore the dynamic behaviors associated with vibration. This model includes contact with the borehole wall allowing a range of stabilization geometries while removing bit-formation interaction effects. The results of exercising the model help develop new insights into both vibration measurement diagnostics and mitigation strategy execution.

Presented here is a review of other physical bottom hole assembly and drilling concepts, and a new novel model. Experimental investigation using the new model for a range of geometries is presented with recorded conditions, annotated video stills and analysis using regression and response surface methods. The analysis when compared to existing industry mitigation methods allows unique insight to the possible effectiveness of such methods. A numerical simulation of the system was also performed and its results compared to the laboratory tests. Results show that a shaft system alone can generate stick-slip and whirl behaviors. Such behaviors occur in distinct regions. Another conclusion of this work is that a popular method for inferring stick-slip from acceleration measures is not reliable for the system used in this study.

CHAPTER 1.INTRODUCTION

1.1 General Description

Rotary oil well drilling is a process used to seek reserves of hydrocarbons in the earth. A drill string is composed of lighter tubulars (drill pipe) and heavier tubulars (drill collars). The drill string is hung from surface and the bit is set down on the bottom of the hole allowing the weight of the lower part of the string to rest on the bit. Rotation of the drill string at the surface allows torque transmission to a drill bit. The weight on the lower section of the string and torque from the string's rotation cause the bit to engage and break the rock. The rock cuttings are removed by circulating fluid, which allows the drilling of the hole to advance. This lower section of the string supplying the weight on the bit (WOB) is called the bottom hole assembly (BHA). The drill collars are often accompanied by stabilizer components to provide support to the BHA and desired alignment of the drill bit. (Jansen 1993)

The high cost of inefficient drilling and component failures spur examination of their causes. Drilling mechanics problem have been credited with 75% of nonproductive time incidents, low rate-of-penetration presents hidden costs, more trips, lost-in-hole charges and increased charges for services. (Burgess 1995) (Ashley et al. 2001) The estimated savings from vibration reduction project alone was \$7,500 per meter drilled totaling more than 1 million dollars (Kriesels 1999). In the past thirty years, vibration's role in reducing rate of penetration has been discussed continuously. (Deily et al. 1968)(Zannoni et al. 1993)(Wu 2010) The lost time due to equipment failures and less than optimal drilling rates are both great reasons for any drilling engineer to be interested in BHA vibration.

1.2 Current Practice Limitations

The BHA is out of sight so direct observation is impossible. The current technology only allows for sensors in a limited number of points, normally only one location: the Measurement While Drilling tools (MWD). It is impossible to interpret the mode shape from just one location. The transmission of this data regularly in the range of the number of seconds between reports. Reconstructed solutions logically are non-unique. This leads to the de facto method for real time vibration mitigation, trial and error After the 1993 SPE forum

series on Drilling Vibration, Anadrill planned to have an internal workshop later that year to collect best practices on vibration mitigation. The results of this internal workshop were summarized in Burgess and Martin (1995). It is assumed that this table was used in internal Anadrill / Schlumberger materials and given to clients and drillers as a quick reference, and hence we have the now famous “Anadrill Vibration Mitigation Method”. A plot of these ideas made it into other related works (Schultz 2005).

1.3 Problem Statement

So what may be done to advance an understanding of the dynamic behaviors in the BHA. This study seeks is to develop an improved understanding of the dynamic behaviors in the BHA in order realize the significance of current to methods for evaluating and planning vibration control for drilling systems and suggest improvements. The methods employed need to allow for direct observation of the two popular culprits “stick-slip” and “whirl”, and will attempt a predictive modeling method.

Currently industry has one set of thumb rules for all conditions and BHAs. Is one enough? Stabilizer placement is often scrutinized to reduce vibrations. Shaft vibration theory is exercised in the design of BHAs. Based on shaft behaviors alone can one see an impact, or is only related to different drill bits? Do different BHA geometries manifest different behaviors for similar operating conditions.

1.4 Hypotheses

To address this problem the follow hypotheses are suggested.

- 1) A flexible shaft system without a drill bit will not experience stick slip or whirl.
- 2) Flexible shaft systems of varying stabilization geometries will produce the same levels and types of vibrations over a range of conditions.
- 3) Vibration levels in a flexible shaft are a function of rotation speed and axial load, and manifest regionally as suggested by the Anadrill Methods materials

After reviewing others models and what has been done the formulation of experiments to test the hypothesis will be explored.

CHAPTER 2.LITERATURE REVIEW

This section will show how field observations and laboratory models have addressed Practitioners from the field and from the lab pursue identifying fundamental mechanisms that should be accounted for in vibration mitigation workflows.

2.1 Stick-Slip and Whirl

Stick-slip and whirl need to be defined before going any further in this discussion. Stick-slip is the cyclic reduction and corresponding increase of instantaneous rotation speed. While Whirl the behavior experienced where the instantaneous center of rotation is in motion around an average center. While authors may attempt to refine to a greater detail how to recognize the behaviors with surface or downhole observations, this general description will due for now. (including Zannoni 1993, Van Den 2000, Kasner 1938, and Chen 1999) The description of whirl is considered forward if the motion of the center of rotation is in the same direction as its rotation, if the motion is reversed, this is called backward.

2.2 Mechanisms

With this rudimentary definition of stick slip and whirl presented consider what others have done to identify the mechanism creating one or both conditions. First, consider the existing work around a mechanistic understanding. Dunayevsky et. Al (1985, 1993) present a mechanism where the dynamic component of axial load on the BHA (WOB fluctuation or axial vibration) may induce lateral vibrations or lateral resonance. This system is based on a simply supported column where the axial load oscillation matches with the lateral natural frequencies resulting in parametric resonance. The work outlines a workflow where first the deflections or buckling state is found then free vibration analysis for lateral and axial modes is performed, then the wave motion and severity is calculated. This style of model is called a critical speed model and has recognized limitations, it will not simulate the development of a vibration, and it only addresses parametric resonance. An improvement of the critical speed style analysis also known as forced frequency analysis is presented and validated in detail by Apostol et al. (1990) using adding mass and damping coefficients successfully in lateral modes.

Now consider how this fits with concurrent recognition of behaviors. Besalsow and Payne (1988) built on an understanding of parametric factors and investigated in the field with an instrumented unit in the top drive. The study shows the excitation frequency may be of multiples and fractions of the rotation speed. The work suggests that resonance allows damaging vibration. Another parametric rotation coefficient is founded on backward whirl, as the ratio of the hole or drill collar and the difference between the hole size and the drill collar size. From experimental data the authors allow some slip or damping by allowing a second coefficient between 0.8 and 1. Forward whirl is also identified as harmonics and multiples of rotary speed. Torsional resonances are also reported on.

Aldred and Sheppard (1992) introduced a mechanistic physical model dubbed “the rolling log”. The experimental apparatus consisted of a 10 meter drill collar mounted horizontally and rotated through a range of speeds. (Figure 1) A 25 cm confining ring was placed across the center of the collar at 5 meters, the collar was again rotated until contact occurred. The experiment was repeated again with lubricant on the confining ring. In this model the rotation speed and the condition of the confining ring could be adjusted to study effects on transverse motion (whirl behavior). Aldred and Sheppard (1992) point out the shortcoming of harmonic analysis (forced frequency, critical speed) is the lack of an accounting for the interaction with the borehole. While harmonic models stop at contact and declare criticality, perhaps a more realistic model needs to account for what happens after contact: the drill string experiences radial acceleration due to inelastic collision and acceleration tangentially due to friction. This supports a mechanistic understanding that if the transverse (lateral) energy builds with each impact then the impacts may become self-sustaining. Once this behavior was initiated, reducing rotation speed was not an effective means of control. Increasing speed increased the frequency of the shocks until backward whirl was initiated. It is suggested this happens when the centrifugal force is higher than the restoring force acting on the collar (gravity and elasticity). Another conclusion was that predicting optimal parameters to avoid shock is usually not possible, and that a real time trial and error method is appropriate.

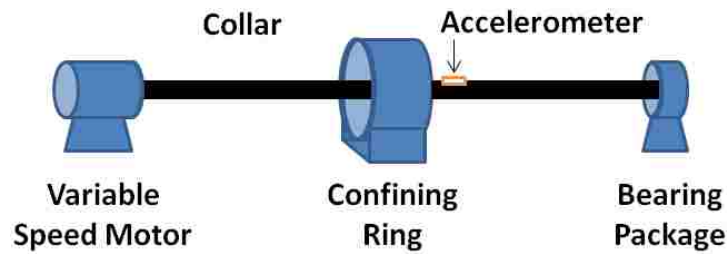


Figure 1. “Rolling Log” experiment.

The popularity of trial and error methods with real-time measurement of vibration have evolved and been widely adopted, while in this author’s opinion mechanistic modeling has remained relatively at the same level. Again, attempts to develop a mechanistic physical model for the drill string and BHA was attempted by Mihajlovic (2004). Mihajlovic et al. presented their work with a flywheel based laboratory device with another flywheel mounted to the base of a long shaft. (Figure 2) A DC motor drives the upper flywheel attached to a shaft connected to the lower flywheel equipped with a disk style brake. The device’s break voltage could be adjusted to explore the shaft’s torsional behavior under load.

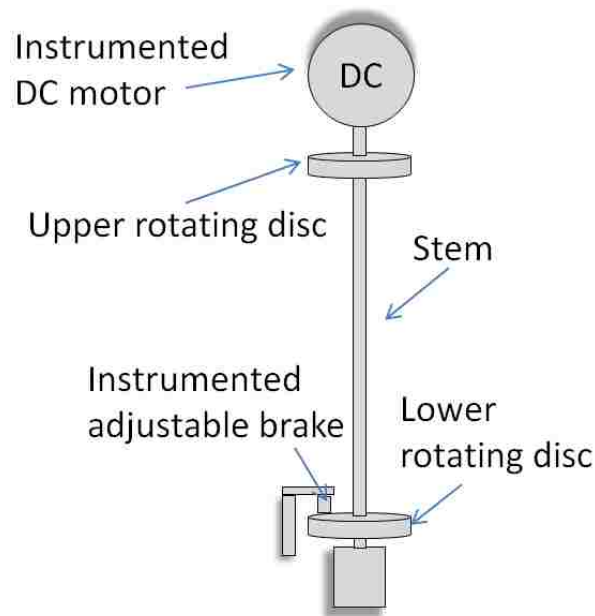


Figure 2. Dual rotating disc connected by stem experiment. (redrawn from Mihajlovic 2004)

The “rolling log” and the “flywheel” models both capture a specific mechanism and its role with rotation speed changes. However, the mechanisms are not inclusive of other parameters the driller has to

work with, namely weight on bit. The axial load effect on a shaft system may be significant. Wauer (1982) discussed the stability of a rotating axial loading shaft, specifically exploring axial load and rotation speed parameters ranges depending on the presence of internal and external damping. (Figure 3) Jansen (1993) acknowledges the power of this type of rotor dynamics model and critical speed model but recognizes that the analogy is hampered by the nonlinear effects caused by drilling fluid, stabilizer clearance, friction and borehole wall contact. To investigate these considerations Jansen developed a numerical model he believed to be more representative. He made a mass-spring model of a drill collar section supported between two stabilizers, which is a rotating shaft between two bearings in fluid. The system is allowed to take axial load, and numerically friction in the system could be adjusted. (Figure 4)

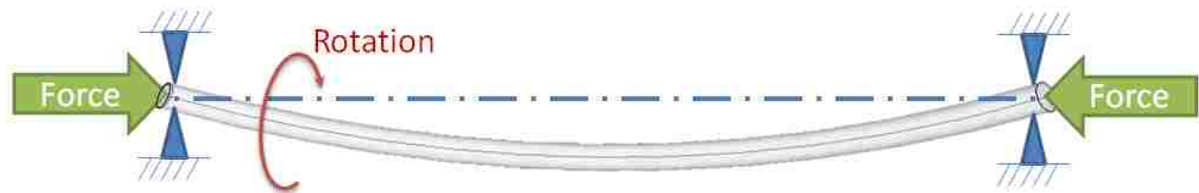


Figure 3. Rotor model. (redrawn from Wauer 1982)

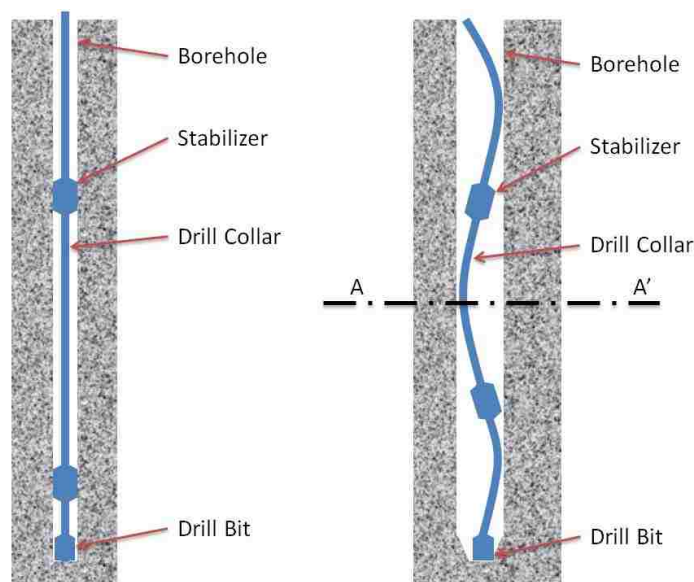


Figure 4. BHA sketches. (redrawn from Jansen 1993)

A discussion of Jansen's numerical model is included in the dimensionless analysis section in the appendix.

Abbassian and Dunayevsky (1998) presented a mechanistic model that exploited three simple systems: torsional vibration in the string, lateral dynamics of the bit, and coupled torsional-lateral vibration of the bit-string assembly. The models are combined to present a mechanistic model of the stability zone concept. One of the assumptions of this model is continuous contact with the side of the wellbore akin to forward whirl. Results of exploring the parameter space of this model mimic the concepts presented in Burgess and Martin (1995). The authors acknowledge the results match the field based experiences despite the assumptions and simplification of the model.

CHAPTER 3.METHODS

3.1 Hypothesis Testing Objectives

Industry and theoretical mathematic agree whirl and stick-slips are actions in play for flexible shaft systems. This section will explore the development and operation of a physical experiment that will allow testing the hypothesis:

- 1) A flexible shaft system without a drill bit will not experience stick slip or whirl.
- 2) Flexible shaft systems of varying stabilization geometries will produce the same levels and types of vibrations over a range of conditions.
- 3) Vibration levels in a flexible shaft are a function of rotation speed and axial load, and manifest regionally as suggested by the Anadrill Methods materials that support the continued successful use of the method.

To address the first hypothesis a physical flexible shaft that will be constructed will be operated across a range of conditions and the model must demonstrate cyclic variation in instantaneous speed, or motion of the rotating section around a center.

To address the second hypothesis the first will be have found null and the different geometries of shafts will have been tested. If the different shafts manifest different types and levels at the same input parameters over a range of parameters then this hypothesis will also be false.

The third hypothesis can be demonstrated by creating a parameter response “map” or surface for each shaft based on measured responses to the parameters of the Anadrill method rotation speed and axial load. The principles of the method will be compared to the response space.

To satisfy a point of the hypotheses are applicable to flexible shaft systems bit (rock breaking excitation factor, bladed pivoting excitation) mechanisms will be excluded. Also a computation model results will support the investigation to completely exclude bit effects and help test the second and third hypotheses.

It was suggested by a committee member that the buckling limit was possibly the regional threshold for stick-slip. This introduces another hypothesis:

- 4) Does the flexible shaft system only experience Stick-Slip above a buckling limit.

This additional hypothesis necessitates that buckling limits be modeled and tested also.

3.2 Model Scaling Requirements from Dimensionless Analysis

Examining Jansen's S (path solution) for whirl (Jansen 1992), determining whirl type provides insights to scaling a physical model:

$$S = \sin(\eta_b + \eta R_c)$$

η_b is the scaled backward whirl speed is a dimensionless Backward Whirl speed with units 1/t divided by natural frequency with units 1/t.

η is the second term in this equation is the ratio of input rotation speed to the natural angular frequency.

R_c is the slipless collar ratio is the collar diameter divided by the quantity of the collar diameter subtracted from the hole diameter.

What is in this solution are terms made from the frequency and clearance diameters. Natural frequency in this case is the square root of quantity of the stiffness divided by the mass. No lengths of the beam have made it into the solution.

Given that the diameters in the test system are similar to diameters used in the field. In fact the test fixture is about a 4 inch collar in a 6 inch annulus with 5-3/4 inch stabilizers. This could be a size combination used in the field. The other term in the solution is natural frequency. The suggested solution is the square root of the stiffness divided by the mass. Another thing to consider is that frequency is inversely proportional to length. A unit length (1 foot) of steel collars in this size have a natural frequency of 92,979 Hz. The same unit length of the test fixtures shaft has a frequency of 4,086 Hz. Steel is about 22.76 times higher in frequency. Therefore for this system using the solution form from Jansen the equivalent system to five (5) feet of shaft [4x1 inch] is 113 feet of [4x1 inch] collars. It should be noted that this is the same scaling factor found using the graphical solution method using another set of equations (Fox 1987) described in the Appendix. The appendix also includes a general discussion on dimensionless

analysis, several discussions on scaling including a summary dimensionless treatment of Euler-Bernoulli beam theory, a similitude like approach, and more discussion on Jansen's mathematical solution.

3.3 New Model Origins

The model developed for this experiment sought to focus on vibration modes and shaft deformation effects. The Wauer (1982) model makes the case clear that axial load should have a significant effect on the deformation and therefore influence on the stability of a rotating shaft. However, the Aldred and Sheppard (1992) experiment, and Mihajlovic et al. (2004) experiment both neglect to explore this response. The physical model developed for this study developed after study of Jansen's considerations and numerical results as previously introduced.

The physical model used in this study (Figure 5) is a flexible shaft with various stabilizer ring configurations, rotated and subject to axial load from the top. The shaft is subject to annular constraint with a base of a rotating table on a load sensor below. A discussion on the effects of the bottom boundary condition is presented in the appendix. An option of the annular constraint was the use of transparent piece that allowed for direct visual observation and recording. The shaft used in the experiment had an acceleration and gyroscopic measurement package at its midpoint.

The anticipated advantages of this configuration over the "rolling log" is the axial load adjustment and sensing, the continuous constraint, and the ability to operate the fixture at any inclination desired from vertical to horizontal. Contrasted to Mihajlovic's (2004) model the flexible shaft allows for observations of lateral deflection. The model intentionally does not attempt to include an analog for bit effects.

3.4 Using Acceleration and Gyroscope Measurement to Measure BHA dynamics

The development and testing of down hole dynamics measurement tools started with accelerometers. Perhaps this is because accelerometers were already being used in down hole tools for surveying. Attempts were made using one, two, three and four accelerometers recording or reporting acceleration while the string was in motion (Deily 1968). Some tools located the accelerometers in the middle of the BHA in a sonde, others in the body of the collars.

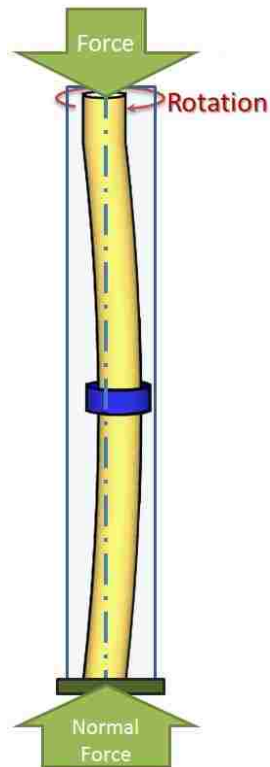


Figure 5. Shaft and annular constraint with axial load force and rotation labels.

Today the use of accelerometers and gyroscopes in drilling measurement tools is wide spread. Diagnosis of vibration modes from acceleration measures was shown by Zannoni, Cheatham et al. (1993) with mathematics, laboratory work and field tests validating the methods for measuring BHA motion commonly used today. Many more examples of interpretation system have appeared in literature from the DDS tool by Warren and Oster (1998) and its peer tools by Robnett, Hood et al. (1999), Ashley, McNary et al. (2001) and Halsey, Kyllingstad et al. (1986) that use similar principles. A robust explanation of the combination of the testing of the tool is found in literature (Zannoni, Cheatham et al. 1993) and US patent 5864058 (Chen 1999).

Figure 6 shows the orientation of the sensor package inside the flexible shaft.

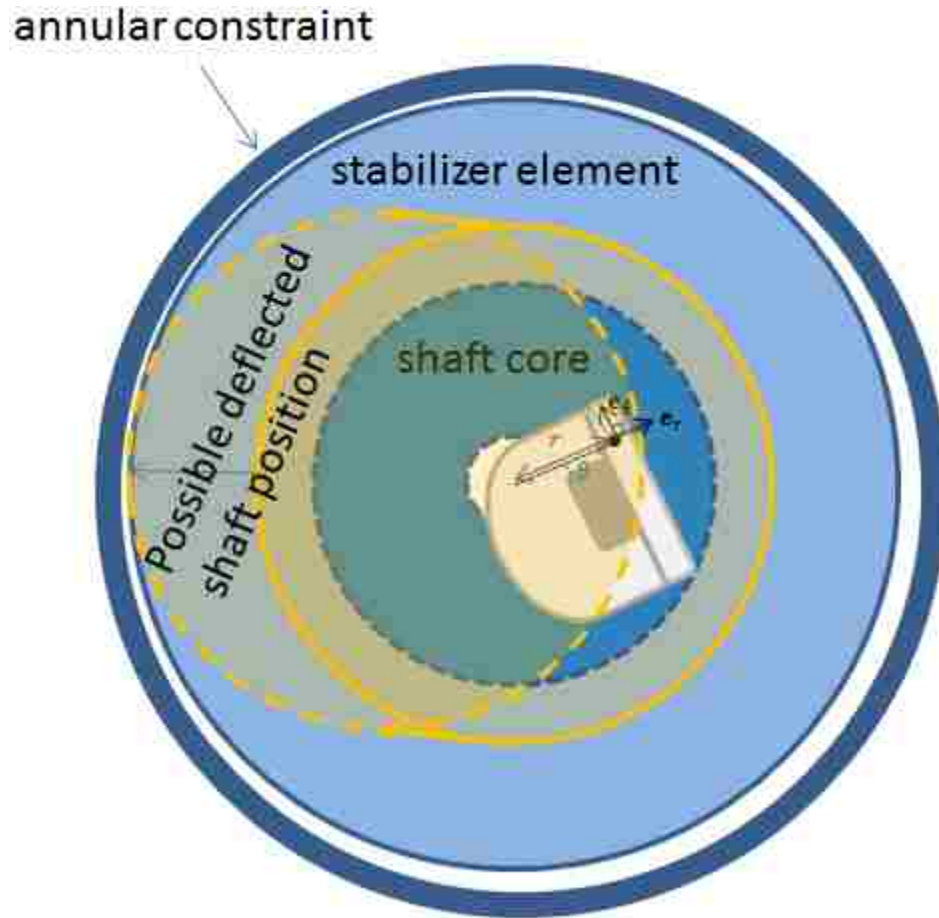


Figure 6. Sensor location inside cross section including shaft stabilizer and annular constraint boundaries.

This investigation focuses on developing an improved mechanism for understanding dynamic behaviors that generate vibration. The proposed mechanism investigated with the physical model described above and discussion on the materials and attempted scaling of the model presented in the Appendix III. The experimental fixture could be used in two ways. One method is a directed manner designed to accomplish and demonstrate specific behaviors, and second is experimental operating in a range of parameters and various configurations designed to capture the occurrence of specific behaviors relative to each other.

The experiments focus use four shaft configurations. Shaft A has no stabilizer elements on it, it is perhaps analogous to a slick BHA. Shaft B one stabilizer on third the shaft length from the free end of the

shaft (the bottom). Shaft C has two stabilizers dividing the shaft into even thirds. Shaft D has one stabilizer in the center of the shaft. (Figure 7)

The upper boundary condition of the system is driven by a motor and the displacement of the upper point to create axial load. Discussion about the drive and motor selection are presented in the appendix. One objective for this endpoint as used in the final testing presented in this study was that the drive would supply constant rotation speed at various torque levels. In the screen phase of model development a constant torque drive was explored. The application of axial load was accomplished with continuous, and fixed displacements of the upper rotation point. In normal drilling operations with the bit advancing through formation, a method to attempt to maintain a specific axial load, or load window is employed. In this study the test fixture supplied displacement (lowering) of the shaft, the axial load was measured at the lower boundary condition. The results including the screening measurement are presented in the next chapter.

The lower boundary condition was also scrutinized. In the main experiments presented in this work the bottom point of the shaft in fixture sat on a disk that sat inside the fixture. This endpoint was selected after experiences with other endpoint conditions during the screening tests, and preparation for a previous analysis strategy. During screening several different boundary conditions were examined. Two of the simplest conditions for a rotating shaft were considered, pinned in the center and free rotation were examined. The results of the boundary condition comparison tests are presented in the results section.

3.5 Physical Model Data Collection

Data to construct response ‘map’ was collected in two styles of parameter variation. The first style held rotation speed constant and incrementally tested different levels of axial load. This was repeated for several rotation speeds across the experimental range. The second style was to set the axial displacement (to a given static axial load) and incrementing the rotation speed, then when the range of speeds was explored, attempting to increase the load and repeat. Force at the base, accelerations and angular position were recorded near a target of 100 hz. The rotation speed of the driving motor was also recorded. The data was then processed to create response maps in the input rotation speed and achieved axial load space for different interpretable measures. The where vibration from a single lateral orientation, the difference in the

two perpendicular lateral acceleration measures (torsional – radial), and an instantaneous rotation speed index.

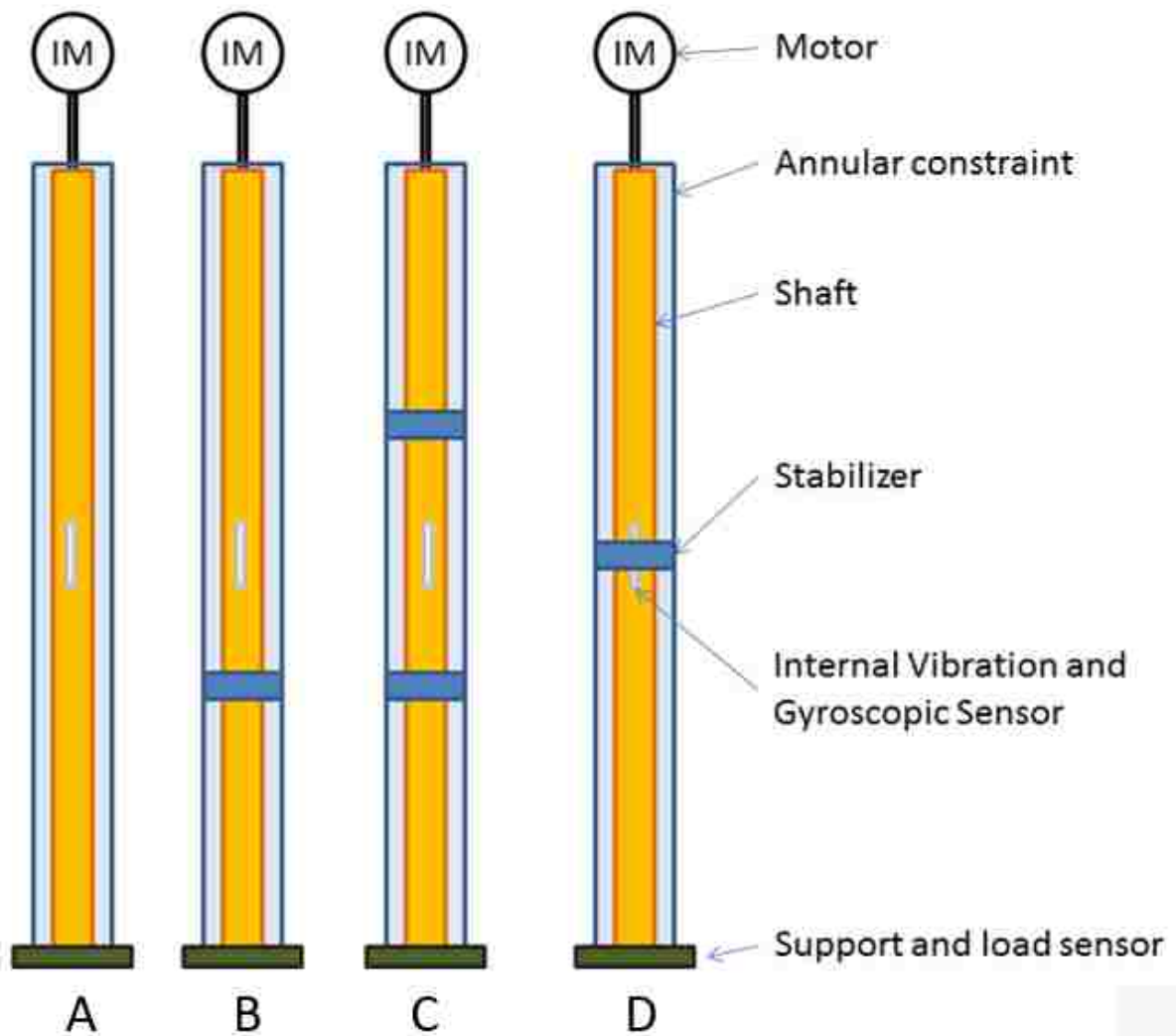


Figure 7. Shaft configurations used in testing presented in the ‘Stability Approach’ flexible shaft system tests. sensor location side view, including shaft stabilizer and annular constraint boundaries.

3.6 Prestress Numerical Modal Analysis for Rotor Dynamic Behaviors in Ansys(TM)

Traditional modal analysis of beams does not account for rotational effects, rotor dynamic analysis does not necessarily account for axial load effects, therefore a two operation process was developed to include both axial loading and rotational effects in the modal analysis. This “preloaded” or “prestress” modal model

produces the response frequencies of the system. This system could be considered unique where most rotor systems do not have axial loads of the magnitudes of a drilling BHA. The system's rotation speed is plotted through the responses and the intersections are points that high resonant or high vibration is predicted to occur. This intersection is called a critical speed. The results from a range of axial loaded rotor dynamic models were aggregated to be presented on a cross plot of axial load vs. rotation speed. (Figure 13) This style plot is significant because weight-on-bit (axial load) and rotation speed are two variables the driller may readily adjust while drilling. The Campbell diagram is significant only because it is a graphical tool for displaying rotor stability equation results. The rotor dynamics simulation also predicts the orbit or whirl direction (backward vs. forward) of the shaft, and if that orbit is considered stable. In this case a stable whirl is one that remains in a constant mode preferentially for the given parameters. This is relevant to oilfield discussion as stability is a desirable property in bit design, it is undesirable in the analysis of BHAs. For Drillers typically stability is viewed with a positive connotation, although again for BHAs in this study the connotation is negative. Backward whirl is known to be damaging to bits (Dupriest and Sowers 2010), where forward whirl is often placed in the acceptable column for bits. (Chen 1999)

The use of the commercial finite element platform and environment allowed for investigations with both beam type elements and tubes made of many smaller elements because of the software's ability to automatically generate meshes for the solutions, and iteratively solve what might otherwise be difficult solutions. The platform also has the ability to integrate more complex geometry, although it is not demonstrated in this work. The workflow employed took the laboratory materials information as input into the engineering data section. The geometry was input in the design modeler. A mesh was generated. A loading problem was then executed. This step is where the axial load was applied and solved. This "static structural" solution was then used along with the rotating velocity in the setup of the modal, rotor dynamics solution. (Figure 8) Critical speed data and Campbell plot results were collected for a range of load scenarios then presented in a similar format to the lab results being plotted with rotation speed vs. axial load.

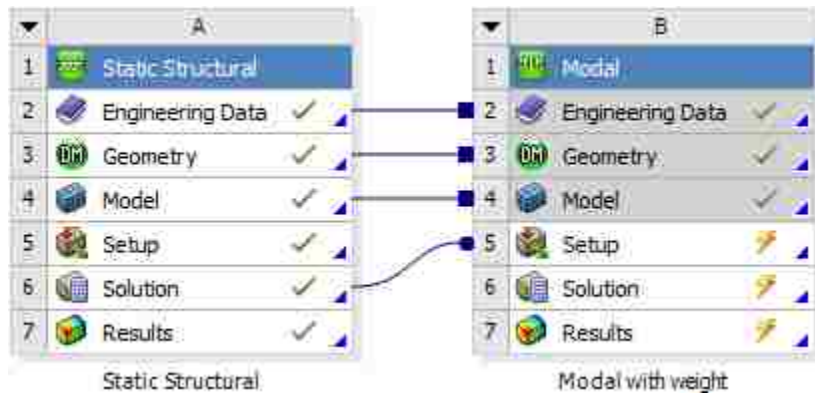


Figure 8. This figure shows the “prestress” solution method. Simply the beam is loaded first in a static model [box A], then loaded to the next analysis [box B].

After material properties were resolved in the lab and confirmed with literature they were assigned to a geometric model. (Figure 9) The geometric model may be made of “beam” type elements that capture the properties of simple equivalent geometries or meshes of solid elements. In this study the stabilizer geometry change created an abrupt diameter change and the additional mass of the sensor package lead to using a shaft broken into many “solid” elements.

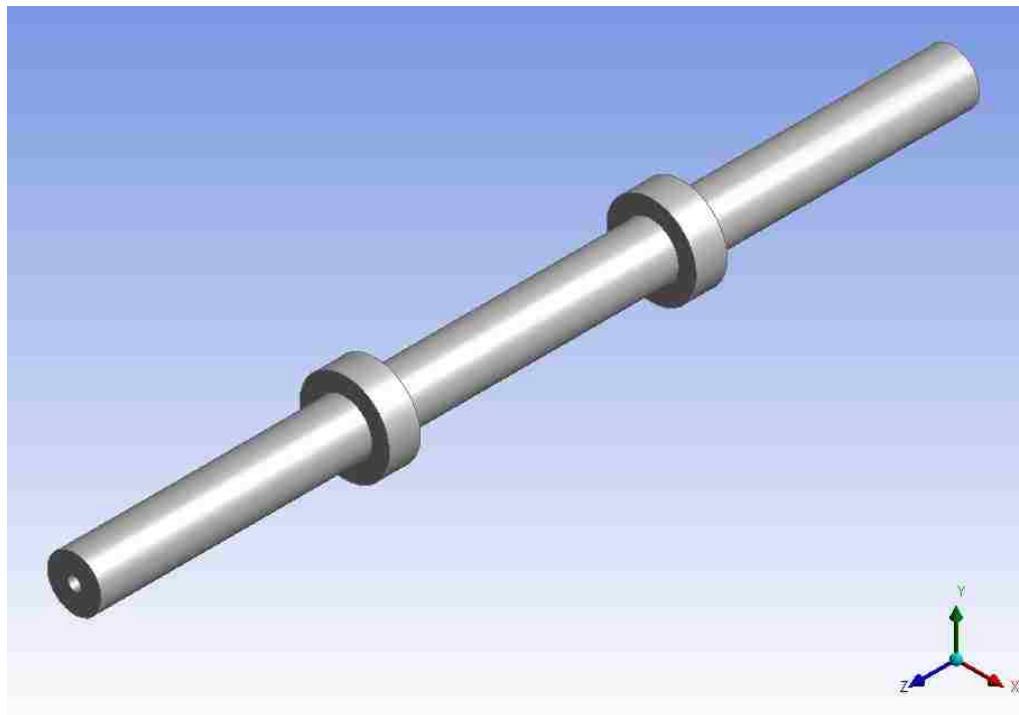


Figure 9. An example of premesh geometry.

Then the geometry is given a mesh. (Figure 9)

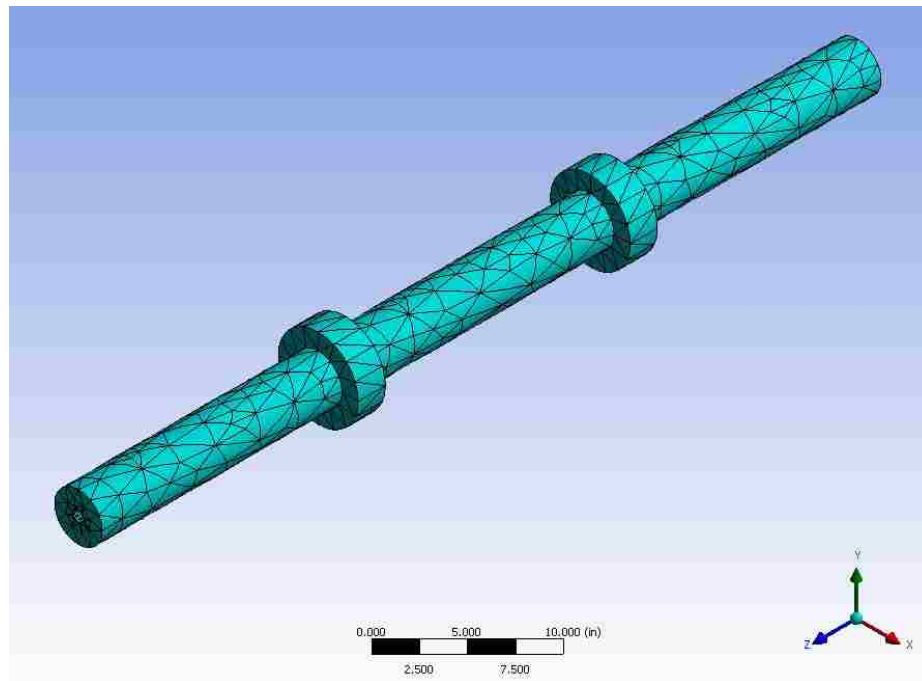


Figure 10. The meshed model is shown for the simulation geometry.

A static simulation of force similar to that used for the buckling calculations is performed. The solution to axial loading is fed into the prestress state of the eigenvalue problem across a range of rotational speeds. (Figure 11) This solution is used to make the Campbell diagram. (Figure 12)

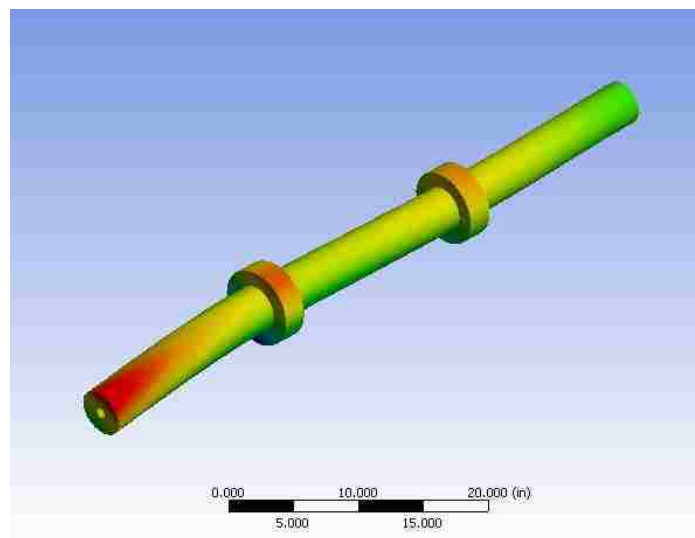


Figure 11. A deformed and stressed model result example. Stress level is visualized here green increasing to red.

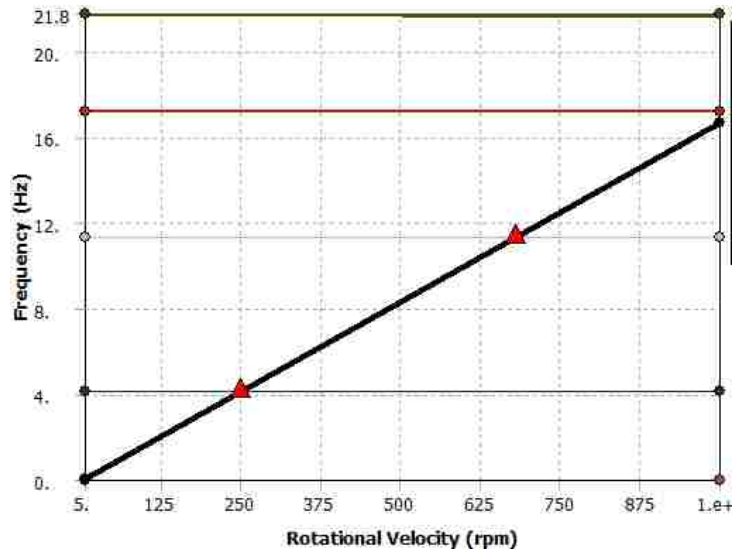


Figure 12. Campbell diagram results showing the modes as: undetermined, forward (FW), backward (BW) and stable or unstable. An excitation frequency is overlaid (thick line) and where this crosses the modes a red triangle is placed to indicate the existence of a critical speed.

Table 1. The Campbell Diagram Output Table. In this table the first two mode are identified by the direction is undetermined, and indication of chaotic motion. In mode shape 3, 5 and 6 unstable backward whirl is predicted, in mode shape 4 unstable forward whirl is predicted. A single (1) ratio is used to related the RPM to the natural frequencies. The intersection of that imposed frequency and the natural frequency results in the identification of a critical speed.

○	Mode - 1 - UNDETERMINED - UNSTABLE
○	Mode - 2 - UNDETERMINED - UNSTABLE
●	Mode - 3 - BW - UNSTABLE
○	Mode - 4 - FW - UNSTABLE
●	Mode - 5 - BW - UNSTABLE
●	Mode - 6 - BW - UNSTABLE
—	RATIO = 1
▲	CRITICAL SPEED

The Campbell diagram shows the system frequencies and the excitation frequencies. Where the system and excitation frequencies overlap is called a critical speed. In this study for the rotation speeds examined the frequency lines did not have much slope so the system frequencies where the critical speeds, however that is not always the case. Where it may be common in a system with a drill bit to use some frequency that is a related to the bit properties in this study a ratio of one was used. For a range of applied axial loads used in the study the critical speeds where collected and plotted and annotated. (Figure 13)

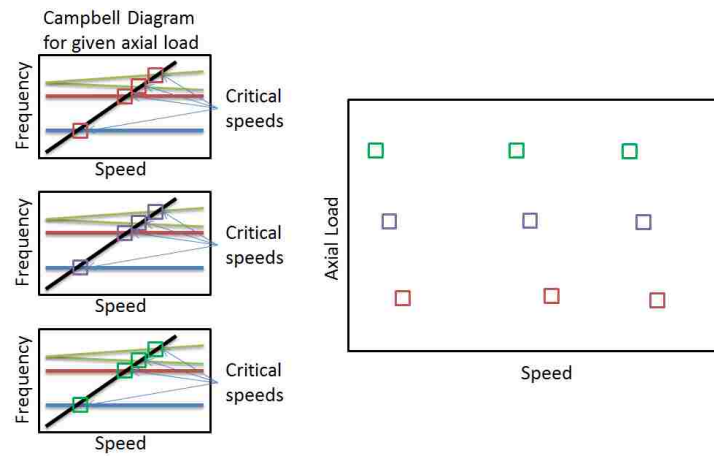


Figure 13. Diagram of extracting critical speed results from Campbell diagrams and making a axial load vs. rotation speed parameter map.

CHAPTER 4.RESULTS

This section first presents some screening measurements exemplify details needed to discuss the hypotheses. The buckling results are presented. Video still are shown demonstrating whirl in the fixture.. Then presents the parameter maps generated for the different shaft configurations are presented. Results from the numerical model are presented also.

4.1 Screening Measurement 1: Long Period Stick-slip Behavior

The objective of this screening experiment was to detail the rotation speed changes for a shaft geometry (BHA stabilizer placement about center and three quarters to the bottom a possible analog to a 30-60 nominal assembly) and the slowest operating parameters expected to experience stick-slip behaviors in the test fixture. Figure 14 and Figure 15 show the measured behaviors of the test fixture shaft during a stick-slip event. Figure 16 and Figure 17 show a six second window of the same event.

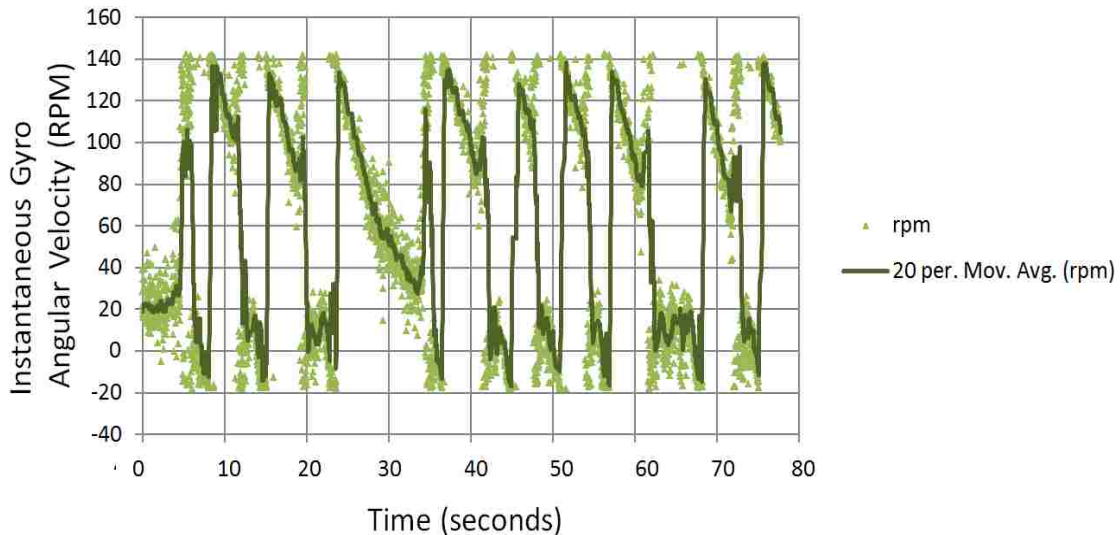


Figure 14. Stick-slip event. 80 second window of a long period stick-slip event: Instantaneous rotation speed.

This event can summarily categorized by the characteristic separation in the average magnitudes of the tangential and radial acceleration measures. A great number of insights can be drawn from this example. First during the rotating phase the instantaneous rotation speed is oscillating but slowly decreasing. Then

the reduced rotation speed phase starts, along with elevated measured vibration. During the reduced rotation speed period vibration continues. Looking at the plot of the six second window (Figure 17), the system can be more clearly observed to have increased vibration levels about a second before the rotation reduces. Then nearly two seconds of vibration levels reduce and nearly a second of reverse rotation is possible. This pattern is illustrated in Figure 18. The system in this case is most calm vibration-wise during this period of reverse rotation.

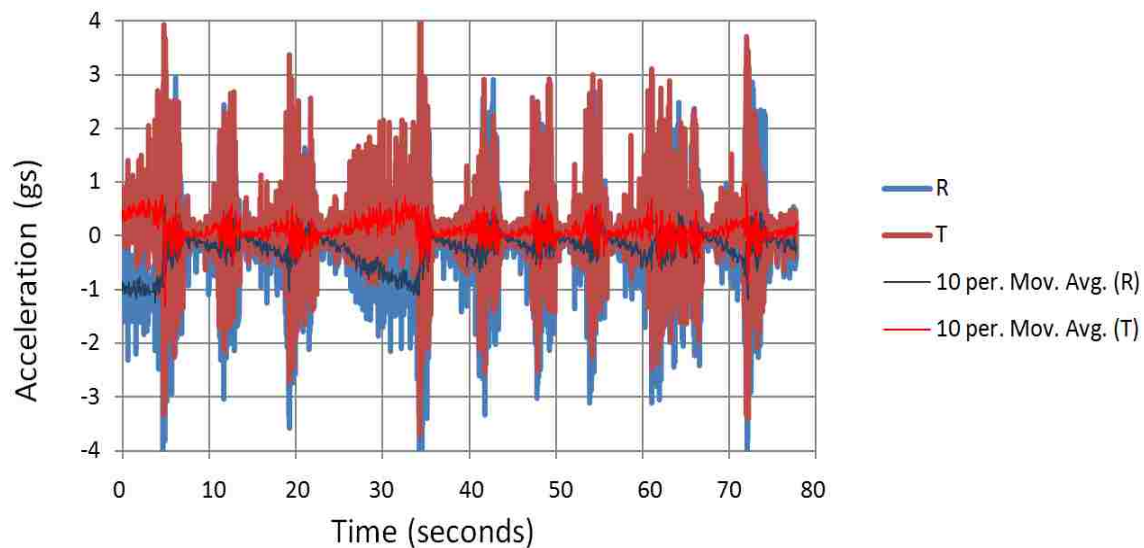


Figure 15. Stick-slip event. 80 second window of a long period stick-slip event: radial and tangential acceleration. The values for the radial position are plotted as negative to better see the average values.

4.2 Screening Measurement 2: Axial Load Variation

This example experiment was designed to demonstrate the axial load sensing ability of the test apparatus during a very different looking torsional or stick slip event developing from a whirling, axial event. Attempting to hold a constant axial load the oscillation of the load is clearly seen. (Figure 19) The magnitude of the phenomena decreases as rotary speed increases from about 200 to 240 instantaneous average RPM. The occurrence of the highest lateral acceleration occurs on the low side of the axial load cycle, as can be clearly seen in Figure 20 and illustrated in Figure 21. The red star identifies one observed boundary load, this will be discussed more in the next section.

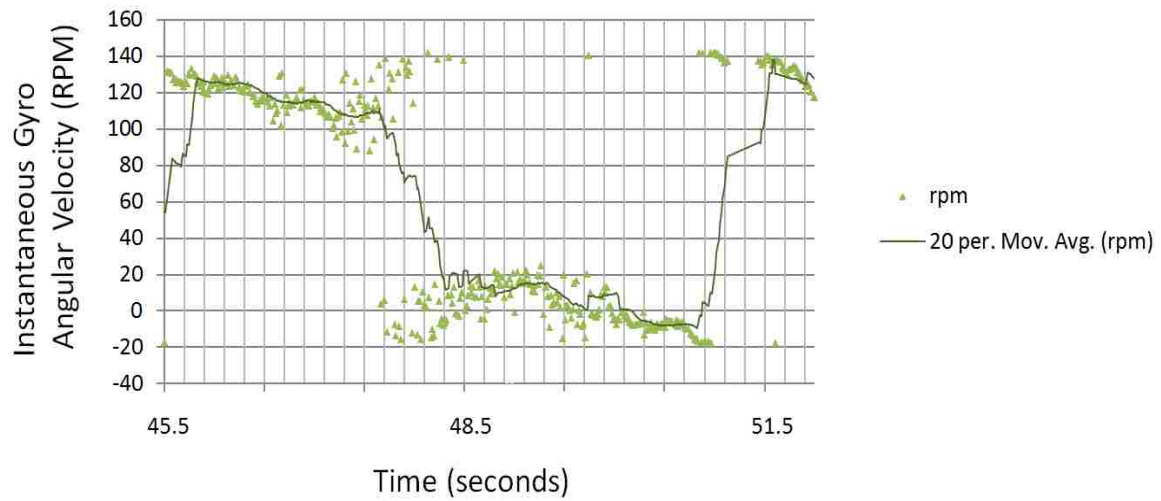


Figure 16. Stick slip event. Six second window of a long period stick-slip event: Instantaneous rotation speed.

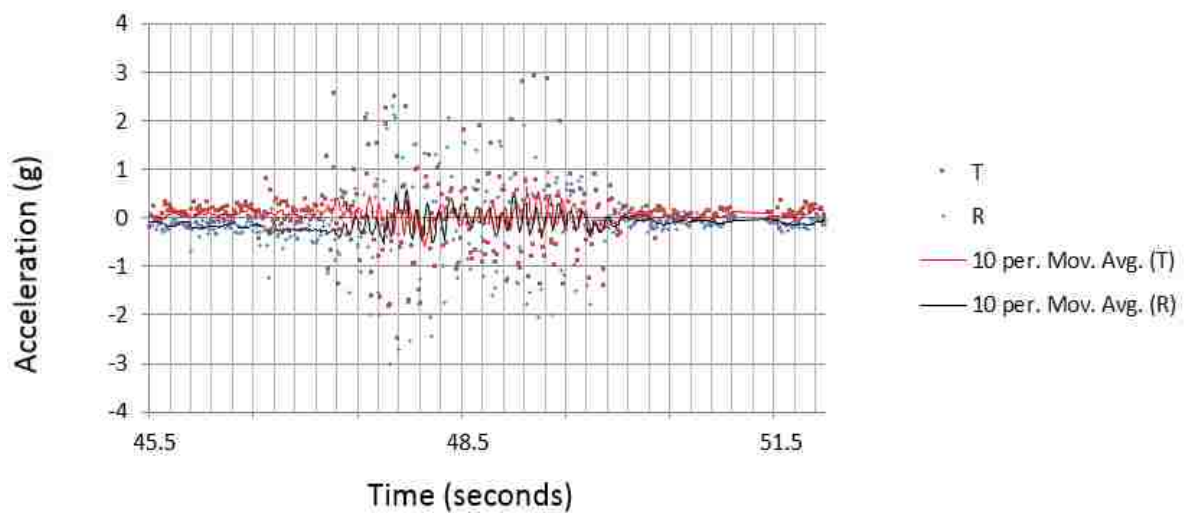


Figure 17. Six second window of a long period stick-slip event: radial and tangential acceleration.

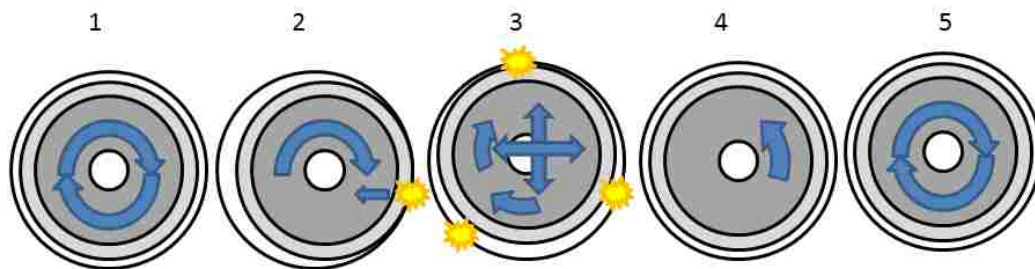


Figure 18. The observed cycle of the “long period” stick-slip event.

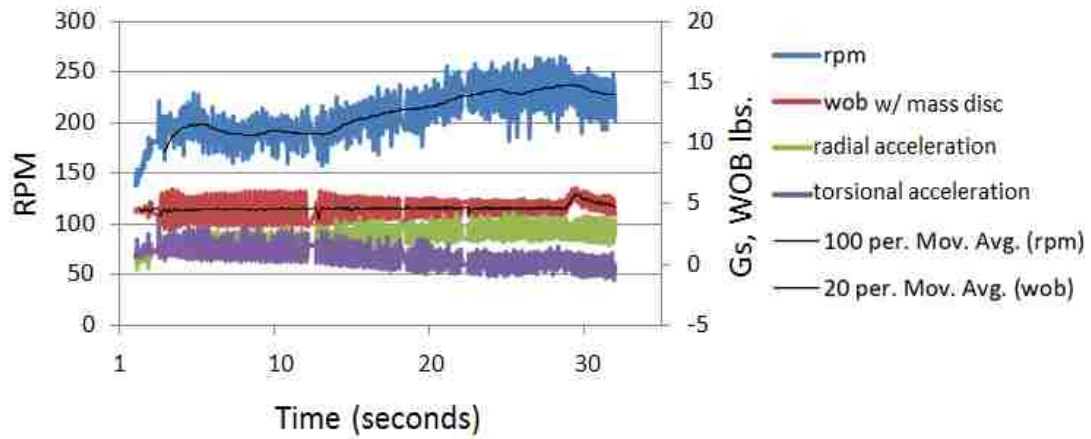


Figure 19. RPM, force, and lateral accelerations for a 40 second window demonstrating axial load oscillation.

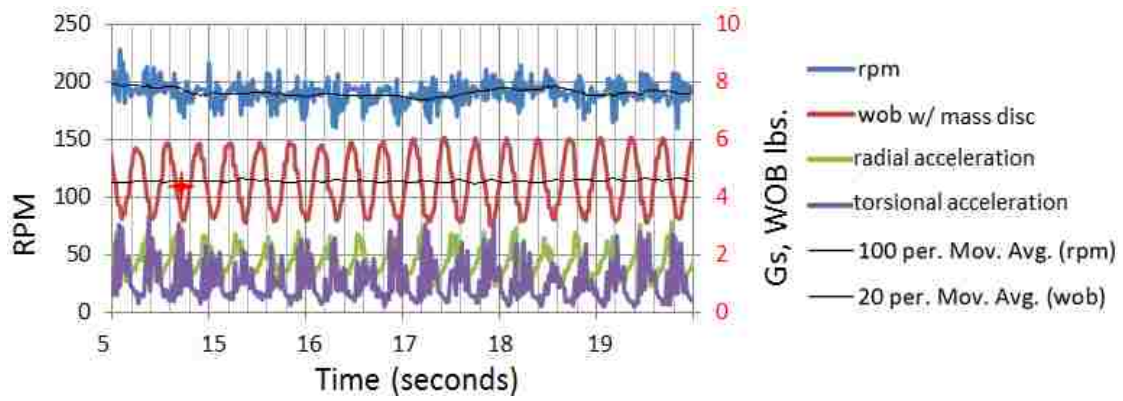


Figure 20. RPM, force, and lateral accelerations for a 6 second window demonstrating axial load oscillation.

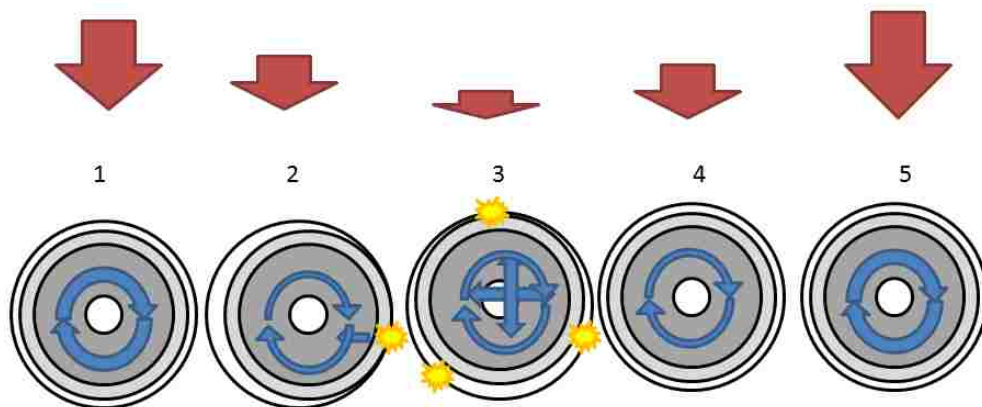


Figure 21. Cycle of axial load variation.

4.3 Experiment 3: Buckling Deflection

The deflection tests were performed with the annular constraint in place, the flexible shaft was loaded axially while force was measured at the base of the shaft until deflection was noted. The shaft was then unloaded. . In the tests the flexible shaft would be loaded then unloaded until the onset of sinusoidal buckling and then unloaded to a lower minimum value. This cycle continued several times. Then the shaft was loaded until a point of helical buckling, unloaded and the cycle repeated. Finally the shaft was loaded and unloaded from helical buckling while being slowly (about 5 rpm) rotated from the top, as in all cases the loads at the point of buckling were recorded. The deflection test was repeated for the four configurations presented.

Here the results from the laboratory testing and computational modeling show the performance of the model, highlighting mechanistic behavior.

4.4 Results from the Physical Experiments

This section reviews the results from the laboratory experiments, first looking at the calculations and buckling. Then presents the observed rotating test results.

4.4.1 Buckling Deflection Calculation

The theoretical buckling load for a similar shaft was estimated using Wu's (1993) formula as presented in the Appendix III.

$$\begin{aligned} \text{Where } E &= 203 \text{ psi} \\ I &= 12.51728 \text{ in}^4 \\ W_e &= 0.011066 \text{ lb. / in.} \end{aligned}$$

Resulting in a critical sinusoidal buckling force of 1.73 lbs., and 3.77 lbs. for helical buckling force. Later this result will be used to help analysis the upper load limits. A comparison with the results from Euler and Ansys™ is presented later.

4.4.2 Buckling Deflection Experiments

The values are shown with colored horizontal lines in the following for reference: Figure 22 shows the resulting loads for Shaft A: the first region where sinusoidal buckling contact was initiated, the second

region where coiling or helical buckling started, and the third region where helical buckling with rotation could be clearly identified. Figure 23 and Figure 24, show the same pattern. Figure 25 shows the similar pattern although in the first and second region of contact, one could see the coil start at almost the exact same point as the initial contact. Another way to say that would be that at the moment of buckling contact a coiling had already initiated.

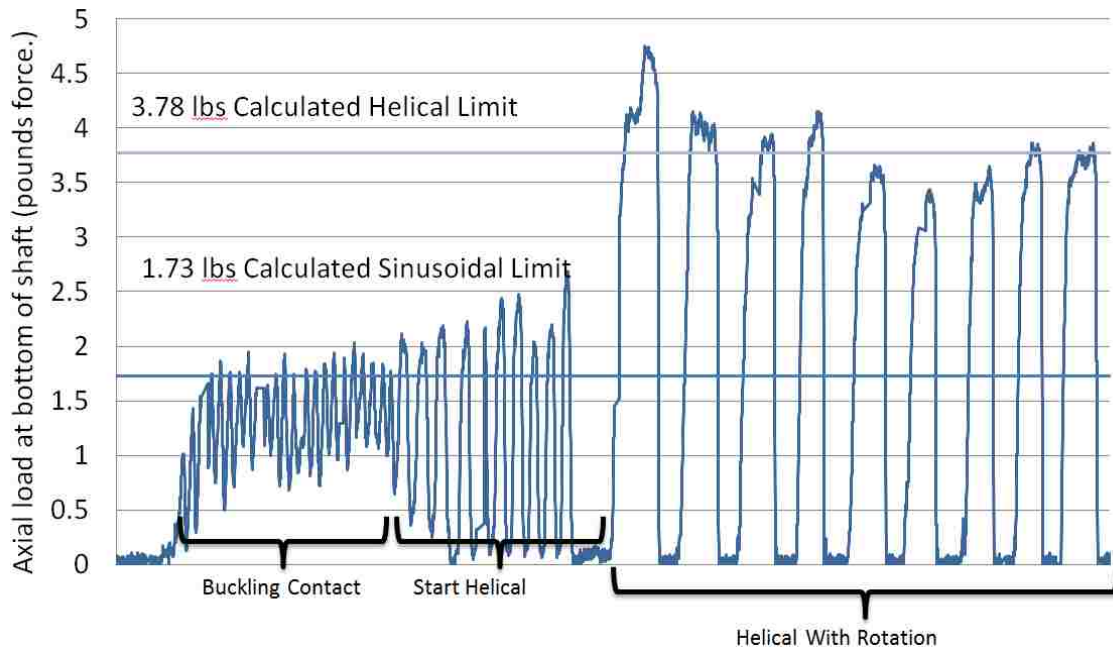


Figure 22. Shaft (A) buckled within 0.25 lbs. of the calculated value of 1.73lbs., helical behavior was observed just over 2 lbs. axial load, Helical with 5 RPM rotation was nearer to the calculated helical value of 3.78lbs.

4.4.3 Axial Load Boundary During Rotation Analysis

In each battery of rotating tests above 5 RPM the maximum linear travel afforded by the fixture was 3.6 inches. This deflection produced sinusoidal buckling in the buckling tests. This value will be called the axial load boundary. The maximum load during the tests for a particular rotation speed were fit with a maxima line, then that line was fit with a linear and polynomial line. A fit value in the form of R-squared was also found. Figure 26 shows for shaft A the scatter plot of data points for a combined set of constrained tests in the fixture. It should be noted that the data points in the plot are aggregated and averaged from the

much larger set of collected data. Details of the characteristic of the test can be inferred. The fixed rotation speed ranges are apparent as vertical trends.

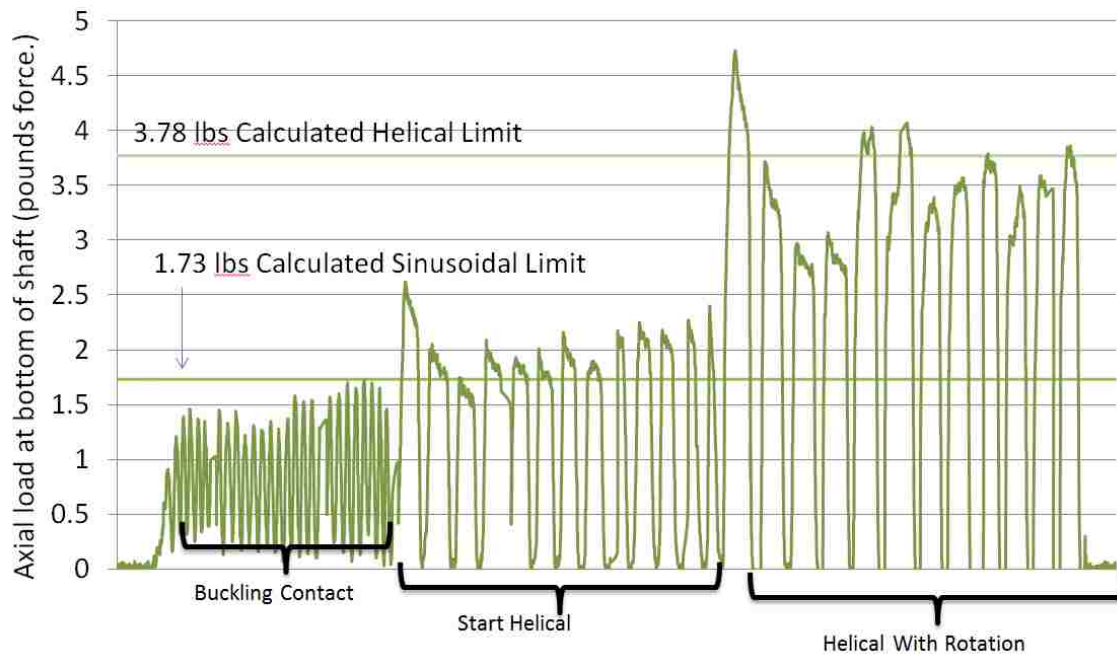


Figure 23. Shaft (B) buckled more than 0.25 lbs. below the calculated value of 1.73lbs., helical behavior was observed just over 2 lbs. axial load in 10/13 cases, Helical with 5 RPM rotation was nearer to the calculated helical value of 3.78lbs., although sometimes was as low as 3 lbs.

Figure 27 shows for shaft B the scatter of data points for a combined set of constrained tests in the fixture. The shaft A load boundary was similar with the exception that at low rotation speeds some higher loads were recorded. Shaft B did not have the same low rotation speed character measured. Both A and B have a limit of about 1 lb. at 600 RPM.

Figure 28 shows for shaft C the scatter of data points for a combined set of constrained tests in the fixture with the axial load limit boundary points. Shaft C's response is unique in a couple of ways. First, the boundary is not continuously decreasing, and for the fixed thrust tests it seemed to converge around 1 lb., however in the fixed RPM tests loads above 1.5 lbs. were achievable in the 310 to 480 RPM range. This also resulted in a 6th order polynomial being used for the fit, and the linear fit having a low R value of 0.0029.

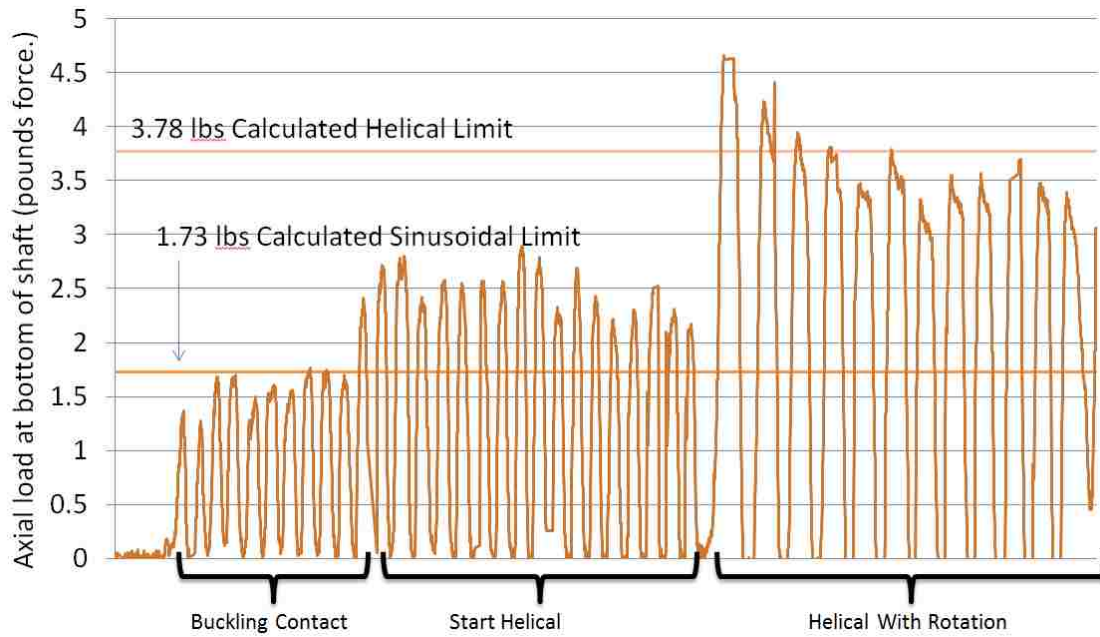


Figure 24. Shaft (C) buckled near the calculated value of 1.73lbs, although some lower than 1.5 lb. results are also observed. Helical behavior was observed over 2.2 lbs. axial load, Helical with 5 RPM rotation was nearer to the calculated helical value of 3.78lbs, although sometimes was as low as 3.3 lbs.

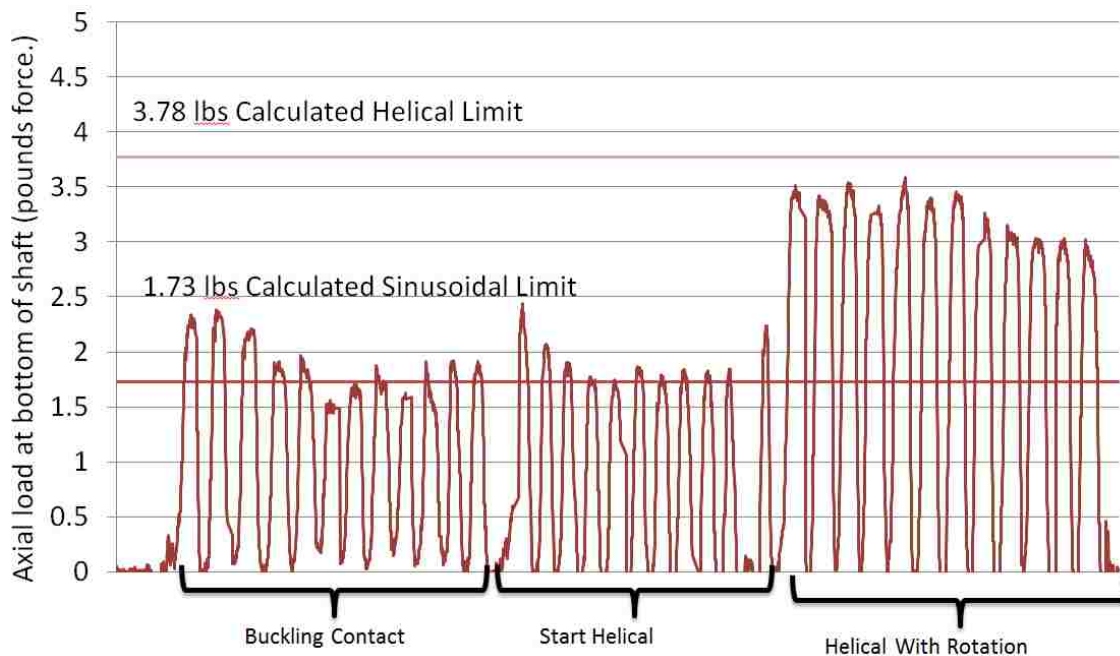


Figure 25. Shaft (D) was different from the other shafts as finding the start of the helical pattern was difficult as the shaft seemed to be wrapping even before contact at about other than the stabilizer. When shaft contact with the hole was found it was consistently lower than the 3.78 lbs. anticipated.

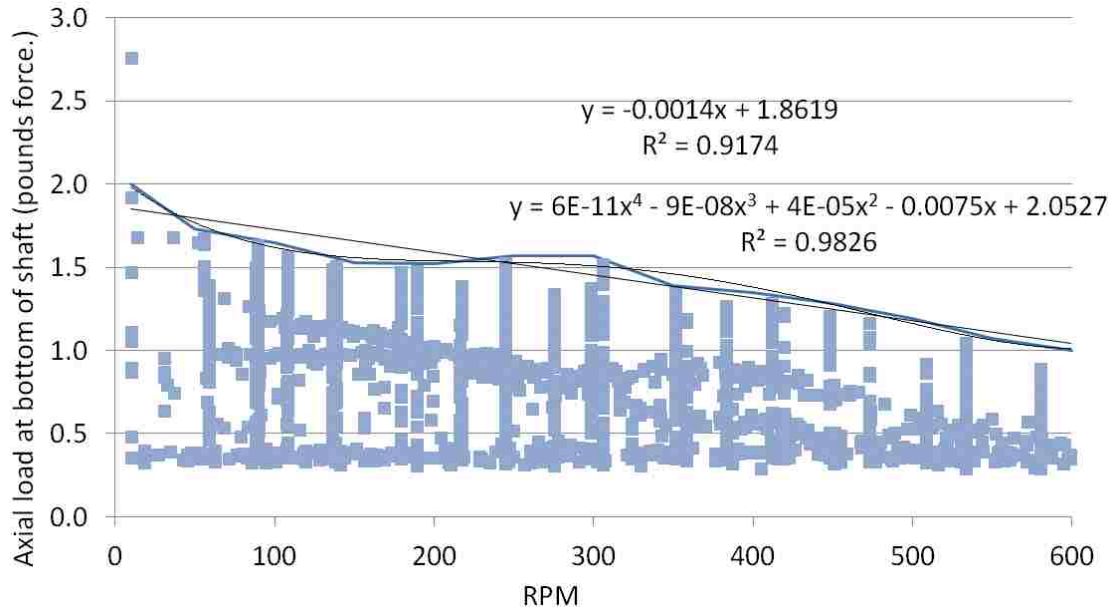


Figure 26. Shaft A axial load boundary. Upper level of achievable axial load to the bottom of shaft A, the sold colored line is a bounding line, the black lines are best fit lines, one linear the other polynomial.

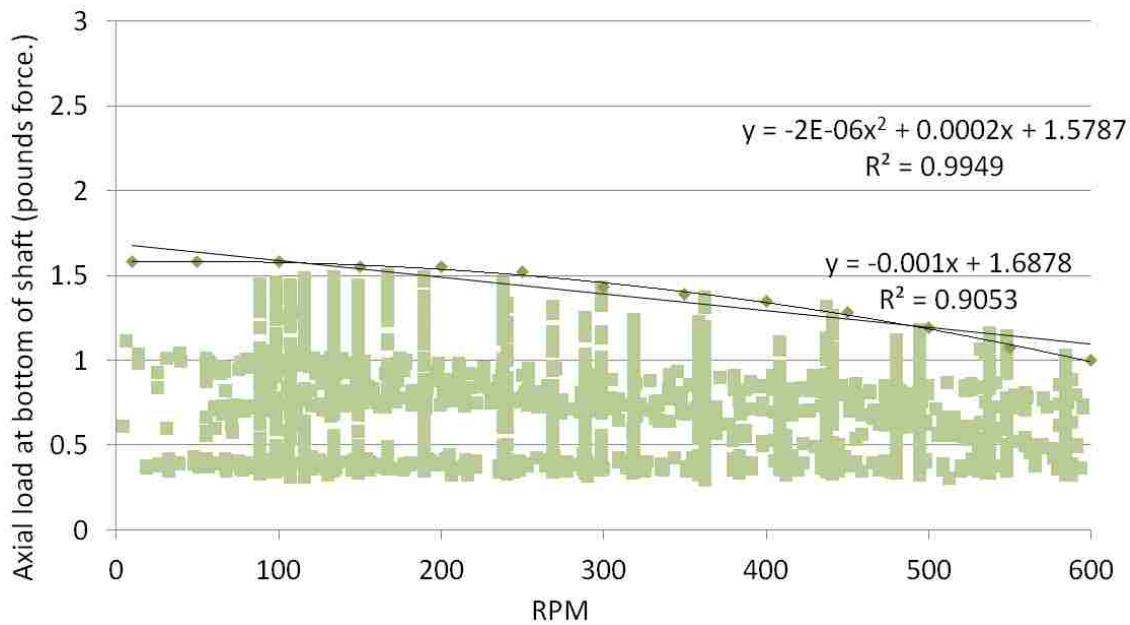


Figure 27. Shaft B axial load boundary. Upper level of achievable axial load to the bottom of shaft B, the diamond points make up a boundary, the black lines are best fit lines, one linear the other polynomial.

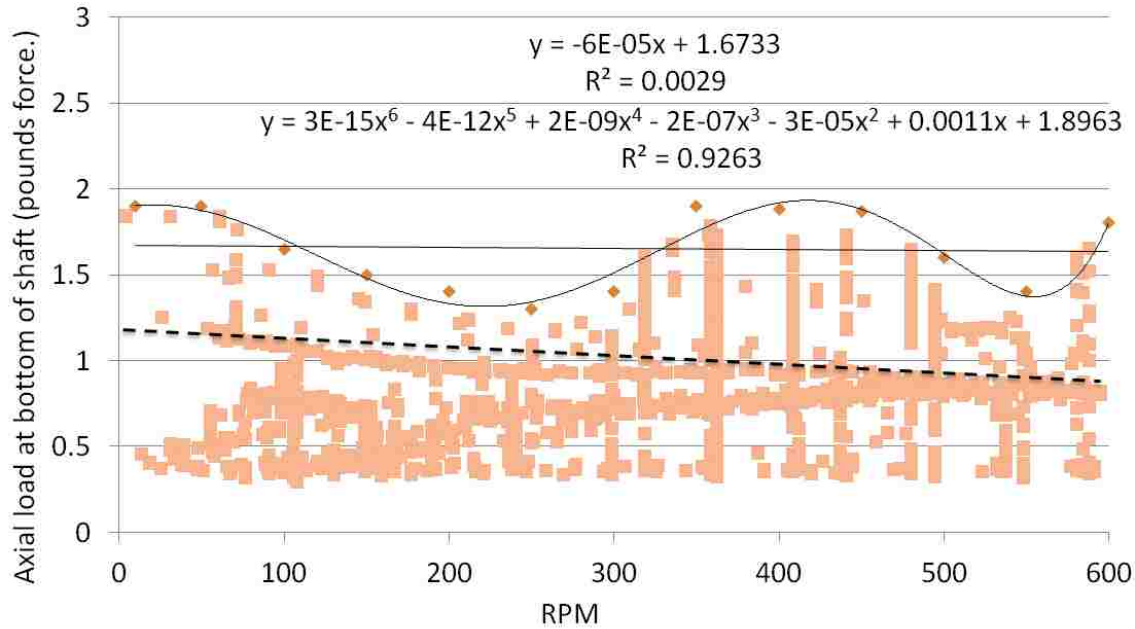


Figure 28. Shaft C axial load boundary. Upper level of achievable axial load to the bottom of shaft C, the diamond points make up a boundary, the black lines are best fit lines, one linear the other polynomial. Take note of the strong trend around 1 lb. that follows a more expected pattern albeit at much less than the calculated buckling load.

Figure 29 shows for shaft D the scatter of data points for a combined set of constrained tests in the fixture with the axial load boundary points. Shaft D shows the same higher achievable loads at low rotation speeds as shaft A.

Table 2 Shows a summary of the axial load boundaries and the fit values for Shafts A,B,C, and D.

4.4.4 Video Stills

Imagining the motion of the shaft is one thing, seeing them on film is another.¹ This study collected some standard rate video (30 frames per second), and some high-speed video to help illustrate the concepts of stick slip and whirl. Presented here are select stills from some of the video collected. Figure 30 and Figure 31 depict a forward synchronous whirl event in the fixture inside the clear annular constraint for the shaft D configuration. The shaft turning clockwise is also orbiting clockwise. The angular velocity of the rotation and the orbit are estimated to be the same since scribe line returns to the same position as the shaft.

¹ The videos are available on youtube under the channel 'drillinglab' <http://www.youtube.com/user/drillinglab>

To the right of each frame is an interpretation of the visual information in the still. The dimensions are distorted for clarity. It should be carefully noted the shaft is slightly deflected inside the fixture, where the illustration does not indicate this deflection. Also the dashed reference line is an inference from the author as this line is out of the view of the camera while it is not facing the shaft.

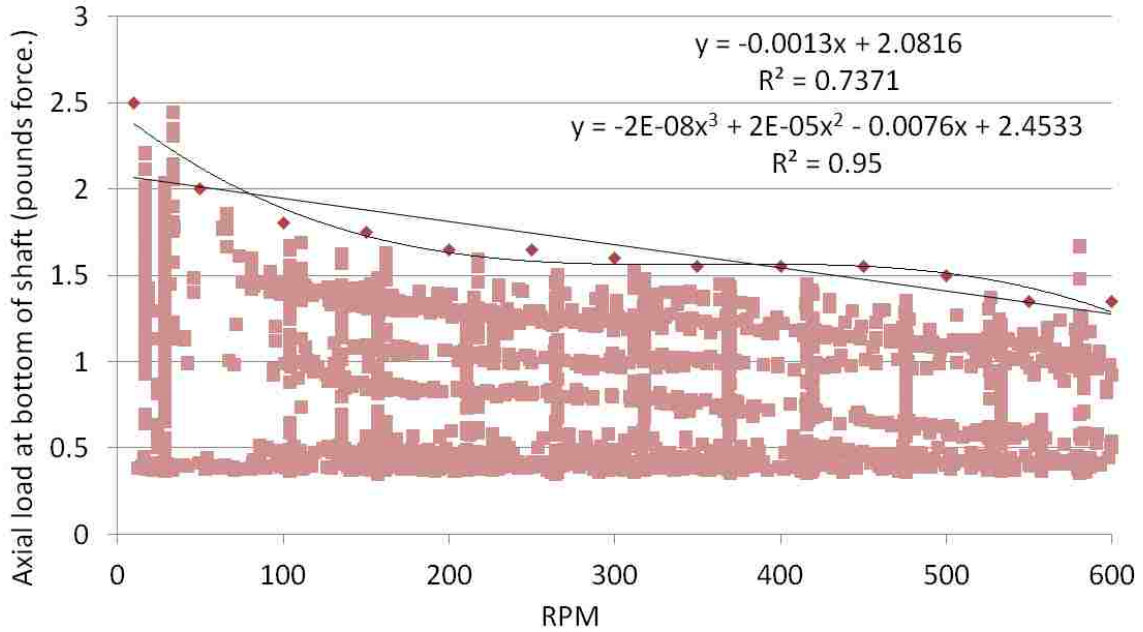


Figure 29. Shaft D axial load boundary Upper level of achievable axial load to the bottom of shaft D, the diamond points make up a boundary, the black lines are best fit lines, one linear the other polynomial.

Table 2. Axial Load Boundary Summary for 3.6 inch Maximum Displacement shows for each shaft configurations the numerically modeled load intercept.

Axial Load Boundary Summary: 3.6 inch Displacement						
Shaft	Linear slope lbs./rpm	Linear Intercept lbs.	Linear R ²	Polynomial Order	Polynomial Intercept lbs.	Polynomial R ²
A	-0.0014	1.86	0.92	4	2.05	0.98
B	-0.001	1.69	0.9	2	1.58	0.91
C	-0.00006	1.67	0.0029	6	1.9	0.93
D	-0.0013	2.08	0.74	3	2.45	0.95

Figure 32 is a sequence of video stills from a 240 frame per second video that has also been captured down to about 60 frame per second to show the orbit effects, however be assured that the higher frame rate

video clearly shows no “stroboscopic” effect or other optical illusion around the orbit of the shaft. A slight blemish in the shaft can be tracked in about the same position in frame 1 and 8. One can note that it takes about 8 stills or 32/240 of a second for the shaft to make a full rotation. One could estimate the RPM: $(240\text{FPS} / 32 \text{ frames to rotate}) * 60 \text{ sec/min} = 450 \text{ RPM}$. Rotation speed was not changed however, a slight decrease in axial load was made that was visually identified as a threshold between behaviors.

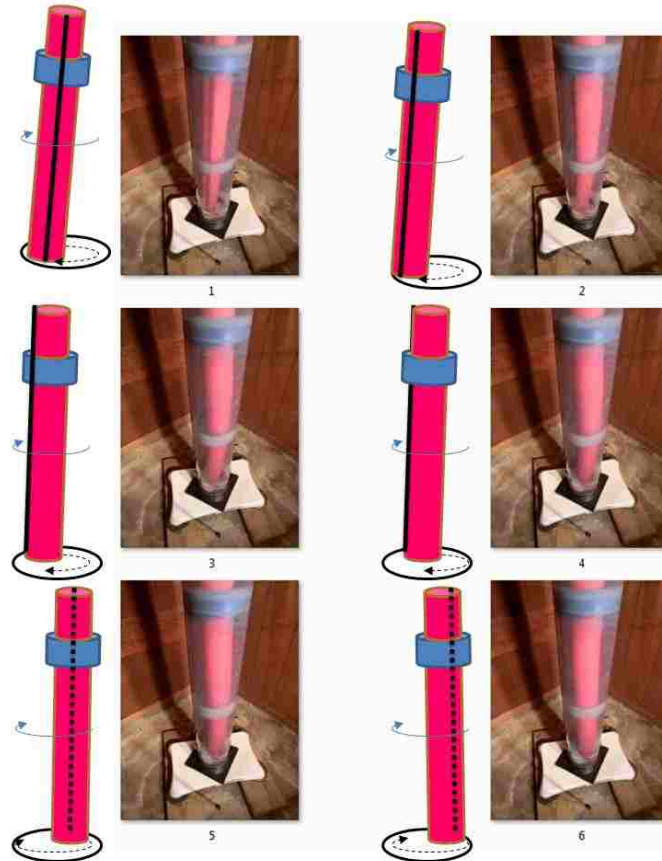


Figure 30. Video stills depicting forward synchronous whirl, Part 1. In the first frame the bottom of the shaft is to the far left in the fixture, in the second frame it has rotated to the back left, in the 3rd and 4th frame it has moved to the back, in the 5th frame in the right side, by frame 6 the shaft has started to come forward again.

Figure 33 depicts the same system in backward whirl. Notice that where before it took about 8 stills to make a whole orbit, it now takes 21. That can be estimated similarly to an orbital angular velocity of 171 RPM. That is a ratio of about $450/171 = 2.63$, this is comparable to the ratio of the shaft diameter and

the fixture base inside diameter of 2.63. Therefore this event could be categorized as a “synchronous” or “gear-like” backward whirl because of the no slip condition or ‘synchronization’ of the shaft outer diameter and the diameter of the lip constraint of the base piece. Examining a longer section of the video this synchronous behavior was not consistent for more than a few cycles at a time before having some slipping. As a caution to the readers, this jargon can lead to some confusion where ‘synchronous’ forward whirl denotes the comparable angular velocities between the shaft rotation and orbit.

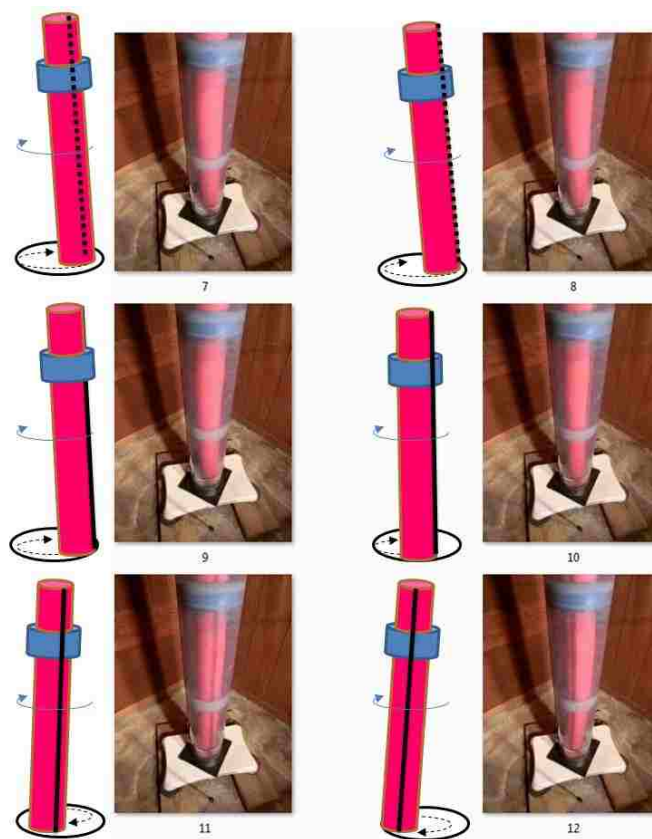


Figure 31. Video stills depicting forward synchronous whirl continued, Part 2. In frame 7 8 and 9 the shaft coming around to forward, by 12 the shaft has just about returned to the position in frame 1. Notice that the ‘scribe’ line has also returned to the original position.

4.4.5 *Vibration Response Surface Experiments*

The rotating tests recorded acceleration levels, using a response surface emulating the field generated parameter maps. Presented are boundary surface plots of the torsional measured position vibrations, the

difference between the two measured in plane accelerations and the gyro measured values formed into an index value.

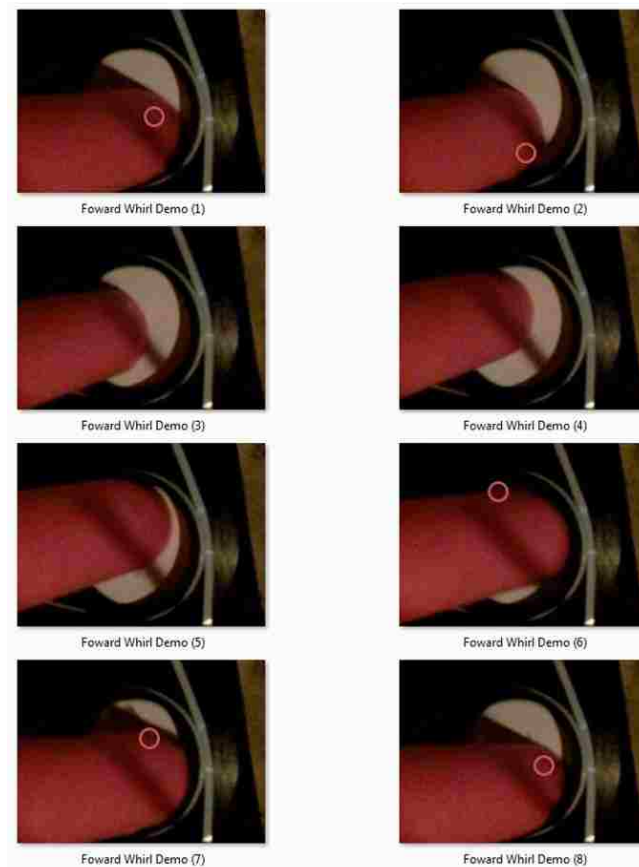


Figure 32. Clockwise rotation filmed with the annual constraint removed showing forward whirl. 60 frames per second stills. The shaft rotating clock wise is also orbiting clock wise around the base constraint. The circle highlights a blemish that is helping visually track rotation.

Figure 34 shows the torsional vibration response surface. On the X-axis is the rotation speed of the fixture, on the Y-axis is the force recorded at the bottom of the shaft. The surface bounds the average one second vibration for the particular set of parameters. Superimposed is the demonstrated axial load limit. This plot is designed to mimic the design of the Anadrill (Schultz 2005) parameter map method for identifying and mitigating vibration.

Figure 35 shows Shaft B's vibration response. It possesses definite geometry but not much is going on below 150 RPM with the exception of the tail of a feature that runs through the map. It is also important

to note that this shaft configuration had the most difficulty transferring force, it was also the farthest below the expected calculated values in the buckling tests. The slope of the response area follows the buckling limit closely.

Figure 36. shows shaft C's vibration response in terms of acceleration averages for a range of axial loads and rotation speeds. Shaft C is unique in the group that it has acceleration values as high as 4g even at low RPM and in the less than 0.75 lb. range. Shaft C's response is also unique in that it has a band of lower vibration (less than 1 g's) around 0.75 lbs. Also the low vibration even at values as large as 400 RPM @ 1.75 lbs. resulting in less than one g.

Figure 37. shows shaft D's vibration response in terms of acceleration averages for a range of axial loads and rotation speeds. Shaft D had an ever increasing vibration response to RPM. Only a small section around 550 RPM and 0.6 lbs. had unusual stability.

At this point in the analysis one can see the characteristic response of the four shafts is similar, although each shaft configuration has some unique elements. Shaft A only developed vibration as high as 3 g's in a few spots, while the others had a fairly consistent ramp from 0 to 5g's. Shaft B was uniquely limited in how much axial load it could develop despite having the same maximum axial displacement applied. It also had a kind of band of elevated vibration right through it. Shaft C also had a kind of band of elevated vibration. Now let's consider the Sperry diagnostic method for identifying stick-slip behaviors, separation of the acceleration values.

Figure 38 shows upper boundry of the separation in the measured average torsional and radial position values for shaft A. Using an algorithm inspired by the Sperry-Sun method, the whirl mode may be predicted. Over a range period of time lateral vibration is just noise in the averaging of the rotation speed. The difference in the values is an indication of a change in mode of vibration. Shaft A had an elevated difference around 300 RPM and 1.25 lbs. It is worth noting that even at the highest points in the parameter range the response is not greatest.

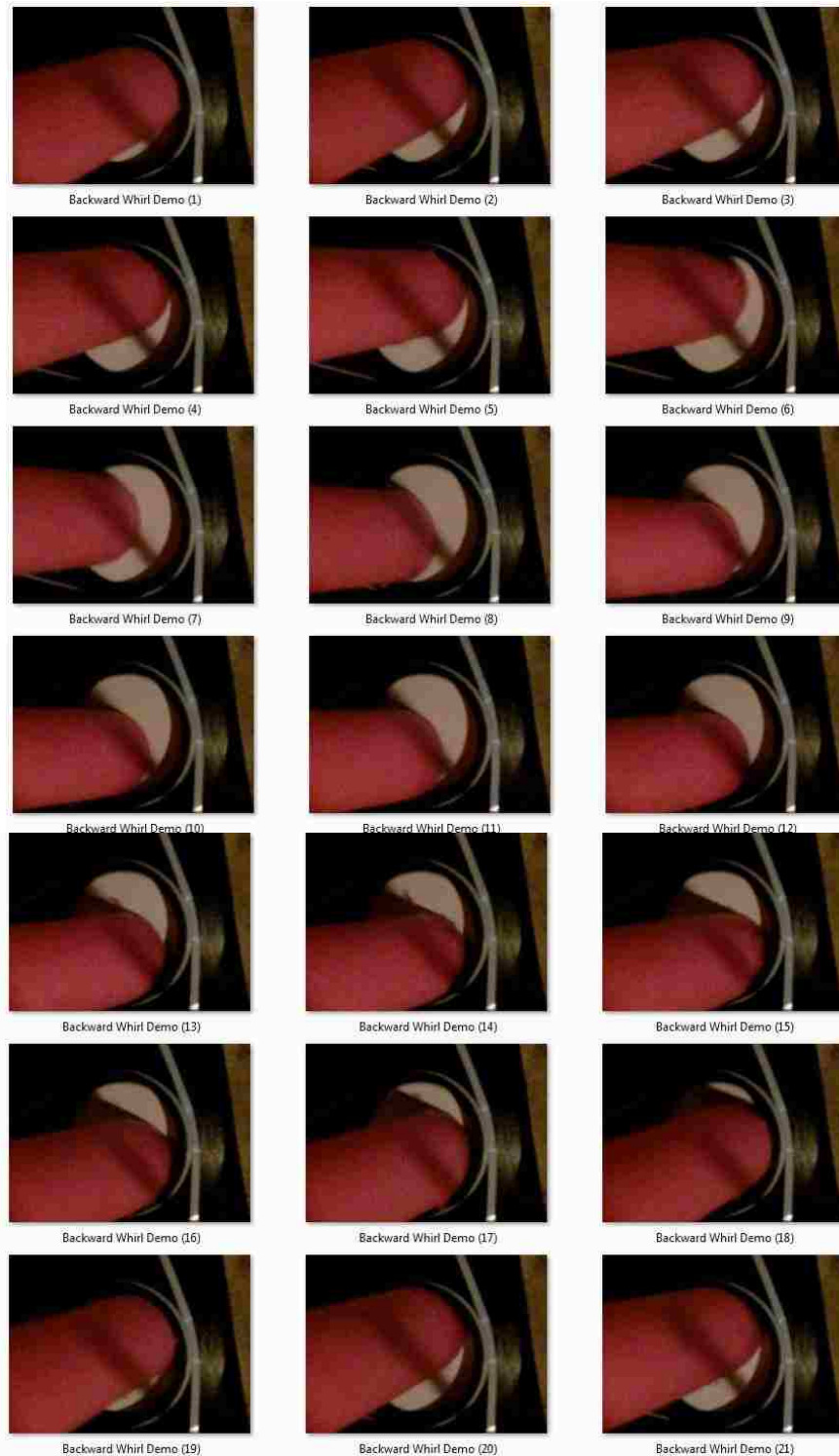


Figure 33. Clockwise rotation filmed with the annual constraint removed showing backward whirl. 60 frames per second stills. The shaft rotating clock wise is also orbiting counter clock wise around the base constraint. The blemish is difficult to track in the stills, however it stand out prominently in the video.

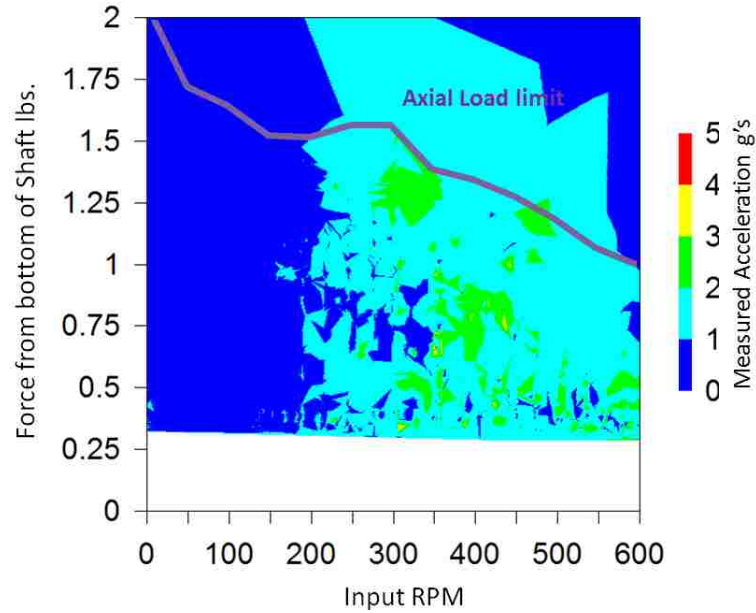


Figure 34. Shaft A torsional vibration response surface. This plot designed to mimic the Anadrill mitigation method regions shows regions of different average vibration levels. In this case for shaft A, vibration from the torsional orientated accelerometer 1 second averages, increases from less than 1g's to above 1g's around 200 RPM. Levels between 1g's and 2 g's past this point with a few regions with values up to 3 g's scattered through map.

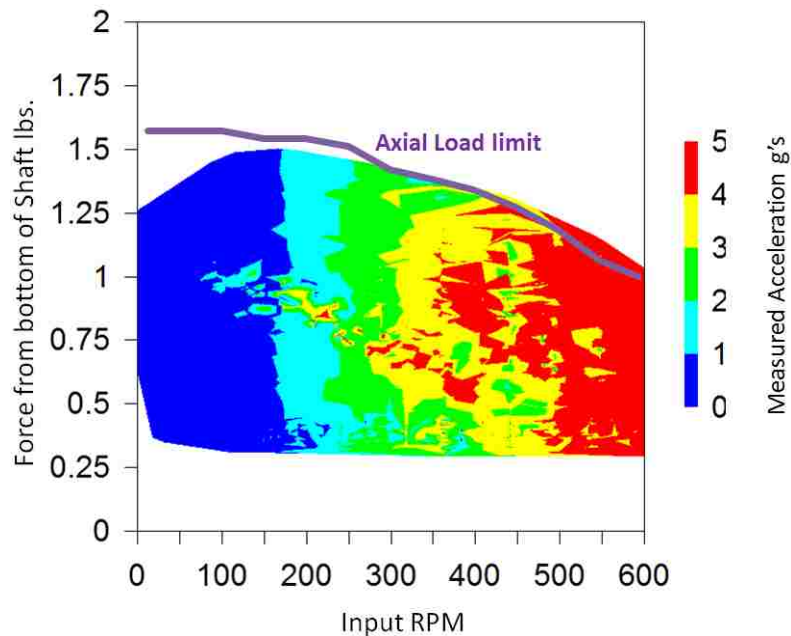


Figure 35. Shaft B torsional vibration response surface. The force vs. RPM, average acceleration parameter map for shaft B shows an increase of vibration response as RPMs increase. From less than 1 g's at 100 RPM up to 5 g's around 500 RPM. Also a near linear feature cuts across the range with elevated levels, Starting at 100 RPM and 1 lb., going to 400 RPM and 0.5 lbs. A second feature of elevated vibration sits around 1 lb. and 400 RPM.

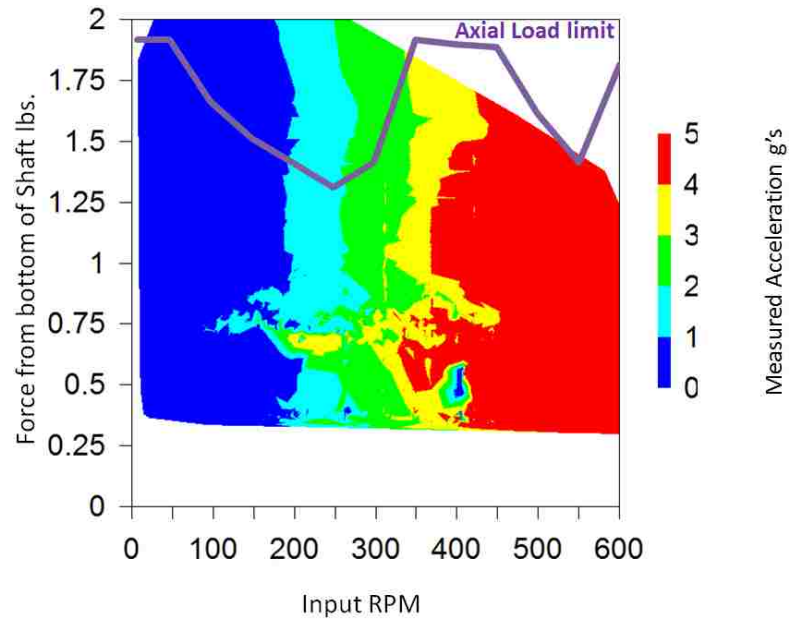


Figure 36. Shaft C torsional vibration response surface. The force vs. RPM, average acceleration parameter map for shaft C is a sharp contrast from the other shafts, having measured average acceleration of more than 4 g's in the lower force lower RPM region around 0-300 RPM and less than 0.75 lbs. The area between 300-400 RPM has mostly less than 1 g's. Past 400 RPMs there is some elevated vibration present.

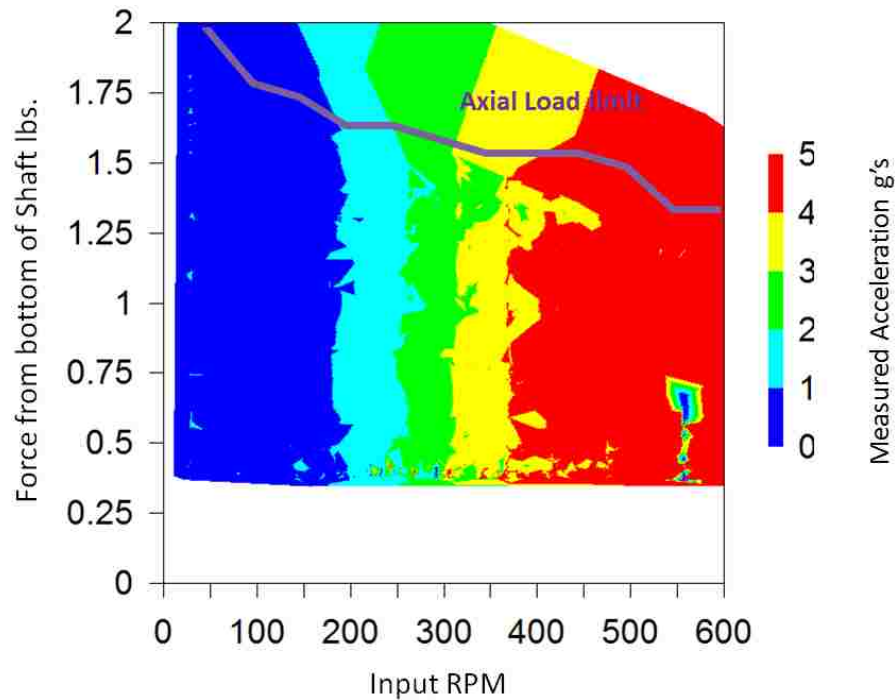


Figure 37. Shaft D torsional vibration response surface. The force vs. RPM, average acceleration parameter map for shaft D is much like that of Shaft B without the bands of elevated response. Vibration's measured show an increase from less than 1 g's around 175 RPM, to 4 g's by 350 RPM.

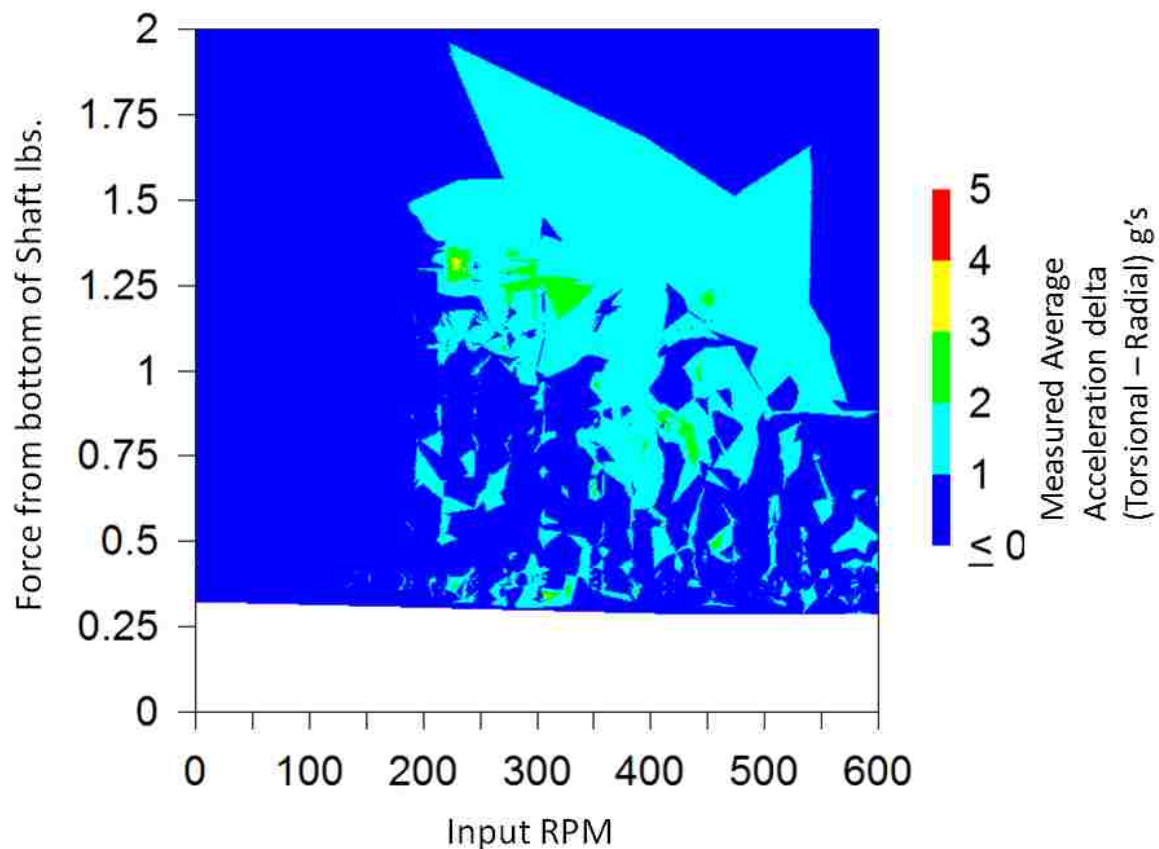


Figure 38. Shaft A vibration separation response surface. Parameter map response for the difference of the two in plane acceleration measures the torsional and radial measures for shaft A. The largest delta is around 1.25 lbs. and 200 RPM.

Figure 39 is the same style of plot for shaft B. Shaft B's response takes on a different character in that it is constantly increasing with RPM. This is a carryover from the near linear effect in vibration increase seen for the stabilized shafts.

Figure 40 shows the same response for shaft C. The response here is sufficiently complicated not to be generalized well by a one-dimensional function of rotation speed. Specifically note that the region above 550 RPM and above 0.75lbs. experiences about the same as the region around 300 RPM of between 2 and 3 gs.

Figure 41 shows the shows upper boundry of the separation in the measured average torsional and radial position values for shaft D. Shaft D's response is fairly one dimensional with the exception of the

region right around 550 RPM and 0.65 RPM that is less than 1 g's. This was noted as physically a very 'smooth running' parameter during physical observation for both shafts configured in this fashion and is not an artifact of processing.

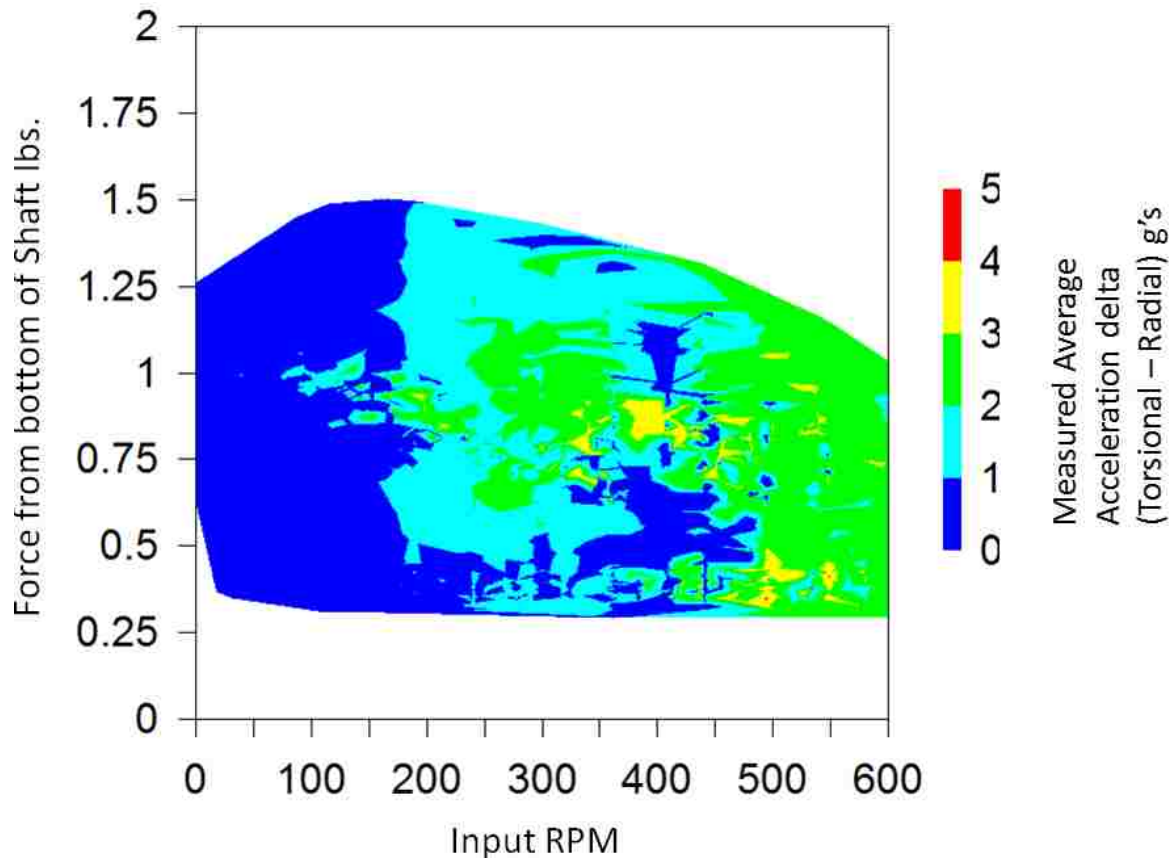


Figure 39. Shaft B vibration separation response surface. Parameter map response for the difference of the two in plane acceleration measures the torsional and radial measures for shaft B. Shaft B is different from Shaft A's response, above 350 RPM the separation increases to past 3 g's in places.

The delta average acceleration measure produced unique regional distributions for each shaft configuration. Next let's look at the gyroscopic results. It has already been shown that a level of torsional vibration was fairly ubiquitous, especially past 200 RPM. The gyroscopic measure is perhaps a more direct way to identify stick-slip behavior. Two index values are established for the sake of simplification. If a minimum recorded continuous RPM data point inside a one second sample qualifies, the parameters for that entire second period where consider qualified for stick-slip measures. The first qualifier was a RPM point near zero (less than 10) when the input average was at least 10 greater. The second qualifier was a

RPM point that was less than half the total RPM observed from the motor. In the screening tests dimensionless stick-slip was presented. In the index presented in this section a 2 point value is equivalent to a 0.5 or greater dimensionless stick-slip. The index presented in the results here included the ‘near stopped’ ten RPM or less factor to highlight the near stop condition. The equivalent In the preliminary case the motor slowed down significantly during some behaviors, that did not appear to happen with the AC drive and induction motor. The effect was that stick-slip behaviors had a shorter period. The qualified points are displayed to demonstrate where stick-slip is occurring.

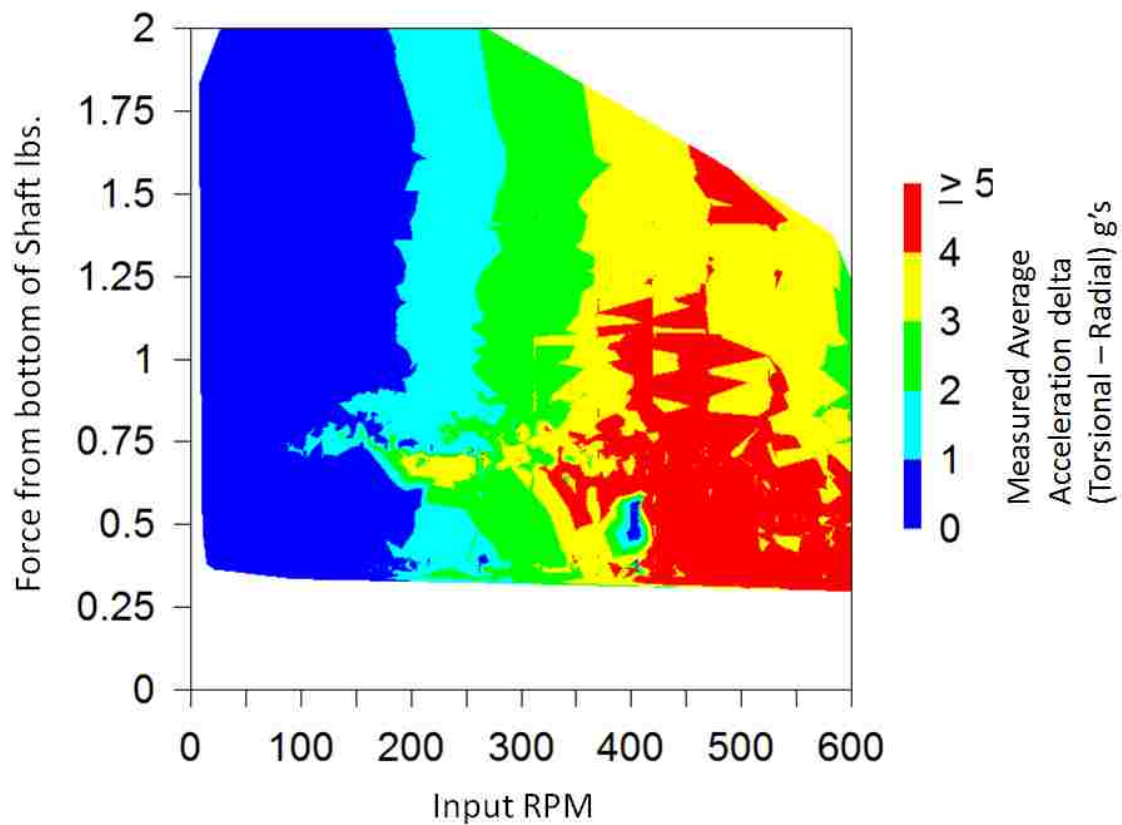


Figure 40. Shaft C vibration separation response surface. Parameter map response for the difference of the two in plane acceleration measures the torsional and radial measures for shaft C. In shaft C the vibration separation past 350 RPM takes off past 4 g's.

Figure 42 shows the bound for the stick-slip index values for shaft A. The index is assigned one point for having a sample less than 10 RPMs slower than the input, and 2 points for having a minimum measured average less than half the input speed. Three points for both conditions. A green peak or plateau has one point, a yellow peak or plateau has two points. Red regions are experiencing both conditions, near

zero rotation speed and a minimum of one half rotation speed. Shaft A is experiencing qualifying stick-slip conditions regularly below 100 RPM independent of axial load and above 1.5 lbs. independent of RPM. The values around 600 RPM that are manifesting in all of the tests may be an artifact of the control scheme of the drive system.

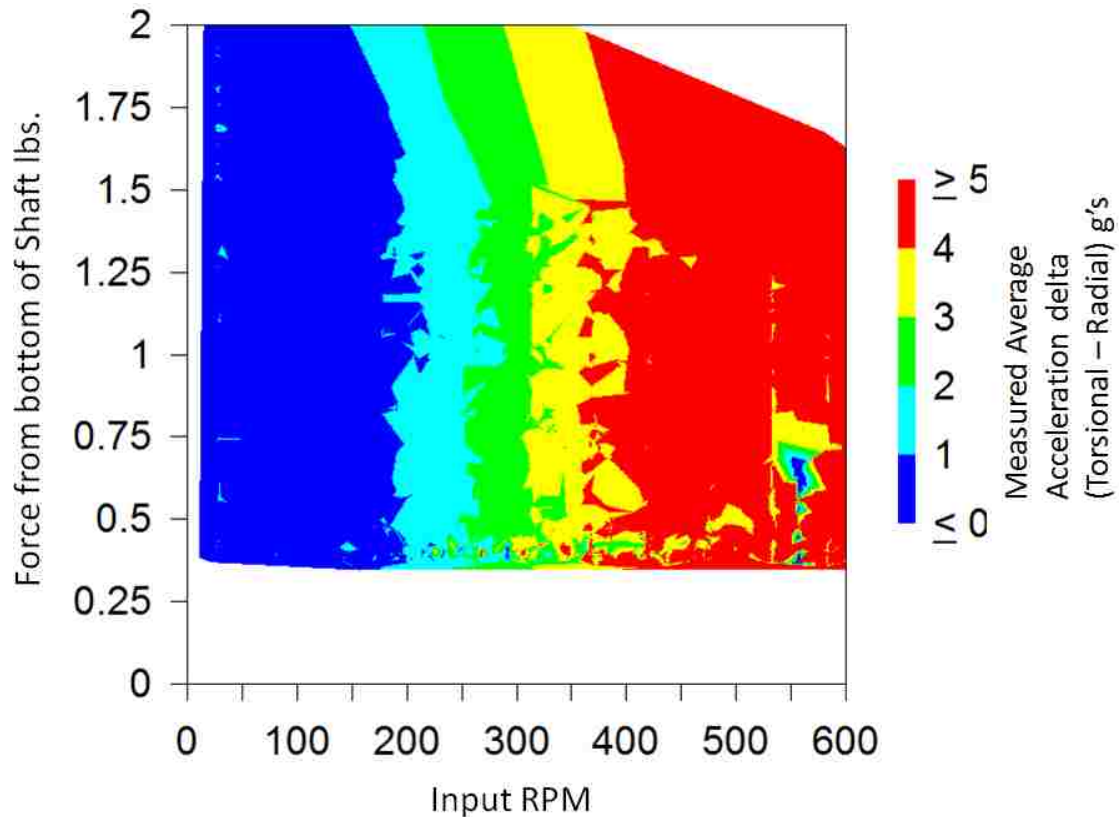


Figure 41. Shaft D vibration separation response surface. Parameter map response for the difference of the two in plane acceleration measures the torsional and radial measures for shaft D. Shaft D is the most pronounced increase, mostly due to having the smallest values for radial acceleration.

Figure 43 shows the bound for the stick-slip index values for shaft B. Shaft B was mostly free of qualifying values above 120 PRM.

Figure 44 shows the bound for the stick-slip index values for shaft C. Shaft C is moderately free of qualifying responses with the exception of “bands” of vibration that cross through the parameter space. The band manifestation will be addressed further in the discussion section.

Figure 45 shows the bound for the stick-slip index values for shaft D. Shaft D has qualifying responses below 150 RPM. It also has a band around 0.4 lbs. and another region around 250 RPM and 1 lb.

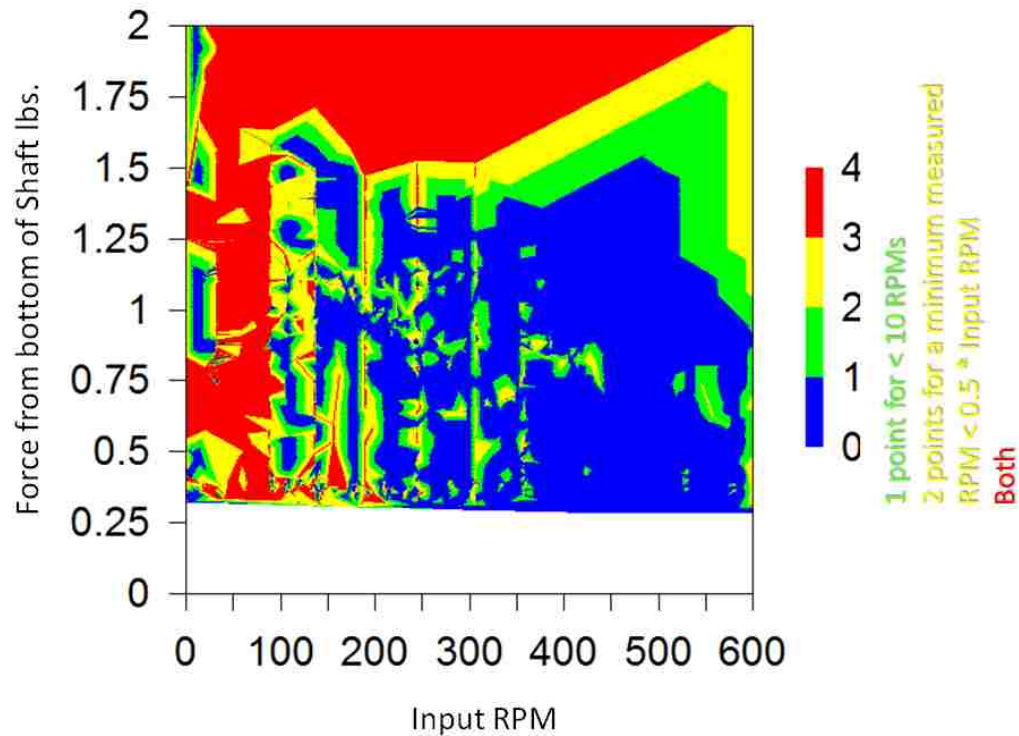


Figure 42. Shaft A stick-slip index response surface. Parameter map response for proceed values from gyroscope and fixture speed differences for Shaft A. Stick-slip index values manifest in places below 400 RPM regularly, the region above the axial load ~ 1.7 lbs. qualifies for stick-slip nearly throughout.

The test battery shows the similarities and distinction of each configuration. Figure 46 shows a summary of the previous surface response figures.

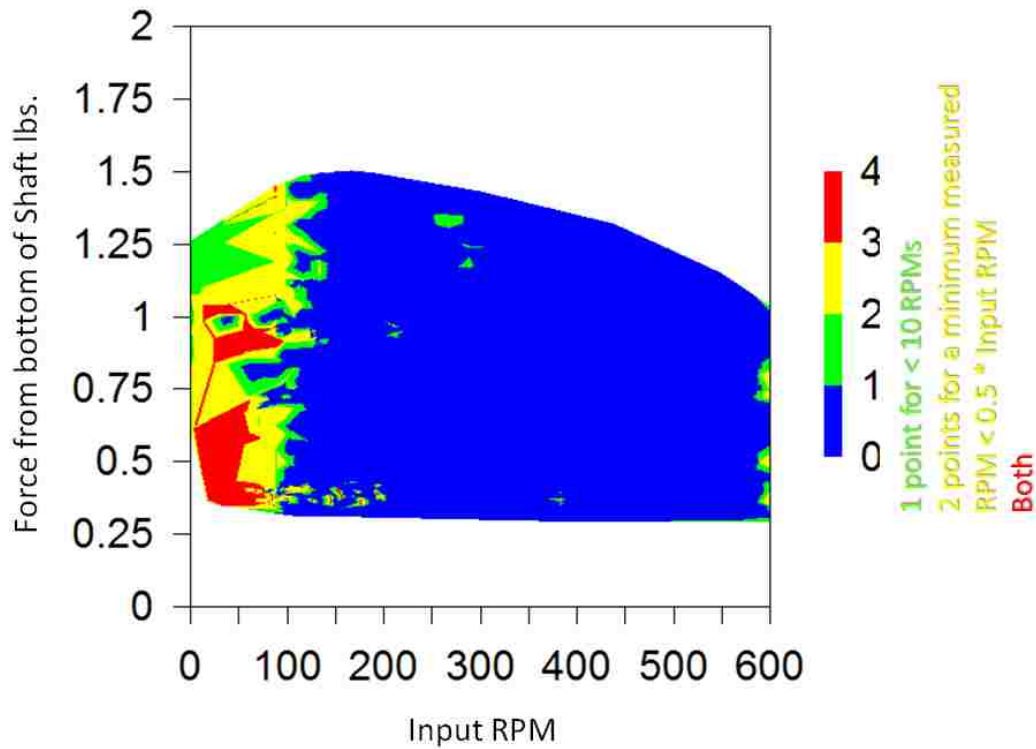


Figure 43. Shaft B stick-slip index response surface. Parameter map response for proceed values from gyroscope and fixture speed differences for Shaft B. The higher loads were not achieved on shaft B so it is hard to say what would happen above the calculated buckling values. The region qualifies for stick slip around 50 RPM and 0.3 - 1.1 lbs.

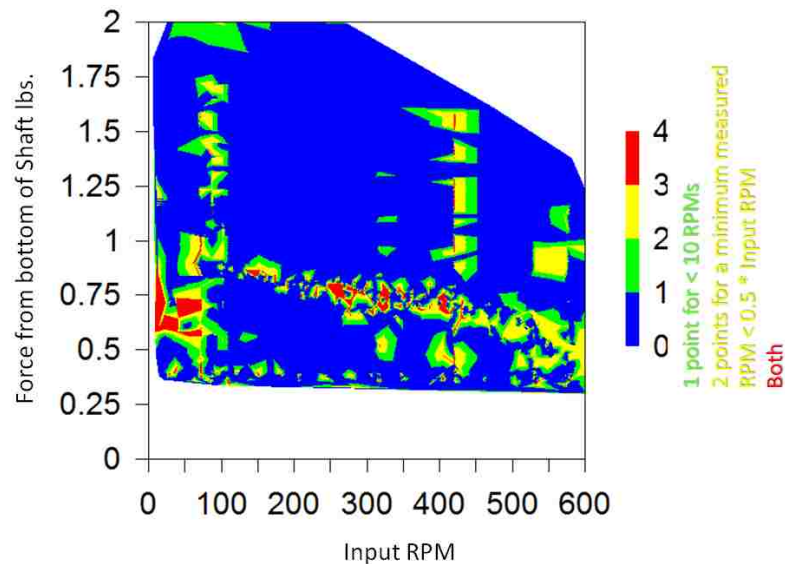


Figure 44. Shaft C stick-slip index response surface. Parameter map response for proceed values from gyroscope and fixture speed differences for shaft C. Shaft C manifests a stripe qualifying as stick-slip around 0.7 lbs. and around 80 and 425 RPM. This response is very different than the previous examples.

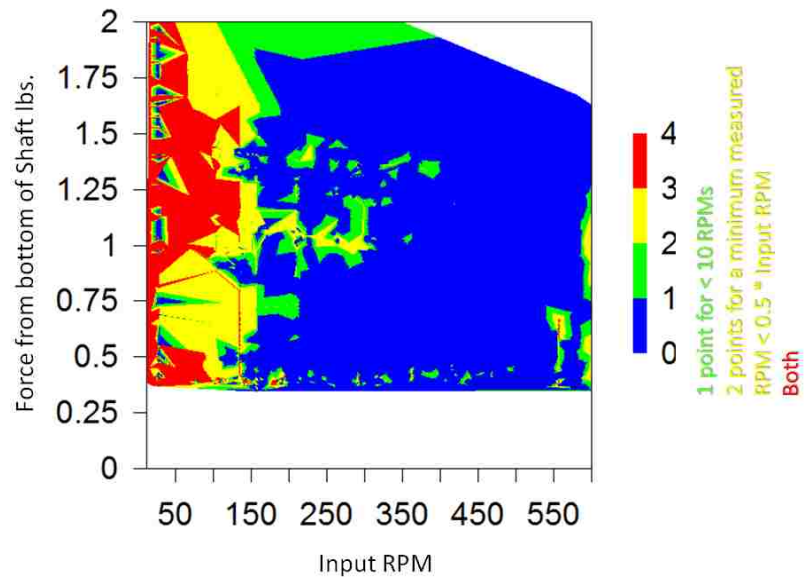


Figure 45. Shaft D stick-slip index response surface. Parameter map response for proceed values from gyroscope and fixture speed differences for shaft D. Stick-slip was mostly on the left side and upper left in this plot. Some sliver of far right behaviors also existed.

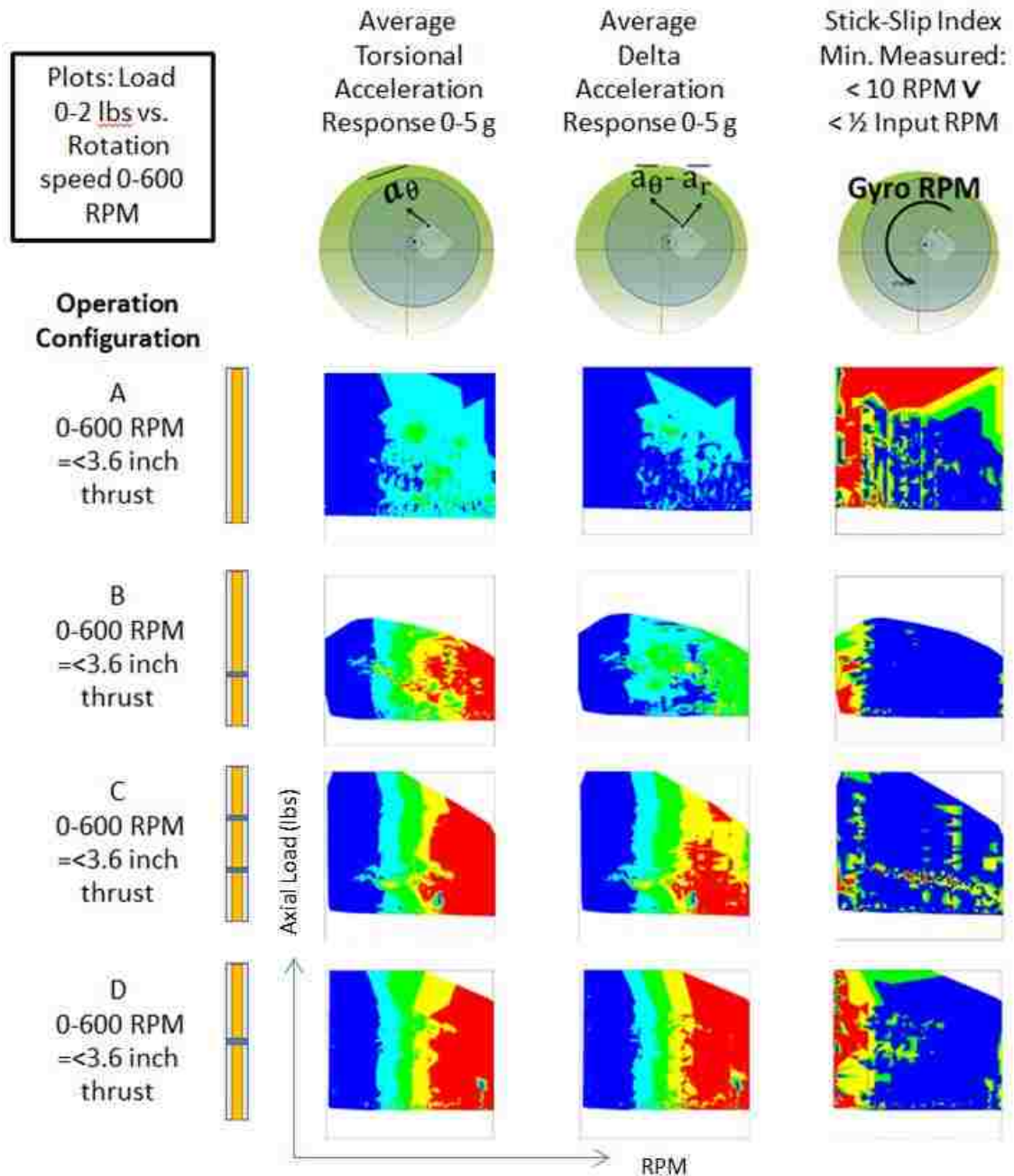


Figure 46. Summary image showing the average torsional acceleration, the average delta acceleration, and the stick slip index as calculated by gyro measurements. Plotted in the rotation speed axial load space. Note here the different results for the different geometries. Shafts B and C have a different response at high RPM and moderate loads. Shaft A has a region of high stick-slip index along the high load range, dissipating some at higher RPMs.

4.5 Results from the Numerical Experiments

4.5.1 Numerical Simulation of Buckling

A detailed treatment of the buckling calculations is presented in Appendix IV. Table 3 presents the results of established formulas and the numerical simulation results from Ansys(TM).

Table 3. Buckling Results for Euler, Wu and Numerical Simulation.

Method	Value	Units
Euler Buckling pin /pin	6.848	Pounds force
Euler Buckling fixed / free	1.712	Pounds force
Wu	1.717	Pounds force
Ansys(TM) (linear buckle pin /pin)	6.732	Pounds force
Ansys(TM) (linear buckle fixed /free)	1.696	Pounds force

It is notable that Euler fixed/free solution is less than 0.3% different to the Wu (1993) solution. Figure 47 and Figure 48 show the graphical version of the numerical buckling results. It is interesting to note the insights from this type of visualization is that buckled members here “buckle” first or deform the most at the unsupported points.

4.5.2 Numerical Simulation of Vibration Mode

The values calculated for buckling behaviors are 99% the same between the numerical simulation and the simple calculation. The recorded values from the experiments are within the range of the calculated values also. The modeled results have been shown to have R-squared values greater than 0.9, so this would seem to be an acceptable match. The modal simulation does not produce a direct analog to the acceleration values measured. Instead, the modal analysis simply predicts regions of special behaviors. In the unstable critical speed regions one would expect impacts and elevated vibration values, in the stable critical speed regions one could possibly expect lower or higher values and fewer impacts.

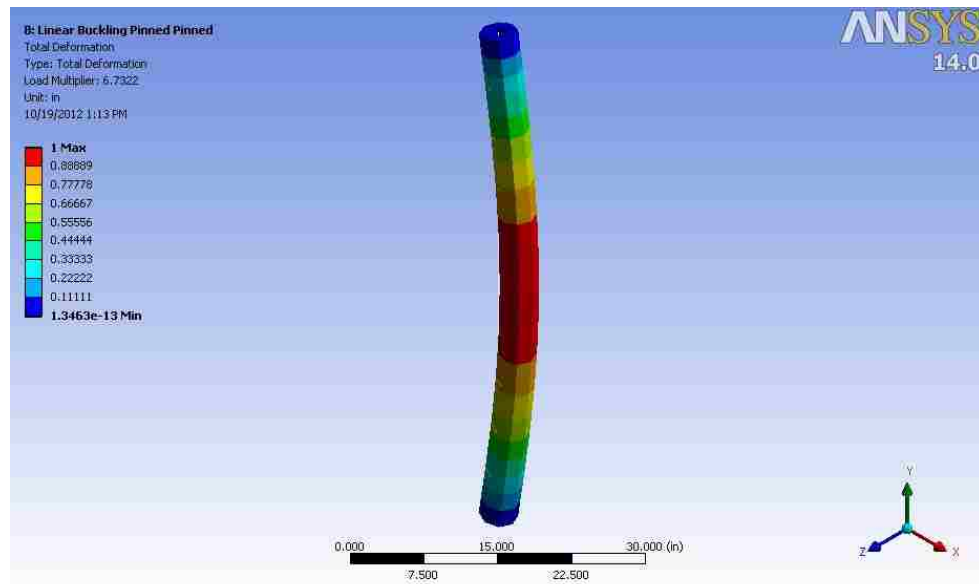


Figure 47. A screen capture of the graphical representation of the buckling simulation. It is worth noting the red that is of value one on the scale is multiplied by the load multiplier 6.7322 lbsf. The boundary conditions here are both ends pinned. One might also not that the column is only “buckled” in the center.

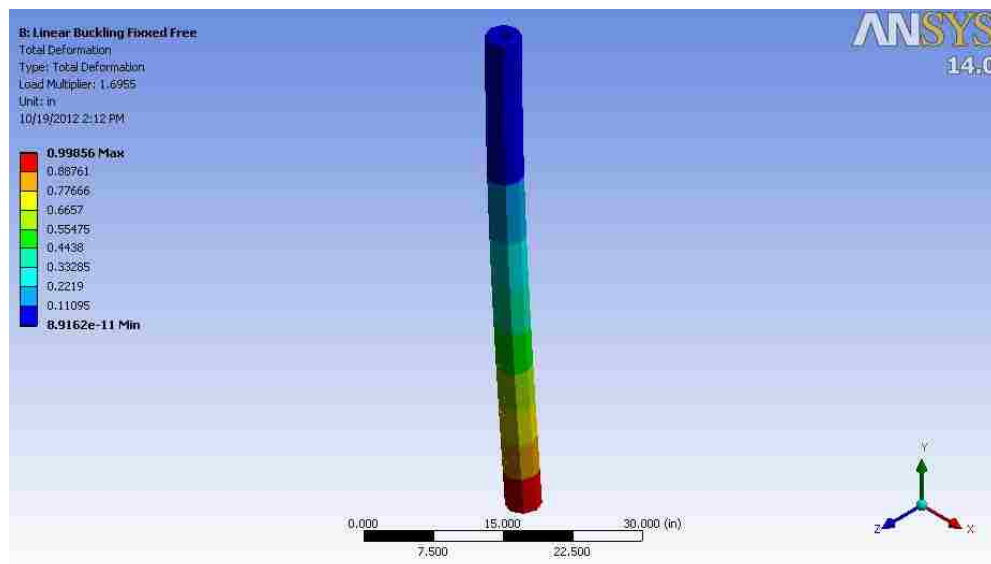


Figure 48. A screen capture of the graphical representation of the buckling simulation. It is worth noting the red that is of value one on the scale is multiplied by the load multiplier 1.6955 lbsf. The boundary conditions here is that the one end is free the other fixed. One might also not that the column is only “buckled” at the bottom.

The shaft A configuration is predicted to have both backward and forward whirl results, however none are expected to have stability based on numerical model modal results. (Figure 49)

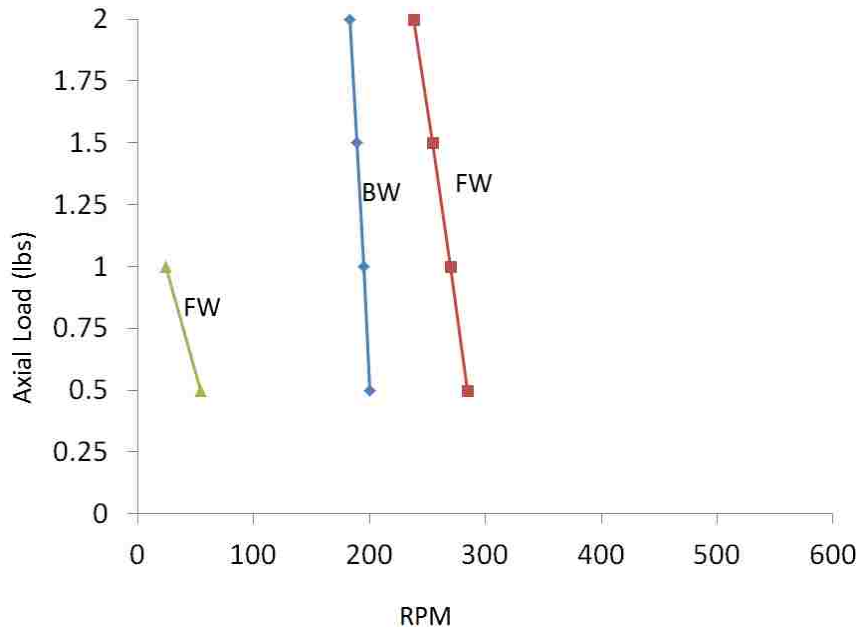


Figure 49. Shaft A modal results. The aggregated prestress modal results for the shaft A assembly. The analysis predicted three unstable whirl phenomena in the parameter space examined.

The Shaft B simulation had unique results for the set, critical speed trends changed from forward to backward whirl predictions and both forward and backward whirl regions found stability. Also the stable regions were not linearly connected. (Figure 50)

The Shaft C results only predicted backward whirling. This whirling was stable at the 300 RPM and half pound load point. (Figure 51)

The Shaft D results predicted stability at the higher load ends of both whirl lines. (Figure 52)

The modal results share a critical speed solution around 1 to one half pound load for around 25 to 50 RPM. For shaft A this region was predicted to be in forward whirl, for assemblies C and D backward. Assembly B's response is unique in that this region transitioned. Shafts A, B and C also share a region around 250 to 300 RPM across the range. It might be noted that the slope of the loaded critical speed lines are not parallel. Figure 53 shows overlaid the results of the numerical models for the four shaft systems.

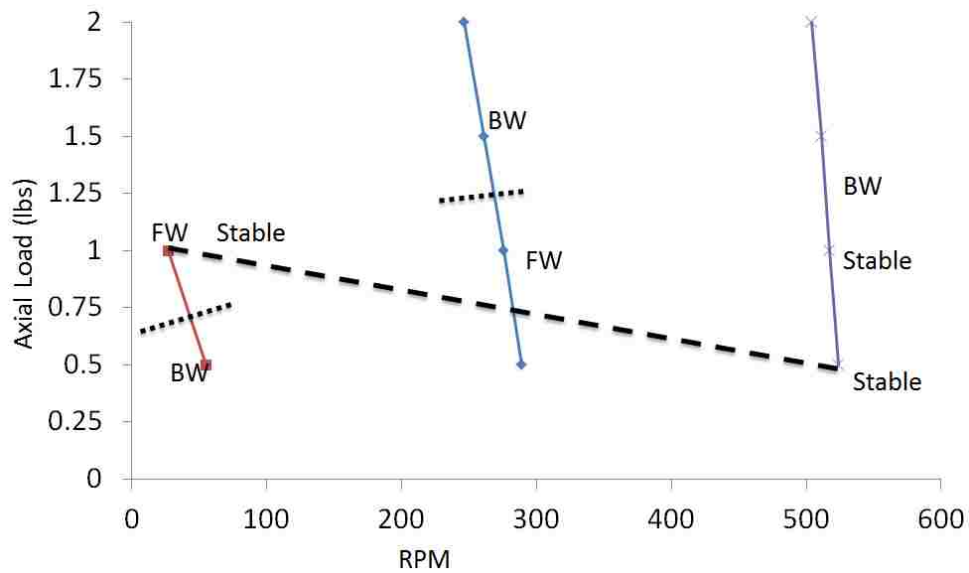


Figure 50. Shaft B modal results. The aggregated prestress modal results for the shaft B assembly. The analysis predicted three trends of critical speeds, the lower speed range one and the upper most speed range had stable regions. Also, the results predicted that two of the regions would transition from forward to backward depending on the loading conditions. A dashed line connects the stable regions. A dotted like separated Backward and forward whirl on a trend line.

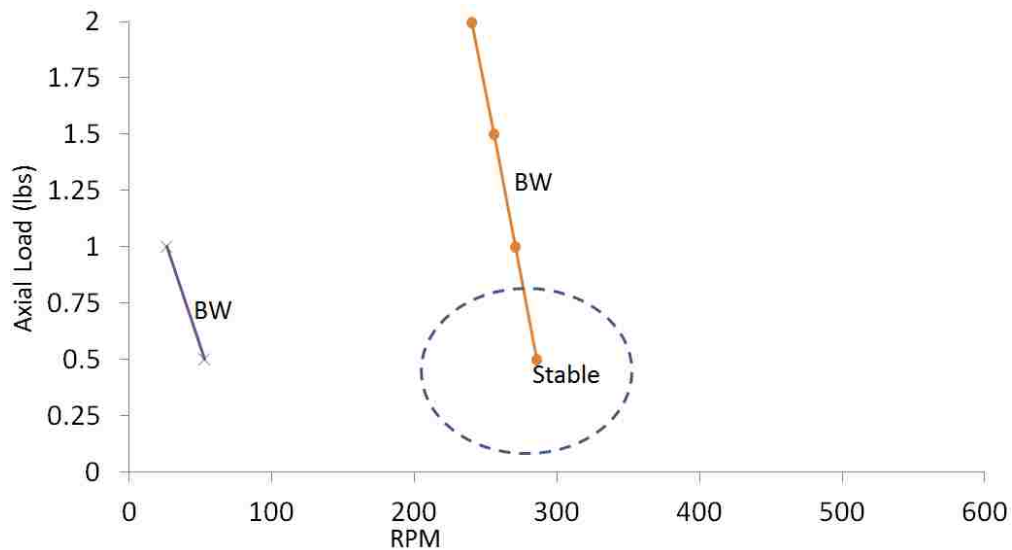


Figure 51. Shaft C modal results. The aggregated prestress modal results for the shaft C assembly. Two backward whirl trends are predicted with a stable region in the lower load range for the trend around 300 RPM. A dashed line circle is placed around the observed stable point.

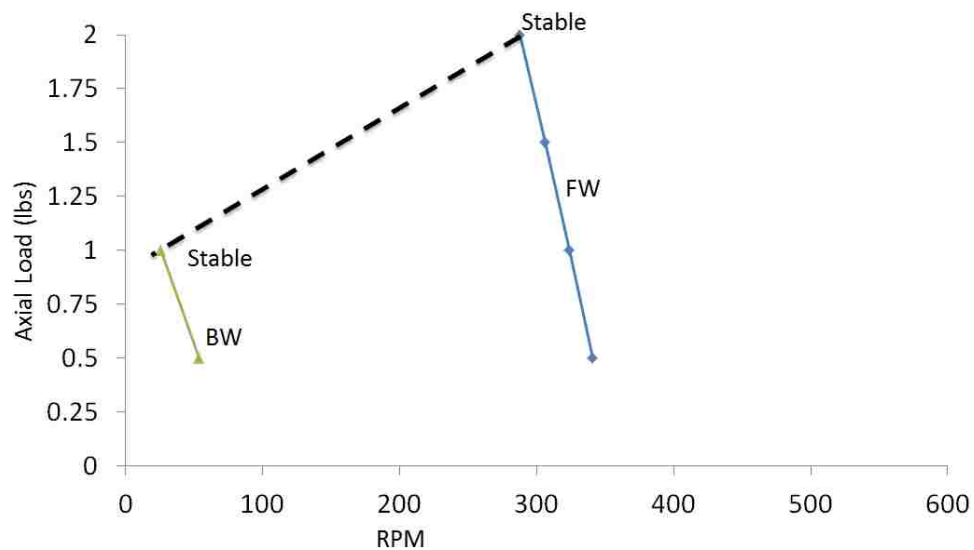


Figure 52. Shaft D modal results. The aggregated prestress modal results for the shaft D assembly. Two whirl trends predicted, both with stable regions in the higher axial load portion of the trend. A dashed line connects the stable regions.

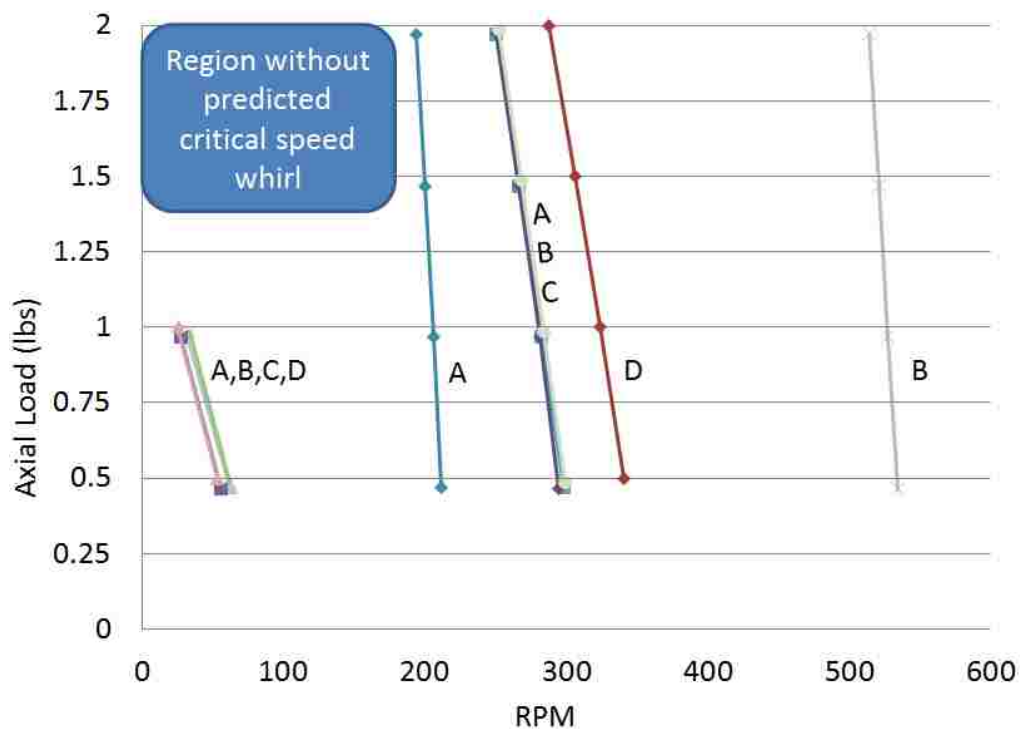


Figure 53. Modal results overlay for shafts A, B, C, D. Simulated critical speed results for all four shaft together. A slight offset was allowed to show the overlapping points better.

CHAPTER 5.DISCUSSIONS

5.1 Prestress Modal Simulation and Experimental Results on the Response Surface

This section The modal simulation results allow the opportunity to compare the method to what happened in the lab. Examination may reveal if acceleration values crossing the unit thresholds can be related.

In shaft A the threshold around 1 g is mostly between the second and third critical speed lines. (Figure 54) It could also be observed that the local minima for the axial load limit line is along the second critical speed lines path. Vibration above one g follows the threshold defined by the second and third critical speed lines.

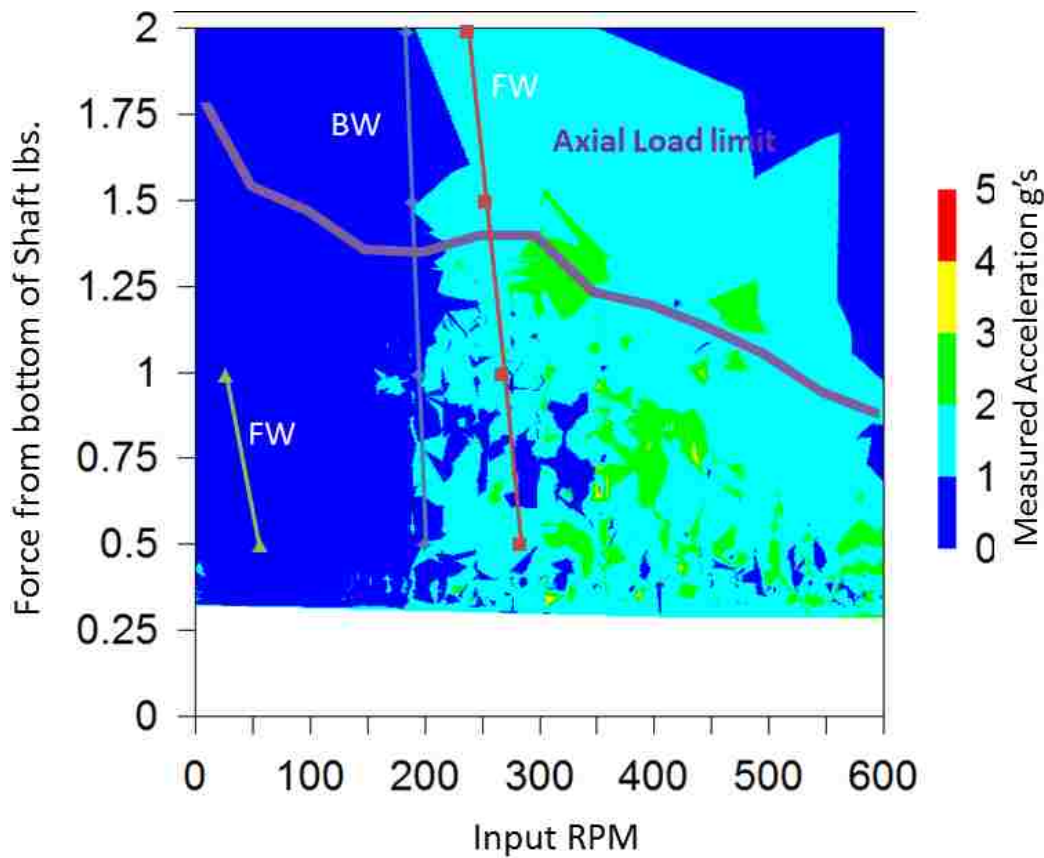


Figure 54. Shaft A torsional vibration response surface with modal simulation results. Simulated critical speed results imposed on the torsional acceleration measurements for shaft A. Notice the critical speed line around 200 RPM crosses the axial load line at a local minima.

Shaft B may also be compared to the critical speed results. (Figure 55) First the stable regions on the critical speed line near 525 RPM are in a region of the highest torsional vibration results. The transition

between backward and forward is near the axial load limit threshold for the critical speed region around 300 RPM. The stable regions connection line trends with an elevated vibration level from the first and third critical speed lines. This might be noteworthy as typically one might expect lower levels of vibration in a “stable” condition.

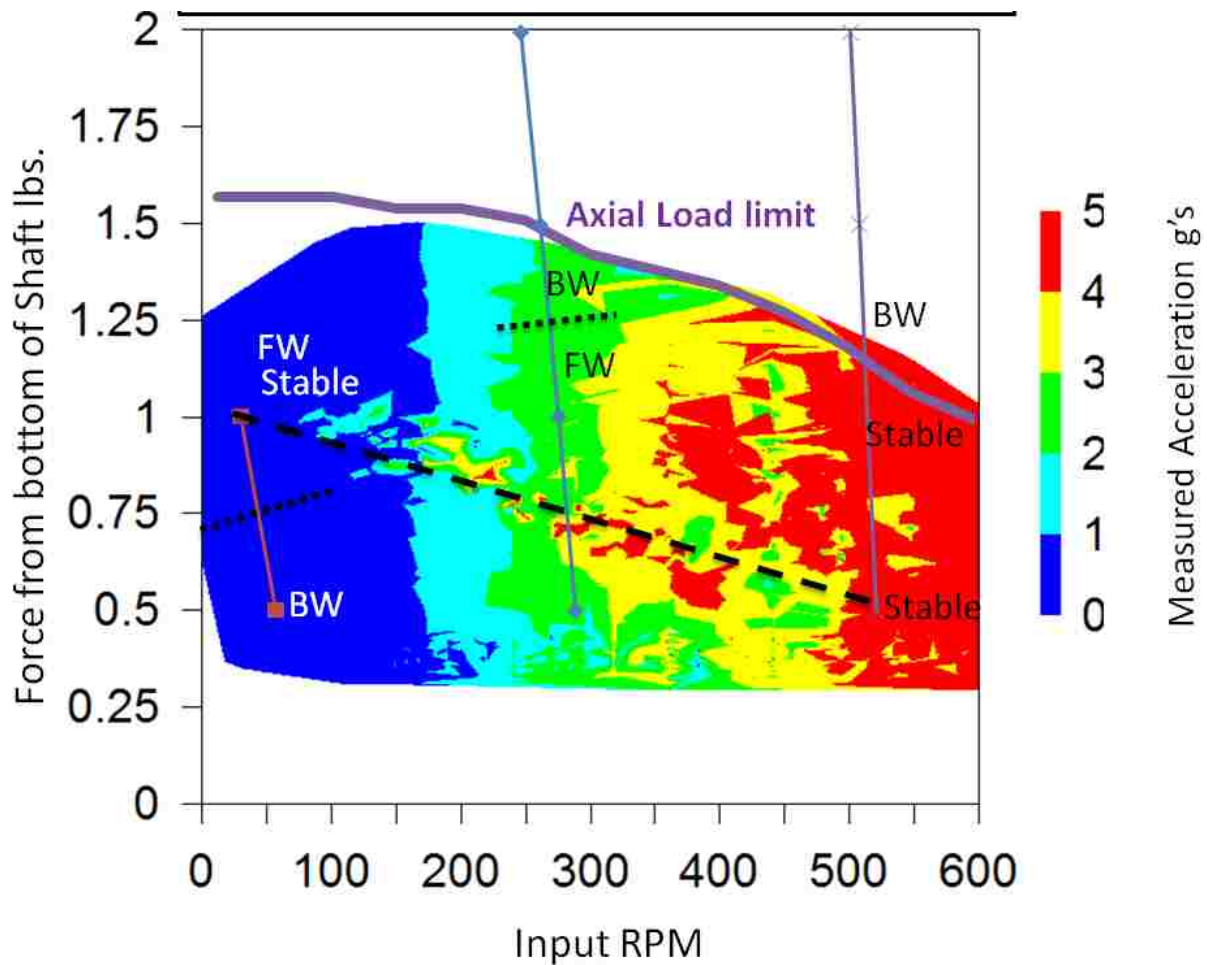


Figure 55. Shaft B torsional vibration response surface with modal simulation results. Simulated critical speed results imposed on the torsional acceleration measurements for shaft B.

Shaft C again exhibits a local minima of the axial load line limit line near a backward critical speed line. (Figure 56) Again greater vibration levels are in a “stable” region. The unusually low vibration area around half a pound and 410 RPM is more than 100 RPM from that stable point on the critical speed plot.

Shaft D has a faint trend around 25 RPM that may correlate to the stable backward whirl prediction. (Figure 57) Again an elevated vibration level near a stable prediction. Shaft D also presents the only stable

region above the plotted axial load limit and the connection between the two stable regions does not correlate to anything the acceleration shading would indicate.

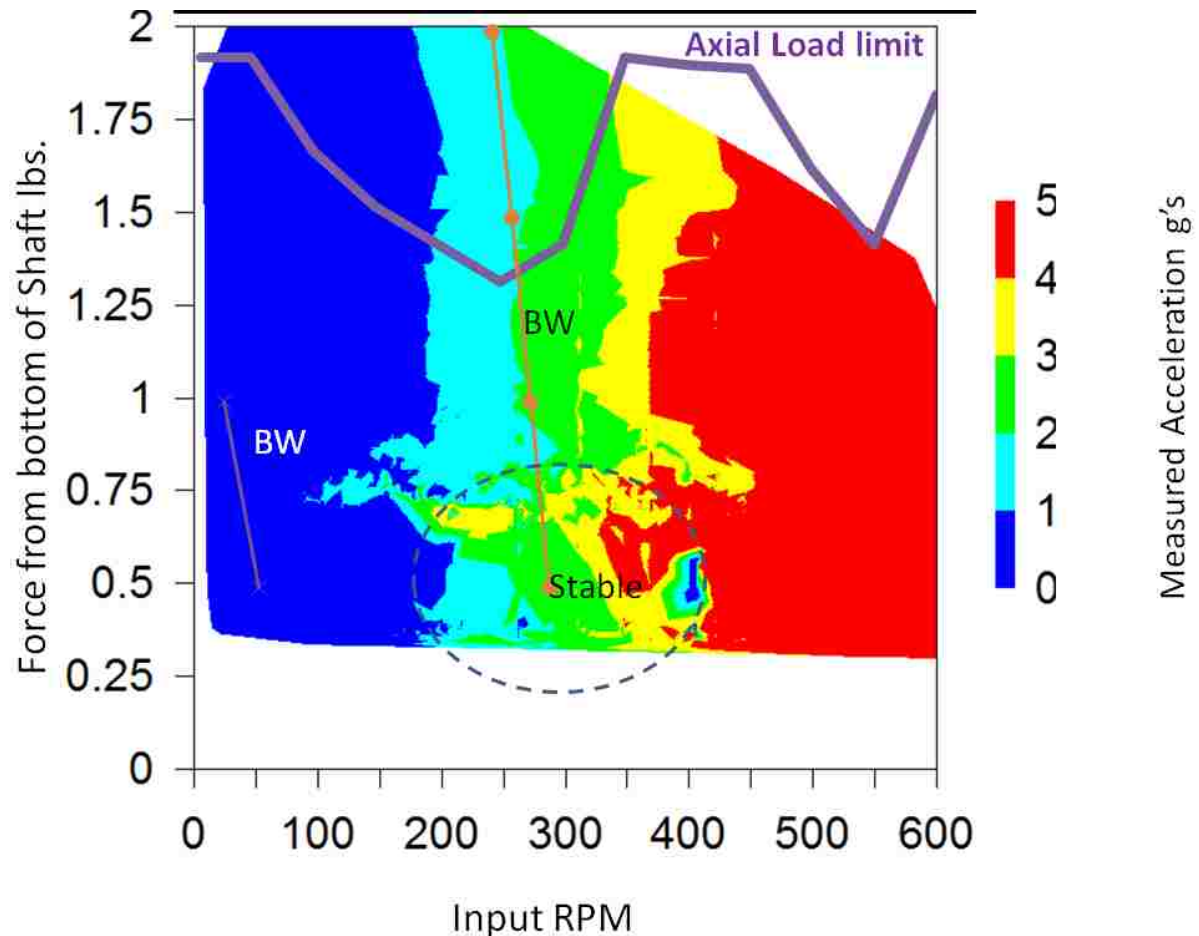


Figure 56. Shaft C torsional vibration response surface with modal simulation results. Simulated critical speed results imposed on the torsional acceleration measurements for shaft C. Notice the critical speed line around 300 RPM crosses the axial load line at a local minima.

Looking at the Modal plots revealed a few trends, one of which was the load limit lines that had local minima, assemblies B and C had a critical speed line for backward whirl through them. The prediction of stability from the analysis correlated with increased vibration levels about one g. The comparison with the stick slip index values was not noteworthy and the plots are not presented here although one can exam the plots presented here. The Modal method predicted whirling all over the parameter range, reinforcing the idea that whirl is present all very often. However, a second look reveals that that at the 1.5 and 2 pound

loading no whirl was predicted until at least 160 RPM. Still the trend with the local minima is related to buckling, and it was recognized from the buckling simulation was that the method matched the non-rotating results well.

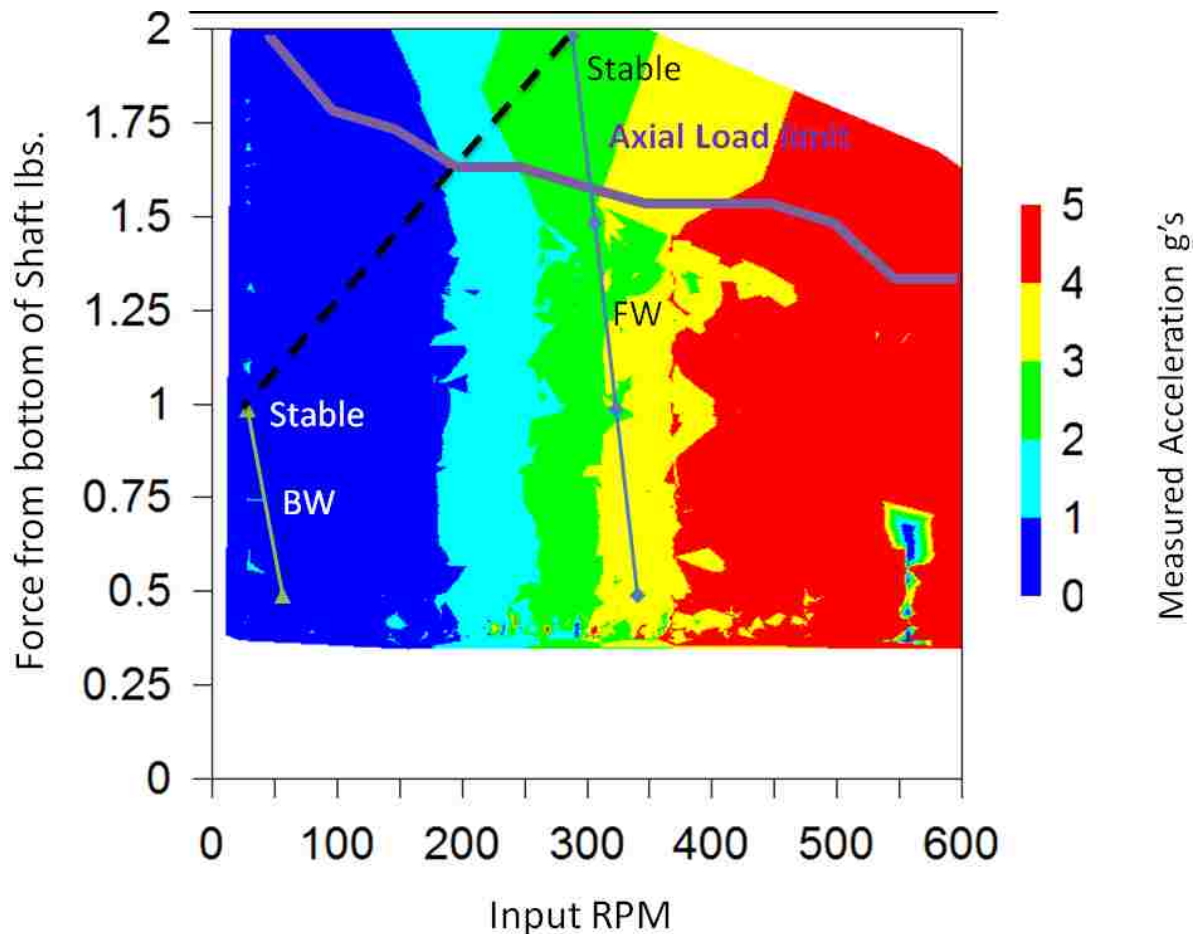


Figure 57. Shaft D torsional vibration response surface with modal simulation results. Simulated critical speed results imposed on the torsional acceleration measurements for shaft D.

In the results section an examination of the lower boundary condition was made. One major discrepancy noticed for the dimensionless stick-slip plot was that the lower bound of the force range was relatively stable at ~0.10 lbs lower, this is the same as the weight of the 1 by 4 inch pin. (Figure 58) The region of elevated values around 30-130 RPM and 0.4 lbs present in the pinned boundary and not the free

boundary suggests for this load a greater side force was present. Possibly this is due to the lack of distance for displacement of the shaft.

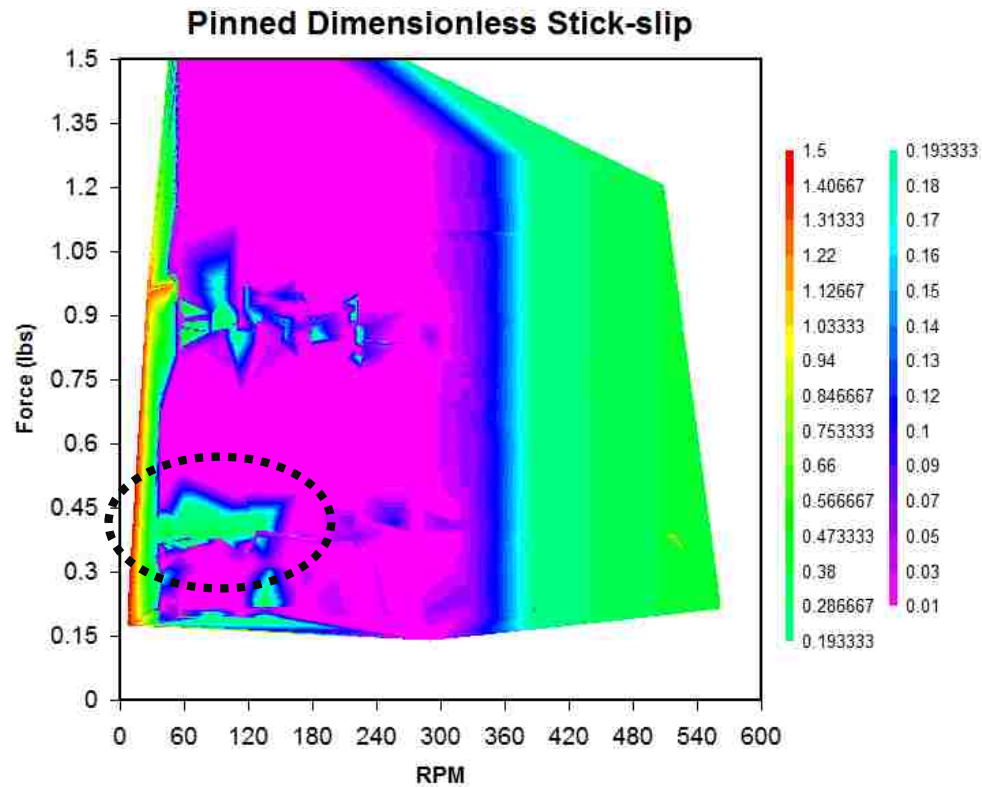




Figure 58. Pinned dimensionless slick-slip screening test. The region around 0.4 lbs load and 90 RPM is circled, this region was not present in the free endpoint condition. In this case it is possible that the increased side load due having no displacement at the bottom increased this measure.

5.2 Discussion of Mitigation Method

The question around the application of the “Anadrill Method” warrants some discussion. (Burgess and Martin 1995) First let’s revisit Table 4 and look at the potential fixes.

Table 4. Vibration Mitigation Table for Stick-slip and Ehrl- edited. (Burgess and Martin 1995)

Vibration	Potential Cure	Directions of travel on RPM vs Load Plot
Stick-Slip	STOP – reduce WOB and increase RPM	
BHA whirl	STOP - reduce RPM and increase WOB	

The question now is if one followed the cures suggest could it be effective to arrive in a lower severity region of operating parameters. Looking at Figure 59 and Figure 60 the answer is simply “Yes”, although some additional insight to the application is gleaned too. From the starting position one (1) for stick-slip perhaps only reducing axial load (WOB) is necessary, however from starting position two (2) perhaps only increasing RPM is necessary. So how would a practitioner know what potential steps to take, so do both. Also, some pragmatism is built into the combination of doing both, as perhaps a reduction of rate of penetration could be avoided by the other parameter compensating for loss of energy. The suggestion that the boundaries are more often diagonal as suggested by Dunayevsky’s (1998) work was not observed.

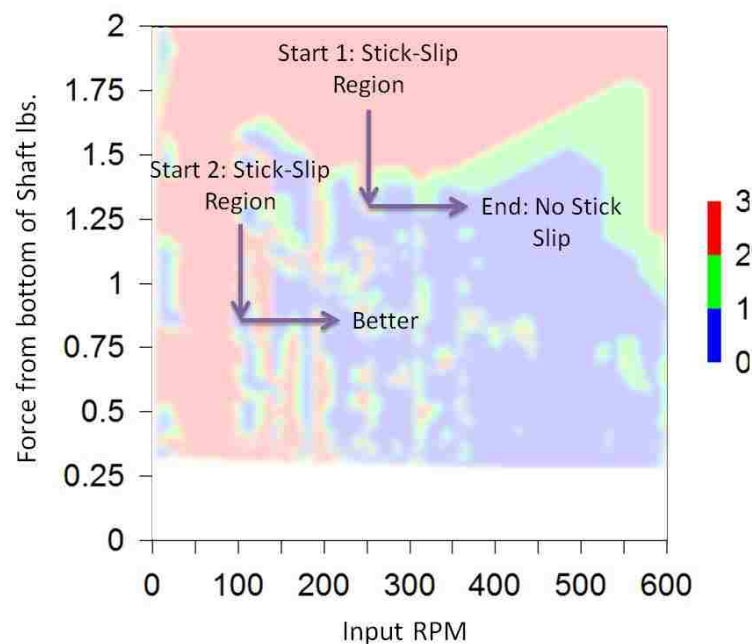


Figure 59. Stick-slip index response surface with Stick-slip mitigation. Work through stick-slip mitigation on shaft a response surface.

The next question addressed is the mapping of region boundaries using a shaft system analog to the BHA. This means no bit effects and no drill string effects are being accounted for directly by the model. Yes regions could be mapped, however with other effects; the effects of the drive system were still present

and can be noted in the difference between the preliminary system and the test fixture used for the final test battery. Placement of stabilizers had effects as can be seen in Figure 46.

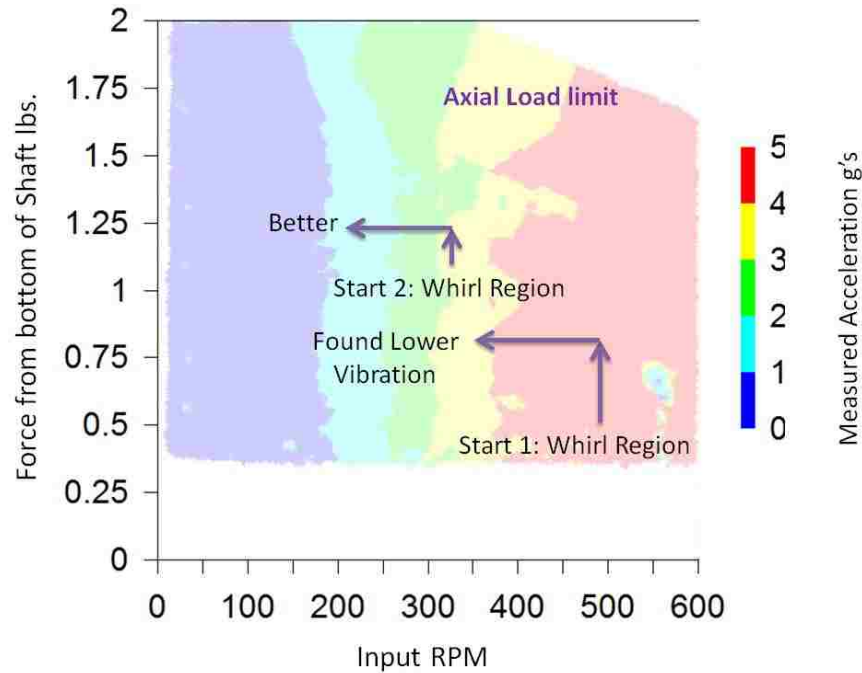


Figure 60. Shaft D torsional vibration surface with whirl response mitigation. Work through whirl mitigation on shaft a response surface.

The simulation results provided some unique insights. The buckling simulation aligned well, however so did the simpler calculations. Critical speed lines established a theoretical region without whirl, the region aligns notionally with industry methods. (Figure 61) Critical speeds nor stable whirling regions predicted by rotor dynamics modal analysis could be correlated with directly vibration intensity most notable for “stable” critical speed regions. Also, the critical speed region prediction did align with the experimentally observed local minima of the axial load limits. The critical speed threshold was seen to be the vibration severity threshold as exemplified by shaft A.

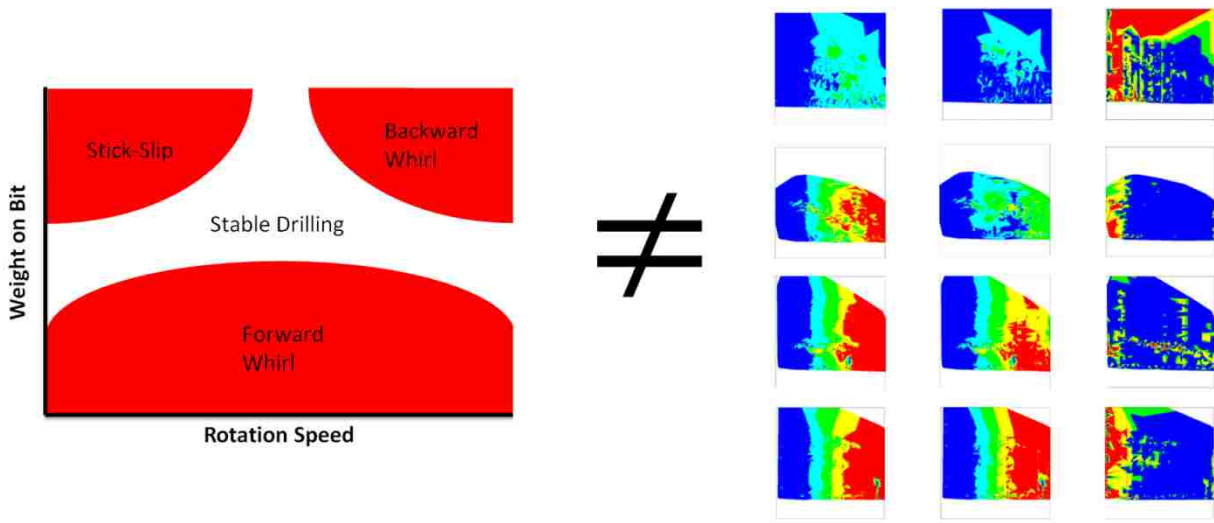
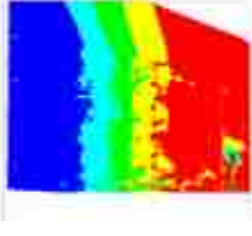
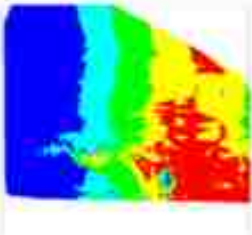
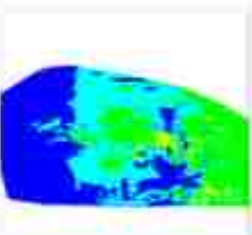
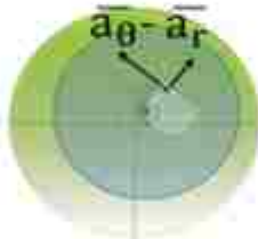


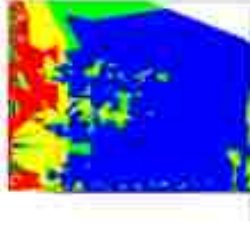
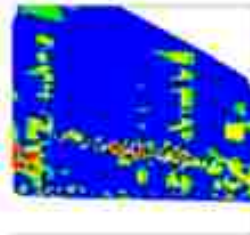
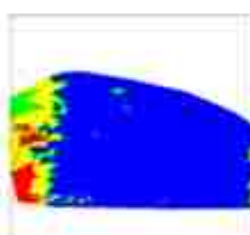
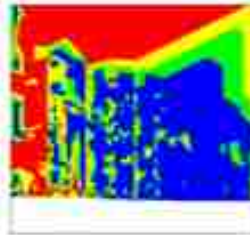
Figure 61. The image suggested by the Anadrill method is clearly not that of any part of response surfaces.

This interpretation method is based on the idea that the lateral components of the measured vibration should cancel out when subtracted leaving only the elevated response from angular acceleration. This interpretation should be revisited as based on the results in this experiment it is not a good indicator for variation in rotation speed.

Average
Delta
Acceleration
Response 0-5 g



Stick-Slip Index
Min. Measured:
< 10 RPM $\sqrt{}$
< ½ Input RPM



\neq

Figure 62. Comparison of the “Sperry-Sun” method to the stick-slip index.

CHAPTER 6.CONCLUSIONS

In this study the flexible shaft system has been observed to achieve the behaviors of stick-slip and whirl without the use of an analog for a drill string or bit. It is not the suggestion that other components be ignored in practice, but that the behaviors and phenomena of BHA vibration have been shown to fit into the industry's de facto standard method of mitigation. This presentation of the rotating flexible shaft system is so far unique, and presents a usable set of examples for discussion on stick-slip and whirl.

6.1 Evaluating Hypotheses

- 1) A flexible shaft system without a drill bit will not experience stick slip or whirl.

This is shown false repeatedly. First in the time based standalone, time based results. As shown in the video stills, and finally by the parameter map plots. Also the numerical modeling supports who and how this is possible.

- 2) Flexible shaft systems of varying stabilization geometries will produce the same levels and types of vibrations over a range of conditions.

This proven false. The responses recorded and the numerical model results clearly show that the stabilization geometry creates variation in level and types of vibration.

- 3) Vibration levels in a flexible shaft are a function of rotation speed and axial load, and manifest regionally as suggested by the Anadrill Methods materials that support the continued successful use of the method.

Yes and no. When the rules were applied to the response surfaces the expected reduction in vibration level was eventually reached. However the imagery that had developed along with the model was not observed in the lab or with numerical simulation. This could be perhaps due to the lack of a bit effect in either model.

- 4) Does the flexible shaft system only experience Stick-Slip above a buckling limit.

No stick-slip was observed in all models in the low rotation speed region. However in the case of the slick assembly a large region of stick slip did occur when the system was operated past is axial load limit. It has not been previously discussed but many BHA are perhaps designed so

that at the upper end of the operating WOB range a non-stabilized section of the BHA is making a tangency point with the borehole wall and achieving this stick-slip.

6.2 Mitigation Method Findings

The Anadrill mitigation method was seen to be good go-by if one were to apply it to the behaviors and response of the flexible shaft systems in the test fixture. Navigating the response surface parameter map with Anadrill's rules results in decreasing the magnitude of the measured symptoms of the dysfunction. (as seen in section in 5.2)

6.3 Measurement and Diagnoses

Another significant finding of this study is that two accelerometer based methods to measure and diagnose stick-slip could be improved on. (Figure 46) The current method as employed with the test fixture simply did not match the results of direct measurement from the gyroscope package. It is entirely possible the uptake of that method depends on elevated vibration being absent during stick-slip driven dysfunction. (Dunayevsky 1998) This is important when one considers the next conclusion...

6.4 Effects of BHA Geometry

Qualifying stick-slip and vibration recognized as whirl observed in the flexible shaft system where not mutually exclusive, although the manifestation of one could influence the magnitude of the other. (Wu 2010) Down hole dynamic conditions need to be mitigated to promote improved performance, however in this study, the flexible shaft system typically transitioned from manifesting one dysfunction to the other, (Figure 21) and as seen in Figure 46. This begs the question, when reduced to the lowest magnitudes possible, what type of remaining dysfunction is preferred. Unfortunately, the experiments with the flexible shaft system did not address this question.

The slick shaft (shaft geometry A) was the only of the four geometries that exhibited stick slip at an axial load threshold consistently. (Figure 48) This threshold was above the calculated sinusoidal buckling and measured average axial load limits. This suggests that proper stabilizer placement can effect buckling related stick-slip conditions. One should remember that possibly in any drilling BHA the top of the

assembly is not stabilized as it is not common practice to place stabilizers in this region. This gives the BHA designer another reason to check weight on bit expectations for the job. This geometry also was the only one that did not experience its highest levels of vibration at the highest range of rotation speed.

Shaft D exhibited a unique reduced vibration area at high rotation speed in the lower axial force range. This zone or sweet spot was achieved in multiple tests. (Figure 46) This gives credit to the belief that a properly designed BHA can be relatively calm vibration wise even at rotation speeds as high as 550 RPM. No suggestion of how to achieve this design is made.

In this study the shaft geometries with stabilization exhibited measured torsional vibration that increased directly to rotation speed. (Section 4.4.5)

CHAPTER 7. FUTURE DIRECTIONS

Again, this study demonstrated that the simple system of the rotating flexible shaft could produce both whirl and stick-slip behavior. (sections 4.1 and 4.2) This should give renewed hope to would-be numerical modelers, however the simulation approach used in this study did not compare the predicted amplitudes of vibration. This would be a worthwhile follow up work. The preliminary tests demonstrated the effects and coupling with the drive that could result in stick-slip events with a 6 to 9 second period including a period of effective backward rotation. (section 4.14.2) Changing the drive system did not eliminate qualified stick-slip behaviors, however it did reduce the period of such behaviors to one or two seconds, where the drive was still turning and the stall was in the shaft itself. This finding reinforces the importance of factors outside the dynamics of the shaft alone. Future modelers should seek to incorporate drive controllers that can mimic a range of responses reflective of the various drives used in industry and drill bit effects to better approach the boundary conditions experienced by a drilling system.

BIBLIOGRAPHY

- A. Lubinski, W. S. A., J.L. Logan (1961). Helical Buckling of Tubing Sealed in Packers. 36th Annual Fall Meeting of SPE, Dallas.
- Ashley, D. K., X. M. McNary, et al. (2001). Extending BHA Life with Multi-Axis Vibration Measurements. SPE/IADC Drilling Conference. Amsterdam, Netherlands, Copyright 2001, SPE/IADC Drilling Conference.
- Brandel, B. a. L., R. S. (2001). "Negative Poisson's ratio polyethylene foams." Journal of Materials Science 36: 5885-5893.
- Brett, J. F. (1992). "The Genesis of Torsional Drillstring Vibrations." SPE Drilling Engineering(09).
- Burgess, T. M. and C. A. Martin (1995). Wellsite Action on Drilling Mechanics Information Improves Economics. SPE/IADC Drilling Conference. Amsterdam, Netherlands, 1995 Copyright 1995, SPE/IADC Drilling Conference.
- Chen, C.-K. D. (1999). Detecting and reducing bit whirl. U. S. P. Office, Baroid Technology, Inc.
- Croucher, M. (2012). "De Moivre's Theorem for Trig Identities." Retrieved March 20, 2012, from <http://demonstrations.wolfram.com/DeMoivresTheoremForTrigIdentities/>.
- Dawson R., P. P. R. (1984). "Drillpipe Buckling in Inclined Holes." Journal of Petroleum Technology(October).
- de S.M. Costa, F. and P. R. Ribeiro (1997). Finite Element Modeling of the Mechanical Behavior of Unbalanced Drillcollars. Latin American and Caribbean Petroleum Engineering Conference. Rio de Janeiro, Brazil, 1997 Copyright 1997, Society of Petroleum Engineers, Inc.
- Deily, F. H., Dareing, D. W., Paff, G. H., Ortloff, J. E., and Lynn, R. D. (1968). "Downhole Measurement of Drill String Forces and Motions." ASME Publication: Journal of Engineering for Industry: p. 217
- Duff, R. (2007). Observation and Modeling of Torsional Vibration Regimes. National Technical Conference and Exhibition, American Association of Drilling Engineers (AADE), Houston Texas.
- Dunayevsky, V. A. and F. Abbassian (1998). "Application of Stability Approach to Bit Dynamics." SPE Drilling & Completion(06).
- Dupriest, F. E., W. C. Elks, et al. (2011). "Borehole-Quality Design and Practices To Maximize Drill-Rate Performance." SPE Drilling & Completion(06).

Dupriest, F. E. and W. L. Koederitz (2005). Maximizing Drill Rates with Real-Time Surveillance of Mechanical Specific Energy. SPE/IADC Drilling Conference. Amsterdam, Netherlands, SPE/IADC Drilling Conference.

Dupriest, F. E. and S. F. Sowers (2010). "Maintaining Steerability While Extending Gauge Length To Manage Whirl." SPE Drilling & Completion(06).

Dupriest, F. E., J. W. Witt, et al. (2005). Maximizing ROP With Real-Time Analysis of Digital Data and MSE. International Petroleum Technology Conference. Doha, Qatar, International Petroleum Technology Conference.

Dykstra, M. W. (1996). Nonlinear Drillstring Dynamics. Ph.D. Dissertation, University of Tulsa.

Elsborg, C. C. and G. Grindhaug (2006). Planning and Detailed BHA Vibration Modeling Lead to Performance Step Change Drilling Deviated 24-in. Hole Section, Offshore Norway. IADC/SPE Drilling Conference. Miami, Florida, USA, Society of Petroleum Engineers.

Euler, L. (1744). Methodus inveniendi lineas curvas maximi minimive proprietate gaudentes sivesolutio problematis isoperimetrici latissimo sensu accepti. Lausanne, Geneva, Marc-MichelBousquet & Co.

Fear, M. J., F. Abbassian, et al. (1997). The Destruction of PDC Bits by Severe Slip-Stick Vibration. SPE/IADC Drilling Conference. Amsterdam, Netherlands, Society of Petroleum Engineers.

Fox, C. (1987). An introduction to the calculus of variations, Courier Dover Publications.

Gerbaud, L., S. Menand, et al. (2006). PDC Bits: All Comes From the Cutter/Rock Interaction. IADC/SPE Drilling Conference. Miami, Florida, USA, Society of Petroleum Engineers.

GMBH, P. S. (2011). Laboratory Experiments, Physics. 37070 Göttingen, Germany 21330.

Greenwood, D. T. (1965). Principles of dynamics. USA, Prentice-Hall.

Halsey, G. W., A. Kyllingstad, et al. (1986). Drillstring Torsional Vibrations: Comparison Between Theory and Experiment on a Full-Scale Research Drilling Rig. SPE Annual Technical Conference and Exhibition. New Orleans, Louisiana, 1986 Copyright 1986, Society of Petroleum Engineers.

Jaing, Wu. and J.-W. H.C. (1993). Preventing Helical Buckling of Pipes in Extended Reach

and Horizontal Wells. ETCE Drilling Technology Symposium. Houston, Texas.

Jansen, J.D. (1992). Whirl and Chaotic Motion of Stabilized Drill Collars SPE Drilling engineer 7 (2): 107-114 SPE-20930-PA. Copyright 1992, Society of Petroleum Engineers.

- Jansen, J. D. (1993). PhD dissertation Delft University of Technology.
- Kasner, E. (1911). "The group of turns and slides and the geometry of turbines." American Journal of Mathematics 33: 193-202.
- Kasner, E. a. C., John de. (1938). "The geometry of the whirl-motion group G6: elementary invariants." Bull. Amer. Math. Soc. Volume 44 (Number 6): 399-403.
- Kriesels, P.C., Keultjes, W.J.G., et al. (1999). Cost Savings through an Integrated Approach to Drillstring Vibration Control. SPE/IADC Middle East Drilling Technology Conference, Abu Dhabi, United Arab Emirates, Society of Petroleum Engineers.
- Ledgerwood, L. W., O. J.-m. Hoffmann, et al. (2010). Downhole Vibration Measurement, Monitoring and Modeling Reveal Stick-Slip as a Primary Cause of PDC Bit Damage in Today's Applications. SPE Annual Technical Conference and Exhibition. Florence, Italy, Society of Petroleum Engineers.
- Lindberg, H. E., and Florence, A. L., (1987). Dynamic Pulse Buckling, Martinus Nijhoff Publishers.
- Lubinski, A. (1950). A study On the Buckling Of Rotary Strings.
- Menand, S., H. Sellami, et al. (2008). How Drillstring Rotation Affects Critical Buckling Load? IADC/SPE Drilling Conference. Orlando, Florida, USA, 2008, IADC/SPE Drilling Conference.
- Menand, S., H. Sellami, et al. (2006). Buckling of Tubulars in Actual Field Conditions. SPE Annual Technical Conference and Exhibition. San Antonio, Texas, USA, Society of Petroleum Engineers.
- Menand, S., H. Sellami, et al. (2009). "Buckling of Tubulars in Simulated Field Conditions." SPE Drilling & Completion(06).
- Mensa-Wilmot, G., S. P. Langdon, et al. (2010). Drilling Efficiency and Rate of Penetration: Definitions, Influencing Factors, Relationships, and Value. IADC/SPE Drilling Conference and Exhibition. New Orleans, Louisiana, USA, Society of Petroleum Engineers.
- Mihajlovic, N., Van Veggel, A.A., Van de Wouw, N., Nijmeijer, H. (2004). Friction-induced Torsional Vibrations in an Experimental Drill-String System. 23rd IASTED Conference on Modelling, Identification and Control, Grindelwald, Switzerland.
- Osnes, S. M., P. A. Amundsen, et al. (2009). Vibration Measurements: A Time for Standardisation. SPE/IADC Drilling Conference and Exhibition. Amsterdam, The Netherlands, Society of Petroleum Engineers.
- Pelfrene, G., H. Sellami, et al. (2011). Mitigating Stick-Slip In Deep Drilling Based On Optimization Of PDC Bit Design. SPE/IADC Drilling Conference and Exhibition. Amsterdam, The Netherlands, Society of Petroleum Engineers.

Pessier, R. C. and M. J. Fear (1992). Quantifying Common Drilling Problems With Mechanical Specific Energy and a Bit-Specific Coefficient of Sliding Friction. SPE Annual Technical Conference and Exhibition. Washington, D.C., Society of Petroleum Engineers Inc.

Raap, C., A. D. Craig, et al. (2011). Drill Pipe Dynamic Measurements Provide Valuable Insight Into Drill String Dysfunctions. SPE Annual Technical Conference and Exhibition. Denver, Colorado, USA, Society of Petroleum Engineers.

Reckmann, H., P. Jogi, et al. (2010). MWD Failure Rates Due to Drilling Dynamics. IADC/SPE Drilling Conference and Exhibition. New Orleans, Louisiana, USA, 2010, IADC/SPE Drilling Conference and Exhibition.

Robnett, E. W., J. A. Hood, et al. (1999). ANALYSIS OF THE STICK-SLIP PHENOMENON USING DOWNHOLE DRILLSTRING ROTATION DATA. SPE/IADC Drilling Conference. Amsterdam, Netherlands, Copyright 1999, SPE/IADC Drilling Conference.

Schlumberger. (2011). "Stick-slip phenomenon." Retrieved 26 July 2011

Schultz, M., Hol, Barbara, Hernandez, Floyd, Sheritt, Allen, Harmer, Richard and Nutter, Nathan Rose Greg. (2005). Continuous Improvement Through Optimized Drilling Performance, AADE-05-NTCE-09. Houston, Texas.

Smyth, G. F., A. M. Evans, et al. (2011). Extension of Gauge Length to Reduce Vibrations and Improve Drilling Performance. SPE/IADC Drilling Conference and Exhibition. Amsterdam, The Netherlands, Society of Petroleum Engineers.

Teale, R. (1965). "The Concept of Specific Energy in Rock Drilling." Intl. J. Rock Mech. Mining Sci: 57-73.

Technology, A. (2011). "WellDrill Technical Data Sheet." 2011.

Thomson, W. T. (1973). Theory of vibration with applications, AA press.

Tucker, R. W., Wang, C., (1999). "An integrated model for drill-string dynamics." Journal of Sound and Vibration 224 (1): 123-165.

Van Den Steen, L. (2000). Drilling assembly with reduced stick-slip tendency, United States. US, Shell Oil Company Houston, TX. 6166654.

Warren, T. M. and J. H. Oster (1998). Torsional Resonance of Drill Collars with PDC Bits in Hard Rock. SPE Annual Technical Conference and Exhibition. New Orleans, Louisiana, 1998 Copyright 1998, Society of Petroleum Engineers Inc.

Wauer, J. (1982). "On the Stability of Rotating, Axially loaded, Homogeneous Shafts." Int. J. Solids Structures 18: 459-466.

Waughman, R. J., J. V. Kenner, et al. (2002). Real-Time Specific Energy Monitoring Reveals Drilling Inefficiency and Enhances the Understanding of When to Pull Worn PDC Bits. IADC/SPE Drilling Conference. Dallas, Texas, Copyright 2002, IADC/SPE Drilling Conference.

Wu, X., L. C. Paez, et al. (2010). Decoupling Stick-slip and Whirl to Achieve Breakthrough in Drilling Performance. IADC/SPE Drilling Conference and Exhibition. New Orleans, Louisiana, USA, 2010, IADC/SPE Drilling Conference and Exhibition.

Zannoni, S. A., C. A. Cheatham, et al. (1993). Development and Field Testing of a New Downhole MWD Drillstring Dynamics Sensor. SPE Annual Technical Conference and Exhibition. Houston, Texas, 1993 Copyright 1993, Society of Petroleum Engineers, Inc.

APPENDIX I: ADDITIONAL PROCEDURES AND EQUIPMENT SETTINGS

It is the perceived responsibility that a laboratory experiment such as this leave enough documentation that one could recreate the results independently. Therefore this section of the appendix presents documentation to utilize the novel sensor array configuration used in this study.

This section includes operating details and calibration procedures specific to the tools used in this study. The use of the equipment is not intended to be a commercial endorsement by the author or LSU of the brand or product, it is simply included for completeness and transparency. This work used several measurement and control apparatus including:

The Nintendo Wii Remote “wiimote” with motion plus in the preliminary tests, and the Wii Remote plus.

The Nintendo Wii Balance Board

Wireless Bluetooth PC dongles, with the GlovePie application and custom scripts

A Philmore Variable Transformer

An Automation Direct GS1-10P5 AC Drive, with the Gsoft application.

Additional Information

Information about the Nintendo hardware is ubiquitous, however detailed information is in the help files for GlovePie.

Information about the GS1 controller is currently available from automation direct at:

[http://www.automationdirect.com/ad/Shopping/Catalog/Drives/GS1_\(120_-z- 230_VAC_V-z-Hz_Control\)/GS1_Drive_Units_\(120_-z- 230_VAC\)/GS1-10P5](http://www.automationdirect.com/ad/Shopping/Catalog/Drives/GS1_(120_-z- 230_VAC_V-z-Hz_Control)/GS1_Drive_Units_(120_-z- 230_VAC)/GS1-10P5)

The manual is currently available at:

<http://www.automationdirect.com/static/manuals/gs1m/gs1m.html>

None of the values were changed from the default settings except P4.00 was adjusted to 5 to allow frequency (speed) to be changed over PC software.

GlovePie is a software written and distributed by Carl Kenner. The software interfaces with many PC and console gaming peripherals / controllers including the wiimote. The application allows custom scripts to be written to interface with the PC. The application also allows logging data files and visualizing device measures. The application is currently available at: <http://glovepie.org/glovepie.php>. Below are examples of the scripts used in this study.

```
Wii remote Calibration
//-----
// WiiAutomatedCalibration.PIE
//
// Developer: Winko Erades van den Berg
// E-mail : winko@winko-erades.nl
// Developed: 13 February 2010
// Modified: 13 February 2010
// Version: 1.0
//
// Description:
// Automated calibration for your Wiimote!
// Place the Wiimote face up on a flat surface.
// Wait for Calibration = 100 %
//-----

// Set your Wiimote LEDs to your liking. Binary value, 1-15
var.leds = 1

// Determinate Offset
if var.calibrate < 200 then
var.XOS = var.XOS + Wiimote.RawForceX
var.YOS = var.YOS + Wiimote.RawForceY
var.ZOS = var.ZOS + Wiimote.RawForceZ

var.xOffset = var.XOS / var.calibrate
var.yOffset = var.YOS / var.calibrate
var.zOffset = var.ZOS / var.calibrate

var.calibrate = var.calibrate + 1
var.calibration = var.calibrate * 100 / 200
endif

// Calibration
if var.XOS > 0 then
var.xRot = Wiimote.RawForceX - var.xOffset
else
var.xRot = Wiimote.RawForceX + var.xOffset
endif

if var.YOS > 0 then
```

```

var.yRot = Wiimote.RawForceY - var.yOffset
else
var.yRot = Wiimote.RawForceY + var.yOffset
endif

if var.ZOS > 0 then
var.zRot = Wiimote.RawForceZ - var.zOffset
else
var.zRot = Wiimote.RawForceZ + var.zOffset
endif

// Debug window output
debug = "Calibration=" + var.calibration + "% " + " X=" + var.xRot + " Y=" + var.yRot + " Z=" +
var.zRot

//Glovescript
//-----
// GyroRPM_BB_Accel.PIE
//
// By: Richard Duff
// rduff1@lsu.edu
//
// This script reads the gyro position and calculates and returns rotation speed
// in RPM, it also returns the self-calibrated values of the accel package, and
// reads the self-calibrated load values of a Wii Balance board.
// the sample rate may be adjusted.
// The screen will show the current Rotation speed and axial force in lbs.
// a file named output.txt will contain the accel values, the angular position
// the calculated rotation speed, the total balance board load, and a
// self-calculated distribution of the balance board load.
//-----

// seems to work well between .1 and 120 Hz
PIE.FrameRate = 100hz
//convert time into seconds.
var.t=time*86400

//Writes motion data to file, roll speed/6 is to conver deg/sec to RPM, weight / 2.2 is kg to lbs.
OutputToFile(RemoveUnits(var.t)+", "+Wiimote.gx + ", " + Wiimote.gy + ", " + Wiimote.gz + ", "
+ wiimote.MotionPlus.GyroRoll + ", " + RemoveUnits(wiimote.MotionPlus.RollSpeed/6) + ", " +
RemoveUnits(BalanceBoard.Weight/2.20462262) + " , " + BalanceBoard.JoyY + " , " +
BalanceBoard.JoyX )

//full debug output (using this debug output was slowing the right speed on my poor t61, even with
the SSD.
//debug = RemoveUnits(var.t)+' sec, TOR: '+wiimote.gx+' , RAD: '+wiimote.gy+' , RPM:
'+RemoveUnits(wiimote.MotionPlus.RollSpeed/6)+' , LBS: '

```

```
+RemoveUnits(BalanceBoard.Weight/2.20462262) + ', OUT: '+BalanceBoard.JoyY+', Right
'+BalanceBoard.JoyX
```

```
//used debug output
debug = 'RPM: '+RemoveUnits(wiimote.MotionPlus.RollSpeed/6)+' LBS: '
+RemoveUnits(BalanceBoard.Weight/2.20462262)
```

Drive Selection

A calibration check of the wiimote involves running the calibration script and seeing if the offsets have changed. If the offsets changed more than 5% then it was suggested that the tests be reran. If the offsets were found to be always changing the offset could be applied to the recorded values.

A check of the balance board involved staking four 2.5 lb. weights into the center of the balance board checking the value returned for each weight. If the balance board returns more than more than 2% difference then it was suggested the tests be reran.

During the development of the physical model prototype versions used DC motors. An early production version of the experiment was developed employed a variable transformer on a “softstart” motor. The softstart motor’s characteristic was that it did not come to full torque from full stop. One the transformer it’s torque was proportional to its speed. This performance was recognized and the desire to have a motor more capable of holding a constant torque even at low rotation speeds was sought to mimic the current generation of AC drives on drilling rigs. This system used a digital variable frequency AC drive with an inverter duty motor to achieve this goal. The associated diagrams for the motors and control schemes can be seen in Figure 63 and Figure 64.

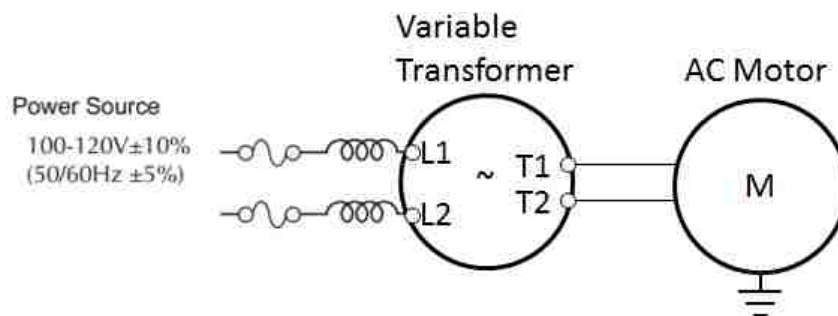


Figure 63. Motor RPM control scheme used in preliminary testing.

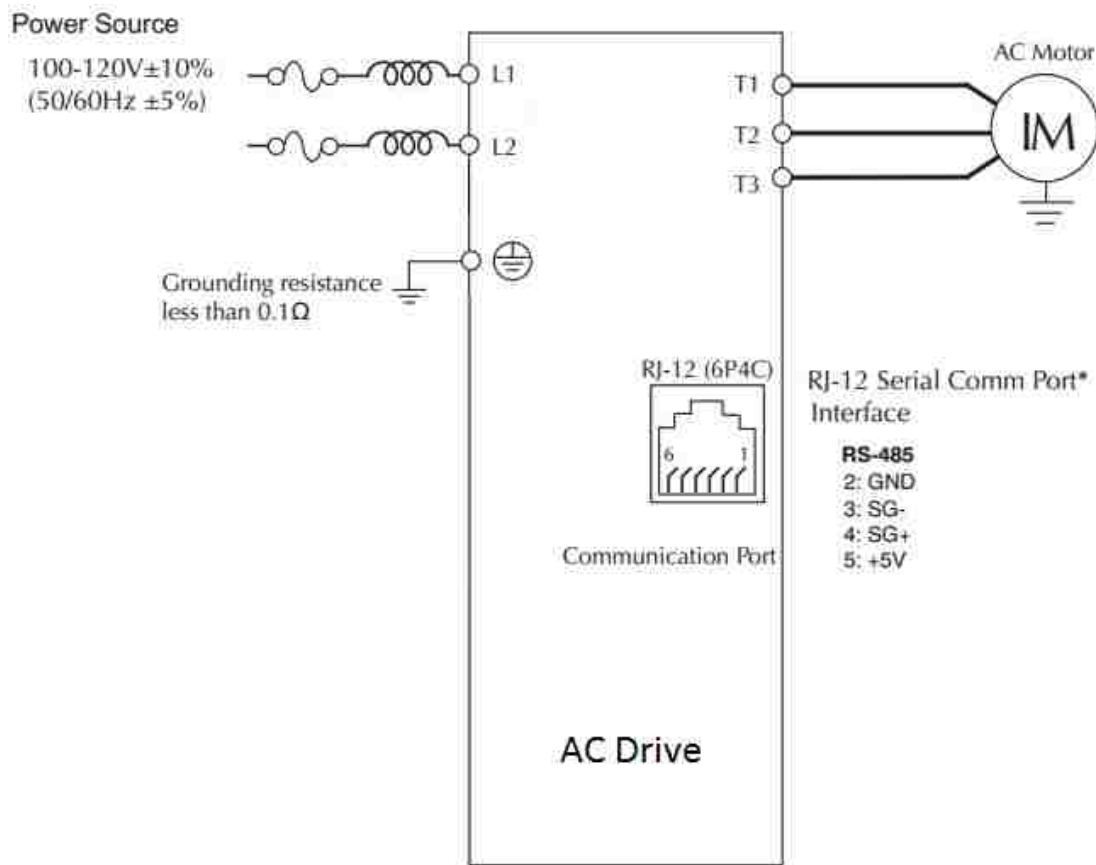


Figure 64. Wiring diagram for 0.5 HP inverter-duty AC motor attached to a 0.5 HP AC drive.

Using Acceleration and Gyroscope Measurement to Measure BHA dynamics

The development and testing of down hole dynamics measurement tools started with accelerometers. Perhaps this is because accelerometers were already being used in down hole tools for surveying. Attempts were made using one, two, three and four accelerometers recording or reporting acceleration while the string was in motion (Deily 1968). Some tools located the accelerometers in the middle of the BHA in a sonde, others in the body of the collars.

Today the use of accelerometers and gyroscopes in drilling measurement tools is wide spread. Diagnosis of vibration modes from acceleration measures was shown by Zannoni, Cheatham et al. (1993) with mathematics, laboratory work and field tests validating the methods for measuring BHA motion commonly used today. Many more examples of interpretation system have appeared in literature from the

DDS tool by Warren and Oster (1998) and its peer tools by Robnett, Hood et al. (1999), Ashley, McNary et al. (2001) and Halsey, Kyllingstad et al. (1986) that use similar principles. A robust explanation of the combination of the testing of the tool is found in literature (Zannoni, Cheatham et al. 1993) and US patent 5864058 (Chen 1999). Figure 6 shows the orientation of the sensor package inside the flexible shaft.

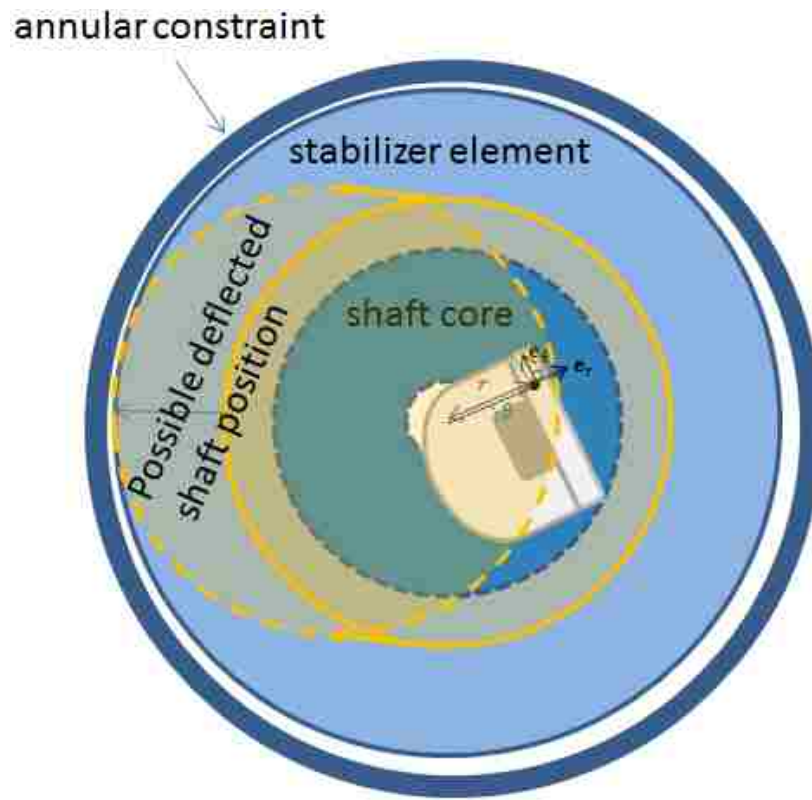


Figure 65. Sensor location inside cross section including shaft stabilizer and annular constraint boundaries.

This investigation focuses on developing an improved mechanism for understanding dynamic behaviors that generate vibration. The proposed mechanism investigated with the physical model described above and discussion on the materials and attempted scaling of the model presented in the Appendix III. The experimental fixture could be used in two ways. One method is a directed manner designed to accomplish and demonstrate specific behaviors, and second is experimental operating in a range of

parameters and various configurations designed to capture the occurrence of specific behaviors relative to each other.

Boundary Condition Friction Reduction Comparison.

In the main experiments presented in this work the bottom point of the shaft in fixture sat on a disk that sat inside the fixture. This endpoint was selected after experiences with other endpoint conditions during the screening tests, and preparation for a previous analysis strategy. During screening several different boundary conditions were examined. The shaft has a tendency to deflect and lift off some force during rotation. This is why for equal deflection the upper load limit is usually trending down. It is worthwhile to explore the endpoint effects.

To begin exploring the possible effects of the bottom point two new bottom endpoints were tested. For one test the bottom support disk was allowed to freely rotate, and second the bottom support disk was allowed to rotate freely and had a small extension that mated with the bottom of the test fixture shaft. For the sake of this discussion the first condition will be called “free” and the second “pinned” It is believed that the effects in the first case was a reduction in friction, and in the second a reduction in friction and a centering of the base of the shaft.(

Figure 66)

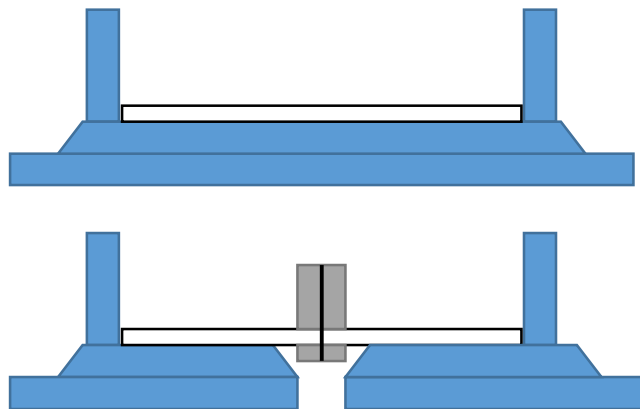


Figure 66. A cross section representing modifications made the lower shaft receiver in the test fixture. The upper case the white disk is free to turn in the fixture, in the second case the disk is again free to spin

however the end of the shaft is mated over the grey pin. The intention is to keep the shaft centered at the bottom. Material was removed below the pin to keep the pin from touching the receiver.

A slick shaft was used to in a screening demonstration to compare the endpoint effects. The first set of plots is the average acceleration measured for the parameter range plotted. (Figure 67) The second set of plots introduces a dimensionless stick-slip index. (Figure 68) This number takes the difference between the average recorded RPM and the shaft RPM then divides by the shaft RPM.

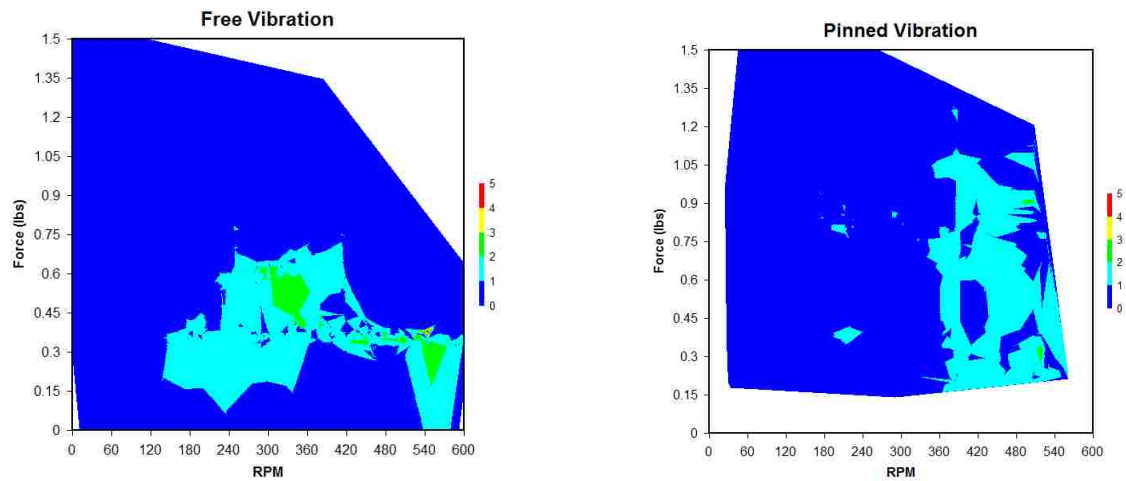


Figure 67. The recorded vibration from a single location in the shaft for the two boundary conditions examined. The free condition looks much the same as it did in the earlier testing. The Pinned condition on the right is devoid of the slightly elevated vibration levels 300 RPM and 0.6 lbs force.

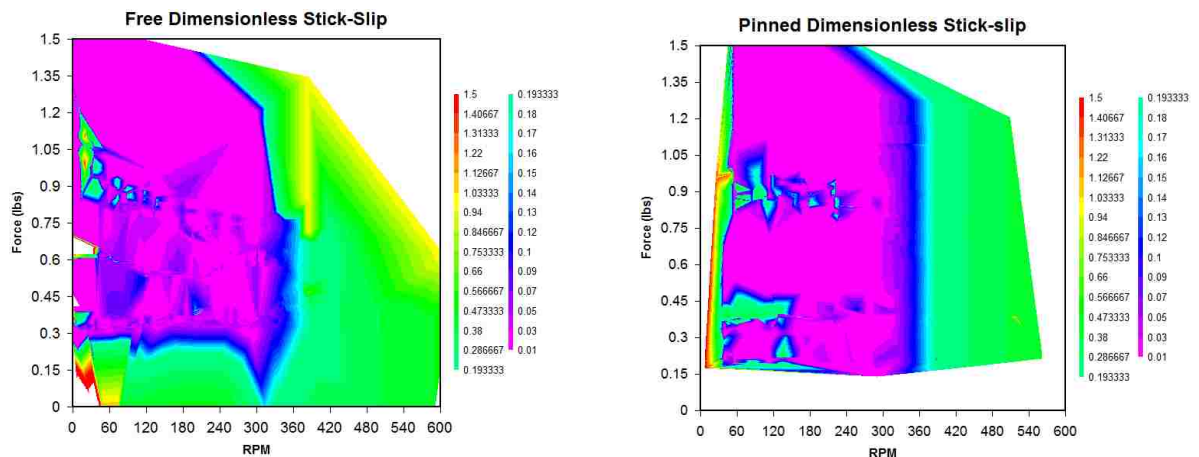


Figure 68. The stick-slip index in this case, dimensionless stick-slip pattern looks largely similar for both endpoints, both plots have an elevated feature around 0.9 lbs force extending from the left side of the plot, and an elevated level on the bottom edge. Between 300-360 RPM is where both plots pick up ten time in magnitude. Looking over to the Modal results the feature around 0.9 lbs on the left of each graph

is at a forward whirl critical speed, and the 300 RPM boundary is parallel to a second forward whirl critical speed.

It should be noted that the endpoint changes presented minor changes to the behaviors of the shaft, however the shape of the response surfaces are comparable. Future work may wish to explore the effect of the lower boundary condition further.

APPENDIX II: ACCELERATION MEASUREMENTS CALCULATION SYSTEMS

Schemes of Measurement

The cross section starting from an at rest position in the center of the hole can be completely described with the location of the center point and the radial location of a designated point along the edge. Accelerometer placement at the center of the cross section of the shaft or in the body of the shaft is like industry schemes for measurement. Allow the cross section of the shaft to be described as a circle with radius R_s with a local polar origin of $(0,0^\circ)$. Measurement (the sensor position) may be located at $(0,0^\circ)$ or at $(R,90^\circ)$, where R is a positive distance less than R_s . (Figure 69) When r shows up later know that this represents that at the places it is being used, it is still possibly a geometry variable - a not yet fixed value.

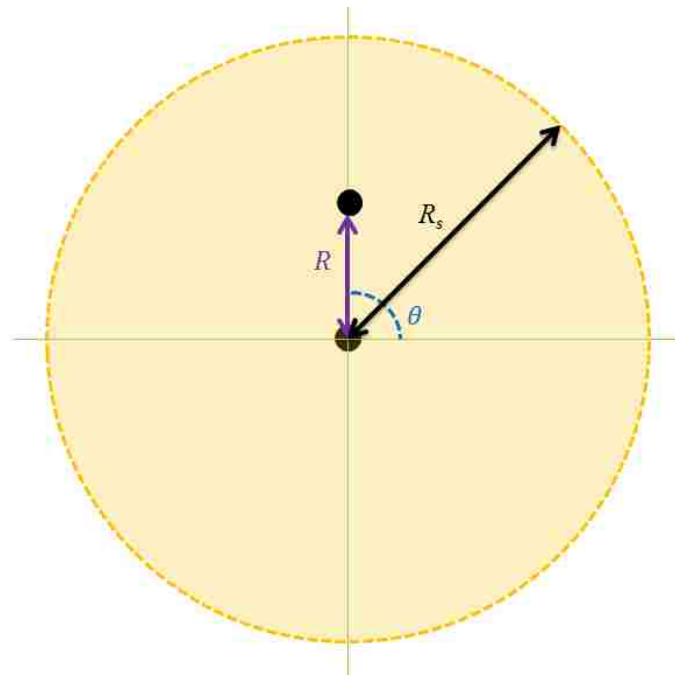


Figure 69. Depiction of potential positions for the sensor in a shaft, showing the origin, R and R_s .

Motion

The shaft cross section will be considered for three systems of motion (Figure 70): circular motion where the angular rate of rotation is not constant (non-uniform), non-uniform circular motion with a lateral motion and two simultaneous non-uniform circular motions.



Figure 70. Non-uniform rotation, non-uniform rotation with lateral motion and two non-uniform motion paths.

Before going further into the results of such motion two discussions of the acceleration of an object, in this case the sensor package, are presented. The first discussion is made using Cartesian like references and the second is an attempt to show a similar proof in polar coordinates. Also, to make this attractive and comprehensible to a wider range of readers the first discussion will use Leibniz's notation, and in the second Newton's notation. As a reminder Leibniz's notation the derivative of the function $x = f(t)$ is written $\frac{dx}{dt}$, in Newton's notation the same could be written \dot{x} . Also as a reminder a unit vector is a vector with length of unity, 1. In this presentation the unit vectors in the first explanation will be \mathbf{i} and \mathbf{j} for Cartesian and \mathbf{u}_r and \mathbf{u}_θ for the polar non-uniform rotating reference frame (then quickly converted to Cartesian) Figure 71, however later when the rotating reference frame is showed for polar and curvilinear they will be \mathbf{e}_θ and understand that it will always be normal to \mathbf{e}_r so still always linearly independent following perceived convention of the respected systems.(Figure 72)

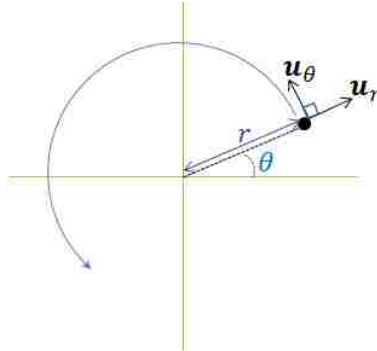


Figure 71. Unit vectors \mathbf{u}_r and \mathbf{u}_θ for the polar non-uniform rotating reference frame.

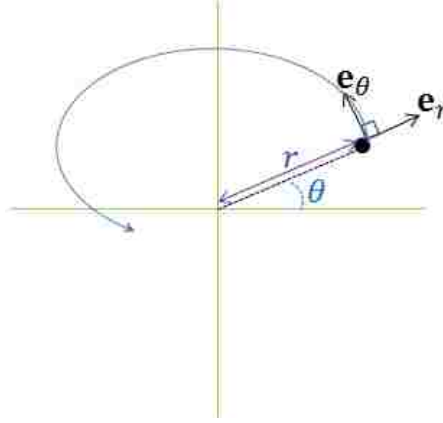


Figure 72. Unit vectors e_θ and e_r are linearly independent, for the polar curvilinear reference frame.

Starting our discussion with the Cartesian unit vectors description, these polar unit vectors can be expressed in terms of Cartesian unit vectors in the x and y directions, denoted \mathbf{i} and \mathbf{j} respectively:

$$\mathbf{u}_r = \cos\theta \mathbf{i} + \sin\theta \mathbf{j} \quad \text{Equation 1}$$

and

$$\mathbf{u}_\theta = -\sin\theta \mathbf{i} + \cos\theta \mathbf{j} \quad \text{Equation 2}$$

To find velocity differentiate. Where the angular velocity ω is $\frac{d\theta}{dt}$.

$$\mathbf{v} = R_s \frac{d\mathbf{u}_r}{dt} = R_s \frac{d}{dt} (\cos\theta \mathbf{i} + \sin\theta \mathbf{j}) = R_s \frac{d\theta}{dt} (-\sin\theta \mathbf{i} + \cos\theta \mathbf{j}) = R_s \frac{d\theta}{dt} \mathbf{u}_\theta = \omega R_s \mathbf{u}_\theta$$

$$\text{Equation 3}$$

The result shows that the magnitude of the velocity is ωR_s .

Taking the next derivative with time,

$$\frac{d\mathbf{u}_\theta}{dt} = -\frac{d\theta}{dt} \mathbf{u}_r = -\omega \mathbf{u}_r \quad \text{Equation 4}$$

Then the find acceleration, \mathbf{a} :

$$\mathbf{a} = R_s \left(\frac{d\omega}{dt} \mathbf{u}_\theta - \omega^2 \mathbf{u}_r \right) \quad \text{Equation 5}$$

The radial and tangential components may be seen as

$$\mathbf{a}_r = -\omega^2 R_s \mathbf{u}_r \quad \text{and} \quad \mathbf{a}_\theta = R_s \frac{d\omega}{dt} \mathbf{u}_\theta \quad \text{Equation 6 and Equation 7}$$

So for the sensor in the body rotating at changing speed the radial and tangential components of acceleration are seen. In the notation $(\mathbf{u}_r, \mathbf{u}_\theta)$

This acceleration result becomes:(Figure 73)

$$(-\omega^2 R, R \frac{d\omega}{dt}) \quad \text{Equation 8}$$

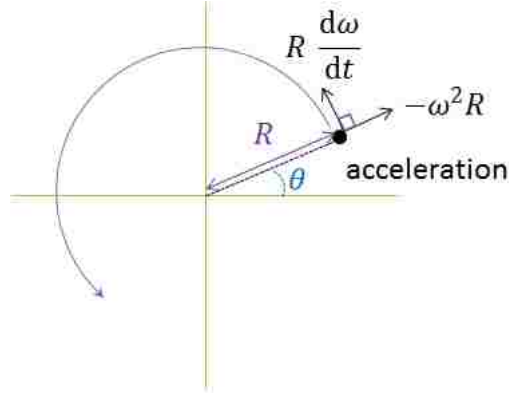


Figure 73. Acceleration of a rotating point in non-uniform circular motion.

Previously the non-uniform circular motion for the measurement point in the BHA was described with unit vectors \mathbf{u}_r and \mathbf{u}_θ almost immediately going to Cartesian like \mathbf{i} and \mathbf{j} , with results in Leibniz's notation for the derivatives. Here as stated, the same unit vectors \mathbf{u}_r and \mathbf{u}_θ will be presented as \mathbf{e}_r and \mathbf{e}_θ solved with Newton's notation for the derivatives with polar coordinates in a curvilinear system with a treatment using imaginary numbers. Figure 72 shows we are going to call the radial unit vector \mathbf{e}_r . This always points from the origin to the instantaneous position of the sensor or possibly the distance from the instantaneous center of rotation to the average center of rotation (Figure 74, Figure 75). Also we will call the tangential unit vector \mathbf{e}_θ and understand that it will always be normal to \mathbf{e}_r increasing in the direction θ . This no different than when we defined \mathbf{u}_r and \mathbf{u}_θ before.

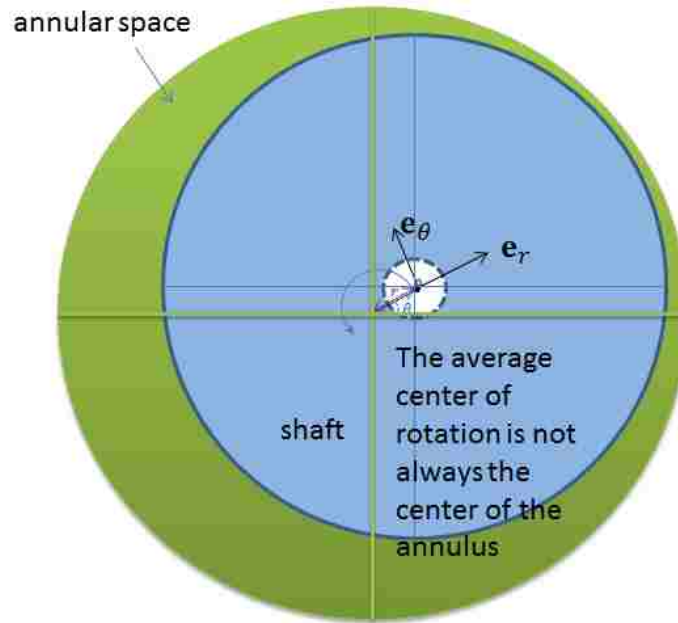


Figure 74. The center of the rotating shaft rotating (orbiting) about an average center of rotation.

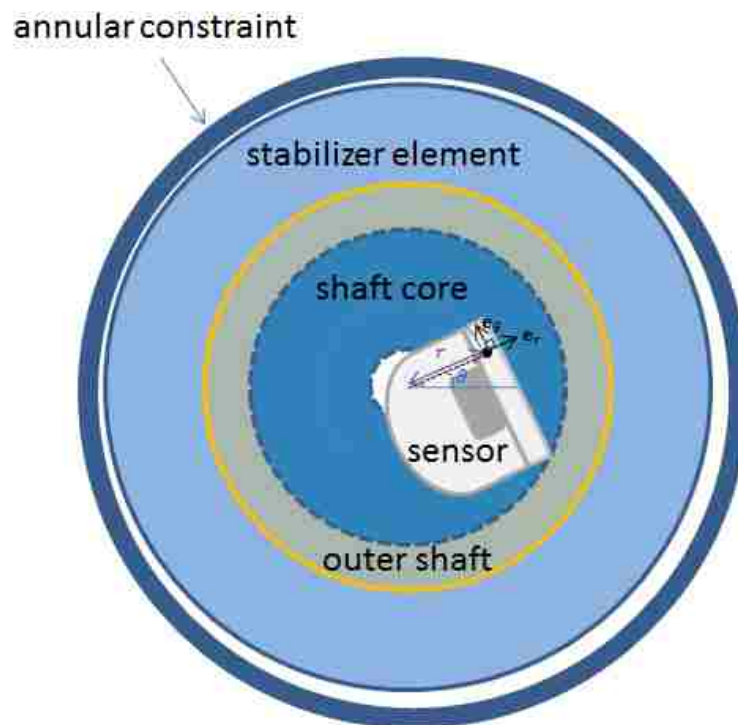


Figure 75. The sensor position in the rotating shaft.

Figure 76 shows a possible configuration of the shaft in the annular “hole” while whirling. Presented here to highlight the two-step approach is possible, and to help understand the systems measured response.

However, the following derivation still only applies to the system in Figure 74 or Figure 75, not yet the combined system.

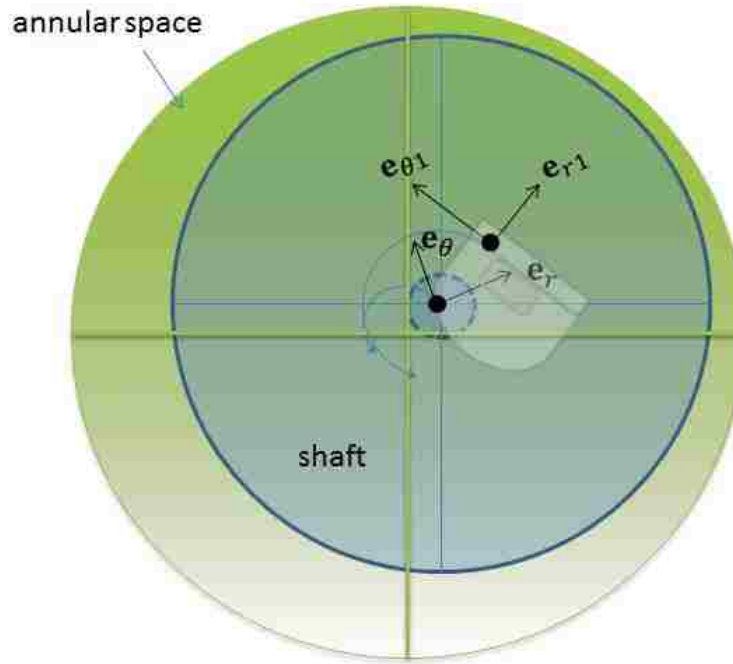


Figure 76. An amalgamation of Figure 74, Figure 75: Unit vectors \mathbf{e}_θ and \mathbf{e}_r are on the reference co-rotating frame at the instantaneous center of rotation, from origin at the average center of rotation, Unit vectors $\mathbf{e}_{\theta 1}$ and $\mathbf{e}_{r 1}$ are on a reference co-rotating frame at the sensor location, from the center of the shaft. Note the scale is distorted here to better show the position and relationships.

The position vector \mathbf{r} of the sensor location or shaft center can then be written.

$$\mathbf{r} = r \mathbf{e}_r \quad \text{Equation 9}$$

The vector \mathbf{r} is in the direction as the radial unit vector \mathbf{e}_r and is of length r . Now, the velocity of the sensor can be written

$$\mathbf{v} = \dot{\mathbf{r}} = v_r \mathbf{e}_r + v_\theta \mathbf{e}_\theta \quad \text{Equation 10}$$

Where \mathbf{v} is the velocity vector, the derivative of the position vector \mathbf{r} . In Newton's notation we write derivatives with a dot. So $\dot{\mathbf{r}}$, v_r and v_θ are the radial velocity and tangential velocity respectively.

Following along this same line of notation for the acceleration if you like

$$\mathbf{a} = \dot{\mathbf{v}} = \ddot{\mathbf{r}} = a_r \mathbf{e}_r + a_\theta \mathbf{e}_\theta \quad \text{Equation 11}$$

Where \mathbf{a} is the acceleration vector, and a_r and a_θ are the radial accelerations and tangential accelerations respectively. So far nothing about this has been specifically polar coordinates, so how could this be expressed in the sensors polar coordinates r and θ . One could simply take the derivative with time and find.

$$\mathbf{v} = \dot{r} \mathbf{e}_r + r \dot{\mathbf{e}}_r \quad \text{Equation 12}$$

This situation now with $\dot{\mathbf{e}}_r$ being the time derivative of the radial unit vector, is non-zero because \mathbf{e}_r changes direction as the object moves. It may not be clear how to find $\dot{\mathbf{e}}_r$. Let's consider the following method with complex numbers and revisit this situation.

A complex number z where x and y are real and i is the square root of -1 (and imaginary number). Here we would say x is the real part and y is the imaginary part because of the i coefficient. Please take care at this point not to recall that before when we used i and j for the Cartesian co-rotating reference frame, this i is not the same. This can be written

$$\mathbf{z} = \mathbf{x} + i\mathbf{y} \quad \text{Equation 13}$$

Alternatively this could be represented

$$\mathbf{z} = (\mathbf{x}, \mathbf{y}) \quad \text{Equation 14}$$

This reminds us of a way to visualize complex numbers, in the complex plane; however, we are going to stick with the i coefficient notation. (Figure 77)

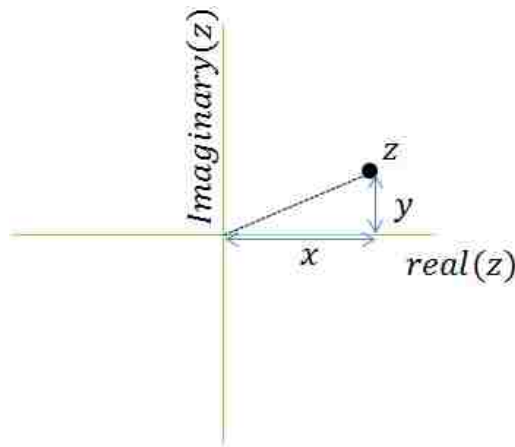


Figure 77. The components of the complex number z , depicted on a Cartesian plane.

The modulus of the complex number is follows

$$|z| = \sqrt{x^2 + y^2} \quad \text{Equation 15}$$

A famous complex analysis known as de Moivre's theorem, allows us to the complex number $e^{i\theta}$, where θ is real. (Croucher 2012)

$$e^{i\theta} = \cos\theta + i \sin\theta \quad \text{Equation 16}$$

So following this visualization where the real and imaginary parts form the head of the vector and the origin the tail. Then the length of the vector could be given as

$$|e^{i\theta}| = \sqrt{\cos^2\theta + \sin^2\theta} = 1 \quad \text{Equation 17}$$

Here $e^{i\theta}$ has been made a unit vector. And that this $e^{i\theta}$ unit vector here is like our e^r for a location with a polar coordinate (measured counter clockwise from the real axis) is θ . To get the corresponding tangential unit vector e_θ If we multiply by i Then complex number $ie^{i\theta}$ can be written making use of $i^2 = -1$. This is also a unit vector. (Figure 78)

$$|ie^{i\theta}| = \sqrt{\sin^2\theta + \cos^2\theta} = 1 \quad \text{Equation 18}$$

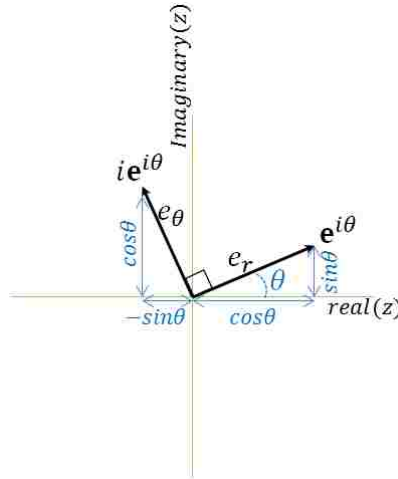


Figure 78. The components of the complex number z substituted with terms from Moivre's theorem, depicted on a Cartesian plane.

This vector is normal to \mathbf{e}^r in the direction of increasing θ . As seen in the Figure 78. Clearly $i\mathbf{e}^{i\theta}$ can now be identified as the tangential unit vector \mathbf{e}_θ .

Getting back to the object in non-uniform circular motion in the complex plane. We can represent the instantaneous position vector of this sensor with the complex number

$$\mathbf{z} = r \mathbf{e}^{i\theta} \quad \text{Equation 19}$$

With the $r(t)$ being the sensor's radial distance from the origin, and where $\theta(t)$ is the angular bearing to the real axis. Now, \mathbf{z} can be the position vector for the sensor, then $\dot{\mathbf{z}}$ is the sensor's velocity vector. Differentiating with respect to time we get,

$$\dot{\mathbf{z}} = \dot{r} \mathbf{e}^{i\theta} + r \dot{\theta} i \mathbf{e}^{i\theta} \quad \text{Equation 20}$$

Differentiating again with respect to time.

$$\ddot{\mathbf{z}} = (\ddot{r} - r \dot{\theta}^2) \mathbf{e}^{i\theta} + (r \ddot{\theta} + 2\dot{r} \dot{\theta}) i \mathbf{e}^{i\theta} \quad \text{Equation 21}$$

Comparing this to the equations from before, and recalling that $\mathbf{e}^{i\theta}$ is analogous with \mathbf{e}_r and $i\mathbf{e}^{i\theta}$ with \mathbf{e}_θ

$$\mathbf{v} = \dot{\mathbf{r}} = v_r \mathbf{e}_r + v_\theta \mathbf{e}_\theta \quad \text{Equation 22}$$

$$\mathbf{a} = \dot{\mathbf{v}} = \ddot{\mathbf{r}} = a_r \mathbf{e}_r + a_\theta \mathbf{e}_\theta \quad \text{Equation 23}$$

We obtain with substitution.

$$v_r = \dot{r} \quad \text{Equation 24}$$

$$v_\theta = r \dot{\theta} = r \omega \quad \text{Equation 25}$$

Where ω is the object's instantaneous angular velocity. Continuing the substitution

$$a_r = \ddot{r} - r \dot{\theta}^2 = \ddot{r} - r \omega^2 \quad \text{Equation 26}$$

$$a_\theta = r \ddot{\theta} + 2\dot{r} \dot{\theta} = r \dot{\omega} + 2\dot{r} \omega \quad \text{Equation 27}$$

The recognized elegance of this derivation is that the complex analysis has taken care of the fact that the unit vectors \mathbf{e}_r and \mathbf{e}_θ change direction as the sensor moves.

So let us consider the special case of the sensor in the tool. Its radius is fixed, but it may experience varying angular velocity. So that $\dot{r} = \ddot{r} = 0$. So the tangential velocity keeps it's the form.

$$\mathbf{v}_\theta = r\boldsymbol{\omega} \quad \text{Equation 28}$$

It's the same as before, except now it is proven for non-uniform in a curvilinear style, as well as circular motion. Similarly with $\dot{r} = \ddot{r} = 0$.

$$\mathbf{a}_r = -r\boldsymbol{\omega}^2 \quad \text{Equation 29}$$

Again it's the same as before, except now it is proven for non-uniform, as well as uniform circular motion. Finally looking at the tangential acceleration.

$$\mathbf{a}_\theta = r\dot{\boldsymbol{\omega}} \quad \text{Equation 30}$$

This

Now, going back to the system of the cross section of the rotating shaft. The results shown in $\mathbf{a}_r = -\omega^2 R \mathbf{s} \cdot \mathbf{u}_r$ and $\mathbf{a}_\theta = R_s \frac{d\omega}{dt} \mathbf{u}_\theta$ Equation 6 and Equation 7, $\mathbf{a}_r = -r\boldsymbol{\omega}^2$ Equation 29, $\mathbf{a}_\theta = r\dot{\boldsymbol{\omega}}$ Equation 30 are consistent with the understanding presented in (Zannoni, Cheatham et al. 1993) Sperry-Sun's "Drillstring Dynamics Sensor". At the time it was recognized that the terms of the non-uniform rotation solution between the sensor and the center of the shaft also needed to be added to the terms for the motion of the shaft around the in annulus.

In the case of the body experiencing a secondary lateral motion while rotating the additional rotation would be added. Consideration for the orientation must be accounted for.

$$(\mathbf{a}_r + \mathbf{a}_{l1} , \mathbf{a}_\theta + \mathbf{a}_{l2}) \quad \text{Equation 31}$$

The result will be dependent on the function of the lateral motion. If the lateral motion is its own non-uniform circular motion on the origin of the cross section. In this way we can deal with decoupled acceleration contributors, acceleration from the rotation of the body, and acceleration from the motion of

the bodies center. If the lateral terms are assumed to come from a path from Figure 70, the calculation for coupling may still be needed, as some special cases of fixed alignment or synchronization may arise. Unless we include a sensor to know the orientation of the body we would not be able to properly couple the terms. As the sensor response is considered let us consider if that important. The situation is not dire in this study as sensor packages employed in this study the IDDS and the Wii remote plus have a dynamic orientation measure.

Sensor Response

Now consider the placement of accelerometers in the cross section of the shaft. Consider the effects of placement of the accelerometer at $(0,0^\circ)$ or at $(R,90^\circ)$, where R is a positive distance less than R_s . In the phenomenon where the rotation speed changes but the center of rotation does not move. Centrally placed measurement would equal zero. Placed at $(R,90^\circ)$, the radial response and the tangential response would be:²

$$-\omega^2 R \mathbf{u}_r, R \frac{d\omega}{dt} \mathbf{u}_\theta$$

For a simple harmonic function such as: $\omega(t) = \sin(t)$ (Figure 79)

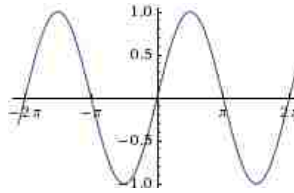


Figure 79. Simple harmonic function.

The response would be:

$$(2 \sin(t) \cos(t), \cos(t))$$

² Calculated using the WolframAlpha engine an online version of Maple the URLS link to the worked equations. <http://www.wolframalpha.com/input/?i=derivative+%CF%89%28t%29%3Dsin%28t%29%5E2>, <http://www.wolframalpha.com/input/?i=derivative+%CF%89%28t%29%3Dsin%28t%29>, <http://www.wolframalpha.com/input/?i=derivative%28t+%2F+2x+-+floor%28t%2F2x%29+%29>, <http://www.wolframalpha.com/input/?i=derivative+%CF%89%28t%29%3D+%28t+%2F+2x+-+floor%28t%2F2x%29%29%5E2>

For oscillation like a “saw tooth” function: $\omega(t) = t/2L - [t/2L]$ (Figure 80)³

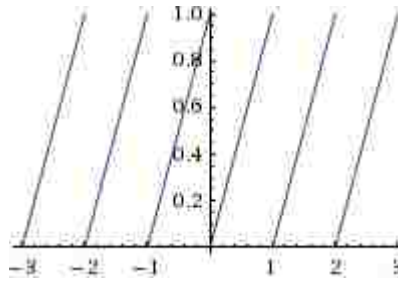


Figure 80. Saw tooth function

The response would be:

$$\left(\frac{t}{2x^2} - \text{Floor}\left[\frac{t}{2x}\right] \right) / x - \left(\frac{t}{2x^2} - \text{Floor}'\left[\frac{t}{2x}\right] \right) / (2x^2) + \left(\text{Floor}\left[\frac{t}{2x}\right] - \text{Floor}'\left[\frac{t}{2x}\right] \right) / x, -(-1 + \text{Floor}'\left[\frac{t}{2x}\right]) / (2x) \quad \text{Equation 32}$$

It should be clear at this point that the response of the harmonic function and the saw tooth function will be very different, where the simple harmonic function will continue to be harmonic the saw tooth’s character will be emphasized in the response as “spikes”. (Figure 81)

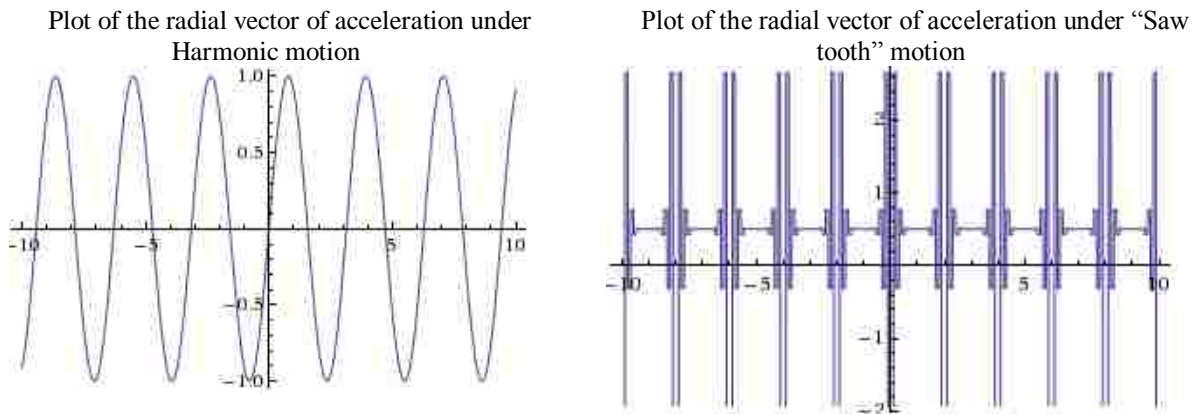


Figure 81. Plots depicting the response of the radial component of acceleration for harmonic and saw tooth functions of motion.

³ In this case we are using the floor function, to create the saw tooth wave. The “Floor” function rounds down to the nearest integer. The notation $[x]$ using the “Floor” bracket that looks kind of like the capitol letter “L” open and reversed “L” to close. In the solution I have elected to write it out Floor[x]

This example of functions for the rotational velocity function can be explored further. The learning here is that the responses from something with discontinuity like a “stick-slip” saw tooth, will have a distinct response from a harmonic torsional spring.

Until now, we have looked at non-uniform circular motion (torsional vibration) of a rotating shaft that was rotating about its center. Now consider the lateral motion, deflection, or whirl of the rotating shaft. Centrally placed measurement would now register the motion of the center of the shaft just as the tangentially placed response did for point in the body of the previously described case. Measurement in the cross section would record both the motions of the center orbit and the motions of the sensor point. The math problem is the same, non-uniform speed of rotation in a circular path. It is applicable to both components. The magnitudes will be potentially different, reflecting the radius’ magnitude and the function of the motion.

In application this scenario, where the rotating shaft is also orbiting around the annulus, the location of the sensor in the plane of the hole is unknown. Adding a direct measurement such as a gyroscope or magnetometer may help better separate the acceleration of combined radial or tangential forces. The placement of the accelerometers in the body of the tool would appear to capture more effects than when in the center of the tool, however if a center located gyroscope or direct measure of the rate of rotation was available then center located measurements may be more useful or usable.

At this point several anticipated motion paths could be further explored and evaluated for response, however the usefulness of this line of investigation may have the most impact showing the wide range of difference between harmonic oscillation, and saw tooth oscillation.

APPENDIX III: PHYSICAL MODEL DEVELOPMENT

Establishing a Physical Model

Presented here is a discussion of the scaling terms for the flexible shaft model used in this project.

To develop an analog physical model of the drilling BHA the parts of the system were identified and relevant properties determined so the system could be scaled. Scaling commonly refers to a transformation that enlarges or reduces the size of system components, the attempt in this case is to reduce the BHA to something small enough to have in the lab with forces safe to observe but still large enough to instrument. Examination of scaling will cover three factors, acceleration's relationship with force, beam deflection, and beam vibration.

Looking at the system of a deflected shaft, first consider this form of Newton's second law:

$$\mathbf{F} = \mathbf{ma} \quad \text{Equation 33}$$

Where F is force, m is mass, and a is acceleration. Next consider that mass in terms of the length of the shaft.

$$\mathbf{m} = \mu\Delta x \quad \text{Equation 34}$$

Where μ is linear density and x is the length of the shaft.

Combining the equation 23 and 24 and rearranging we get:

$$\mathbf{F}/\mu\Delta x = \mathbf{a} \quad \text{Equation 35}$$

So to preserving a similar response of acceleration can be accomplished with a proportional reduction of force, length, and liner density.

Next consider the deflection of the shaft in terms of it being an Euler-Bernoulli beam with an applied transverse load F

$$EI \frac{d^4 w}{dx^4} = F \quad \text{Equation 36}$$

Where E is Young's modulus, I is the area moment of inertial of the cross section, and w is the deflection of the neutral axis of the beam. Rearrange by multiplying each side by the length.

$$\frac{d^4 w}{dx^4} = F/EI \quad \text{Equation 37}$$

This makes a case for reducing force by Young's modulus times Area moment of inertial proportionally.

Young's modulus can be calculated by dividing the tensile stress, σ by the tensile strain, ϵ :

$$E \equiv \frac{\sigma}{\epsilon} = \frac{F/A_0}{\Delta L/L_0} = \frac{FL_0}{A_0 \Delta L} \quad \text{Equation 38}$$

Where F is the force applied to the object, A_0 is the original cross-sectional area through which the force is applied, ΔL is the amount by which the length of the object changes, L_0 is the original length of the object.

Finally, consider the vibration. Where L is the length, and the force F is now $q(x)$ a simple dynamic beam under axial load described in the Euler-Lagrange equation with solution S is: (Fox 1987)

$$S = \int_0^L \left[\frac{1}{2} \mu \left(\frac{\partial^2 w}{\partial t} \right)^2 - \frac{1}{2} EI \left(\frac{\partial^2 w}{\partial x^2} \right)^2 + q(x)w(x, t) \right] dx \quad \text{Equation 39}$$

The first term represents the kinetic energy, the second term is the potential energy due to internal forces, and the third term is the potential energy due to the load $q(x)$. The terms for the linear mass (oilfield weight per unit length) μ , Young's Modulus E (which contribute to stiffness), and the force $q(x)$ and the displacement $w(x, t)$ are all represented. Therefore, a linear scaling of each term is recognized

What this calls for is a linear proportionate reduction in linear mass, stiffness, and force to achieve analog results for changes in length. For a system of similar geometry in cross section and I (which contribute to stiffness), then density is an appropriate factor. The system we are scaling from is the steel drill collars used in a real drilling BHA, as listed in Table 5.

Table 5. Drill Collar System Properties.

Property	Steel System (Drill Collars) – Typical range
Density, specific weight	7.75–8.05 g/cm ³ ,65.5 ppg
Length	500 ft,
Linear Mass 4 x 1 inch collar	40 lbs. / ft
Young's Modulus	200 GPa; 29,000,000 lbf/in ²
Weight on Bit (Axial Load)	Range: 2,267- 27,215 daN ⁴ 5,000 – 60,000 lbs. force estimate center

The linear mass of the steel BHA system of this geometry is about 40 lb./ft (weight). The shaft material is about .029 g/cm³ or 0.24 ppg. The cross section area of a 4 x 1 collar is about 12 sq. in and a displacement of 0.0145 bbl./ft, or 0.61 gallons/ft. The linear mass is then 0.24 gallon/ft*0.61 ppg = .145 lbs./ft. The analog system's nominal target shaft size is about 5 feet or 1.524 meters. The model's shaft linear mass is 0.00265 times that of steel.

The suggested analog system shares the cross section of 6 inch hole having nominal 4 x 1 inch shaft, I will be the same regardless of the material. The Young's modulus of steel is 200 GPa, The Young's modulus of the shaft material is estimated around 1 MPa. (Brandel 2001) In the Lab it was estimated around 1.4 MPa , as presented in the young's modulus subsection. This system is solved graphically in Figure 82.

The force applied to the system can be controlled, so it will be calculated based on the scale factor selected. Considering the effects of the scaling, a concentration in length drives the equivalent linear mass up. That is to say 100 feet of steel to be modeled in 10 feet would be a material ten (10) times greater in weight. Similarly the stiffness would decrease, a material that can stretch one (1) foot per 100 feet would now need to stretch one (1) foot per ten (10) feet. The ratio will be the original property divided by the analog systems property. Then the coefficient scale factor would be this ratio adjusted for the reduction in length. Figure 82 shows the convergence of the scale factors for the linear density and Young's modulus (

⁴ Oilfield daN = Kg force

E) by Second moment of inertia factor (I). In a discussion framed as scaling factor groups one could make EI (Young's modulus (E), Second moment of inertia factor (I)) a group, and L (length L) a second group.

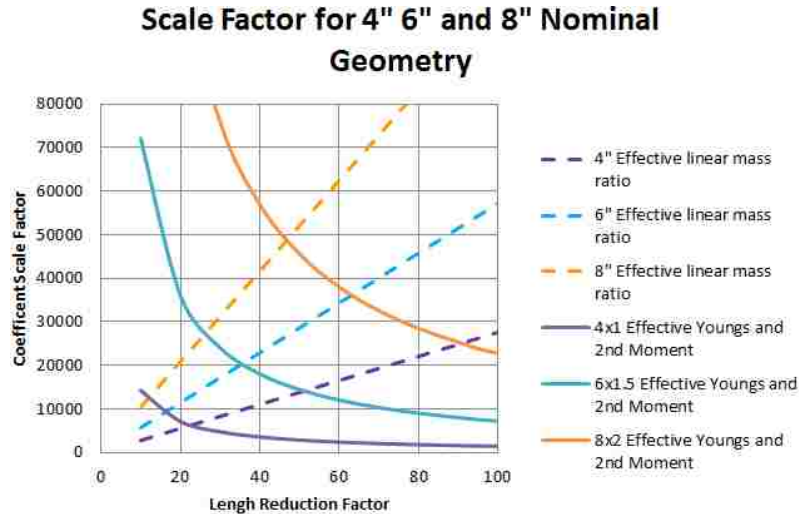


Figure 82. Scale factor's convergence. This plot shows two families of lines. The first family the dashed lines are the effective linear mass ratio, the second family solid lines is the scaled second moment multiplied by Young's Modulus. Both factors come from Equation 39. Where the similarly colored lines cross the equation is matched to the physical model systems properties.

The comparison generates has a matching scaled length reduction factors of 22, 35 and 47 respectively. That means the target 5 foot shaft is equivalent to a 110 foot, 175 foot and 235 foot sections of lower BHA drill collars respectively.

A complete typical lower BHA might contain anywhere from 90 feet to 240 feet of drill collars, or the complete BHA may contain more depending on the desired loads to be provided to the bit. This analysis scaling exercise demonstrates that the proposed system is fairly comparable analog at least honoring Newton's second law, Euler-Bernoulli deflection, and Euler-Bernoulli beam vibration for BHA components in the 4" to 8" nominal drill collar or 6" to 12-1/4" hole size range. It is difficult to say it is a great analog without having an equation that describes the behaviors expressly targeted, and for that matter having it in a dimensionless form. This description and scaling of a drilling BHS system could be a study onto itself.

Other Properties of the Proposed Physical Model

The physical properties of the proposed model are of particulate interest when considering the validity of the comparison to a field drilling system made of Steel components drilling rock. For this reason some discussion about testing and measurement of shear modulus, Young's modulus, spring constants, of the shaft is of interest. Also, friction between of the shaft and the annulus and the shaft and the bottom hole material is worth discussing.

Mass and Density

To estimate the mass and density, the shaft material was cut into twenty 1 cm x 1 cm cubes. The weight of each cube, and a combination of all the cubes was measured.

Shear Modulus

Shear modulus is defined as the ratio of shear stress to shear strain. The shear modulus of rods may be measured experimentally with a torsional pendulum. (Figure 83)



Figure 83. Torsional pendulum shaft redrawn from (GMBH 2011).

The period of a torsional pendulum may be written:

$$T = 2\pi \sqrt{\frac{I_z}{D_T}} \quad \text{Equation 40}$$

Where

I_z is the polar moment

D_T is the torsional modulus

Or

$$T = 2\pi \sqrt{I_z \cdot \frac{2}{\pi} \cdot \frac{L}{G} R^{-2}} \quad \text{Equation 41}$$

Where

T is the period of vibration

I_z is the polar moment

L is the length of the shaft

G is the Shear Modulus

And R is the radius of the shaft.

In the laboratory the top of the shaft is fixed and the bottom free with some added mass was wound and released for a series of different masses and starting angular positions. Now, the angular pendulum's period should be independent of mass or initial position. The measured rotation speed can be plotted and the period estimated from the plot. This period can be used to calculate the shear modulus using the equations above. This value was not used in the scaling equations for the system.

Young's Modulus

Young's modulus is the ratio of uniaxial stress over the uniaxial strain during the period that Hooke's Law is true. It can be calculated experimentally by the slope of the stress-strain curve created during a tensile test.

To test this in the lab the shaft was loaded with various amounts and the displacement measured. Young's modulus was then calculated. In the scaling section the value of 1 MPa or 145 psi was already

suggested. This was obtained by recording 0.35 inch deformation on a 60 inch long tube 4x1 inch tube from a 10 lb. force.

Spring Constant

Similar to young's modulus the spring constant may be measured experimentally during a tensile test. This value relates the force exerted by a spring to its distance, the difference being the spring constant is not independent of geometry. So once Young's modulus is calculated as the quantity force divided by area times the quantity length divided change in length for that force. So for a spring that this means Young's modulus times the area times the total length is equivalent to a spring constant for that specific geometry. Nominally about 7000 N/m for the shaft systems used in this experiment.

Friction Factor

Friction is the force resisting the relative motion of solid surfaces in contact, fluid layers or other material elements. Dry friction between solid surfaces is divided into static friction for non-moving surfaces and kinetic friction for surfaces in motion. For static and kinetic friction the interaction of two materials moving past one another can be described using a friction coefficient, that coefficient is the ratio of the force resisting motion and the force pushing them together.

This number is not discussed in the scaling exercise, so now is a fair time to calculate it. To estimate the dry friction a simple experiment was designed to find the friction force. A sample of material was prepared and loaded into the test fixture. While the sample was pushed slowly, one end of the test fixture was elevated until the material glided freely down fixture. The tests were repeated without the nudging to get started, no measurable difference in angle was apparent. The pitch also known as the angle of repose was measured and recorded by both a gravity and a gyro based sensor. The test was repeated, then another sample was repaired and tested similarly for a total of eight repetitions each. The size and weight of the samples were measured and recorded. The first set of samples averaged 0.078 lbs. (0.0353 kilograms). This system has a widely accepted solution derived from Newton's second law. (Figure 84)

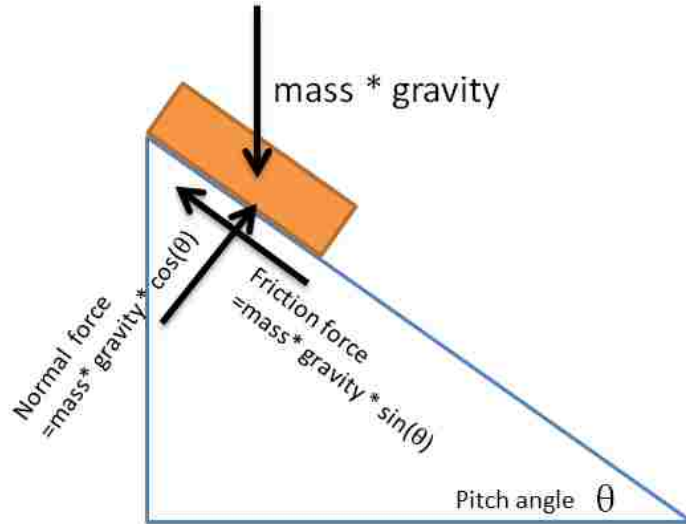


Figure 84. Free body diagram for solution to friction force calculation.

The first set of 12 inch (0.3048 meter) long samples for the shaft material fell at an average pitch angle of 39 degrees. Taking gravity to be 9.81 m/s^2 [it cancels out later, as does the weight] the friction force is calculated as 0.218 Newtons, the normal force to be 0.27 Newtons. The friction coefficient is simply the ratio of the friction force over the normal force can be found:

$$F_f = \mu N \quad \text{Equation 42}$$

where

F_f = frictional force (Newtons)

μ = frictional coefficient

N = normal force (Newtons)

This can be estimated as $\tan(\text{pitch angle}) = \mu$. Here the average friction coefficient was calculated to 0.81. No reference was found for the shaft material on the annulus material to compare this number to however published values for what might be considered a similar material (clear plastic) of Poly(methyl methacrylate) (Plexiglas) are about 0.8. This value of coefficient of friction is not used further in this work and is provided here solely as reference.

Dimensionless Analysis on Scaling of a System (Buckingham)

Dimensional equations for physical systems may be simplified when several quantities of the same kind are included and when the physical properties of the system are not expected to change during the operation. The quantities may then be described by a ratio. For example, if a shaft is of a particular diameter and length, and does not change during the operation, then this relationship could be made into a ratio. This ratio would be useful if the diameter and the length of the shaft are used in an equation. Similarly if an equation describes a property of a material and lengths and the system shall remain geometrically similar to itself in all cases then the formulation of the equations can be further reduced to be only a function of quantities. For the described relationship, if all the quantities involved are considered then this formulation might be considered a complete equation. A complete equation will have unitless coefficients. Unitless coefficients used in this fashion are also known as dimensionless numbers.

The value of dimensionless numbers presents itself when one can form a simpler function that completely captures a behavior. For example for engineering purposes the dimensionless wave numbers can be tabulated as functions of the slenderness ratio defined by the length of the beam to the radius of gyration of the cross section so that the natural frequencies of a system can be obtained directly for given physical and geometric properties. (Han et al. 1999) It is further understood that differences in beam models monotonically decreases with an increasing slenderness ratio. This is because less slender beams have a greater influence from second order effects. The drill string bottom hole assembly system is very slender, perhaps examining the simpler Euler-Bernoulli theory beam will present an insight.

Transverse vibration theory or beam theory presents a number of potential solutions to beam vibration problems. The difficulty with all solutions in regard to the rotary drilling system is an assumption of the endpoint behaviors. Four popular models are Euler-Bernoulli, Rayleigh, shear and Timoshenko. The most comprehensive model appears to be what is known as the Timoshenko model, it can be described as adding rotary inertia to the shear model or shear distortion to the Rayleigh model. A dimensionless style comparison between the models and the results is presented in (Han et al. 1999) Jansen approaches the boundary condition issues by exploring the behaviors between stabilizers. Examining his methods will

reveal additional dimensionless quantities of interest. However first, consider the Euler-Bernoulli model. To help follow the discussion on dimensioned and dimensionless numbers an * after a quantity will denote it is dimensional, following the convention in Han et al. 1999. Solving the vibration of a beam problems begins by describing the potential and kinetic energy and of the bending beam. The potential energy of a uniform beam may be given as:

$$E^*_{potential\ bending} = \frac{1}{2} \int_0^{L^*} E^* I^* \left(\frac{\partial^2 v^*(x^*, t^*)}{\partial x^{*2}} \right)^2 dx^*$$

Where E^* is Young's Modulus, I^* is the area moment of inertia of the cross-section about the neutral axis $v^*(x^*, t^*)$, the transverse deflection (v^*) at position x^* , time t^* , and the length of the beam is L^* . To attempt to get closer to a complete equation the distances can all be made unitless, by dimensioned length being made a 'unit length' of unity, then beam is described with:

$$L = \frac{L^*}{L^*} = 1$$

$$v = v^*/L^*$$

$$x = x^*/L^*$$

Now the potential energy can be rewritten:

$$E^*_{potential\ bending} = \frac{1}{2} \int_0^1 \frac{E^* I^*}{L^*} \left(\frac{\partial^2 v(x, t)}{\partial x^2} \right)^2 dx$$

Following Buckingham's advice this term $\frac{E^* I^*}{L^*}$ that is now a unitless term

$$E_{potential\ bending} = \frac{1}{2} \int_0^1 \left(\frac{\partial^2 v(x, t)}{\partial x^2} \right)^2 dx$$

The kinetic energy of moving (translating) a point on the beam

$$E^*_{kinetic\ trans} = \frac{1}{2} \int_0^{L^*} \rho^* A^* \left(\frac{\partial v^*(x^*, t^*)}{\partial t^*} \right)^2 dx^*$$

Where ρ^* is the density of the beam and A^* is the cross sectional area. Again following Buckingham's advice A^* can be non-demensionalized by L^{*2} and L^{*2} is really just L^* times L^* . Time t will be $1/\omega_1^*$ where

ω_1^* is the first natural frequency of the system. This will be found later. Then following Han the kinetic energy is non-dimensionalized by $\frac{E^* I^*}{L^*}$, to write:

$$E_{kinetic\ trans} = \frac{1}{2} \int_0^1 \rho^* \frac{L^{*6} \omega_1^{*2}}{E^* I^*} A \left(\frac{\partial v(x, t)}{\partial t} \right)^2 dx$$

By non-dimensionalizing ρ^* the density with $\frac{E^* I^*}{L^{*6} \omega_1^{*2}}$ the equation simplifies too:

$$E_{kinetic\ trans} = \frac{1}{2} \int_0^1 \rho A \left(\frac{\partial v(x, t)}{\partial t} \right)^2 dx$$

Now the dimensionless Lagrangian, defined by $E_{kinetic\ trans} - E_{potential\ bending}$ can be written:

$$L = \frac{1}{2} \int_0^1 \left[\left(\rho A \frac{\partial v(x, t)}{\partial t} \right)^2 - \left(\frac{\partial^2 v(x, t)}{\partial x^2} \right)^2 \right] dx$$

Following along with the virtual work, non-conservative force $f(x, t)$ method suggested by Han one will arrive with a governing equation of motion using Hamilton's principle that can be solved with Eigen function expansion.

$$f(x, t) = \rho A \frac{\partial^2 v(x, t)}{\partial t^2} - \frac{\partial^4 v(x, t)}{\partial x^4}$$

$$\frac{\partial^2 v}{\partial x^2} \delta \left(\frac{\partial v}{\partial x} \right) \Big|_0^1 = 0$$

$$\frac{\partial^3 v}{\partial x^3} \delta v \Big|_0^1 = 0$$

Stop here and consider the physical meaning of this equation now. v is dimensionless displacement, with derivatives $\frac{\partial v}{\partial x}$ is dimensionless slope, $\frac{\partial^2 v}{\partial x^2}$ moment, and $\frac{\partial^3 v}{\partial x^3}$ dimensionless shear. The variation in the displacement is zero, meaning it is always the same value. The vibrating system has reached a steady state. This system will have predictable wave shapes.

Han goes on to show that the wave shapes look generally the same for all 4 discussed methods. The first wave shape is a cantilever (one node), the second a single peak (two nodes), the third looks something like a sign wave cycle (three nodes), and the fourth is just a bit longer than one and a half sign wave cycles (four nodes). In each case the node count includes a fixed boundary condition. So in this simple case both the mode shape and the frequency can be predicted with dimensionless analyses. (Han et al. 1999) Will the same be true for a rotor dynamics approach?

Dimensionless Linear Rotor Dynamics (After Jansen (1992))

The motion of a drill collar section can be examined as the behaviors between stabilizer positions. This idealized model is presented here for analysis with dimensionless numbers. This will allow one to examine the first bending mode at constant rotary speed with a mass-spring system with two degrees of freedom.

First examine the basic equations, then some of the neglected effects will come back in to play later. The equations of motion of a whirling system neglecting gravity, fluid forces, stabilizer clearance, and friction are neglected are as follows (Den Hartog 1956) can be described as a point in the midway plane between stabilization:

$$m\ddot{x}_1 + kx_1 = me_0\Omega^2\cos(\Omega t) \text{ and } m\ddot{x}_2 + kx_2 = me_0\Omega^2\sin(\Omega t)$$

Where the m is equivalent mass and the dots above are differentiation with respect to time., e_0 is the eccentricity of the center of the mass, Ω is the rotary speed, t is time, and k is the equivalent bending stiffness.

Following rotor dynamics conventions a compact notation for complex variables will be used. The complex coordinate:

$$x = x_1 + ix_2$$

Represents the displacements x_1 and x_2 of the geometric center of the drill collars. Similarly following convention here the primed coordinate:

$$x' = x'_1 + ix'_2$$

represents the displacement of the center of mass.

If gravity, drilling fluid, collar clearance, and friction are neglected then the remaining forces acting on the collars are inertial forces and restoration forces. Following the established complex notation, the inertial forces caused by accelerations can be written as:

$$F_m = -F\ddot{m}'$$

And the restoration forces caused by bending can be written as:

$$F_k = -kx$$

The position of the center of mass rotation around the geometric center may be written:

$$x' = x + e_0 \exp(i\Omega t + i\zeta_0)$$

Where ζ_0 is the initial phase angle. Now, substituting the second derivative of this equation into the equation for the inertial forces and adding the force components in the equation of motion.

$$m\ddot{x} + kx = me_0\Omega^2 \exp(i\Omega t)$$

This simplifies the original two equations of motion with the use of the complex notation.

Fluid effects introduce nonlinearity by assuming the collars experience an added mass force and drag force.

$$F_f = -m_f\ddot{x} - c_f|\dot{x}|\dot{x}$$

Where m_f is the equivalent added mass and c_f is the equivalent fluid damping coefficient. The effect of stabilizer friction and clearance is most easily expressed in polar coordinates:

$$F_k = -k \left[(q - s_o) + i\phi \left(s_o - \frac{s_o^2}{q} \right) \right] \exp(i\theta)$$

Where s_o is half the difference in the hole diameter and stabilizer size; and the friction angle ϕ is the arc tan of the dimensionless coefficient of friction between the stabilizer and the borehole wall. Contact with the wall is accounted by including the formula:

$$F_w = -[(1 + iS\mu_c)k_w(q - c_0) - c_w\dot{q}] \exp(i\theta) \text{ and } S = \sin(\dot{\theta} + \Omega R_c)$$

Where c_0 is the collar clearance, R_c is the ratio of the collars to the difference in the hole diameter and collar size; μ_c is the dimensionless coefficient of friction between the collars and the borehole wall; k_w is penalty stiffness, c_w is a damping coefficient. The effect of gravity is expressed as

$$F_g = -imgf_b \sin(\alpha_i)$$

Where g is the acceleration caused by gravity, f_b is the buoyancy factor, and α_i is the borehole inclination.

Now following Jansen the force components can be scaled by the following dimensionless parameters:

$$y = x/c_0$$

Scaling the Cartesian displacement by the collar clearance. The clearance is the largest the collar can move so this is like the slenderness gyration;

$$r = q/c_0$$

Scaling the Cartesian deflection by the collar clearance creates a second slenderness gyration term;

$$\beta = \frac{m_f + m}{m}$$

Buoyancy factor;

$$\delta = s_0/c_0$$

Ratio of stabilizer clearance and collar clearance;

$$\epsilon = e_0/c_0$$

Ratio of collar eccentricity and collar clearance;

$$\eta = \Omega/\omega$$

Ratio of input rotation speed to the natural angular frequency;

$$\xi = c_f c_0/m$$

Ratio of fluid damping coefficient times collar clearance to mass;

$$\tau = \omega t$$

Dimensionless time, again the natural angular frequency is multiplied by the time;

$$Q_g = F_g/(c_0 k)$$

Ratio of gravity to the collar clearance multiplied by an equivalent bending stiffness;

$$\rho = k/k_w$$

Ratio of equivalent bending stiffness to penalty stiffness;

$$v = c_w/(m\omega)$$

Dimensionless wall damping, ratio of damping to mass times natural angular frequency;

$$Q_k = F_k/(c_0 k)$$

Scaled restoring force. Ratio of restoration force to collar clearance times equivalent stiffness;

Where:

$$\omega = \sqrt{\frac{k}{m}}$$

is the natural angular frequency.

Now differentiating to scaled time τ and following Jansen's example results in a strongly nonlinear equation. Jansen's results show that if collar eccentricity is included forward whirl solutions are possible and if it is neglected backward whirl with slipping stabilizers solutions exist.

Jansen is able to further find a factor S for backward whirl such that if S is equal to one means that collar slip is driving whirl, if S is negative one then collars are experiencing whirl-resisting slip.

$$S = \sin(\eta_b + \eta R_c)$$

Where η_b =the scaled backward whirl speed, and η is again the scaled rotary speed and R_c is the slipless whirl collar ratio. (Jansen 1992) Following this line of logic under ideal conditions one could predict the type of whirl knowing only the geometry of the tool and hole, and the natural angular frequency. This demonstrates the power of dimensionless analysis.

Application to Physical Model Scaling (repeated in body of dissertation)

Examining Jansen's S (path solution) for whirl, determining whirl type provides insights to scaling a physical model:

$$S = \sin(\eta_b + \eta R_c)$$

η_b is the scaled backward whirl speed is a dimensionless Backward Whirl speed with units 1/t divided by natural frequency with units 1/t.

η is the second term in this equation is the ratio of input rotation speed to the natural angular frequency.

R_c is the slipless collar ratio is the collar diameter divided by the quantity of the collar diameter subtracted from the hole diameter.

What is in this solution are terms made from the frequency and clearance diameters. Natural frequency in this case is the square root of quantity of the stiffness divided by the mass.

Given that the diameters in the test system are similar to diameters used in the field. In fact the test fixture is about a 4 inch collar in a 6 inch annulus with 5-3/4 inch stabilizers. This could be a size combination used in the field. The other term in the solution is natural frequency. The suggested solution is the square root of the stiffness divided by the mass. Another thing to consider is that frequency is inversely proportional to length. A unit length (1 foot) of steel collars in this size have a natural frequency of 92,979 Hz. The same unit length of the test fixtures shaft has a frequency of 4,086 Hz. Steel is about 22.76 times higher in frequency. Therefore for this system using the solution form from Jansen the equivalent system to five feet of shaft [4x1 inch] is 113 feet of [4x1 inch] collars. It should be noted that this is the same scaling factor found using the graphical solution method using another set of equations (Fox 1987).

APPENDIX IV: ANSYS™ MODELING OF EXPERIMENTAL SYSTEM

Where appropriate finite element models were designed to mirror the laboratory experiments. Ansys(TM) is a commercial engineering simulation software developer that makes a range of products. In this study the Ansys(TM) Workbench, Mechanical was employed. Specifically, the static structural, linear buckling, modal and transient structural systems were used to model specific parts of the laboratory experiments. The purpose of including the experiments and the results here are to back up the laboratory tests and expand the explanation of those experiments allowing greater theoretical analysis. Additionally the computational model may show the open door to take the experimental philosophy to a full size system.

Euler Buckling

Euler developed for an ideal column (straight, homogeneous, free from internal stress) the maximum load that could be handled before entering an unstable state. In this state any lateral force will cause the column to fail by buckling. (Euler 1744)

The image shows a mathematical formula for Euler's critical load, which is
$$F_{cr} = \frac{\pi^2 EI}{K^2 L^2}$$
 where F_{cr} is the critical force, E is the modulus of elasticity, I is the area moment of inertia, K is the column effective length factor, and L is the unsupported length of the column.

Equation 43

where

F = maximum or critical force (vertical load on column),

E =modulus of elasticity,

I =area moment of inertia,

L = unsupported length of column,

K = column effective length factor, whose value depends on the conditions of end support of the column, as follows.

For both ends pinned (hinged, free to rotate), $K= 1.0$.

For both ends fixed, $K= 0.50$.

For one end fixed and the other end pinned, $K= 0.699....$

For one end fixed and the other end free to move laterally, $K= 2.0$.

The limitations of the ideal column had led to many empirically support formulas. For real systems including BHAs and casing, demining the boundary conditions, the K factor is difficult. Perhaps, more significant the added complication of the annular contacts as early introduction of lateral forces empirical formulas are favored for predicting the buckling loads.

Early Oilfield theories about buckling were developed by Lubinski. (Lubinski 1950) (A. Lubinski 1961) Euler buckling has been adapted into oilfield terms with the introduction of the effective weight (buoyant weight). Discussion of tubular constrained in an annulus discuss two modes, initial sinusoidal buckling and (final or lock up) helical buckling. This convention of lock up is that in the helical mode transferring any axial force to the end of the string is difficult.

For vertical wellbores the discussions of buckling regularly target at what critical force does the buckling mode initiate.

For sinusoidal buckling.

$$F_{\sin} = 2 (E I W_e / r)^{0.5} \quad \text{Equation 44}$$

Where W_e is the effective weight, the buoyed weight.

Dawson and Paslay included the effects of inclination by introducing a trigonometry term. (Dawson R. 1984)

$$F_{\sin} = 2 (E I W_e \sin(\alpha) / r)^{0.5} \quad \text{Equation 45}$$

Where α is the inclination of the wellbore.

Wu and Juvkam-Wold (Wu and H.C. 1993) moved away from defining a radial clearance and simply defined

$$F_{\sin} = 2.55 (E I W_e^2)^{1/3} \quad \text{Equation 46}$$

This practice for calculating initial (sinusoidal) buckling developed into helical buckling estimates.

$$F_{hel} = 5.55 (E I W_e^2)^{1/3} \quad \text{Equation 47}$$

The top of the helical buckled pipe was found by finding the force just for the first buckle to find the length of the bucked section short of the length reduced or supported by the buckling,

$$F_{hel,t} = 5.55 (E I W_e^2)^{1/3} - W_e L_{hel} \quad \text{Equation 48}$$

$$F_{hel,t} = 0.14 (E I W_e^2)^{1/3} \quad \text{Equation 49}$$

The length of the initial “helix” is then found to be

$$L_{hel} = (16\pi^2 EI / W_e^2)^{1/3} \quad \text{Equation 50}$$

The significance of all of this is that the top of the helical buckling load is very close to zero, this supports the use of the “buckling neutral point” (the place where effective axial load is zero) could be used to define the top of a section for potential helical buckling. The implication here is that potentially the entire compression section of the BHA is subject to helical buckling.

Actually, some general consensus has arrived as to the onset of sinusoidal buckling in straight wells, the same should not be said about helical buckling. Using a coefficient (λ) to the sinusoidal buckling equation, some authors have found values between 2.83 and 5.65.

$$F_{hel} = \lambda(E I W_e \sin(\alpha) / r)^{0.5} \quad \text{Equation 51}$$

Menard et al. 2008 suggests that the 2.83 is the onset of the helix, and 5.65 is coefficient to the load of a full helical drill string. These authors also found that the helical buckling load of a rotating member is about half of the value for the member not rotating, and that down hole dynamics such as snaking (lateral motion in the bottom of the wellbore) and backward whirl may occur as a result of buckling.

Calculations

For the calculations on the experimental systems buckling the following values were used (Table 6) and results found (Table 7)

Table 6. Values used for Buckling Calculation

Term	Value	Units
Tube outer diameter	4	Inch (in)
Tube inner diameter	1.6	Inch (in)
Tube Length	60	Inch (in)
Young's modulus (E)	203*	Pounds per square inch (psi)
Poisson's Ratio	0.03	
Density	1.81*	Pounds per square foot
	*approximate from experiment	

Table 7. Buckling Calculation Results

Method	Value	Units
Euler Buckling pin /pin	6.848	Pounds force
Euler Buckling fixed / free	1.712	Pounds force
Wu (1993)	1.717	Pounds force
Ansys(TM) (linear buckle pin /pin)	6.732	Pounds force
Ansys(TM) (linear buckle fixed /free)	1.696	Pounds force

It is notable that Euler fixed/free solution is less than 0.3% different to the Wu (1993) solution.

Dynamic buckling

Another category of buckling called dynamic buckling, where an axial impact force creates loads via a shock wave effect that momentarily buckles the column is also known. This shockwave is also known as a stress wave travels down and back up the column. (Lindberg 1987)



Equation 52

Where σ is the impact stress,
 L is the length of the rod,
 c is the elastic wave speed,
 h is the smaller lateral dimension of a rectangular rod.

Torsion

The drill string transmits torque to the drill bit through the BHA. The drill collars in the BHA are significantly shorter, and stiffer than the drill pipe, however the possibility of torsion effects in the BHA's

drill collars remains. The simplest form of a torsion effect may be the increased stresses influence on deflection and buckling. (Menand, Sellami et al. 2006) (Menand, Sellami et al. 2008) (Menand, Sellami et al. 2006) (Menand, Sellami et al. 2009) From a dynamics perspective the torsion spring or pendulum may be simpler. A similar phenomena to dynamic buckling may also occur in torsion although it will not be discussed in this section as an isolated phenomena.

Torsional Effects on Buckling

Rotation and torsion have been shown to reduce the threshold at which a member will buckle.

Torsional Spring Pendulum

As long as torsional springs are not turned past their elastic limit they obey an angular form of Hooke's Law.

 Equation 53

The torsional pendulum is analogous to the spring mass oscillator. This will be detailed more in the next section on resonance, with a description of the simple harmonic oscillator. That is the general equation of motion is:

 Equation 54

In cases where damping is small,

 Equation 55

As in the case of a pendulum. The frequency of vibration is near the natural resonate frequency.

 Equation 56

The general solution to this system with no driving force, called the transient solution is,

 Equation 57

Where

$$\omega = \sqrt{\omega_n^2 - \alpha^2} = \sqrt{\omega_n^2 - (\sigma/2I)^2}$$

Equation 58

Definition of terms

Term	Unit	Definition
θ	radians	Angle of deflection from rest position
I	kg m^2	Moment of inertia
c	$\text{kg m}^2/\text{s}$	Rotational friction (damping)
σ	N m	Coefficient of torsion spring
T	N m	Drive torque
ω_n	Hz	Undamped (or natural) resonant frequency
ω_{un}	rad/s	Undamped resonant frequency in radians
ω_d	Hz	Damped resonant frequency
ω_{dn}	rad/s	Damped resonant frequency in radians
τ	s	Reciprocal of damping time constant
ϕ	rad	Phase angle of oscillation
r	m	Distance from axis to where force is applied

Resonance Behaviors

Having touched on torsional resonance in the last section, preventing resonance designs and behaviors, lateral, axial, or torsional are usually the first thing that comes to mind in mitigating BHA vibration. The concept around critical speed identification is popular in industry, and its software workflows.⁵ Industry has identified critical speed avoidance as instrumental in avoiding damaging vibration. It is this authors opinion that: Industry perhaps believes that most BHA's avoid harmful vibration by design, however maybe subject to rotation speeds or bit excitation that is more harmful than another. The discussion of resonance will explore what supports such notions, and how such notions perhaps should be specific to particular systems.

Galileo recognized resonance in pendulums and musical strings, the behavior occurs with all types of vibration and waves. Resonance is simply the tendency of a system to oscillate at a greater amplitude

⁵ Based on industry software like WellPlan critical speed, APS welldrill critical speed, scan drill critical speed identifier.

depending on the frequency. At a resonant frequency the system can have a large amplitude of vibration with even small driving forces, as the system stores and constructs vibration energy. When a system can easily exchange energy between ‘types of energy analogies’ (from potential energy to kinetic energy, or from mechanical energy to kinetic energy to impact) resonance is likely to occur. For example as a pendulum swings its potential energy from the top of the swing converts to kinetic energy until the bottom of the swing and then begins converting back to potential as the pendulum rises. However, some losses occur in the system, the losses create a damping effect.

A physical system is said to have degrees of freedom (a set off independent displacements, rotations, or deformations, that completely describe the position and orientation of the system), and for each degree of freedom, a resonant frequency may exist. In this sense, pendulums, torsional pendulums, and other single degree of freedom systems have a single resonance frequency. A system such as continuously described deforming beam, column or rod, may have an infinite number of degrees of freedom, and possibly an infinite number of resonance frequencies.

This situation is not as dire as it might seem having potentially infinite critical frequencies. The natural frequencies in such systems will be harmonics (an integer multiple) of the fundamental frequency (the first natural frequency). The behaviors of such systems near the critical frequencies will also depending on the degree of damping in the system. One model is the viscous damping model. In this model the damping force is a result of a damping constant multiplied by the system’s velocity. The spring force is a result of a spring constant multiplied by the system’s position, while the mass is the coefficient of acceleration when calculating force. If the coefficients are arranged this system can be written as:

$$m\ddot{x} = -c\dot{x} - kx \quad \text{Equation 59}$$

$$F = m\ddot{x} + c\dot{x} + kx \quad \text{Equation 60}$$

Where

F is the force

m is the mass

x is displacement with the dots being derivatives, velocity and acceleration.

k is the spring constant
and c is the damping constant (Greenwood 1965)

The viscous damping model is just one of many models used to describe vibration. The ‘structural damping model’ or ‘hysteretic model’ is often better used to describe the internal damping of a material. In this type of model the damping force is proportional to the displacement but in phase with the velocity.

Returning to under-damped systems again, let us introduce a concept of tuning, or quality to the resonance. A more tuned or higher quality system losses less energy at the resonance frequency. A driven system that is ‘tuned’ will have greater amplitudes of vibration but tighter and smaller range of frequencies that to achieve resonance.

Rotor dynamic Behaviors

The mathematics of rotors includes two more terms. The first is a gyroscopic effect that couples rotational degrees of freedom to a spinning axis. This is typically written as G. The second term modifies apparent stiffness depending on rotational velocity. This term can produce unstable motion. Typically it will be written as B. Taking the previous equation and writing in a matrix form we have:

Including the new terms:

$$[\mathbf{M}]\{\ddot{\mathbf{u}}\} + ([\mathbf{C}] + [\mathbf{G}])\{\dot{\mathbf{u}}\} + ([\mathbf{K}] + [\mathbf{B}])\{\mathbf{u}\} = \{\mathbf{f}\}$$

Notice that the terms now need to be in matrix notation.

The gyroscopic effect may be represented with a skew symmetric matrix that couples the degrees of freedom on the planes perpendicular to the spin axis depending on the rotational velocity. It can be written:

$$[\mathbf{M}]\{\ddot{\mathbf{q}}\} + \Omega[\mathbf{G}]\{\dot{\mathbf{q}}\} + [\mathbf{K}]\{\mathbf{q}\} = \mathbf{0} \text{ Equation 61}$$

$$[\mathbf{G}] = \begin{bmatrix} 0 & 0 & 0 & 0 & 0 \\ 0 & \ddots & \ddots & \ddots & \vdots \\ 0 & \ddots & 0 & 0 & 0 \\ 0 & \ddots & 0 & 0 & I_p \\ 0 & \dots & 0 & -I_p & 0 \end{bmatrix} \text{ Equation 62}$$

Where the polar moment, negative polar moment goes in the position of the relevant mass elements.

Determining the whirling behaviors is an eigenvalue problem. This type of linear algebra challenge can be addressed in a number of ways, numerical methods, mathematical framework softwares, and fit for purpose solutions. In the case of this study a fit for purpose solution was employed that included not only an eigenvalue solver but tools to assist in forming the problem in the form of a commercial finite element modeling package.

APPENDIX V: ADDITIONAL RESULTS

Numerical Model of Response

Simple numerical models of the response were created. The objective of this type of model is not to emulate sophisticated BHA models, but to provide a go by for future research or to equip operations personal with concepts to make better decisions when more sophisticated models are unavailable, or simply perhaps more than necessary for the potential impact of the situation. Information in the Appendix III and V is provided to assist this future effort.

The axial load limit for the given displacement thrust was previously introduced. Shaft C had an unusual response with little decline, perhaps because of having two centralization points. Taking the average of the other three a decline of 0.0012 lbs. per RPM might be expected. This should not be surprising as the effective length of the system is being reduced by the deflection of the whirling shaft. Accepting the scaling factor of 53,174 for an 8 inch equivalent system, that would only be a loss of about 65 lbs. per RPM. This may be a moot point for an actual drilling rig operated by a brake handle because the drilling is slacking off weight, not typically inputting a linear feed rate. In a time drill operation this correction could be looked into further if RPM changes in the operation are taking place. It was not established in this study what the perceived surface loads would be.

If one were to compare these results to a simple model such as that presented by Wauer (Wauer 1982) then one could infer that this system is in the region 2/region 3 boundary where internal damping is smaller than external damping. This insight may open the door for a method to qualify damping factors in field systems. When one is at a static buckling point does rotation extend or diminish the load capability before buckling?

Numerical Model of Torsional Vibration for Experimental Fixture.

A function describing the relationship between input rotation speed and measured torsional vibration measurements may be made.(Table 8) Where n is the rotation speed in RPM. (useable when RPM <500 and axial load is under the axial load limit)

Table 8. Torsional Vibration Modeled vs. Rotation Speed.

A	$a_{\theta} = 0.003n + .143$	$R^2=0.504$
B	$a_{\theta} = -4 \times 10^{-08}n^3 + 3 \times 10^{-05}n^2 - 0.0035n - 0.1065$	$R^2=0.871$
C	$a_{\theta} = -7 \times 10^{-08}n^3 + 6 \times 10^{-05}n^2 - 0.0034n + 0.086$	$R^2=0.928$
D	$a_{\theta} = -7 \times 10^{-08}n^3 + 6 \times 10^{-05}n^2 - 0.0037n + 0.1449$	$R^2=0.843$

In this type of case it is not suggested that one would or could try to use this information in the field while drilling because the experiment, by design and hence the results, neglected to include a cutting structure effects.

Numerical Model of Transverse (Lateral) Vibration for Experimental Fixture.

Aldred and Sheppard (1992) suggest the relationship between rotary speed and transverse acceleration is monotonic increasing with no evidence of resonant structure using data from Vandiver et al. (Case studies of bending vibrations and whirling motion of drill collars. SPEDE Dec. 1990 p.282-290.)

Figure 85 shows a plot of overlaying the results and trends from this study.

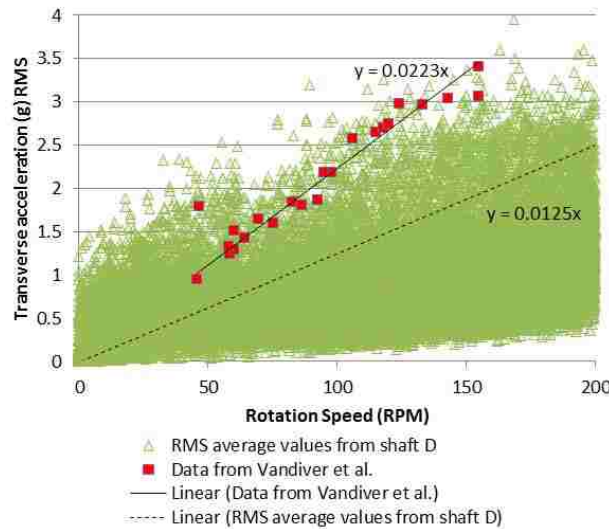


Figure 85. Rotation speed vs. acceleration comparison: The trend of the RMS values from Vandiver et al. is almost double in magnitude of the found in this study, with slopes of 0.0125 in this study vs. 0.0223 from the reference data.

Observations on Free Vibration Tests

The free vibration test was not achievable for the entire range of parameters. Rotation speed much above 300 RPM caused the shaft to cantilever out of the base constraint. This fact combined with the threshold response observed in the successful tests showed that above a rotation speed of about 250 RPM the Shafts without constraint experienced resonance. Perhaps the most important thing that can be gleaned from this series of tests is that a definite threshold existed where before a certain rotation speed the shaft was whirling with a degree of angular velocity flux, and after it was vibrating at a higher mode, and the angular velocity oscillations reduced.

Observations on Vibration Response Surface Analysis

The response surface method revealed that each shaft geometry had a unique bound on the maximum average response for vibration. The occurrence of banding in the response is in line with predictions made by commercial numerical models. Figure 86 takes shaft A's plots for vibration and stick-slip side by side for sake of discussion. The heavy grey line divides each plot into two regions, one region dominated with elevated vibration another by qualifying stick-slip responses.

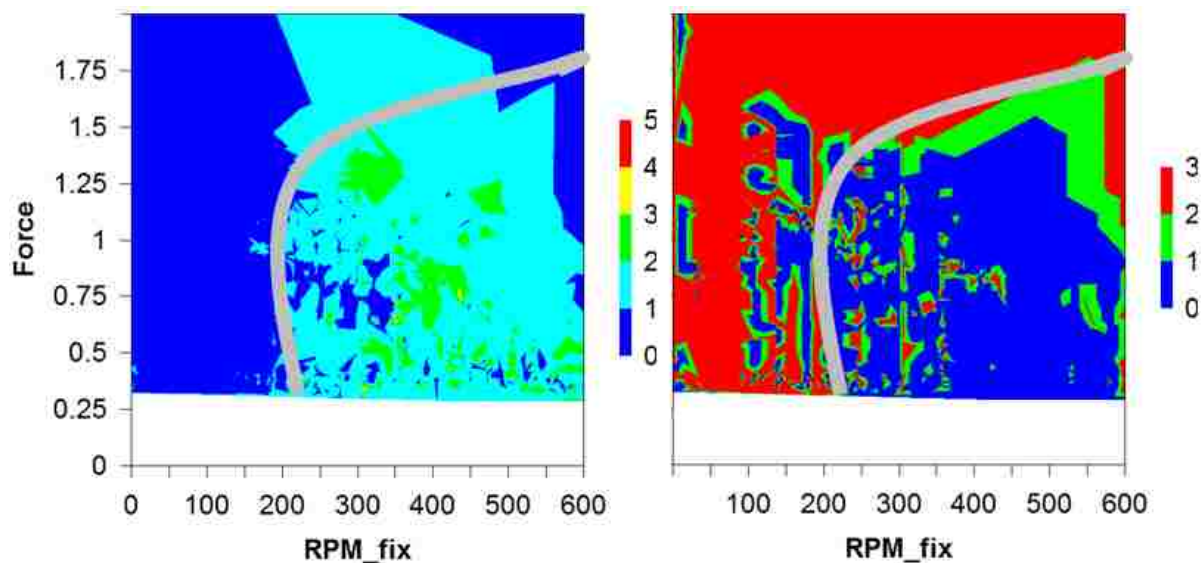


Figure 86. Shaft A torsional vibration and stick-slip. For shaft A, looking side by side, notice the grey curved as a suggested boundary between the region with elevated stick-slip and elevated vibration.

Figure 87 like the previous figure is a composite of two figures with an added suggested boundary line. This line is simply a visual indicator for discussion unlike the axial load boundary that was a measured value. In this case the boundary suggested is a straight line and not a curve. The suggestion here clearly is that in regions dominated by vibration, stick-slip is uncommon and vice versa.

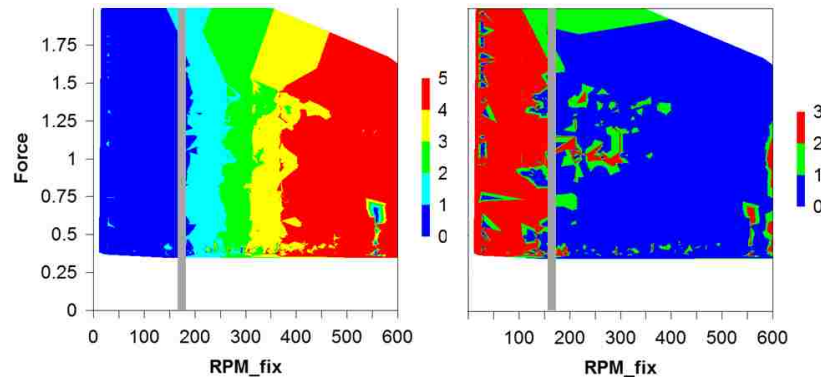


Figure 87. Shaft D torsional vibration and stick-slip. For shaft D, looking at the figures side by side, notice the grey curved as a suggested boundary between the region with elevated stick-slip and elevated vibration.

Figure 88 is again the plots of the torsional vibration region and the qualified stick-slip response. Following the hypothesis that one can make a division between the occurrence of vibration and stick-slip does not look effective here. A suggested bound of qualifying stick-slip events overlaid on the vibration response does not seem to be solely inclusive or exclusive. However one could make the argument that the stick-slip is not “dominating the region” it is simply occurring as a banded behavior.

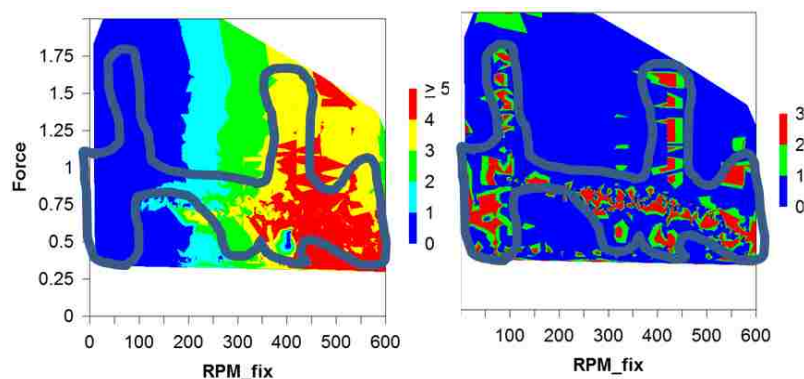


Figure 88. Shaft C torsional vibration and stick-slip. For shaft C, looking at the figures side by side, notice the grey curved as a suggested boundary between the region with elevated stick-slip, however it does not fit to well as an exclusion of elevated vibration.

The test battery shows the similarities and distinction of each configuration. Figure 46 shows a summary of the previous surface response figures. The patterns of the regions emerge clearly, and what stands out specifically, if one were to use the diagnosis of stick-slip behaviors using acceleration measured difference in torsional acceleration and radial acceleration instead of a direct angular measure, misdiagnosis would seem inevitable. In this study it seems this may largely be due to the lower magnitude of the average recorded radial position accelerations. For that matter, the tiny gyro used was a video game controller performed. Industry should take note and consider using this type of equipment, if not for survey, perhaps simply for an additional down hole measure of rotation speed that is not dependent on magnetometers.

The parameter maps for whirl and some for stick-slip too, did not have the anticipated curve to them as they do in the only other dual dysfunction (whirl and stick-slip in compatible frame work) model. Dunayevsky and Abbassian (1998) attributes this character to a term called torque decay. This factor could be present in the bit or the drill string in measures not achievable by the shaft only model. Alternatively, skillfully building a realistic torque decay function into a motor controller could be an option for further research, however arriving at a direct measure of that value from the field seems elusive with conventional measurement.

The following are the report results from selected Ansys™ runs.

APPENDIX VI: ANSYS™ REPORTS



Project

First Saved	Monday, October 29, 2012
Last Saved	Friday, November 09, 2012
Product Version	14.0 Release
Save Project Before Solution	No
Save Project After Solution	No



Contents

- [Units](#)
- [Model \(A4, B4\)](#)
 - [Geometry](#)
 - [Solid](#)
 - [Point Mass](#)
 - [Coordinate Systems](#)
 - [Connections](#)
 - [Joints](#)
 - [Fixed - Ground To Solid](#)
 - [Springs](#)
 - [Mesh](#)
 - [Named Selections](#)
 - [Static Structural \(A5\)](#)
 - [Analysis Settings](#)
 - [Force](#)
 - [Solution \(A6\)](#)
 - [Solution Information](#)
 - [Results](#)
 - [Modal 2 \(B5\)](#)
 - [Pre-Stress \(Static Structural\)](#)
 - [Analysis Settings](#)
 - [Rotational Velocity](#)
 - [Solution \(B6\)](#)
 - [Solution Information](#)
 - [Results](#)
 - [Campbell Diagram](#)
- [Material Data](#)
 - [Iifoam](#)

Units

TABLE 1

Unit System	U.S. Customary (in, lbm, lbf, s, V, A) Degrees RPM Fahrenheit
Angle	Degrees
Rotational Velocity	RPM
Temperature	Fahrenheit

Model (A4, B4)

Geometry

TABLE 2
Model (A4, B4) > Geometry

Object Name	Geometry
State	Fully Defined
Definition	
Source	C:\Users\vdiz\Desktop\shaft a final_files\dp0\SYSDMSYS.agdb
Type	DesignModeler
Length Unit	Inches
Element Control	Program Controlled
Display Style	Body Color
Bounding Box	
Length X	3.502 in
Length Y	3.502 in
Length Z	57.25 in
Properties	
Volume	522.08 in ³
Mass	0.84697 lbm
Scale Factor Value	1.
Statistics	
Bodies	1
Active Bodies	1
Nodes	32279
Elements	20561
Mesh Metric	None
Basic Geometry Options	
Parameters	Yes
Parameter Key	DS
Attributes	No
Named Selections	No
Material Properties	No
Advanced Geometry Options	
Use Associativity	Yes
Coordinate Systems	No

Reader Mode Saves Updated File	No
Use Instances	Yes
Smart CAD Update	No
Attach File Via Temp File	Yes
Temporary Directory	C:\Users\vdiz\AppData\Local\Temp
Analysis Type	3-D
Decompose Disjoint Faces	Yes
Enclosure and Symmetry Processing	Yes

TABLE 3
Model (A4, B4) > Geometry > Parts

Object Name	<i>Solid</i>
State	Meshed
Graphics Properties	
Visible	Yes
Glow	0.4
Shininess	0.6
Transparency	1
Specularity	0.8
Definition	
Suppressed	No
ID (Beta)	16
Stiffness Behavior	Flexible
Coordinate System	Default Coordinate System
Reference Temperature	By Environment
Material	
Assignment	lifoam
Nonlinear Effects	Yes
Thermal Strain Effects	Yes
Bounding Box	
Length X	3.502 in
Length Y	3.502 in
Length Z	57.25 in
Properties	
Volume	522.08 in ³
Mass	0.54697 lbm
Centroid X	-8.5495e-018 in
Centroid Y	3.0387e-017 in
Centroid Z	-3.4198e-018 in
Moment of Inertia Ip1	149.07 lbm·in ²
Moment of Inertia Ip2	149.07 lbm·in ²
Moment of Inertia Ip3	0.87247 lbm·in ²
Statistics	
Nodes	32279
Elements	20561
Mesh Metric	None

TABLE 4
Model (A4, B4) > Geometry > Point Masses

Object Name	<i>Point Mass</i>
State	Fully Defined
Scope	
Scoping Method	Geometry Selection
Geometry	1 Face
Coordinate System	Global Coordinate System
X Coordinate	0. in
Y Coordinate	0.8 in
Z Coordinate	0. in
Location	Defined
Definition	
Mass	0.3 lbm
Mass Moment of Inertia X	0. lbm·in ²
Mass Moment of Inertia Y	0. lbm·in ²
Mass Moment of Inertia Z	0. lbm·in ²
Suppressed	No
Behavior	Deformable
Pinball Region	All

Coordinate Systems

TABLE 5
Model (A4, B4) > Coordinate Systems > Coordinate System

Object Name	<i>Global Coordinate System</i>
State	Fully Defined
Definition	
Type	Cartesian
Coordinate System ID	0.
Origin	
Origin X	0. in
Origin Y	0. in
Origin Z	0. in

Connections

Directional Vectors	
X Axis Data	[1. 0. 0.]
Y Axis Data	[0. 1. 0.]
Z Axis Data	[0. 0. 1.]

TABLE 6
Model (A4, B4) > Connections

Object Name	Connections
State	Fully Defined
Auto Detection	
Generate Automatic Connection On Refresh	Yes
Transparency	
Enabled	Yes

TABLE 7
Model (A4, B4) > Connections > Joints

Object Name	Joints
State	Fully Defined
Definition	
Connection Type	Joint
Scope	
Scoping Method	Geometry Selection
Geometry	All Bodies
Auto Detection	
Tolerance Type	Slider
Tolerance Slider	0.
Tolerance Value	0.14366 in
Use Range	No
Group By	Bodies
Search Across	Bodies
Fixed Joints	No
Revolute Joints	No

TABLE 8
Model (A4, B4) > Connections > Joints > Joints

Object Name	Fixed - Ground To Solid
State	Fully Defined
Definition	
Connection Type	Body-Ground
Type	Fixed
Suppressed	No
Reference	
Coordinate System	Reference Coordinate System
Mobile	
Scoping Method	Geometry Selection
Scope	1 Face
Body	Solid
Initial Position	Unchanged
Behavior	Deformable
Pinball Region	All

TABLE 9
Model (A4, B4) > Connections > Springs

Object Name	Longitudinal - Ground To Solid		Longitudinal - Ground To Solid	Longitudinal - Ground To Solid
State	Suppressed		Fully Defined	Suppressed
Graphics Properties				
Visible	Yes		No	Yes
Definition				
Type	Longitudinal			
Spring Behavior	Both (Linear)			
Longitudinal Stiffness	100. lbf/in		1.e+007 lbf/in	
Longitudinal Damping	0. lbf·s/in			
Preload	None			
Suppressed	Yes		No	Yes
Spring Length	5. in			
Scope				
Scope	Body-Ground			
Reference				
Scoping Method	Geometry Selection			
Coordinate System	Global Coordinate System			
Reference X Coordinate	0. in			
Reference Y Coordinate	5. in			
Reference Z Coordinate	10. in		28.625 in	-10. in
Reference Location	Defined			
Behavior	Rigid			
Pinball Region	All			
Mobile				
Scoping Method	Geometry Selection			
Scope	1 Face			

Body	Solid		
Coordinate System	Global Coordinate System		
Mobile X Coordinate	0. in	-6.1188e-017 in	0. in
Mobile Y Coordinate	-1.7984e-016 in	3.633e-017 in	-1.7984e-016 in
Mobile Z Coordinate	10. in	28.625 in	-10. in
Mobile Location	Defined		
Behavior	Deformable	Rigid	
Pinball Region	All		

TABLE 10
Model (A4, B4) > Connections > Longitudinal - Ground To Solid > Command Snippet

Object Name	Commands (APDL)
State	Suppressed
File	
File Name	
File Status	File not found
Definition	
Suppressed	No
Target	Mechanical APDL
Input Arguments	
ARG1	100.
ARG2	100.
ARG3	100.
ARG4	100.
ARG5	
ARG6	
ARG7	
ARG8	
ARG9	

Model (A4, B4) > Connections > Longitudinal - Ground To Solid > Commands (APDL)

```
! Commands inserted into this file will be executed just after the spring definition.
! The material, type, and real number for this spring is equal to the parameter "_sid".
! Active UNIT system in Workbench when this object was created: U.S. Customary (in, lbm, lbf, s, V, A) temperature units of F
!arg1=Kxx, arg2=Kyy arg3=Kxy agr4=Kyx arg5=Cxx arg6=Cyy arg7=Cxy arg8=Cyx
!By default the bearing element is symmetric means Kxy=Kyx and Cxy=Cyx

et,_sid, 214
keyopt,_sid, 2,0 !keyopt(2)=0 means in xy plane
!keyopt,_sid, 3,1 !Use keyopt(3)=1 if the element is non symmetric
r,_sid,arg1,arg2,arg3,arg4,arg5,arg6
rmore,arg7,arg8
```

TABLE 11
Model (A4, B4) > Connections > Longitudinal - Ground To Solid > Command Snippet

Object Name	Commands (APDL)
State	Fully Defined
File	
File Name	
File Status	File not found
Definition	
Suppressed	No
Target	Mechanical APDL
Input Arguments	
ARG1	100.
ARG2	100.
ARG3	100.
ARG4	100.
ARG5	
ARG6	
ARG7	
ARG8	
ARG9	

Model (A4, B4) > Connections > Longitudinal - Ground To Solid > Commands (APDL)

```
! Commands inserted into this file will be executed just after the spring definition.
! The material, type, and real number for this spring is equal to the parameter "_sid".
! Active UNIT system in Workbench when this object was created: U.S. Customary (in, lbm, lbf, s, V, A) temperature units of F
!arg1=Kxx, arg2=Kyy arg3=Kxy agr4=Kyx arg5=Cxx arg6=Cyy arg7=Cxy arg8=Cyx
!By default the bearing element is symmetric means Kxy=Kyx and Cxy=Cyx

et,_sid, 214
keyopt,_sid, 2,0 !keyopt(2)=0 means in xy plane
!keyopt,_sid, 3,1 !Use keyopt(3)=1 if the element is non symmetric
r,_sid,arg1,arg2,arg3,arg4,arg5,arg6
rmore,arg7,arg8
```

TABLE 12
Model (A4, B4) > Connections > Longitudinal - Ground To Solid > Command Snippet

Object Name	Commands (APDL)
State	Suppressed

File	
File Name	
File Status	File not found
Definition	
Suppressed	No
Target	Mechanical APDL
Input Arguments	
ARG1	100.
ARG2	100.
ARG3	100.
ARG4	100.
ARG5	
ARG6	
ARG7	
ARG8	
ARG9	

Model (A4, B4) > Connections > Longitudinal - Ground To Solid > Commands (APDL)

```

! Commands inserted into this file will be executed just after the spring definition.
! The material, type, and real number for this spring is equal to the parameter " _sid".
! Active UNIT system in Workbench when this object was created: U.S. Customary (in, lbm, lbf, s, V, A) temperature units of F
!arg1=Kxx, arg2=Kyy arg3=Kxy agr4=Kyx arg5=Cxx arg6=Cyy arg7=Cxy arg8=Cyx
!By default the bearing element is symmetric means Kxy=Kyx and Cxy=Cyx

et,_sid,214
keyopt,_sid,2,0 !keyopt(2)=0 means in xy plane
!keyopt,_sid,3,1 !Use keyopt(3)=1 if the element is non symmetric
r,_sid,arg1,arg2,arg3,arg4,arg5,arg6
rmore,arg7,arg8

```

Mesh

TABLE 13
Model (A4, B4) > Mesh

Object Name	<i>Mesh</i>
State	Solved
Defaults	
Physics Preference	Mechanical
Relevance	40
Sizing	
Use Advanced Size Function	Off
Relevance Center	Coarse
Element Size	Default
Initial Size Seed	Active Assembly
Smoothing	High
Transition	Fast
Span Angle Center	Medium
Minimum Edge Length	2.51330 in
Inflation	
Use Automatic Inflation	None
Inflation Option	Smooth Transition
Transition Ratio	0.272
Maximum Layers	5
Growth Rate	1.2
Inflation Algorithm	Pre
View Advanced Options	No
Patch Conforming Options	
Triangle Surface Mesher	Program Controlled
Advanced	
Shape Checking	Standard Mechanical
Element Midside Nodes	Program Controlled
Straight Sided Elements	No
Number of Retries	0
Extra Retries For Assembly	Yes
Rigid Body Behavior	Dimensionally Reduced
Mesh Morphing	Disabled
Defeaturing	
Pinch Tolerance	Please Define
Generate Pinch on Refresh	No
Automatic Mesh Based Defeaturing	On
Defeaturing Tolerance	Default
Statistics	
Nodes	32279
Elements	20561
Mesh Metric	None

Named Selections

Static Structural (A5)

TABLE 14
Model (A4, B4) > Analysis

Object Name	Static Structural (A5)
State	Solved
Definition	
Physics Type	Structural
Analysis Type	Static Structural
Solver Target	Mechanical APDL
Options	
Environment Temperature	71.6 °F
Generate Input Only	No

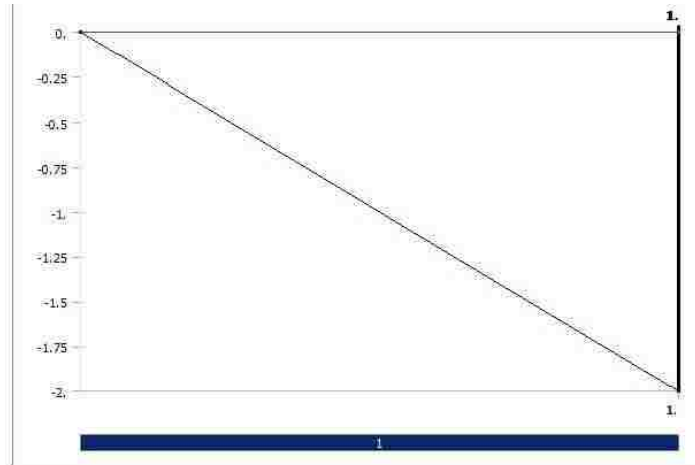
TABLE 15
Model (A4, B4) > Static Structural (A5) > Analysis Settings

Object Name	Analysis Settings
State	Fully Defined
Restart Analysis	
Restart Type	Program Controlled
Status	Done
Step Controls	
Number Of Steps	1.
Current Step Number	1.
Step End Time	1. s
Auto Time Stepping	Program Controlled
Solver Controls	
Solver Type	Program Controlled
Weak Springs	Program Controlled
Large Deflection	Off
Inertia Relief	Off
Restart Controls	
Generate Restart Points	Program Controlled
Retain Files After Full Solve	Yes
Nonlinear Controls	
Force Convergence	Program Controlled
Moment Convergence	Program Controlled
Displacement Convergence	Program Controlled
Rotation Convergence	Program Controlled
Line Search	Program Controlled
Stabilization	Off
Output Controls	
Stress	Yes
Strain	Yes
Nodal Forces	No
Contact Miscellaneous	No
General Miscellaneous	No
Calculate Results At	All Time Points
Cache Results in Memory (Beta)	Never
Max Number of Result Sets	Program Controlled
Analysis Data Management	
Solver Files Directory	C:\Users\rdlz\Desktop\shaft a final_files\dp0\SYSTEMECHAN
Future Analysis	Prestressed analysis
Scratch Solver Files Directory	
Save MAPDL db	No
Delete Unneeded Files	Yes
Nonlinear Solution	No
Solver Units	Active System
Solver Unit System	Bin

TABLE 16
Model (A4, B4) > Static Structural (A5) > Loads

Object Name	Force
State	Fully Defined
Scope	
Scoping Method	Geometry Selection
Geometry	1 Face
Definition	
ID (Beta)	158
Type	Force
Define By	Components
Coordinate System	Global Coordinate System
X Component	0. lbf (ramped)
Y Component	0. lbf (ramped)
Z Component	-2. lbf (ramped)
Suppressed	No

FIGURE 1
Model (A4, B4) > Static Structural (A5) > Force



Solution (A6)

TABLE 17
Model (A4, B4) > Static Structural (A5) > Solution

Object Name	Solution (A6)
State	Solved
Adaptive Mesh Refinement	
Max Refinement Loops	3
Refinement Depth	2
Information	
Status	Done

TABLE 18
Model (A4, B4) > Static Structural (A5) > Solution (A6) > Solution Information

Object Name	Solution Information
State	Solved
Solution Information	
Solution Output	Solver Output
Newton-Raphson Residuals	0
Update Interval	2.5 s
Display Points	All
FE Connection Visibility	
Activate Visibility	Yes
Display	All FE Connectors
Draw Connections Attached To	All Nodes
Line Color	Connection Type
Visible on Results	No
Line Thickness	Single
Display Type	Lines

TABLE 19
Model (A4, B4) > Static Structural (A5) > Solution (A6) > Results

Object Name			Directional Deformation	Normal Stress
State		Solved		
Scope				
Scoping Method		Geometry Selection		
Geometry		All Bodies		
Definition				
Type		Directional Deformation	Normal Stress	
Orientation		X Axis	Z Axis	
By		Time		
Display Time		Last		
Coordinate System		Global Coordinate System		
Calculate Time History		Yes		
Identifier				
Suppressed		No		
Results				
Minimum		-8.0791e-005 in	-0.22232 psi	
Maximum		9.5799e-005 in	-0.21515 psi	
Information				
Time		1 s		
Load Step		1		
Substep		1		
Iteration Number		1		
Integration Point Results				
Display Option			Averaged	

Modal 2 (B5)

TABLE 20
Model (A4, B4) > Analysis

Object Name	<i>Modal 2 (B5)</i>
State	Solved
Definition	
Physics Type	Structural
Analysis Type	Modal
Solver Target	Mechanical APDL
Options	
Generate Input Only	No

TABLE 21
Model (A4, B4) > Modal 2 (B5) > Initial Condition

Object Name	<i>Pre-Stress (Static Structural)</i>
State	Fully Defined
Definition	
Pre-Stress Environment	Static Structural
Pre-Stress Define By	Program Controlled
Reported Loadstep	Last
Reported Substep	Last
Reported Time	End Time
Contact Status	Use True Status

TABLE 22
Model (A4, B4) > Modal 2 (B5) > Analysis Settings

Object Name	<i>Analysis Settings</i>
State	Fully Defined
Options	
Max Modes to Find	6
Limit Search to Range	No
Solver Controls	
Damped	Yes
Solver Type	Full Damped
Rotordynamics Controls	
Coriolis Effect	On
Campbell Diagram	On
Number of Points	2
Output Controls	
Stress	No
Strain	No
Nodal Forces	No
Calculate Reactions	No
General Miscellaneous	No
Cache Results in Memory (Beta)	Never
Damping Controls	
Stiffness Coefficient Define By	Direct Input
Stiffness Coefficient	0.
Mass Coefficient	0.
Analysis Data Management	
Solver Files Directory	C:\Users\rdz\Desktop\shaft a final_files\dp0\SYS-2\MECH\
Future Analysis	None
Scratch Solver Files Directory	
Save MAPDL db	No
Delete Unneeded Files	Yes
Solver Units	Active System
Solver Unit System	Bin

TABLE 23
Model (A4, B4) > Modal 2 (B5) > Rotations

Object Name	<i>Rotational Velocity</i>
State	Fully Defined
Scope	
Scoping Method	Geometry Selection
Geometry	All Bodies
Definition	
Define By	Vector
Magnitude	Tabular Data
Axis	Defined
Suppressed	No

TABLE 24
Model (A4, B4) > Modal 2 (B5) > Rotational Velocity

Points	Rotational Velocity [rpm]
1	5.
2	1000.

Solution (B6)

TABLE 25

Model (A4, B4) > Modal 2 (B5) > Solution	
Object Name	Solution (B6)
State	Solved
Adaptive Mesh Refinement	
Max Refinement Loops	1.
Refinement Depth	2.
Information	
Status	Done

The following bar chart indicates the frequency at each calculated mode.

FIGURE 2
Model (A4, B4) > Modal 2 (B5) > Solution (B6)

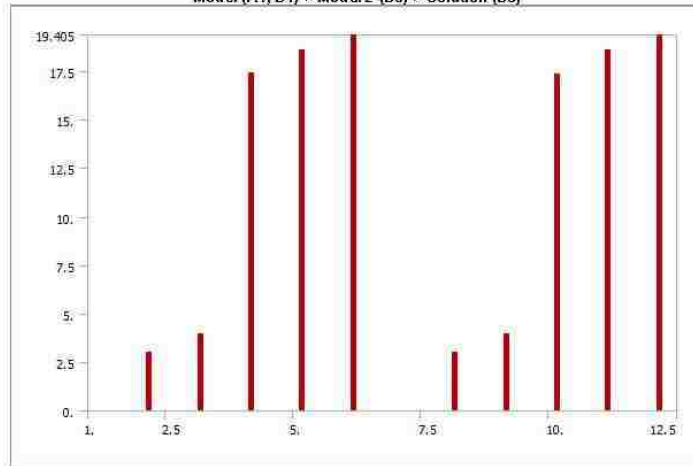


TABLE 26
Model (A4, B4) > Modal 2 (B5) > Solution (B6)

Set	Solve Point	Mode	Damped Frequency [Hz]	Stability [Hz]	Modal Damping Ratio
1		1.	0.	-1.2059	N/A
2.		2.	3.055	-7.6074e-014	2.4902e-014
3.		3.	3.9712	1.4005e-013	-3.5268e-014
4.		4.	17.415	-2.4594e-013	1.4122e-014
5.		5.	18.609	-3.7798e-013	2.0312e-014
6.		6.	19.399	2.776e-013	-1.431e-014
7.		1.	0.	-1.2059	N/A
8.		2.	3.0543	2.6955e-013	-8.8254e-014
9.		3.	3.972	3.5349e-013	-8.8995e-014
10.		4.	17.402	1.1549e-013	-6.6362e-015
11.		5.	18.612	2.6471e-013	-1.4222e-014
12.		6.	19.405	6.7526e-013	-3.4799e-014

TABLE 27
Model (A4, B4) > Modal 2 (B5) > Solution (B6) > Solution Information

Object Name	Solution Information
State	Solved
Solution Information	
Solution Output	Solver Output
Newton-Raphson Residuals	0
Update Interval	2.5 s
Display Points	All
FE Connection Visibility	
Activate Visibility	Yes
Display	All FE Connectors
Draw Connections Attached To	All Nodes
Line Color	Connection Type
Visible on Results	No
Line Thickness	Single
Display Type	Lines

TABLE 28
Model (A4, B4) > Modal 2 (B5) > Solution (B6) > Results

Model (4, 4) / Model 2 (3, 3) / Solution (60) / Results					
Object Name	Directional Deformation	Directional Deformation 2	Directional Deformation 3	Directional Deformation 4	Directional Deformation 5
State	Solved				
Scope					
Scoping Method	Geometry Selection				
Geometry	All Bodies				
Definition					
Type	Directional Deformation				
Orientation	X Axis				

Set Number	1.	2.	3.	4.	5.
Phase Angle	0. °				
Coordinate System	Global Coordinate System				
Identifier					
Suppressed	No				
Results					
Minimum	-1.8706e-003 in	-17.236 in	-13.485 in	-34.193 in	-47.492 in
Maximum	39.812 in	0.29203 in	30.608 in	21.669 in	12.512 in
Information					
Mode	1	2	3	4	5
Reported Frequency	0. Hz	3.055 Hz	3.9712 Hz	17.415 Hz	18.609 Hz
Reported Stability	-1.2059 Hz	-7.6074e-014 Hz	1.4005e-013 Hz	-2.4594e-013 Hz	-3.7798e-013 Hz
Reported Modal Damping Ratio	N/A	2.4902e-014	-3.5268e-014	1.4122e-014	2.0312e-014
Reported Logarithmic Decrement	N/A	-1.5646e-013	2.2159e-013	-8.8731e-014	-1.2763e-013

TABLE 29
Model (A4, B4) > Modal 2 (B5) > Solution (B6) > Directional Deformation

Set	Solve Point	Mode	Damped Frequency [Hz]	Stability [Hz]	Modal Damping Ratio
1.	1.	1.	0.	-1.2059	N/A
2.		2.	3.055	-7.6074e-014	2.4902e-014
3.		3.	3.9712	1.4005e-013	-3.5268e-014
4.		4.	17.415	-2.4594e-013	1.4122e-014
5.		5.	18.609	-3.7798e-013	2.0312e-014
6.		6.	19.399	2.776e-013	-1.431e-014
7.	2.	1.	0.	-1.2059	N/A
8.		2.	3.0543	2.6955e-013	-8.8254e-014
9.		3.	3.972	3.5349e-013	-8.8995e-014
10.		4.	17.402	1.1549e-013	-6.6362e-015
11.		5.	18.612	2.6471e-013	-1.4222e-014
12.		6.	19.405	6.7526e-013	-3.4799e-014

TABLE 30
Model (A4, B4) > Modal 2 (B5) > Solution (B6) > Directional Deformation 2

Set	Solve Point	Mode	Damped Frequency [Hz]	Stability [Hz]	Modal Damping Ratio
1.	1.	1.	0.	-1.2059	N/A
2.		2.	3.055	-7.6074e-014	2.4902e-014
3.		3.	3.9712	1.4005e-013	-3.5268e-014
4.		4.	17.415	-2.4594e-013	1.4122e-014
5.		5.	18.609	-3.7798e-013	2.0312e-014
6.		6.	19.399	2.776e-013	-1.431e-014
7.	2.	1.	0.	-1.2059	N/A
8.		2.	3.0543	2.6955e-013	-8.8254e-014
9.		3.	3.972	3.5349e-013	-8.8995e-014
10.		4.	17.402	1.1549e-013	-6.6362e-015
11.		5.	18.612	2.6471e-013	-1.4222e-014
12.		6.	19.405	6.7526e-013	-3.4799e-014

TABLE 31
Model (A4, B4) > Modal 2 (B5) > Solution (B6) > Directional Deformation 3

Set	Solve Point	Mode	Damped Frequency [Hz]	Stability [Hz]	Modal Damping Ratio
1.	1.	1.	0.	-1.2059	N/A
2.		2.	3.055	-7.6074e-014	2.4902e-014
3.		3.	3.9712	1.4005e-013	-3.5268e-014
4.		4.	17.415	-2.4594e-013	1.4122e-014
5.		5.	18.609	-3.7798e-013	2.0312e-014
6.		6.	19.399	2.776e-013	-1.431e-014
7.	2.	1.	0.	-1.2059	N/A
8.		2.	3.0543	2.6955e-013	-8.8254e-014
9.		3.	3.972	3.5349e-013	-8.8995e-014
10.		4.	17.402	1.1549e-013	-6.6362e-015
11.		5.	18.612	2.6471e-013	-1.4222e-014
12.		6.	19.405	6.7526e-013	-3.4799e-014

TABLE 32
Model (A4, B4) > Modal 2 (B5) > Solution (B6) > Directional Deformation 4

Set	Solve Point	Mode	Damped Frequency [Hz]	Stability [Hz]	Modal Damping Ratio
1.	1.	1.	0.	-1.2059	N/A
2.		2.	3.055	-7.6074e-014	2.4902e-014
3.		3.	3.9712	1.4005e-013	-3.5268e-014
4.		4.	17.415	-2.4594e-013	1.4122e-014
5.		5.	18.609	-3.7798e-013	2.0312e-014
6.		6.	19.399	2.776e-013	-1.431e-014
7.	2.	1.	0.	-1.2059	N/A
8.		2.	3.0543	2.6955e-013	-8.8254e-014
9.		3.	3.972	3.5349e-013	-8.8995e-014
10.		4.	17.402	1.1549e-013	-6.6362e-015
11.		5.	18.612	2.6471e-013	-1.4222e-014
12.		6.	19.405	6.7526e-013	-3.4799e-014

TABLE 33
Model (A4, B4) > Modal 2 (B5) > Solution (B6) > Directional Deformation 5

Set	Solve Point	Mode	Damped Frequency [Hz]	Stability [Hz]	Modal Damping Ratio
-----	-------------	------	-----------------------	----------------	---------------------

1.	1.	1.	0.	-1.2059	N/A
2.		2.	3.055	-7.6074e-014	2.4902e-014
3.		3.	3.9712	1.4005e-013	-3.5268e-014
4.		4.	17.415	-2.4594e-013	1.4122e-014
5.		5.	18.609	-3.7798e-013	2.0312e-014
6.		6.	19.399	2.776e-013	-1.431e-014
7.	2.	1.	0.	-1.2059	N/A
8.		2.	3.0543	2.6955e-013	-8.8254e-014
9.		3.	3.972	3.5349e-013	-8.8995e-014
10.		4.	17.402	1.1549e-013	-6.6362e-015
11.		5.	18.612	2.6471e-013	-1.4222e-014
12.		6.	19.405	6.7526e-013	-3.4799e-014

TABLE 34
Model (A4, B4) > Modal 2 (B5) > Solution (B6) > Results

Object Name	Directional Deformation 6
State	Solved
Scope	
Scoping Method	Geometry Selection
Geometry	All Bodies
Definition	
Type	Directional Deformation
Orientation	X Axis
Set Number	6.
Phase Angle	0. °
Coordinate System	Global Coordinate System
Identifier	
Suppressed	No
Results	
Minimum	-27.054 in
Maximum	13.7 in
Information	
Mode	6
Reported Frequency	19.399 Hz
Reported Stability	2.776e-013 Hz
Reported Modal Damping Ratio	-1.431e-014
Reported Logarithmic Decrement	8.9912e-014

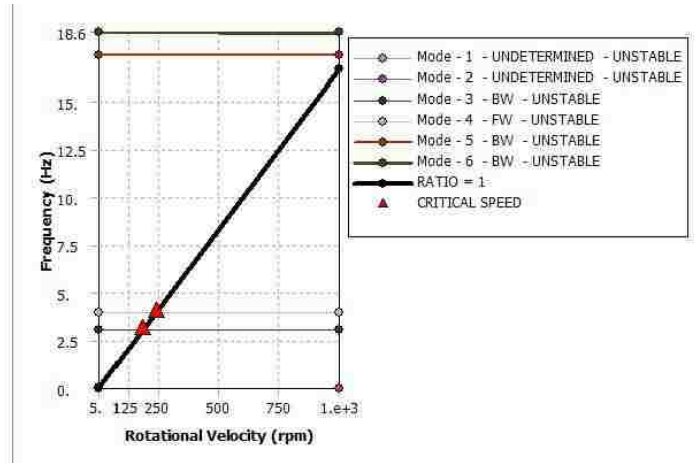
TABLE 35
Model (A4, B4) > Modal 2 (B5) > Solution (B6) > Directional Deformation 6

Set	Solve Point	Mode	Damped Frequency [Hz]	Stability [Hz]	Modal Damping Ratio
1.	1.	1.	0.	-1.2059	N/A
2.		2.	3.055	-7.6074e-014	2.4902e-014
3.		3.	3.9712	1.4005e-013	-3.5268e-014
4.		4.	17.415	-2.4594e-013	1.4122e-014
5.		5.	18.609	-3.7798e-013	2.0312e-014
6.		6.	19.399	2.776e-013	-1.431e-014
7.	2.	1.	0.	-1.2059	N/A
8.		2.	3.0543	2.6955e-013	-8.8254e-014
9.		3.	3.972	3.5349e-013	-8.8995e-014
10.		4.	17.402	1.1549e-013	-6.6362e-015
11.		5.	18.612	2.6471e-013	-1.4222e-014
12.		6.	19.405	6.7526e-013	-3.4799e-014

TABLE 36
Model (A4, B4) > Modal 2 (B5) > Solution (B6) > Result Charts

Object Name	Campbell Diagram
State	Solved
Scope	
Rotational Velocity Selection	Rotational Velocity
Campbell Diagram Controls	
Y Axis Data	Frequency
Critical Speed	Yes
Ratio	1.
Sorting	Yes
Axis	
X Axis Label	Rotational Velocity
X Axis Range	Program Controlled
X Axis Minimum	5. RPM
X Axis Maximum	1000. RPM
Y Axis Label	Frequency
Y Axis Range	Program Controlled
Y Axis Minimum	0. Hz
Y Axis Maximum	18.612 Hz
Definition	
Suppressed	No

FIGURE 3
Model (A4, B4) > Modal 2 (B5) > Solution (B6) > Campbell Diagram



Model (A4, B4) > Modal 2 (B5) > Solution (B6) > Campbell Diagram

Mode	Whirl Direction	Mode Stability	Critical Speed	5 rpm	1000 rpm
1.	UNDETERMINED	UNSTABLE	NONE	0. Hz	0. Hz
2.	UNDETERMINED	UNSTABLE	NONE	0. Hz	0. Hz
3.	BW	UNSTABLE	183.29 rpm	3.056 Hz	3.0543 Hz
4.	FW	UNSTABLE	238.28 rpm	3.9712 Hz	3.972 Hz
5.	BW	UNSTABLE	NONE	17.415 Hz	17.402 Hz
6.	BW	UNSTABLE	NONE	18.609 Hz	18.612 Hz

Material Data

lifoam

TABLE 37
lifoam > Constants

Density	1.0477e-003 lbm in ⁻³
---------	----------------------------------

TABLE 38
lifoam > Isotropic Elasticity

Temperature F	Young's Modulus psi	Poisson's Ratio	Bulk Modulus psi	Shear Modulus psi
203		3.e-002	71.986	98.544



Project

First Saved	Monday, October 29, 2012
Last Saved	Thursday, November 08, 2012
Product Version	14.0 Release
Save Project Before Solution	No
Save Project After Solution	No



Contents

- [Units](#)
- [Model \(A4, B4\)](#)
 - [Geometry](#)
 - [Solid](#)
 - [Point Mass](#)
 - [Coordinate Systems](#)
 - [Connections](#)
 - [Joints](#)
 - [Fixed - Ground To Solid](#)
 - [Springs](#)
 - [Mesh](#)
 - [Named Selections](#)
 - [Static Structural \(A5\)](#)
 - [Analysis Settings](#)
 - [Force](#)
 - [Solution \(A6\)](#)
 - [Solution Information](#)
 - [Results](#)
 - [Modal 2 \(B5\)](#)
 - [Pre-Stress \(Static Structural\)](#)
 - [Analysis Settings](#)
 - [Rotational Velocity](#)
 - [Solution \(B6\)](#)
 - [Solution Information](#)
 - [Results](#)
 - [Campbell Diagram](#)
- [Material Data](#)
 - [Iifoam](#)

Units

TABLE 1

Unit System	U.S. Customary (in, lbm, lbf, s, V, A) Degrees RPM Fahrenheit
Angle	Degrees
Rotational Velocity	RPM
Temperature	Fahrenheit

Model (A4, B4)

Geometry

TABLE 2
Model (A4, B4) > Geometry

Object Name	Geometry
State	Fully Defined
Definition	
Source	C:\Users\vdiz\Desktop\shaft b final_files\dp0\SYSDMSYS.agdb
Type	DesignModeler
Length Unit	Inches
Element Control	Program Controlled
Display Style	Body Color
Bounding Box	
Length X	5.874 in
Length Y	5.874 in
Length Z	57.25 in
Properties	
Volume	556.99 in³
Mass	0.88355 lbm
Scale Factor Value	1.
Statistics	
Bodies	1
Active Bodies	1
Nodes	30352
Elements	19400
Mesh Metric	None
Basic Geometry Options	
Parameters	Yes
Parameter Key	DS
Attributes	No
Named Selections	No
Material Properties	No
Advanced Geometry Options	
Use Associativity	Yes
Coordinate Systems	No

Reader Mode Saves Updated File	No
Use Instances	Yes
Smart CAD Update	No
Attach File Via Temp File	Yes
Temporary Directory	C:\Users\vdiz\AppData\Local\Temp
Analysis Type	3-D
Decompose Disjoint Faces	Yes
Enclosure and Symmetry Processing	Yes

TABLE 3
Model (A4, B4) > Geometry > Parts

Object Name	<i>Solid</i>
State	Meshed
Graphics Properties	
Visible	Yes
Glow	0
Shininess	1
Transparency	1
Specularity	1
Definition	
Suppressed	No
ID (Beta)	16
Stiffness Behavior	Flexible
Coordinate System	Default Coordinate System
Reference Temperature	By Environment
Material	
Assignment	lifoam
Nonlinear Effects	Yes
Thermal Strain Effects	Yes
Bounding Box	
Length X	5.874 in
Length Y	5.874 in
Length Z	57.25 in
Properties	
Volume	556.99 in ³
Mass	0.58355 lbm
Centroid X	-4.3274e-017 in
Centroid Y	2.9784e-017 in
Centroid Z	-0.62759 in
Moment of Inertia Ip1	152.59 lbm·in ²
Moment of Inertia Ip2	152.59 lbm·in ²
Moment of Inertia Ip3	1.0842 lbm·in ²
Statistics	
Nodes	30352
Elements	19400
Mesh Metric	None

TABLE 4
Model (A4, B4) > Geometry > Point Masses

Object Name	<i>Point Mass</i>
State	Fully Defined
Scope	
Scoping Method	Geometry Selection
Geometry	1 Face
Coordinate System	Global Coordinate System
X Coordinate	0. in
Y Coordinate	0.8 in
Z Coordinate	0. in
Location	Defined
Definition	
Mass	0.3 lbm
Mass Moment of Inertia X	0. lbm·in ²
Mass Moment of Inertia Y	0. lbm·in ²
Mass Moment of Inertia Z	0. lbm·in ²
Suppressed	No
Behavior	Deformable
Pinball Region	All

Coordinate Systems

TABLE 5
Model (A4, B4) > Coordinate Systems > Coordinate System

Object Name	<i>Global Coordinate System</i>
State	Fully Defined
Definition	
Type	Cartesian
Coordinate System ID	0.
Origin	
Origin X	0. in
Origin Y	0. in
Origin Z	0. in

Directional Vectors	
X Axis Data	[1. 0. 0.]
Y Axis Data	[0. 1. 0.]
Z Axis Data	[0. 0. 1.]

Connections

TABLE 6
Model (A4, B4) > Connections

Object Name	<i>Connections</i>
State	Fully Defined
Auto Detection	
Generate Automatic Connection On Refresh	Yes
Transparency	
Enabled	Yes

TABLE 7
Model (A4, B4) > Connections > Joints

Object Name	<i>Joints</i>
State	Fully Defined
Definition	
Connection Type	Joint
Scope	
Scoping Method	Geometry Selection
Geometry	All Bodies
Auto Detection	
Tolerance Type	Slider
Tolerance Slider	0.
Tolerance Value	0.14462 in
Use Range	No
Group By	Bodies
Search Across	Bodies
Fixed Joints	No
Revolute Joints	No

TABLE 8
Model (A4, B4) > Connections > Joints > Joints

Object Name	<i>Fixed - Ground To Solid</i>
State	Fully Defined
Definition	
Connection Type	Body-Ground
Type	Fixed
Suppressed	No
Reference	
Coordinate System	Reference Coordinate System
Mobile	
Scoping Method	Geometry Selection
Scope	1 Face
Body	Solid
Initial Position	Unchanged
Behavior	Deformable
Pinball Region	All

TABLE 9
Model (A4, B4) > Connections > Springs

Object Name	Longitudinal - Ground To Solid		Longitudinal - Ground To Solid
State	Fully Defined		
Graphics Properties			
Visible	No		
Definition			
Type	Longitudinal		
Spring Behavior	Both (Linear)		
Longitudinal Stiffness	100. lbf/in		1.e+007 lbf/in
Longitudinal Damping	0. lbf·s/in		
Preload	None		
Suppressed	No		
Spring Length	5. in		
Scope			
Scope	Body-Ground		
Reference			
Scoping Method	Geometry Selection		
Coordinate System	Global Coordinate System		
Reference X Coordinate	0. in		
Reference Y Coordinate	5. in		
Reference Z Coordinate	-10. in		28.625 in
Reference Location	Defined		
Behavior	Rigid		
Pinball Region	All		
Mobile			
Scoping Method	Geometry Selection		
Scope	1 Face		

Body	Solid	
Coordinate System	Global Coordinate System	
Mobile X Coordinate	0. in	-6.1188e-017 in
Mobile Y Coordinate	-1.7984e-016 in	3.633e-017 in
Mobile Z Coordinate	-10. in	28.625 in
Mobile Location	Defined	
Behavior	Deformable	Rigid
Pinball Region	All	

TABLE 10
Model (A4, B4) > Connections > Longitudinal - Ground To Solid > Command Snippet

Object Name	Commands (APDL)
State	Fully Defined
File	
File Name	
File Status	File not found
Definition	
Suppressed	No
Target	Mechanical APDL
Input Arguments	
ARG1	100.
ARG2	100.
ARG3	100.
ARG4	100.
ARG5	
ARG6	
ARG7	
ARG8	
ARG9	

Model (A4, B4) > Connections > Longitudinal - Ground To Solid > Commands (APDL)

```
! Commands inserted into this file will be executed just after the spring definition.
! The material, type, and real number for this spring is equal to the parameter "_sid".
! Active UNIT system in Workbench when this object was created: U.S. Customary (in, lbm, lbf, s, V, A) temperature units of F
!arg1=Kxx, arg2=Kyy arg3=Kxy agr4=Kyx arg5=Cxx arg6=Cyy arg7=Cxy arg8=Cyx
!By default the bearing element is symmetric means Kxy=Kyx and Cxy=Cyx

et,_sid, 214
keyopt,_sid, 2,0 !keyopt(2)=0 means in xy plane
!keyopt,_sid, 3,1 !Use keyopt(3)=1 if the element is non symmetric
r,_sid,arg1,arg2,arg3,arg4,arg5,arg6
rmore,arg7,arg8
```

TABLE 11
Model (A4, B4) > Connections > Longitudinal - Ground To Solid > Command Snippet

Object Name	Commands (APDL)
State	Fully Defined
File	
File Name	
File Status	File not found
Definition	
Suppressed	No
Target	Mechanical APDL
Input Arguments	
ARG1	100.
ARG2	100.
ARG3	100.
ARG4	100.
ARG5	
ARG6	
ARG7	
ARG8	
ARG9	

Model (A4, B4) > Connections > Longitudinal - Ground To Solid > Commands (APDL)

```
! Commands inserted into this file will be executed just after the spring definition.
! The material, type, and real number for this spring is equal to the parameter "_sid".
! Active UNIT system in Workbench when this object was created: U.S. Customary (in, lbm, lbf, s, V, A) temperature units of F
!arg1=Kxx, arg2=Kyy arg3=Kxy agr4=Kyx arg5=Cxx arg6=Cyy arg7=Cxy arg8=Cyx
!By default the bearing element is symmetric means Kxy=Kyx and Cxy=Cyx

et,_sid, 214
keyopt,_sid, 2,0 !keyopt(2)=0 means in xy plane
!keyopt,_sid, 3,1 !Use keyopt(3)=1 if the element is non symmetric
r,_sid,arg1,arg2,arg3,arg4,arg5,arg6
rmore,arg7,arg8
```

Mesh

TABLE 12
Model (A4, B4) > Mesh

Object Name	<i>Mesh</i>
State	Solved
Defaults	
Physics Preference	Mechanical
Relevance	40
Sizing	
Use Advanced Size Function	Off
Relevance Center	Coarse
Element Size	Default
Initial Size Seed	Active Assembly
Smoothing	High
Transition	Fast
Span Angle Center	Medium
Minimum Edge Length	2.51330 in
Inflation	
Use Automatic Inflation	None
Inflation Option	Smooth Transition
Transition Ratio	0.272
Maximum Layers	5
Growth Rate	1.2
Inflation Algorithm	Pre
View Advanced Options	No
Patch Conforming Options	
Triangle Surface Mesher	Program Controlled
Advanced	
Shape Checking	Standard Mechanical
Element Midside Nodes	Program Controlled
Straight Sided Elements	No
Number of Retries	0
Extra Retries For Assembly	Yes
Rigid Body Behavior	Dimensionally Reduced
Mesh Morphing	Disabled
Defeaturing	
Pinch Tolerance	Please Define
Generate Pinch on Refresh	No
Automatic Mesh Based Defeaturing	On
Defeaturing Tolerance	Default
Statistics	
Nodes	30352
Elements	19400
Mesh Metric	None

Named Selections

Static Structural (A5)

TABLE 13
Model (A4, B4) > Analysis

Object Name	<i>Static Structural (A5)</i>
State	Solved
Definition	
Physics Type	Structural
Analysis Type	Static Structural
Solver Target	Mechanical APDL
Options	
Environment Temperature	71.6 °F
Generate Input Only	No

TABLE 14
Model (A4, B4) > Static Structural (A5) > Analysis Settings

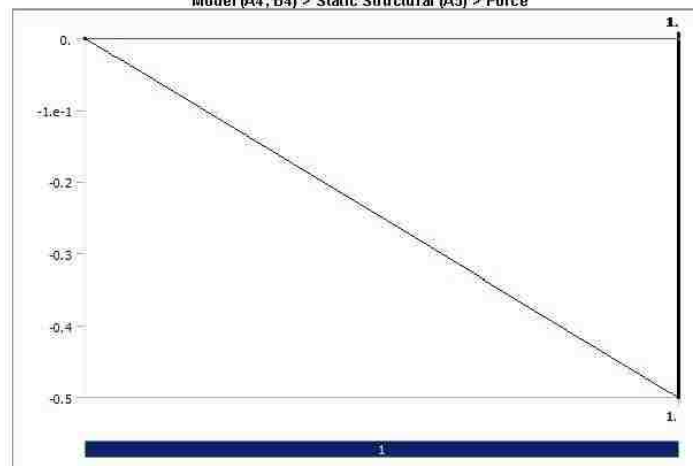
Object Name	<i>Analysis Settings</i>
State	Fully Defined
Restart Analysis	
Restart Type	Program Controlled
Status	Done
Step Controls	
Number Of Steps	1.
Current Step Number	1.
Step End Time	1. s
Auto Time Stepping	Program Controlled
Solver Controls	
Solver Type	Program Controlled
Weak Springs	Program Controlled
Large Deflection	Off
Inertia Relief	Off
Restart Controls	
Generate Restart Points	Program Controlled
Retain Files After Full Solve	Yes
Nonlinear Controls	
Force Convergence	Program Controlled

Moment Convergence	Program Controlled
Displacement Convergence	Program Controlled
Rotation Convergence	Program Controlled
Line Search	Program Controlled
Stabilization	Off
Output Controls	
Stress	Yes
Strain	Yes
Nodal Forces	No
Contact Miscellaneous	No
General Miscellaneous	No
Calculate Results At	All Time Points
Cache Results in Memory (Beta)	Never
Max Number of Result Sets	Program Controlled
Analysis Data Management	
Solver Files Directory	C:\Users\rdz\Desktop\shaft b final_files\dp0\SYSMECH\
Future Analysis	Prestressed analysis
Scratch Solver Files Directory	
Save MAPDL db	No
Delete Unneeded Files	Yes
Nonlinear Solution	No
Solver Units	Active System
Solver Unit System	Bin

TABLE 15
Model (A4, B4) > Static Structural (A5) > Loads

Object Name	Force
State	Fully Defined
Scope	
Scoping Method	Geometry Selection
Geometry	1 Face
Definition	
ID (Beta)	158
Type	Force
Define By	Components
Coordinate System	Global Coordinate System
X Component	0. lbf (ramped)
Y Component	0. lbf (ramped)
Z Component	-0.5 lbf (ramped)
Suppressed	No

FIGURE 1
Model (A4, B4) > Static Structural (A5) > Force



Solution (A6)

TABLE 16
Model (A4, B4) > Static Structural (A5) > Solution

Object Name	Solution (A6)
State	Solved
Adaptive Mesh Refinement	
Max Refinement Loops	3
Refinement Depth	2
Information	
Status	Done

TABLE 17
Model (A4, B4) > Static Structural (A5) > Solution (A6) > Solution Information

Object Name	<i>Solution Information</i>
State	Solved
Solution Information	
Solution Output	Solver Output
Newton-Raphson Residuals	0
Update Interval	2.5 s
Display Points	All
FE Connection Visibility	
Activate Visibility	Yes
Display	All FE Connectors
Draw Connections Attached To	All Nodes
Line Color	Connection Type
Visible on Results	No
Line Thickness	Single
Display Type	Lines

TABLE 18
Model (A4, B4) > Static Structural (A5) > Solution (A6) > Results

Object Name	Directional Deformation	Normal Stress
State	Solved	
Scope		
Scoping Method	Geometry Selection	
Geometry	All Bodies	
Definition		
Type	Directional Deformation	Normal Stress
Orientation	X Axis	Z Axis
By	Time	
Display Time	Last	
Coordinate System	Global Coordinate System	
Calculate Time History	Yes	
Identifier		
Suppressed	No	
Results		
Minimum	-3.891e-005 in	-6.0173e-002 psi
Maximum	6.7717e-005 in	1.2836e-002 psi
Information		
Time	1. s	
Load Step	1	
Substep	1	
Iteration Number	1	
Integration Point Results		
Display Option	Averaged	

Modal 2 (B5)

TABLE 19
Model (A4, B4) > Analysis

Object Name	<i>Modal 2 (B5)</i>
State	Solved
Definition	
Physics Type	Structural
Analysis Type	Modal
Solver Target	Mechanical APDL
Options	
Generate Input Only	No

TABLE 20
Model (A4, B4) > Modal 2 (B5) > Initial Condition

Object Name	<i>Pre-Stress (Static Structural)</i>
State	Fully Defined
Definition	
Pre-Stress Environment	Static Structural
Pre-Stress Define By	Program Controlled
Reported Loadstep	Last
Reported Substep	Last
Reported Time	End Time
Contact Status	Use True Status

TABLE 21
Model (A4, B4) > Modal 2 (B5) > Analysis Settings

Object Name	<i>Analysis Settings</i>
State	Fully Defined
Options	
Max Modes to Find	6
Limit Search to Range	No
Solver Controls	
Damped	Yes
Solver Type	Full Damped
Rotordynamics Controls	
Coriolis Effect	On
Campbell Diagram	On

Number of Points	2
Output Controls	
Stress	No
Strain	No
Nodal Forces	No
Calculate Reactions	No
General Miscellaneous	No
Cache Results in Memory (Beta)	Never
Damping Controls	
Stiffness Coefficient Define By	Direct Input
Stiffness Coefficient	0.
Mass Coefficient	0.
Analysis Data Management	
Solver Files Directory	C:\Users\vdiz\Desktop\shaft b final_files\dp0\SYS-2\MECH\
Future Analysis	None
Scratch Solver Files Directory	
Save MAPDL db	No
Delete Unneeded Files	Yes
Solver Units	Active System
Solver Unit System	Bin

TABLE 22
Model (A4, B4) > Modal 2 (B5) > Rotations

Object Name	Rotational Velocity
State	Fully Defined
Scope	
Scoping Method	Geometry Selection
Geometry	All Bodies
Definition	
Define By	Vector
Magnitude	Tabular Data
Axis	Defined
Suppressed	No

TABLE 23
Model (A4, B4) > Modal 2 (B5) > Rotational Velocity

Points	Rotational Velocity [rpm]
1	5.
2	1000.

Solution (B6)

TABLE 24
Model (A4, B4) > Modal 2 (B5) > Solution

Object Name	Solution (B6)
State	Solved
Adaptive Mesh Refinement	
Max Refinement Loops	1.
Refinement Depth	2.
Information	
Status	Done

The following bar chart indicates the frequency at each calculated mode.

FIGURE 2
Model (A4, B4) > Modal 2 (B5) > Solution (B6)

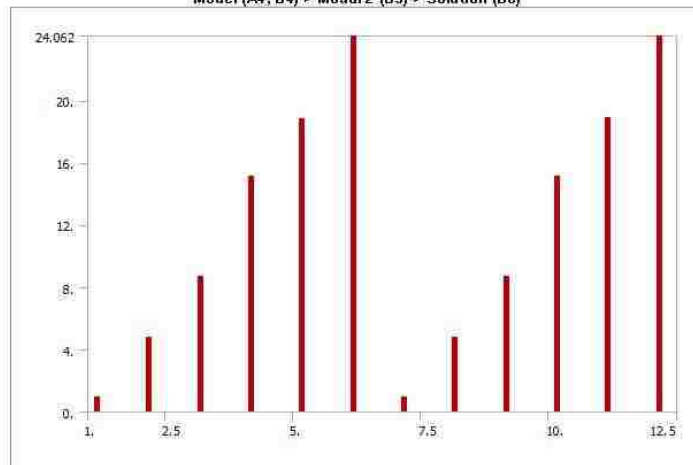


TABLE 25

Model (A4, B4) > Modal 2 (B5) > Solution (B6)					
Set	Solve Point	Mode	Damped Frequency [Hz]	Stability [Hz]	Modal Damping Ratio
1.	1.	1.	0.92538	1.1151e-012	-1.205e-012
2.		2.	4.8321	2.1522e-013	-4.454e-014
3.		3.	8.739	-1.041e-012	1.1912e-013
4.		4.	15.14	-9.2971e-013	6.1409e-014
5.		5.	18.857	1.6772e-012	-8.8942e-014
6.		6.	24.062	1.2422e-012	-5.1627e-014
7.	2.	1.	0.92538	-2.2287e-012	2.4084e-012
8.		2.	4.8319	-3.3064e-013	6.8428e-014
9.		3.	8.7385	-1.8059e-012	2.0665e-013
10.		4.	15.136	-1.718e-012	1.1351e-013
11.		5.	18.863	-1.1914e-012	6.3162e-014
12.		6.	24.061	-7.5084e-013	3.1205e-014

TABLE 26
Model (A4, B4) > Modal 2 (B5) > Solution (B6) > Solution Information

Object Name	Solution Information
State	Solved
Solution Information	
Solution Output	Solver Output
Newton-Raphson Residuals	0
Update Interval	2.5 s
Display Points	All
FE Connection Visibility	
Activate Visibility	Yes
Display	All FE Connectors
Draw Connections Attached To	All Nodes
Line Color	Connection Type
Visible on Results	No
Line Thickness	Single
Display Type	Lines

TABLE 27
Model (A4, B4) > Modal 2 (B5) > Solution (B6) > Results

Object Name	Directional Deformation	Directional Deformation 2	Directional Deformation 3	Directional Deformation 4	Directional Deformation 5
State	Solved				
Scope					
Scoping Method	Geometry Selection				
Geometry	All Bodies				
Definition					
Type	Directional Deformation				
Orientation	X Axis				
Set Number	1.	2.	3.	4.	5.
Phase Angle	0. °				
Coordinate System	Global Coordinate System				
Identifier					
Suppressed	No				
Results					
Minimum	-34.393 in	-33.994 in	-24.229 in	-30.233 in	-46.976 in
Maximum	1.9684e-003 in	13.333 in	4.9369 in	6.8387 in	34.078 in
Information					
Mode	1	2	3	4	5
Reported Frequency	0.92538 Hz	4.8321 Hz	8.739 Hz	15.14 Hz	18.857 Hz
Reported Stability	1.1151e-012 Hz	2.1522e-013 Hz	-1.041e-012 Hz	-9.2971e-013 Hz	1.6772e-012 Hz
Reported Modal Damping Ratio	-1.205e-012	-4.454e-014	1.1912e-013	6.1409e-014	-8.8942e-014
Reported Logarithmic Decrement	7.571e-012	2.7985e-013	-7.4847e-013	-3.8585e-013	5.5884e-013

TABLE 28
Model (A4, B4) > Modal 2 (B5) > Solution (B6) > Directional Deformation

Set	Solve Point	Mode	Damped Frequency [Hz]	Stability [Hz]	Modal Damping Ratio
1.	1.	1.	0.92538	1.1151e-012	-1.205e-012
2.		2.	4.8321	2.1522e-013	-4.454e-014
3.		3.	8.739	-1.041e-012	1.1912e-013
4.		4.	15.14	-9.2971e-013	6.1409e-014
5.		5.	18.857	1.6772e-012	-8.8942e-014
6.		6.	24.062	1.2422e-012	-5.1627e-014
7.	2.	1.	0.92538	-2.2287e-012	2.4084e-012
8.		2.	4.8319	-3.3064e-013	6.8428e-014
9.		3.	8.7385	-1.8059e-012	2.0665e-013
10.		4.	15.136	-1.718e-012	1.1351e-013
11.		5.	18.863	-1.1914e-012	6.3162e-014
12.		6.	24.061	-7.5084e-013	3.1205e-014

TABLE 29
Model (A4, B4) > Modal 2 (B5) > Solution (B6) > Directional Deformation 2

Set	Solve Point	Mode	Damped Frequency [Hz]	Stability [Hz]	Modal Damping Ratio
1.	1.	1.	0.92538	1.1151e-012	-1.205e-012
2.		2.	4.8321	2.1522e-013	-4.454e-014
3.		3.	8.739	-1.041e-012	1.1912e-013
4.		4.	15.14	-9.2971e-013	6.1409e-014
5.		5.	18.857	1.6772e-012	-8.8942e-014

6.		6.	24.062	1.2422e-012	-5.1627e-014
7.		1.	0.92538	-2.2287e-012	2.4084e-012
8.		2.	4.8319	-3.3064e-013	6.8428e-014
9.		3.	8.7385	-1.8059e-012	2.0665e-013
10.		4.	15.136	-1.718e-012	1.1351e-013
11.		5.	18.863	-1.1914e-012	6.3162e-014
12.		6.	24.061	-7.5084e-013	3.1205e-014

TABLE 30
Model (A4, B4) > Modal 2 (B5) > Solution (B6) > Directional Deformation 3

Set	Solve Point	Mode	Damped Frequency [Hz]	Stability [Hz]	Modal Damping Ratio
1.		1.	0.92538	1.1151e-012	-1.205e-012
2.		2.	4.8321	2.1522e-013	-4.454e-014
3.		3.	8.739	-1.041e-012	1.1912e-013
4.		4.	15.14	-9.2971e-013	6.1409e-014
5.		5.	18.857	1.6772e-012	-8.8942e-014
6.		6.	24.062	1.2422e-012	-5.1627e-014
7.		1.	0.92538	-2.2287e-012	2.4084e-012
8.		2.	4.8319	-3.3064e-013	6.8428e-014
9.		3.	8.7385	-1.8059e-012	2.0665e-013
10.		4.	15.136	-1.718e-012	1.1351e-013
11.		5.	18.863	-1.1914e-012	6.3162e-014
12.		6.	24.061	-7.5084e-013	3.1205e-014

TABLE 31
Model (A4, B4) > Modal 2 (B5) > Solution (B6) > Directional Deformation 4

Set	Solve Point	Mode	Damped Frequency [Hz]	Stability [Hz]	Modal Damping Ratio
1.		1.	0.92538	1.1151e-012	-1.205e-012
2.		2.	4.8321	2.1522e-013	-4.454e-014
3.		3.	8.739	-1.041e-012	1.1912e-013
4.		4.	15.14	-9.2971e-013	6.1409e-014
5.		5.	18.857	1.6772e-012	-8.8942e-014
6.		6.	24.062	1.2422e-012	-5.1627e-014
7.		1.	0.92538	-2.2287e-012	2.4084e-012
8.		2.	4.8319	-3.3064e-013	6.8428e-014
9.		3.	8.7385	-1.8059e-012	2.0665e-013
10.		4.	15.136	-1.718e-012	1.1351e-013
11.		5.	18.863	-1.1914e-012	6.3162e-014
12.		6.	24.061	-7.5084e-013	3.1205e-014

TABLE 32
Model (A4, B4) > Modal 2 (B5) > Solution (B6) > Directional Deformation 5

Set	Solve Point	Mode	Damped Frequency [Hz]	Stability [Hz]	Modal Damping Ratio
1.		1.	0.92538	1.1151e-012	-1.205e-012
2.		2.	4.8321	2.1522e-013	-4.454e-014
3.		3.	8.739	-1.041e-012	1.1912e-013
4.		4.	15.14	-9.2971e-013	6.1409e-014
5.		5.	18.857	1.6772e-012	-8.8942e-014
6.		6.	24.062	1.2422e-012	-5.1627e-014
7.		1.	0.92538	-2.2287e-012	2.4084e-012
8.		2.	4.8319	-3.3064e-013	6.8428e-014
9.		3.	8.7385	-1.8059e-012	2.0665e-013
10.		4.	15.136	-1.718e-012	1.1351e-013
11.		5.	18.863	-1.1914e-012	6.3162e-014
12.		6.	24.061	-7.5084e-013	3.1205e-014

TABLE 33
Model (A4, B4) > Modal 2 (B5) > Solution (B6) > Results

Object Name	Directional Deformation 6
State	Solved
Scope	
Scoping Method	Geometry Selection
Geometry	All Bodies
Definition	
Type	Directional Deformation
Orientation	X Axis
Set Number	6.
Phase Angle	0. °
Coordinate System	Global Coordinate System
Identifier	
Suppressed	No
Results	
Minimum	-31.2 in
Maximum	50.646 in
Information	
Mode	6
Reported Frequency	24.062 Hz
Reported Stability	1.2422e-012 Hz
Reported Modal Damping Ratio	-5.1627e-014
Reported Logarithmic Decrement	3.2438e-013

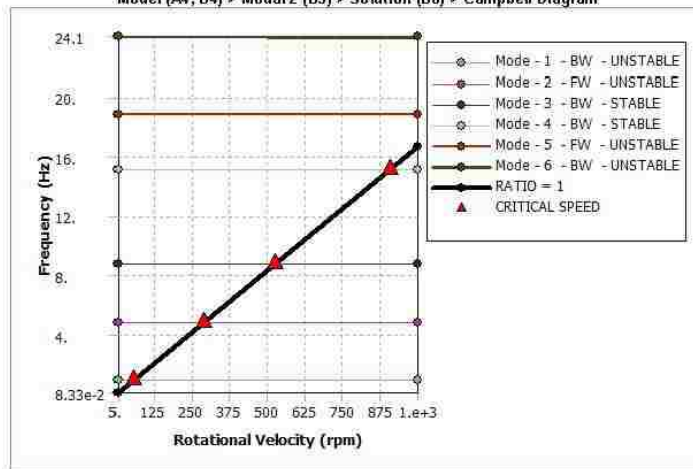
TABLE 34

Model (A4, B4) > Modal 2 (B5) > Solution (B6) > Directional Deformation 6					
Set	Solve Point	Mode	Damped Frequency [Hz]	Stability [Hz]	Modal Damping Ratio
1	1.	1.	0.92538	1.1151e-012	-1.205e-012
2		2.	4.8321	2.1522e-013	-4.454e-014
3		3.	8.739	-1.041e-012	1.1912e-013
4		4.	15.14	-9.2971e-013	6.1409e-014
5		5.	18.857	1.6772e-012	-8.8942e-014
6		6.	24.062	1.2422e-012	-5.1627e-014
7	2.	1.	0.92538	-2.2287e-012	2.4084e-012
8		2.	4.8319	-3.3064e-013	6.8428e-014
9		3.	8.7385	-1.8059e-012	2.0665e-013
10		4.	15.136	-1.718e-012	1.1351e-013
11		5.	18.863	-1.1914e-012	6.3162e-014
12		6.	24.061	-7.5084e-013	3.1205e-014

TABLE 35
Model (A4, B4) > Modal 2 (B5) > Solution (B6) > Result Charts

Object Name	Campbell Diagram
State	Solved
Scope	
Rotational Velocity Selection	Rotational Velocity
Campbell Diagram Controls	
Y Axis Data	Frequency
Critical Speed	Yes
Ratio	1.
Sorting	Yes
Axis	
X Axis Label	Rotational Velocity
X Axis Range	Program Controlled
X Axis Minimum	5. RPM
X Axis Maximum	1000. RPM
Y Axis Label	Frequency
Y Axis Range	Program Controlled
Y Axis Minimum	8.3333e-002 Hz
Y Axis Maximum	24.062 Hz
Definition	
Suppressed	No

FIGURE 3
Model (A4, B4) > Modal 2 (B5) > Solution (B6) > Campbell Diagram



Model (A4, B4) > Modal 2 (B5) > Solution (B6) > Campbell Diagram					
Mode	Whirl Direction	Mode Stability	Critical Speed	5. rpm	1000. rpm
1	BW	UNSTABLE	55.523 rpm	0.92538 Hz	0.92538 Hz
2	FW	UNSTABLE	289.92 rpm	4.8321 Hz	4.8319 Hz
3	BW	STABLE	524.33 rpm	8.739 Hz	8.7385 Hz
4	BW	STABLE	908.16 rpm	15.14 Hz	15.136 Hz
5	FW	UNSTABLE	NONE	18.857 Hz	18.863 Hz
6	BW	UNSTABLE	NONE	24.062 Hz	24.061 Hz

Material Data

lifoam

TABLE 36 lifoam > Constants	
Density	1.0477e-003 lbm in ⁻³

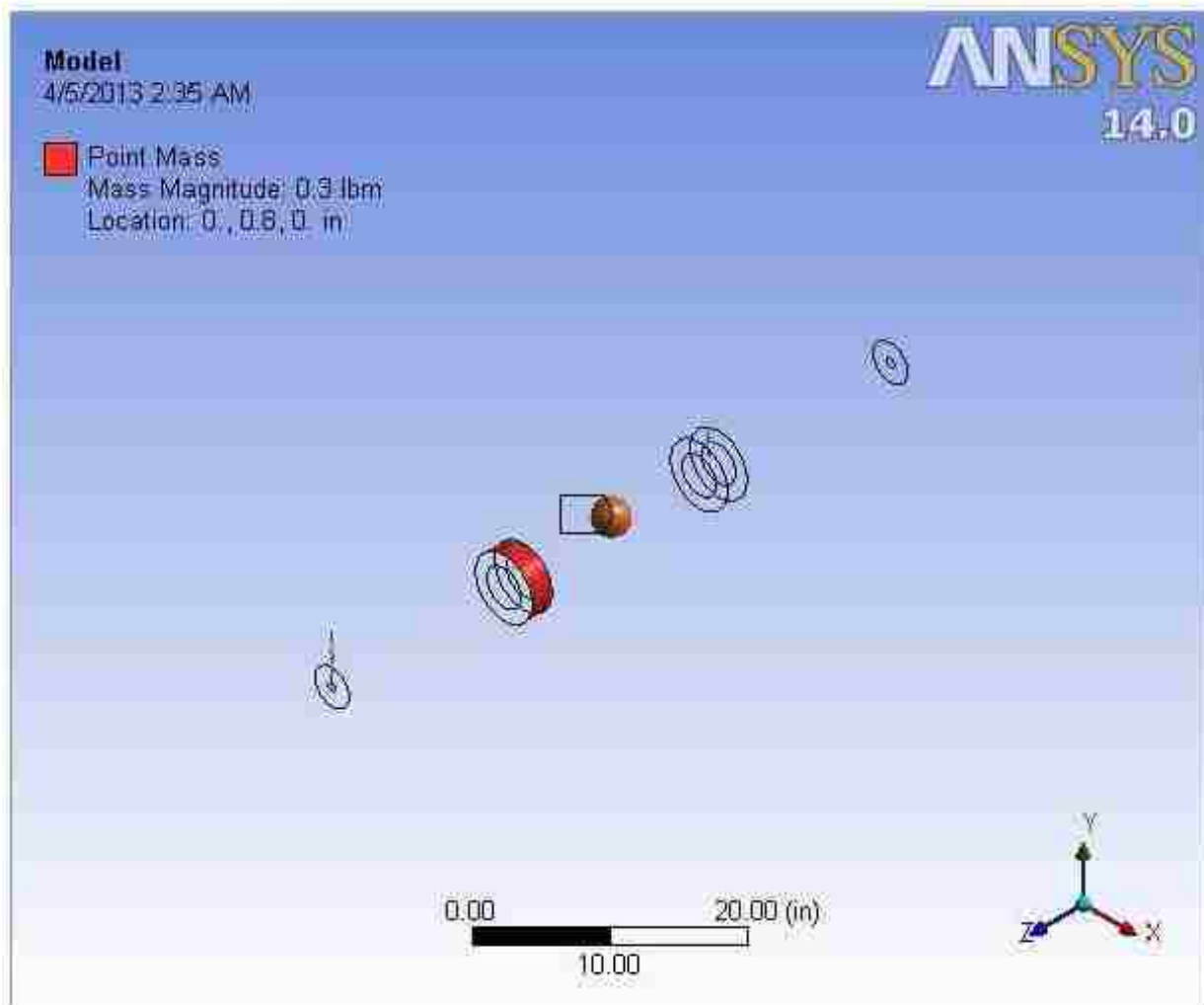
TABLE 37
lifoam > Isotropic Elasticity

Temperature F	Young's Modulus psi	Poisson's Ratio	Bulk Modulus psi	Shear Modulus psi
	203	3.e-002	71.986	98.544



Project

First Saved	Monday, October 29, 2012
Last Saved	Friday, November 09, 2012
Product Version	14.0 Release
Save Project Before Solution	No
Save Project After Solution	No



Contents

- [Units](#)
- [Model \(A4, B4\)](#)
 - [Geometry](#)
 - [Solid](#)
 - [Point Mass](#)
 - [Coordinate Systems](#)
 - [Connections](#)
 - [Joints](#)
 - [Fixed - Ground To Solid](#)
 - [Springs](#)
 - [Mesh](#)
 - [Named Selections](#)
 - [Static Structural \(A5\)](#)
 - [Analysis Settings](#)
 - [Force](#)
 - [Solution \(A6\)](#)
 - [Solution Information](#)
 - [Results](#)
 - [Modal 2 \(B5\)](#)
 - [Pre-Stress \(Static Structural\)](#)
 - [Analysis Settings](#)
 - [Rotational Velocity](#)
 - [Solution \(B6\)](#)
 - [Solution Information](#)
 - [Results](#)
 - [Campbell Diagram](#)
- [Material Data](#)
 - [Iifoam](#)

Units

TABLE 1

Unit System	U.S. Customary (in, lbm, lbf, s, V, A) Degrees RPM Fahrenheit
Angle	Degrees
Rotational Velocity	RPM
Temperature	Fahrenheit

Model (A4, B4)

Geometry

TABLE 2
Model (A4, B4) > Geometry

Object Name	Geometry
State	Fully Defined
Definition	
Source	C:\Users\vdiz\Desktop\shaft c final_files\dp0\SYSDMSYS.agdb
Type	DesignModeler
Length Unit	Inches
Element Control	Program Controlled
Display Style	Body Color
Bounding Box	
Length X	5.874 in
Length Y	5.874 in
Length Z	57.25 in
Properties	
Volume	591.95 in ³
Mass	0.92018 lbm
Scale Factor Value	1.
Statistics	
Bodies	1
Active Bodies	1
Nodes	30264
Elements	19323
Mesh Metric	None
Basic Geometry Options	
Parameters	Yes
Parameter Key	DS
Attributes	No
Named Selections	No
Material Properties	No
Advanced Geometry Options	
Use Associativity	Yes
Coordinate Systems	No

Reader Mode Saves Updated File	No
Use Instances	Yes
Smart CAD Update	No
Attach File Via Temp File	Yes
Temporary Directory	C:\Users\vdiz\AppData\Local\Temp
Analysis Type	3-D
Decompose Disjoint Faces	Yes
Enclosure and Symmetry Processing	Yes

TABLE 3
Model (A4, B4) > Geometry > Parts

Object Name	<i>Solid</i>
State	Meshed
Graphics Properties	
Visible	Yes
Glow	0
Shininess	1
Transparency	1
Specularity	1
Definition	
Suppressed	No
ID (Beta)	16
Stiffness Behavior	Flexible
Coordinate System	Default Coordinate System
Reference Temperature	By Environment
Material	
Assignment	lifoam
Nonlinear Effects	Yes
Thermal Strain Effects	Yes
Bounding Box	
Length X	5.874 in
Length Y	5.874 in
Length Z	57.25 in
Properties	
Volume	591.95 in ³
Mass	0.62018 lbm
Centroid X	1.1562e-017 in
Centroid Y	3.2047e-017 in
Centroid Z	-1.1291e-015 in
Moment of Inertia Ip1	156.59 lbm·in ²
Moment of Inertia Ip2	156.59 lbm·in ²
Moment of Inertia Ip3	1.2961 lbm·in ²
Statistics	
Nodes	30264
Elements	19323
Mesh Metric	None

TABLE 4
Model (A4, B4) > Geometry > Point Masses

Object Name	<i>Point Mass</i>
State	Fully Defined
Scope	
Scoping Method	Geometry Selection
Geometry	1 Face
Coordinate System	Global Coordinate System
X Coordinate	0. in
Y Coordinate	0.8 in
Z Coordinate	0. in
Location	Defined
Definition	
Mass	0.3 lbm
Mass Moment of Inertia X	0. lbm·in ²
Mass Moment of Inertia Y	0. lbm·in ²
Mass Moment of Inertia Z	0. lbm·in ²
Suppressed	No
Behavior	Deformable
Pinball Region	All

Coordinate Systems

TABLE 5
Model (A4, B4) > Coordinate Systems > Coordinate System

Object Name	<i>Global Coordinate System</i>
State	Fully Defined
Definition	
Type	Cartesian
Coordinate System ID	0.
Origin	
Origin X	0. in
Origin Y	0. in
Origin Z	0. in

Connections

Directional Vectors	
X Axis Data	[1. 0. 0.]
Y Axis Data	[0. 1. 0.]
Z Axis Data	[0. 0. 1.]

TABLE 6
Model (A4, B4) > Connections

Object Name	Connections
State	Fully Defined
Auto Detection	
Generate Automatic Connection On Refresh	Yes
Transparency	
Enabled	Yes

TABLE 7
Model (A4, B4) > Connections > Joints

Object Name	Joints
State	Fully Defined
Definition	
Connection Type	Joint
Scope	
Scoping Method	Geometry Selection
Geometry	All Bodies
Auto Detection	
Tolerance Type	Slider
Tolerance Slider	0.
Tolerance Value	0.14462 in
Use Range	No
Group By	Bodies
Search Across	Bodies
Fixed Joints	No
Revolute Joints	No

TABLE 8
Model (A4, B4) > Connections > Joints > Joints

Object Name	Fixed - Ground To Solid
State	Fully Defined
Definition	
Connection Type	Body-Ground
Type	Fixed
Suppressed	No
Reference	
Coordinate System	Reference Coordinate System
Mobile	
Scoping Method	Geometry Selection
Scope	1 Face
Body	Solid
Initial Position	Unchanged
Behavior	Deformable
Pinball Region	All

TABLE 9
Model (A4, B4) > Connections > Springs

Object Name	Longitudinal - Ground To Solid		Longitudinal - Ground To Solid	Longitudinal - Ground To Solid
State	Fully Defined			
Graphics Properties				
Visible	Yes			
Definition				
Type	Longitudinal			
Spring Behavior	Both (Linear)			
Longitudinal Stiffness	100. lbf/in	1.e+007 lbf/in		
Longitudinal Damping	0. lbf·s/in			
Preload	None			
Suppressed	No			
Spring Length	5. in			
Scope				
Scope	Body-Ground			
Reference				
Scoping Method	Geometry Selection			
Coordinate System	Global Coordinate System			
Reference X Coordinate	0. in			
Reference Y Coordinate	5. in			
Reference Z Coordinate	10. in	28.625 in	-10. in	
Reference Location	Defined			
Behavior	Rigid			
Pinball Region	All			
Mobile				
Scoping Method	Geometry Selection			
Scope	1 Face			

Body	Solid		
Coordinate System	Global Coordinate System		
Mobile X Coordinate	0. in	-6.1188e-017 in	0. in
Mobile Y Coordinate	-1.7984e-016 in	3.633e-017 in	-1.7984e-016 in
Mobile Z Coordinate	10. in	28.625 in	-10. in
Mobile Location	Defined		
Behavior	Deformable	Rigid	
Pinball Region	All		

TABLE 10
Model (A4, B4) > Connections > Longitudinal - Ground To Solid > Command Snippet

Object Name	Commands (APDL)
State	Fully Defined
File	
File Name	
File Status	File not found
Definition	
Suppressed	No
Target	Mechanical APDL
Input Arguments	
ARG1	100.
ARG2	100.
ARG3	100.
ARG4	100.
ARG5	
ARG6	
ARG7	
ARG8	
ARG9	

Model (A4, B4) > Connections > Longitudinal - Ground To Solid > Commands (APDL)

```
! Commands inserted into this file will be executed just after the spring definition.
! The material, type, and real number for this spring is equal to the parameter "_sid".
! Active UNIT system in Workbench when this object was created: U.S. Customary (in, lbm, lbf, s, V, A) temperature units of F
!arg1=Kxx, arg2=Kyy arg3=Kxy agr4=Kyx arg5=Cxx arg6=Cyy arg7=Cxy arg8=Cyx
!By default the bearing element is symmetric means Kxy=Kyx and Cxy=Cyx

et,_sid, 214
keyopt,_sid, 2,0 !keyopt(2)=0 means in xy plane
!keyopt,_sid, 3,1 !Use keyopt(3)=1 if the element is non symmetric
r,_sid,arg1,arg2,arg3,arg4,arg5,arg6
rmore,arg7,arg8
```

TABLE 11
Model (A4, B4) > Connections > Longitudinal - Ground To Solid > Command Snippet

Object Name	Commands (APDL)
State	Fully Defined
File	
File Name	
File Status	File not found
Definition	
Suppressed	No
Target	Mechanical APDL
Input Arguments	
ARG1	100.
ARG2	100.
ARG3	100.
ARG4	100.
ARG5	
ARG6	
ARG7	
ARG8	
ARG9	

Model (A4, B4) > Connections > Longitudinal - Ground To Solid > Commands (APDL)

```
! Commands inserted into this file will be executed just after the spring definition.
! The material, type, and real number for this spring is equal to the parameter "_sid".
! Active UNIT system in Workbench when this object was created: U.S. Customary (in, lbm, lbf, s, V, A) temperature units of F
!arg1=Kxx, arg2=Kyy arg3=Kxy agr4=Kyx arg5=Cxx arg6=Cyy arg7=Cxy arg8=Cyx
!By default the bearing element is symmetric means Kxy=Kyx and Cxy=Cyx

et,_sid, 214
keyopt,_sid, 2,0 !keyopt(2)=0 means in xy plane
!keyopt,_sid, 3,1 !Use keyopt(3)=1 if the element is non symmetric
r,_sid,arg1,arg2,arg3,arg4,arg5,arg6
rmore,arg7,arg8
```

TABLE 12
Model (A4, B4) > Connections > Longitudinal - Ground To Solid > Command Snippet

Object Name	Commands (APDL)
State	Fully Defined

File	
File Name	
File Status	File not found
Definition	
Suppressed	No
Target	Mechanical APDL
Input Arguments	
ARG1	100.
ARG2	100.
ARG3	100.
ARG4	100.
ARG5	
ARG6	
ARG7	
ARG8	
ARG9	

Model (A4, B4) > Connections > Longitudinal - Ground To Solid > Commands (APDL)

```

! Commands inserted into this file will be executed just after the spring definition.
! The material, type, and real number for this spring is equal to the parameter " _sid".
! Active UNIT system in Workbench when this object was created: U.S. Customary (in, lbm, lbf, s, V, A) temperature units of F
!arg1=Kxx, arg2=Kyy arg3=Kxy agr4=Kyx arg5=Cxx arg6=Cyy arg7=Cxy arg8=Cyx
!By default the bearing element is symmetric means Kxy=Kyx and Cxy=Cyx

et,_sid,214
keyopt,_sid,2,0 !keyopt(2)=0 means in xy plane
!keyopt,_sid,3,1 !Use keyopt(3)=1 if the element is non symmetric
r,_sid,arg1,arg2,arg3,arg4,arg5,arg6
rmore,arg7,arg8

```

Mesh

TABLE 13
Model (A4, B4) > Mesh

Object Name	<i>Mesh</i>
State	Solved
Defaults	
Physics Preference	Mechanical
Relevance	40
Sizing	
Use Advanced Size Function	Off
Relevance Center	Coarse
Element Size	Default
Initial Size Seed	Active Assembly
Smoothing	High
Transition	Fast
Span Angle Center	Medium
Minimum Edge Length	2.51330 in
Inflation	
Use Automatic Inflation	None
Inflation Option	Smooth Transition
Transition Ratio	0.272
Maximum Layers	5
Growth Rate	1.2
Inflation Algorithm	Pre
View Advanced Options	No
Patch Conforming Options	
Triangle Surface Mesher	Program Controlled
Advanced	
Shape Checking	Standard Mechanical
Element Midside Nodes	Program Controlled
Straight Sided Elements	No
Number of Retries	0
Extra Retries For Assembly	Yes
Rigid Body Behavior	Dimensionally Reduced
Mesh Morphing	Disabled
Defeaturing	
Pinch Tolerance	Please Define
Generate Pinch on Refresh	No
Automatic Mesh Based Defeaturing	On
Defeaturing Tolerance	Default
Statistics	
Nodes	30264
Elements	19323
Mesh Metric	None

Named Selections

Static Structural (A5)

TABLE 14
Model (A4, B4) > Analysis

Object Name	Static Structural (A5)
State	Solved
Definition	
Physics Type	Structural
Analysis Type	Static Structural
Solver Target	Mechanical APDL
Options	
Environment Temperature	71.6 °F
Generate Input Only	No

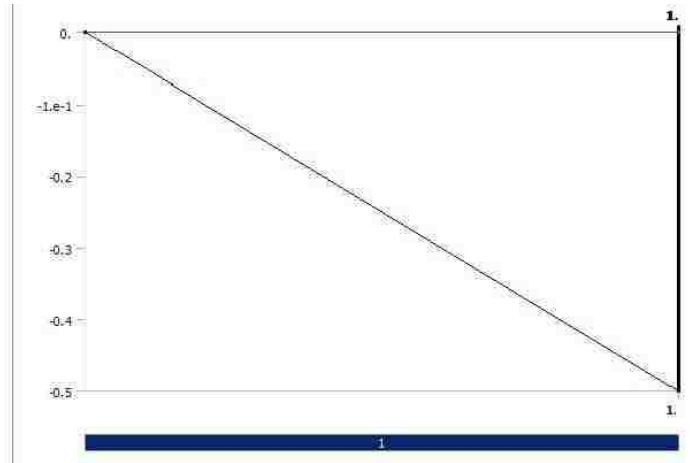
TABLE 15
Model (A4, B4) > Static Structural (A5) > Analysis Settings

Object Name	Analysis Settings
State	Fully Defined
Restart Analysis	
Restart Type	Program Controlled
Status	Done
Step Controls	
Number Of Steps	1.
Current Step Number	1.
Step End Time	1. s
Auto Time Stepping	Program Controlled
Solver Controls	
Solver Type	Program Controlled
Weak Springs	Program Controlled
Large Deflection	Off
Inertia Relief	Off
Restart Controls	
Generate Restart Points	Program Controlled
Retain Files After Full Solve	Yes
Nonlinear Controls	
Force Convergence	Program Controlled
Moment Convergence	Program Controlled
Displacement Convergence	Program Controlled
Rotation Convergence	Program Controlled
Line Search	Program Controlled
Stabilization	Off
Output Controls	
Stress	Yes
Strain	Yes
Nodal Forces	No
Contact Miscellaneous	No
General Miscellaneous	No
Calculate Results At	All Time Points
Cache Results in Memory (Beta)	Never
Max Number of Result Sets	Program Controlled
Analysis Data Management	
Solver Files Directory	C:\Users\rdz\Desktop\shaft c final_files\dp0\SYSTEMECH\
Future Analysis	Prestressed analysis
Scratch Solver Files Directory	
Save MAPDL db	No
Delete Unneeded Files	Yes
Nonlinear Solution	No
Solver Units	Active System
Solver Unit System	Bin

TABLE 16
Model (A4, B4) > Static Structural (A5) > Loads

Object Name	Force
State	Fully Defined
Scope	
Scoping Method	Geometry Selection
Geometry	1 Face
Definition	
ID (Beta)	158
Type	Force
Define By	Components
Coordinate System	Global Coordinate System
X Component	0. lbf (ramped)
Y Component	0. lbf (ramped)
Z Component	-0.5 lbf (ramped)
Suppressed	No

FIGURE 1
Model (A4, B4) > Static Structural (A5) > Force



Solution (A6)

TABLE 17
Model (A4, B4) > Static Structural (A5) > Solution

Object Name	<i>Solution (A6)</i>
State	Solved
Adaptive Mesh Refinement	
Max Refinement Loops	3
Refinement Depth	2
Information	
Status	Done

TABLE 18
Model (A4, B4) > Static Structural (A5) > Solution (A6) > Solution Information

Object Name	<i>Solution Information</i>
State	Solved
Solution Information	
Solution Output	Solver Output
Newton-Raphson Residuals	0
Update Interval	2.5 s
Display Points	All
FE Connection Visibility	
Activate Visibility	Yes
Display	All FE Connectors
Draw Connections Attached To	All Nodes
Line Color	Connection Type
Visible on Results	No
Line Thickness	Single
Display Type	Lines

TABLE 19
Model (A4, B4) > Static Structural (A5) > Solution (A6) > Results

Model (44, 64) = Static Structural (44) = Solution (44) = Results		
Object Name	Directional Deformation	Normal Stress
State	Solved	
Scope		
Scoping Method	Geometry Selection	
Geometry	All Bodies	
Definition		
Type	Directional Deformation	Normal Stress
Orientation	X Axis	Z Axis
By	Time	
Display Time	Last	
Coordinate System	Global Coordinate System	
Calculate Time History	Yes	
Identifier		
Suppressed	No	
Results		
Minimum	-1.8613e-005 in	-5.9266e-002 psi
Maximum	8.5734e-005 in	1.4381e-002 psi
Information		
Time	1, s	
Load Step	1	
Substep	1	
Iteration Number	1	
Integration Point Results		
Display Option	Averaged	

Modal 2 (B5)

TABLE 20
Model (A4, B4) > Analysis

Object Name	<i>Modal 2 (B5)</i>
State	Solved
Definition	
Physics Type	Structural
Analysis Type	Modal
Solver Target	Mechanical APDL
Options	
Generate Input Only	No

TABLE 21
Model (A4, B4) > Modal 2 (B5) > Initial Condition

Object Name	<i>Pre-Stress (Static Structural)</i>
State	Fully Defined
Definition	
Pre-Stress Environment	Static Structural
Pre-Stress Define By	Program Controlled
Reported Loadstep	Last
Reported Substep	Last
Reported Time	End Time
Contact Status	Use True Status

TABLE 22
Model (A4, B4) > Modal 2 (B5) > Analysis Settings

Object Name	<i>Analysis Settings</i>
State	Fully Defined
Options	
Max Modes to Find	6
Limit Search to Range	No
Solver Controls	
Damped	Yes
Solver Type	Full Damped
Rotordynamics Controls	
Coriolis Effect	On
Campbell Diagram	On
Number of Points	2
Output Controls	
Stress	No
Strain	No
Nodal Forces	No
Calculate Reactions	No
General Miscellaneous	No
Cache Results in Memory (Beta)	Never
Damping Controls	
Stiffness Coefficient Define By	Direct Input
Stiffness Coefficient	0.
Mass Coefficient	0.
Analysis Data Management	
Solver Files Directory	C:\Users\vdiz\Desktop\shaft c final_files\dp0\SYS-2\MECH\
Future Analysis	None
Scratch Solver Files Directory	
Save MAPDL db	No
Delete Unneeded Files	Yes
Solver Units	Active System
Solver Unit System	Bin

TABLE 23
Model (A4, B4) > Modal 2 (B5) > Rotations

Object Name	<i>Rotational Velocity</i>
State	Fully Defined
Scope	
Scoping Method	Geometry Selection
Geometry	All Bodies
Definition	
Define By	Vector
Magnitude	Tabular Data
Axis	Defined
Suppressed	No

TABLE 24
Model (A4, B4) > Modal 2 (B5) > Rotational Velocity

Points	Rotational Velocity [rpm]
1	5.
2	1000.

Solution (B6)

TABLE 25

Model (A4, B4) > Modal 2 (B5) > Solution	
Object Name	Solution (B6)
State	Solved
Adaptive Mesh Refinement	
Max Refinement Loops	1.
Refinement Depth	2.
Information	
Status	Done

The following bar chart indicates the frequency at each calculated mode.

FIGURE 2
Model (A4, B4) > Modal 2 (B5) > Solution (B6)

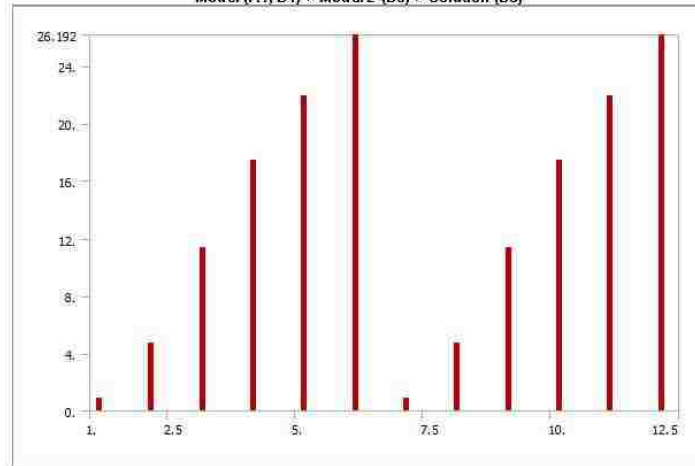


TABLE 26
Model (A4, B4) > Modal 2 (B5) > Solution (B6)

Set	Solve Point	Mode	Damped Frequency [Hz]	Stability [Hz]	Modal Damping Ratio
1	1.	1.	0.89121	2.0811e-012	2.3351e-012
2		2.	4.7771	-7.8685e-013	1.6471e-013
3		3.	11.442	-1.6047e-013	1.4025e-014
4		4.	17.463	-5.7812e-013	3.3105e-014
5		5.	21.953	-9.2402e-013	4.2091e-014
6		6.	26.192	2.3545e-013	-8.9896e-015
7	2.	1.	0.89121	1.3058e-012	-1.4652e-012
8		2.	4.7769	-3.2718e-013	6.8492e-014
9		3.	11.442	1.3137e-013	-1.1482e-014
10		4.	17.463	4.2661e-013	-2.4429e-014
11		5.	21.951	1.7995e-013	-8.1981e-015
12		6.	26.191	5.5906e-013	-2.1345e-014

TABLE 27
Model (A4, B4) > Modal 2 (B5) > Solution (B6) > Solution Information

Object Name	Solution Information
State	Solved
Solution Information	
Solution Output	Solver Output
Newton-Raphson Residuals	0
Update Interval	2.5 s
Display Points	All
FE Connection Visibility	
Activate Visibility	Yes
Display	All FE Connectors
Draw Connections Attached To	All Nodes
Line Color	Connection Type
Visible on Results	No
Line Thickness	Single
Display Type	Lines

TABLE 28
Model (A4, B4) > Modal 2 (B5) > Solution (B6) > Results

Model (4, 4) / Model 2 (3, 3) / Solution (60) / Results					
Object Name	Directional Deformation	Directional Deformation 2	Directional Deformation 3	Directional Deformation 4	Directional Deformation 5
State	Solved				
Scope					
Scoping Method	Geometry Selection				
Geometry	All Bodies				
Definition					
Type	Directional Deformation				
Orientation	X Axis				

Set Number	1.	2.	3.	4.	5.
Phase Angle	0. °				
Coordinate System	Global Coordinate System				
Identifier					
Suppressed	No				
Results					
Minimum	-32.921 in	-35.72 in	-12.648 in	-36.305 in	-55.956 in
Maximum	1.7646e-003 in	11.918 in	11.325 in	16.104 in	66.673 in
Information					
Mode	1	2	3	4	5
Reported Frequency	0.89121 Hz	4.7771 Hz	11.442 Hz	17.463 Hz	21.953 Hz
Reported Stability	-2.0811e-012 Hz	-7.8685e-013 Hz	-1.6047e-013 Hz	-5.7812e-013 Hz	-9.2402e-013 Hz
Reported Modal Damping Ratio	2.3351e-012	1.6471e-013	1.4025e-014	3.3105e-014	4.2091e-014
Reported Logarithmic Decrement	-1.4672e-011	-1.0349e-012	-8.8119e-014	-2.0801e-013	-2.6447e-013

TABLE 29
Model (A4, B4) > Modal 2 (B5) > Solution (B6) > Directional Deformation

Set	Solve Point	Mode	Damped Frequency [Hz]	Stability [Hz]	Modal Damping Ratio
1.	1.	1.	0.89121	-2.0811e-012	2.3351e-012
2.		2.	4.7771	-7.8685e-013	1.6471e-013
3.		3.	11.442	-1.6047e-013	1.4025e-014
4.		4.	17.463	-5.7812e-013	3.3105e-014
5.		5.	21.953	-9.2402e-013	4.2091e-014
6.		6.	26.192	-2.3545e-013	-8.9896e-015
7.	2.	1.	0.89121	1.3058e-012	-1.4652e-012
8.		2.	4.7769	-3.2718e-013	6.8492e-014
9.		3.	11.442	1.3137e-013	-1.1482e-014
10.		4.	17.463	4.2661e-013	-2.4429e-014
11.		5.	21.951	1.7995e-013	-8.1981e-015
12.		6.	26.191	5.5906e-013	-2.1345e-014

TABLE 30
Model (A4, B4) > Modal 2 (B5) > Solution (B6) > Directional Deformation 2

Set	Solve Point	Mode	Damped Frequency [Hz]	Stability [Hz]	Modal Damping Ratio
1.	1.	1.	0.89121	-2.0811e-012	2.3351e-012
2.		2.	4.7771	-7.8685e-013	1.6471e-013
3.		3.	11.442	-1.6047e-013	1.4025e-014
4.		4.	17.463	-5.7812e-013	3.3105e-014
5.		5.	21.953	-9.2402e-013	4.2091e-014
6.		6.	26.192	-2.3545e-013	-8.9896e-015
7.	2.	1.	0.89121	1.3058e-012	-1.4652e-012
8.		2.	4.7769	-3.2718e-013	6.8492e-014
9.		3.	11.442	1.3137e-013	-1.1482e-014
10.		4.	17.463	4.2661e-013	-2.4429e-014
11.		5.	21.951	1.7995e-013	-8.1981e-015
12.		6.	26.191	5.5906e-013	-2.1345e-014

TABLE 31
Model (A4, B4) > Modal 2 (B5) > Solution (B6) > Directional Deformation 3

Set	Solve Point	Mode	Damped Frequency [Hz]	Stability [Hz]	Modal Damping Ratio
1.	1.	1.	0.89121	-2.0811e-012	2.3351e-012
2.		2.	4.7771	-7.8685e-013	1.6471e-013
3.		3.	11.442	-1.6047e-013	1.4025e-014
4.		4.	17.463	-5.7812e-013	3.3105e-014
5.		5.	21.953	-9.2402e-013	4.2091e-014
6.		6.	26.192	-2.3545e-013	-8.9896e-015
7.	2.	1.	0.89121	1.3058e-012	-1.4652e-012
8.		2.	4.7769	-3.2718e-013	6.8492e-014
9.		3.	11.442	1.3137e-013	-1.1482e-014
10.		4.	17.463	4.2661e-013	-2.4429e-014
11.		5.	21.951	1.7995e-013	-8.1981e-015
12.		6.	26.191	5.5906e-013	-2.1345e-014

TABLE 32
Model (A4, B4) > Modal 2 (B5) > Solution (B6) > Directional Deformation 4

Set	Solve Point	Mode	Damped Frequency [Hz]	Stability [Hz]	Modal Damping Ratio
1.	1.	1.	0.89121	-2.0811e-012	2.3351e-012
2.		2.	4.7771	-7.8685e-013	1.6471e-013
3.		3.	11.442	-1.6047e-013	1.4025e-014
4.		4.	17.463	-5.7812e-013	3.3105e-014
5.		5.	21.953	-9.2402e-013	4.2091e-014
6.		6.	26.192	-2.3545e-013	-8.9896e-015
7.	2.	1.	0.89121	1.3058e-012	-1.4652e-012
8.		2.	4.7769	-3.2718e-013	6.8492e-014
9.		3.	11.442	1.3137e-013	-1.1482e-014
10.		4.	17.463	4.2661e-013	-2.4429e-014
11.		5.	21.951	1.7995e-013	-8.1981e-015
12.		6.	26.191	5.5906e-013	-2.1345e-014

TABLE 33
Model (A4, B4) > Modal 2 (B5) > Solution (B6) > Directional Deformation 5

Set	Solve Point	Mode	Damped Frequency [Hz]	Stability [Hz]	Modal Damping Ratio
-----	-------------	------	-----------------------	----------------	---------------------

1.	1.	1.	0.89121	-2.0811e-012	2.3351e-012
2.		2.	4.7771	-7.8685e-013	1.6471e-013
3.		3.	11.442	-1.6047e-013	1.4025e-014
4.		4.	17.463	-5.7812e-013	3.3105e-014
5.		5.	21.953	-9.2402e-013	4.2091e-014
6.		6.	26.192	2.3545e-013	-8.9896e-015
7.	2.	1.	0.89121	1.3058e-012	-1.4652e-012
8.		2.	4.7769	-3.2718e-013	6.8492e-014
9.		3.	11.442	1.3137e-013	-1.1482e-014
10.		4.	17.463	4.2661e-013	-2.4429e-014
11.		5.	21.951	1.7995e-013	-8.1981e-015
12.		6.	26.191	5.5906e-013	-2.1345e-014

TABLE 34
Model (A4, B4) > Modal 2 (B5) > Solution (B6) > Results

Object Name	Directional Deformation 6
State	Solved
Scope	
Scoping Method	Geometry Selection
Geometry	All Bodies
Definition	
Type	Directional Deformation
Orientation	X Axis
Set Number	6.
Phase Angle	0. °
Coordinate System	Global Coordinate System
Identifier	
Suppressed	No
Results	
Minimum	-33.269 in
Maximum	44.63 in
Information	
Mode	6
Reported Frequency	26.192 Hz
Reported Stability	2.3545e-013 Hz
Reported Modal Damping Ratio	-8.9896e-015
Reported Logarithmic Decrement	5.6483e-014

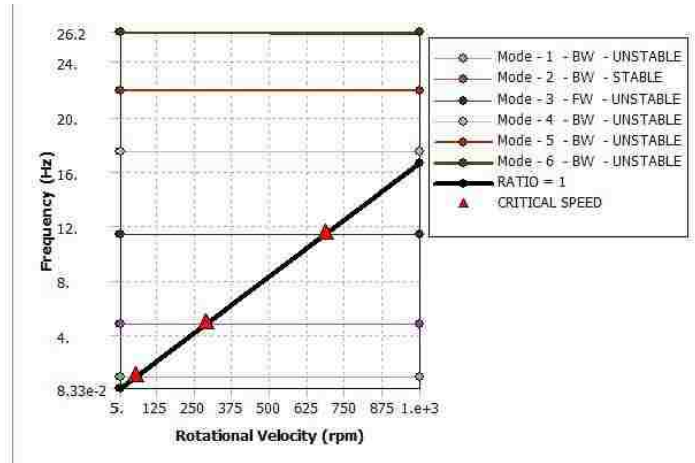
TABLE 35
Model (A4, B4) > Modal 2 (B5) > Solution (B6) > Directional Deformation 6

Set	Solve Point	Mode	Damped Frequency [Hz]	Stability [Hz]	Modal Damping Ratio
1.	1.	1.	0.89121	-2.0811e-012	2.3351e-012
2.		2.	4.7771	-7.8685e-013	1.6471e-013
3.		3.	11.442	-1.6047e-013	1.4025e-014
4.		4.	17.463	-5.7812e-013	3.3105e-014
5.		5.	21.953	-9.2402e-013	4.2091e-014
6.		6.	26.192	2.3545e-013	-8.9896e-015
7.	2.	1.	0.89121	1.3058e-012	-1.4652e-012
8.		2.	4.7769	-3.2718e-013	6.8492e-014
9.		3.	11.442	1.3137e-013	-1.1482e-014
10.		4.	17.463	4.2661e-013	-2.4429e-014
11.		5.	21.951	1.7995e-013	-8.1981e-015
12.		6.	26.191	5.5906e-013	-2.1345e-014

TABLE 36
Model (A4, B4) > Modal 2 (B5) > Solution (B6) > Result Charts

Object Name	Campbell Diagram
State	Solved
Scope	
Rotational Velocity Selection	Rotational Velocity
Campbell Diagram Controls	
Y Axis Data	Frequency
Critical Speed	Yes
Ratio	1.
Sorting	Yes
Axis	
X Axis Label	Rotational Velocity
X Axis Range	Program Controlled
X Axis Minimum	5. RPM
X Axis Maximum	1000. RPM
Y Axis Label	Frequency
Y Axis Range	Program Controlled
Y Axis Minimum	8.3333e-002 Hz
Y Axis Maximum	26.192 Hz
Definition	
Suppressed	No

FIGURE 3
Model (A4, B4) > Modal 2 (B5) > Solution (B6) > Campbell Diagram



Model (A4, B4) > Modal 2 (B5) > Solution (B6) > Campbell Diagram

Mode	Whirl Direction	Mode Stability	Critical Speed	5. rpm	1000. rpm
1	BW	UNSTABLE	53.473 rpm	0.69121 Hz	0.69121 Hz
2	BW	STABLE	296.62 rpm	4.7771 Hz	4.7769 Hz
3	FW	UNSTABLE	686.51 rpm	11.442 Hz	11.442 Hz
4	BW	UNSTABLE	NONE	17.463 Hz	17.463 Hz
5	BW	UNSTABLE	NONE	21.963 Hz	21.961 Hz
6	BW	UNSTABLE	NONE	26.192 Hz	26.191 Hz

Material Data

lifoam

TABLE 37
lifoam > Constants

Density	1.0477e-003 lbm in ⁻³
---------	----------------------------------

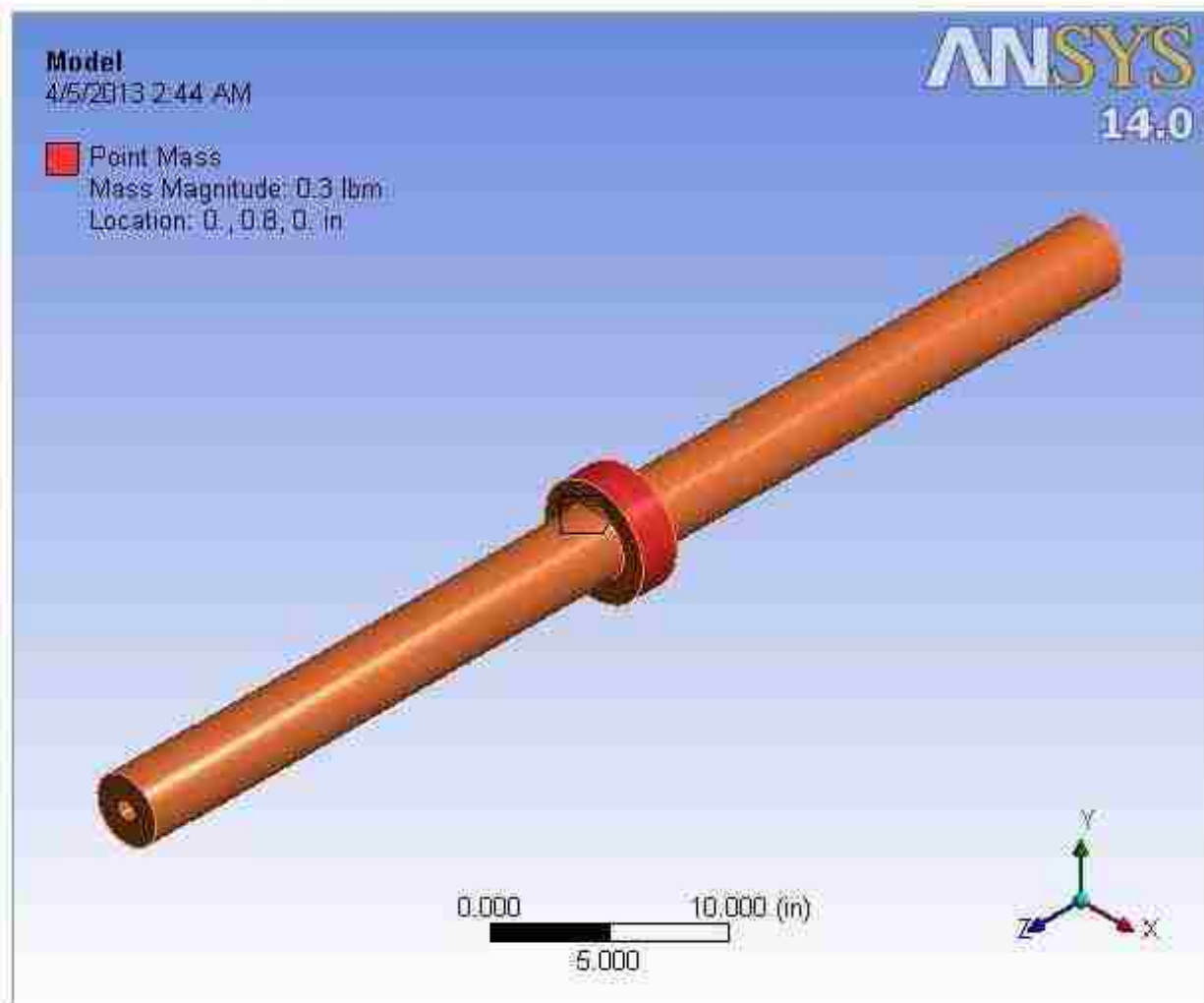
TABLE 38
lifoam > Isotropic Elasticity

Temperature F	Young's Modulus psi	Poisson's Ratio	Bulk Modulus psi	Shear Modulus psi
203		3.e-002	71.986	98.544



Project

First Saved	Monday, October 29, 2012
Last Saved	Friday, November 09, 2012
Product Version	14.0 Release
Save Project Before Solution	No
Save Project After Solution	No



Contents

- [Units](#)
- [Model \(A4, B4\)](#)
 - [Geometry](#)
 - [Solid](#)
 - [Point Mass](#)
 - [Coordinate Systems](#)
 - [Connections](#)
 - [Joints](#)
 - [Fixed - Ground To Solid](#)
 - [Springs](#)
 - [Mesh](#)
 - [Named Selections](#)
 - [Static Structural \(A5\)](#)
 - [Analysis Settings](#)
 - [Force](#)
 - [Solution \(A6\)](#)
 - [Solution Information](#)
 - [Results](#)
 - [Modal 2 \(B5\)](#)
 - [Pre-Stress \(Static Structural\)](#)
 - [Analysis Settings](#)
 - [Rotational Velocity](#)
 - [Solution \(B6\)](#)
 - [Solution Information](#)
 - [Results](#)
 - [Campbell Diagram](#)
- [Material Data](#)
 - [Iifoam](#)

Units

TABLE 1

Unit System	U.S. Customary (in, lbm, lbf, s, V, A) Degrees RPM Fahrenheit
Angle	Degrees
Rotational Velocity	RPM
Temperature	Fahrenheit

Model (A4, B4)

Geometry

TABLE 2
Model (A4, B4) > Geometry

Object Name	Geometry
State	Fully Defined
Definition	
Source	C:\Users\vdiz\Desktop\shaft d final_files\dp0\SYSDMSYS.agdb
Type	DesignModeler
Length Unit	Inches
Element Control	Program Controlled
Display Style	Body Color
Bounding Box	
Length X	5.874 in
Length Y	5.874 in
Length Z	57.25 in
Properties	
Volume	556.99 in³
Mass	0.88355 lbm
Scale Factor Value	1.
Statistics	
Bodies	1
Active Bodies	1
Nodes	30428
Elements	19466
Mesh Metric	None
Basic Geometry Options	
Parameters	Yes
Parameter Key	DS
Attributes	No
Named Selections	No
Material Properties	No
Advanced Geometry Options	
Use Associativity	Yes
Coordinate Systems	No

Reader Mode Saves Updated File	No
Use Instances	Yes
Smart CAD Update	No
Attach File Via Temp File	Yes
Temporary Directory	C:\Users\vdiz\AppData\Local\Temp
Analysis Type	3-D
Decompose Disjoint Faces	Yes
Enclosure and Symmetry Processing	Yes

TABLE 3
Model (A4, B4) > Geometry > Parts

Object Name	<i>Solid</i>
State	Meshed
Graphics Properties	
Visible	Yes
Glow	0
Shininess	1
Transparency	1
Specularity	1
Definition	
Suppressed	No
ID (Beta)	16
Stiffness Behavior	Flexible
Coordinate System	Default Coordinate System
Reference Temperature	By Environment
Material	
Assignment	lifoam
Nonlinear Effects	Yes
Thermal Strain Effects	Yes
Bounding Box	
Length X	5.874 in
Length Y	5.874 in
Length Z	57.25 in
Properties	
Volume	556.99 in ³
Mass	0.58355 lbm
Centroid X	-8.0137e-019 in
Centroid Y	3.7397e-018 in
Centroid Z	-1.6526e-015 in
Moment of Inertia Ip1	149.18 lbm·in ²
Moment of Inertia Ip2	149.18 lbm·in ²
Moment of Inertia Ip3	1.0842 lbm·in ²
Statistics	
Nodes	30428
Elements	19466
Mesh Metric	None

TABLE 4
Model (A4, B4) > Geometry > Point Masses

Object Name	<i>Point Mass</i>
State	Fully Defined
Scope	
Scoping Method	Geometry Selection
Geometry	1 Face
Coordinate System	Global Coordinate System
X Coordinate	0. in
Y Coordinate	0.8 in
Z Coordinate	0. in
Location	Defined
Definition	
Mass	0.3 lbm
Mass Moment of Inertia X	0. lbm·in ²
Mass Moment of Inertia Y	0. lbm·in ²
Mass Moment of Inertia Z	0. lbm·in ²
Suppressed	No
Behavior	Deformable
Pinball Region	All

Coordinate Systems

TABLE 5
Model (A4, B4) > Coordinate Systems > Coordinate System

Object Name	<i>Global Coordinate System</i>
State	Fully Defined
Definition	
Type	Cartesian
Coordinate System ID	0.
Origin	
Origin X	0. in
Origin Y	0. in
Origin Z	0. in

Directional Vectors	
X Axis Data	[1. 0. 0.]
Y Axis Data	[0. 1. 0.]
Z Axis Data	[0. 0. 1.]

Connections

TABLE 6
Model (A4, B4) > Connections

Object Name	<i>Connections</i>
State	Fully Defined
Auto Detection	
Generate Automatic Connection On Refresh	Yes
Transparency	
Enabled	Yes

TABLE 7
Model (A4, B4) > Connections > Joints

Object Name	<i>Joints</i>
State	Fully Defined
Definition	
Connection Type	Joint
Scope	
Scoping Method	Geometry Selection
Geometry	All Bodies
Auto Detection	
Tolerance Type	Slider
Tolerance Slider	0.
Tolerance Value	0.14462 in
Use Range	No
Group By	Bodies
Search Across	Bodies
Fixed Joints	No
Revolute Joints	No

TABLE 8
Model (A4, B4) > Connections > Joints > Joints

Object Name	<i>Fixed - Ground To Solid</i>
State	Fully Defined
Definition	
Connection Type	Body-Ground
Type	Fixed
Suppressed	No
Reference	
Coordinate System	Reference Coordinate System
Mobile	
Scoping Method	Geometry Selection
Scope	1 Face
Body	Solid
Initial Position	Unchanged
Behavior	Deformable
Pinball Region	All

TABLE 9
Model (A4, B4) > Connections > Springs

Object Name	Longitudinal - Ground To Solid		Longitudinal - Ground To Solid
State	Fully Defined		
Graphics Properties			
Visible	No		
Definition			
Type	Longitudinal		
Spring Behavior	Both (Linear)		
Longitudinal Stiffness	100. lbf/in	1.e+007 lbf/in	
Longitudinal Damping	0. lbf·s/in		
Preload	None		
Suppressed	No		
Spring Length	5. in		
Scope			
Scope	Body-Ground		
Reference			
Scoping Method	Geometry Selection		
Coordinate System	Global Coordinate System		
Reference X Coordinate	0. in		
Reference Y Coordinate	5. in		
Reference Z Coordinate	0. in	28.625 in	
Reference Location	Defined		
Behavior	Rigid		
Pinball Region	All		
Mobile			
Scoping Method	Geometry Selection		
Scope	1 Face		

Body	Solid	
Coordinate System	Global Coordinate System	
Mobile X Coordinate	0. in	-6.1188e-017 in
Mobile Y Coordinate	-1.7984e-016 in	3.633e-017 in
Mobile Z Coordinate	0. in	28.625 in
Mobile Location	Defined	
Behavior	Deformable	Rigid
Pinball Region	All	

TABLE 10
Model (A4, B4) > Connections > Longitudinal - Ground To Solid > Command Snippet

Object Name	Commands (APDL)
State	Fully Defined
File	
File Name	
File Status	File not found
Definition	
Suppressed	No
Target	Mechanical APDL
Input Arguments	
ARG1	100.
ARG2	100.
ARG3	100.
ARG4	100.
ARG5	
ARG6	
ARG7	
ARG8	
ARG9	

Model (A4, B4) > Connections > Longitudinal - Ground To Solid > Commands (APDL)

```
! Commands inserted into this file will be executed just after the spring definition.
! The material, type, and real number for this spring is equal to the parameter "_sid".
! Active UNIT system in Workbench when this object was created: U.S. Customary (in, lbm, lbf, s, V, A) temperature units of F
!arg1=Kxx, arg2=Kyy arg3=Kxy agr4=Kyx arg5=Cxx arg6=Cyy arg7=Cxy arg8=Cyx
!By default the bearing element is symmetric means Kxy=Kyx and Cxy=Cyx

et,_sid, 214
keyopt,_sid, 2,0 !keyopt(2)=0 means in xy plane
!keyopt,_sid, 3,1 !Use keyopt(3)=1 if the element is non symmetric
r,_sid,arg1,arg2,arg3,arg4,arg5,arg6
rmore,arg7,arg8
```

TABLE 11
Model (A4, B4) > Connections > Longitudinal - Ground To Solid > Command Snippet

Object Name	Commands (APDL)
State	Fully Defined
File	
File Name	
File Status	File not found
Definition	
Suppressed	No
Target	Mechanical APDL
Input Arguments	
ARG1	100.
ARG2	100.
ARG3	100.
ARG4	100.
ARG5	
ARG6	
ARG7	
ARG8	
ARG9	

Model (A4, B4) > Connections > Longitudinal - Ground To Solid > Commands (APDL)

```
! Commands inserted into this file will be executed just after the spring definition.
! The material, type, and real number for this spring is equal to the parameter "_sid".
! Active UNIT system in Workbench when this object was created: U.S. Customary (in, lbm, lbf, s, V, A) temperature units of F
!arg1=Kxx, arg2=Kyy arg3=Kxy agr4=Kyx arg5=Cxx arg6=Cyy arg7=Cxy arg8=Cyx
!By default the bearing element is symmetric means Kxy=Kyx and Cxy=Cyx

et,_sid, 214
keyopt,_sid, 2,0 !keyopt(2)=0 means in xy plane
!keyopt,_sid, 3,1 !Use keyopt(3)=1 if the element is non symmetric
r,_sid,arg1,arg2,arg3,arg4,arg5,arg6
rmore,arg7,arg8
```

Mesh

TABLE 12
Model (A4, B4) > Mesh

Object Name	<i>Mesh</i>
State	Solved
Defaults	
Physics Preference	Mechanical
Relevance	40
Sizing	
Use Advanced Size Function	Off
Relevance Center	Coarse
Element Size	Default
Initial Size Seed	Active Assembly
Smoothing	High
Transition	Fast
Span Angle Center	Medium
Minimum Edge Length	2.51330 in
Inflation	
Use Automatic Inflation	None
Inflation Option	Smooth Transition
Transition Ratio	0.272
Maximum Layers	5
Growth Rate	1.2
Inflation Algorithm	Pre
View Advanced Options	No
Patch Conforming Options	
Triangle Surface Mesher	Program Controlled
Advanced	
Shape Checking	Standard Mechanical
Element Midside Nodes	Program Controlled
Straight Sided Elements	No
Number of Retries	0
Extra Retries For Assembly	Yes
Rigid Body Behavior	Dimensionally Reduced
Mesh Morphing	Disabled
Defeaturing	
Pinch Tolerance	Please Define
Generate Pinch on Refresh	No
Automatic Mesh Based Defeaturing	On
Defeaturing Tolerance	Default
Statistics	
Nodes	30428
Elements	19466
Mesh Metric	None

Named Selections

Static Structural (A5)

TABLE 13
Model (A4, B4) > Analysis

Object Name	<i>Static Structural (A5)</i>
State	Solved
Definition	
Physics Type	Structural
Analysis Type	Static Structural
Solver Target	Mechanical APDL
Options	
Environment Temperature	71.6 °F
Generate Input Only	No

TABLE 14
Model (A4, B4) > Static Structural (A5) > Analysis Settings

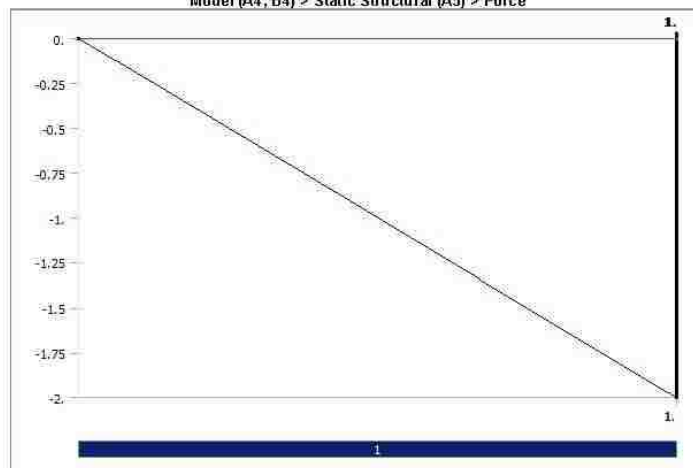
Object Name	<i>Analysis Settings</i>
State	Fully Defined
Restart Analysis	
Restart Type	Program Controlled
Status	Done
Step Controls	
Number Of Steps	1.
Current Step Number	1.
Step End Time	1. s
Auto Time Stepping	Program Controlled
Solver Controls	
Solver Type	Program Controlled
Weak Springs	Program Controlled
Large Deflection	Off
Inertia Relief	Off
Restart Controls	
Generate Restart Points	Program Controlled
Retain Files After Full Solve	Yes
Nonlinear Controls	
Force Convergence	Program Controlled

Moment Convergence	Program Controlled
Displacement Convergence	Program Controlled
Rotation Convergence	Program Controlled
Line Search	Program Controlled
Stabilization	Off
Output Controls	
Stress	Yes
Strain	Yes
Nodal Forces	No
Contact Miscellaneous	No
General Miscellaneous	No
Calculate Results At	All Time Points
Cache Results in Memory (Beta)	Never
Max Number of Result Sets	Program Controlled
Analysis Data Management	
Solver Files Directory	C:\Users\rdz\Desktop\shaft.d\final_files\dp\DSYSMECH\
Future Analysis	Prestressed analysis
Scratch Solver Files Directory	
Save MAPDL db	No
Delete Unneeded Files	Yes
Nonlinear Solution	No
Solver Units	Active System
Solver Unit System	Bin

TABLE 15
Model (A4, B4) > Static Structural (A5) > Loads

Object Name	Force
State	Fully Defined
Scope	
Scoping Method	Geometry Selection
Geometry	1 Face
Definition	
ID (Beta)	158
Type	Force
Define By	Components
Coordinate System	Global Coordinate System
X Component	0. lbf (ramped)
Y Component	0. lbf (ramped)
Z Component	-2. lbf (ramped)
Suppressed	No

FIGURE 1
Model (A4, B4) > Static Structural (A5) > Force



Solution (A6)

TABLE 16
Model (A4, B4) > Static Structural (A5) > Solution

Object Name	Solution (A6)
State	Solved
Adaptive Mesh Refinement	
Max Refinement Loops	3
Refinement Depth	2
Information	
Status	Done

TABLE 17
Model (A4, B4) > Static Structural (A5) > Solution (A6) > Solution Information

Object Name	<i>Solution Information</i>
State	Solved
Solution Information	
Solution Output	Solver Output
Newton-Raphson Residuals	0
Update Interval	2.5 s
Display Points	All
FE Connection Visibility	
Activate Visibility	Yes
Display	All FE Connectors
Draw Connections Attached To	All Nodes
Line Color	Connection Type
Visible on Results	No
Line Thickness	Single
Display Type	Lines

TABLE 18
Model (A4, B4) > Static Structural (A5) > Solution (A6) > Results

Object Name	Directional Deformation	Normal Stress
State	Solved	
Scope		
Scoping Method	Geometry Selection	
Geometry	All Bodies	
Definition		
Type	Directional Deformation	Normal Stress
Orientation	X Axis	Z Axis
By	Time	
Display Time	Last	
Coordinate System	Global Coordinate System	
Calculate Time History	Yes	
Identifier		
Suppressed	No	
Results		
Minimum	-1.5612e-004 in	-0.24091 psi
Maximum	2.437e-004 in	5.2457e-002 psi
Information		
Time	1. s	
Load Step	1	
Substep	1	
Iteration Number	1	
Integration Point Results		
Display Option		Averaged

Modal 2 (B5)

TABLE 19
Model (A4, B4) > Analysis

Object Name	<i>Modal 2 (B5)</i>
State	Solved
Definition	
Physics Type	Structural
Analysis Type	Modal
Solver Target	Mechanical APDL
Options	
Generate Input Only	No

TABLE 20
Model (A4, B4) > Modal 2 (B5) > Initial Condition

Object Name	<i>Pre-Stress (Static Structural)</i>
State	Fully Defined
Definition	
Pre-Stress Environment	Static Structural
Pre-Stress Define By	Program Controlled
Reported Loadstep	Last
Reported Substep	Last
Reported Time	End Time
Contact Status	Use True Status

TABLE 21
Model (A4, B4) > Modal 2 (B5) > Analysis Settings

Object Name	<i>Analysis Settings</i>
State	Fully Defined
Options	
Max Modes to Find	6
Limit Search to Range	No
Solver Controls	
Damped	Yes
Solver Type	Full Damped
Rotordynamics Controls	
Coriolis Effect	On
Campbell Diagram	On

Number of Points	2
Output Controls	
Stress	No
Strain	No
Nodal Forces	No
Calculate Reactions	No
General Miscellaneous	No
Cache Results in Memory (Beta)	Never
Damping Controls	
Stiffness Coefficient Define By	Direct Input
Stiffness Coefficient	0.
Mass Coefficient	0.
Analysis Data Management	
Solver Files Directory	C:\Users\vdiz\Desktop\shaft.d\final_files\dp0\SYS-2\MECH\
Future Analysis	None
Scratch Solver Files Directory	
Save MAPDL db	No
Delete Unneeded Files	Yes
Solver Units	Active System
Solver Unit System	Bin

TABLE 22
Model (A4, B4) > Modal 2 (B5) > Rotations

Object Name	Rotational Velocity
State	Fully Defined
Scope	
Scoping Method	Geometry Selection
Geometry	All Bodies
Definition	
Define By	Vector
Magnitude	Tabular Data
Axis	Defined
Suppressed	No

TABLE 23
Model (A4, B4) > Modal 2 (B5) > Rotational Velocity

Points	Rotational Velocity [rpm]
1	5.
2	1000.

Solution (B6)

TABLE 24
Model (A4, B4) > Modal 2 (B5) > Solution

Object Name	Solution (B6)
State	Solved
Adaptive Mesh Refinement	
Max Refinement Loops	1.
Refinement Depth	2.
Information	
Status	Done

The following bar chart indicates the frequency at each calculated mode.

FIGURE 2
Model (A4, B4) > Modal 2 (B5) > Solution (B6)

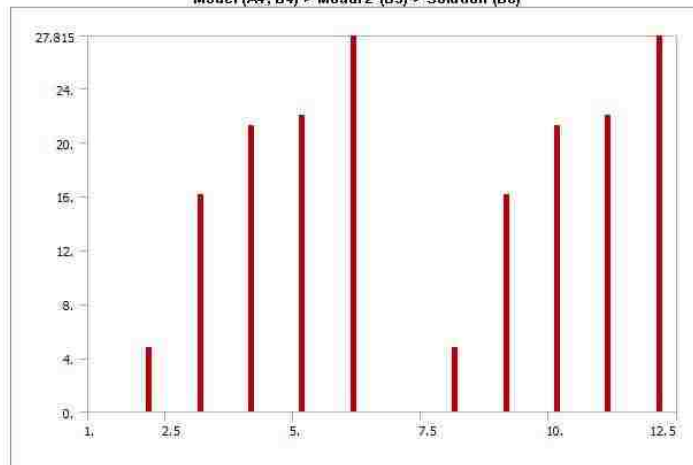


TABLE 25

Model (A4, B4) > Modal 2 (B5) > Solution (B6)					
Set	Solve Point	Mode	Damped Frequency [Hz]	Stability [Hz]	Modal Damping Ratio
1.	1.	1.	0.	1.1533	-1.
2.		2.	4.801	-1.9174e-013	3.9938e-014
3.		3.	16.102	-5.2627e-013	3.2684e-014
4.		4.	21.225	1.5586e-013	-7.3435e-015
5.		5.	22.038	-8.1812e-014	3.7124e-015
6.		6.	27.815	3.4715e-014	-1.2481e-015
7.	2.	1.	0.	-1.1533	N/A
8.		2.	4.801	-1.592e-014	3.3161e-015
9.		3.	16.087	3.1557e-013	-1.9617e-014
10.		4.	21.241	-4.0333e-013	1.8988e-014
11.		5.	22.036	-5.1524e-014	2.3382e-015
12.		6.	27.812	2.0465e-013	-7.3584e-015

TABLE 26
Model (A4, B4) > Modal 2 (B5) > Solution (B6) > Solution Information

Object Name	Solution Information
State	Solved
Solution Information	
Solution Output	Solver Output
Newton-Raphson Residuals	0
Update Interval	2.5 s
Display Points	All
FE Connection Visibility	
Activate Visibility	Yes
Display	All FE Connectors
Draw Connections Attached To	All Nodes
Line Color	Connection Type
Visible on Results	No
Line Thickness	Single
Display Type	Lines

TABLE 27
Model (A4, B4) > Modal 2 (B5) > Solution (B6) > Results

Object Name	Directional Deformation	Directional Deformation 2	Directional Deformation 3	Directional Deformation 4	Directional Deformation 5
State	Solved				
Scope					
Scoping Method	Geometry Selection				
Geometry	All Bodies				
Definition					
Type	Directional Deformation				
Orientation	X Axis				
Set Number	1.	2.	3.	4.	5.
Phase Angle	0. °				
Coordinate System	Global Coordinate System				
Identifier					
Suppressed	No				
Results					
Minimum	-1.8873e-003 in	-16.964 in	-34.497 in	-41.556 in	-50.904 in
Maximum	38.405 in	35.495 in	15.812 in	29.77 in	56.551 in
Information					
Mode	1	2	3	4	5
Reported Frequency	0. Hz	4.801 Hz	16.102 Hz	21.225 Hz	22.038 Hz
Reported Stability	1.1533 Hz	-1.9174e-013 Hz	-5.2627e-013 Hz	1.5586e-013 Hz	-8.1812e-014 Hz
Reported Modal Damping Ratio	-1.	3.9938e-014	3.2684e-014	-7.3435e-015	3.7124e-015
Reported Logarithmic Decrement	N/A	-2.5094e-013	-2.0536e-013	4.6141e-014	-2.3325e-014

TABLE 28
Model (A4, B4) > Modal 2 (B5) > Solution (B6) > Directional Deformation

Set	Solve Point	Mode	Damped Frequency [Hz]	Stability [Hz]	Modal Damping Ratio
1.	1.	1.	0.	1.1533	-1.
2.		2.	4.801	-1.9174e-013	3.9938e-014
3.		3.	16.102	-5.2627e-013	3.2684e-014
4.		4.	21.225	1.5586e-013	-7.3435e-015
5.		5.	22.038	-8.1812e-014	3.7124e-015
6.		6.	27.815	3.4715e-014	-1.2481e-015
7.	2.	1.	0.	-1.1533	N/A
8.		2.	4.801	-1.592e-014	3.3161e-015
9.		3.	16.087	3.1557e-013	-1.9617e-014
10.		4.	21.241	-4.0333e-013	1.8988e-014
11.		5.	22.036	-5.1524e-014	2.3382e-015
12.		6.	27.812	2.0465e-013	-7.3584e-015

TABLE 29
Model (A4, B4) > Modal 2 (B5) > Solution (B6) > Directional Deformation 2

Set	Solve Point	Mode	Damped Frequency [Hz]	Stability [Hz]	Modal Damping Ratio
1.	1.	1.	0.	1.1533	-1.
2.		2.	4.801	-1.9174e-013	3.9938e-014
3.		3.	16.102	-5.2627e-013	3.2684e-014
4.		4.	21.225	1.5586e-013	-7.3435e-015
5.		5.	22.038	-8.1812e-014	3.7124e-015

6.		6.	27.815	3.4715e-014	-1.2481e-015
7.		1.	0.	-1.1533	N/A
8.		2.	4.801	-1.592e-014	3.3161e-015
9.		3.	16.087	3.1557e-013	-1.9617e-014
10.		4.	21.241	-4.0333e-013	1.8988e-014
11.		5.	22.036	-5.1524e-014	2.3382e-015
12.		6.	27.812	2.0465e-013	-7.3584e-015

TABLE 30
Model (A4, B4) > Modal 2 (B5) > Solution (B6) > Directional Deformation 3

Set	Solve Point	Mode	Damped Frequency [Hz]	Stability [Hz]	Modal Damping Ratio
1.		1.	0.	1.1533	-1.
2.		2.	4.801	-1.9174e-013	3.9938e-014
3.		3.	16.102	-5.2627e-013	3.2684e-014
4.		4.	21.225	1.5586e-013	-7.3435e-015
5.		5.	22.038	-8.1812e-014	3.7124e-015
6.		6.	27.815	3.4715e-014	-1.2481e-015
7.		1.	0.	-1.1533	N/A
8.		2.	4.801	-1.592e-014	3.3161e-015
9.		3.	16.087	3.1557e-013	-1.9617e-014
10.		4.	21.241	-4.0333e-013	1.8988e-014
11.		5.	22.036	-5.1524e-014	2.3382e-015
12.		6.	27.812	2.0465e-013	-7.3584e-015

TABLE 31
Model (A4, B4) > Modal 2 (B5) > Solution (B6) > Directional Deformation 4

Set	Solve Point	Mode	Damped Frequency [Hz]	Stability [Hz]	Modal Damping Ratio
1.		1.	0.	1.1533	-1.
2.		2.	4.801	-1.9174e-013	3.9938e-014
3.		3.	16.102	-5.2627e-013	3.2684e-014
4.		4.	21.225	1.5586e-013	-7.3435e-015
5.		5.	22.038	-8.1812e-014	3.7124e-015
6.		6.	27.815	3.4715e-014	-1.2481e-015
7.		1.	0.	-1.1533	N/A
8.		2.	4.801	-1.592e-014	3.3161e-015
9.		3.	16.087	3.1557e-013	-1.9617e-014
10.		4.	21.241	-4.0333e-013	1.8988e-014
11.		5.	22.036	-5.1524e-014	2.3382e-015
12.		6.	27.812	2.0465e-013	-7.3584e-015

TABLE 32
Model (A4, B4) > Modal 2 (B5) > Solution (B6) > Directional Deformation 5

Set	Solve Point	Mode	Damped Frequency [Hz]	Stability [Hz]	Modal Damping Ratio
1.		1.	0.	1.1533	-1.
2.		2.	4.801	-1.9174e-013	3.9938e-014
3.		3.	16.102	-5.2627e-013	3.2684e-014
4.		4.	21.225	1.5586e-013	-7.3435e-015
5.		5.	22.038	-8.1812e-014	3.7124e-015
6.		6.	27.815	3.4715e-014	-1.2481e-015
7.		1.	0.	-1.1533	N/A
8.		2.	4.801	-1.592e-014	3.3161e-015
9.		3.	16.087	3.1557e-013	-1.9617e-014
10.		4.	21.241	-4.0333e-013	1.8988e-014
11.		5.	22.036	-5.1524e-014	2.3382e-015
12.		6.	27.812	2.0465e-013	-7.3584e-015

TABLE 33
Model (A4, B4) > Modal 2 (B5) > Solution (B6) > Results

Object Name	Directional Deformation 6
State	Solved
Scope	
Scoping Method	Geometry Selection
Geometry	All Bodies
Definition	
Type	Directional Deformation
Orientation	X Axis
Set Number	6.
Phase Angle	0. °
Coordinate System	Global Coordinate System
Identifier	
Suppressed	No
Results	
Minimum	-37.098 in
Maximum	2.8658 in
Information	
Mode	6
Reported Frequency	27.815 Hz
Reported Stability	3.4715e-014 Hz
Reported Modal Damping Ratio	-1.2481e-015
Reported Logarithmic Decrement	7.8418e-015

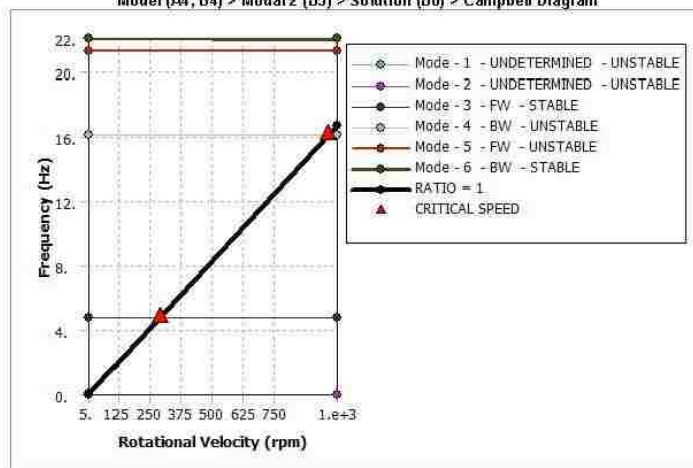
TABLE 34

Model (A4, B4) > Modal 2 (B5) > Solution (B6) > Directional Deformation 6					
Set	Solve Point	Mode	Damped Frequency [Hz]	Stability [Hz]	Modal Damping Ratio
1	1.	1.	0.	1.1533	-1
2		2.	4.801	-1.9174e-013	3.9938e-014
3		3.	16.102	-5.2627e-013	3.2684e-014
4		4.	21.225	1.5586e-013	-7.3435e-015
5		5.	22.038	-8.1812e-014	3.7124e-015
6		6.	27.815	3.4715e-014	-1.2491e-015
7	2.	1.	0.	-1.1533	N/A
8		2.	4.801	-1.592e-014	3.3161e-015
9		3.	16.067	3.1557e-013	-1.9617e-014
10		4.	21.241	-4.0333e-013	1.8988e-014
11		5.	22.036	-5.1524e-014	2.3382e-015
12		6.	27.812	2.0465e-013	-7.3584e-015

TABLE 35
Model (A4, B4) > Modal 2 (B5) > Solution (B6) > Result Charts

Object Name	Campbell Diagram
State	Solved
Scope	
Rotational Velocity Selection	Rotational Velocity
Campbell Diagram Controls	
Y Axis Data	Frequency
Critical Speed	Yes
Ratio	1.
Sorting	Yes
Axis	
X Axis Label	Rotational Velocity
X Axis Range	Program Controlled
X Axis Minimum	5. RPM
X Axis Maximum	1000. RPM
Y Axis Label	Frequency
Y Axis Range	Program Controlled
Y Axis Minimum	0. Hz
Y Axis Maximum	22.038 Hz
Definition	
Suppressed	No

FIGURE 3
Model (A4, B4) > Modal 2 (B5) > Solution (B6) > Campbell Diagram



Model (A4, B4) > Modal 2 (B5) > Solution (B6) > Campbell Diagram					
Mode	Whirl Direction	Mode Stability	Critical Speed	5. rpm	1000. rpm
1.	UNDETERMINED	UNSTABLE	NONE	0. Hz	0. Hz
2.	UNDETERMINED	UNSTABLE	NONE	0. Hz	0. Hz
3.	FW	STABLE	268.06 rpm	4.801 Hz	4.801 Hz
4.	BW	UNSTABLE	965.24 rpm	16.102 Hz	16.087 Hz
5.	FW	UNSTABLE	NONE	21.225 Hz	21.241 Hz
6.	BW	STABLE	NONE	22.038 Hz	22.036 Hz

Material Data

lifoam

TABLE 36
lifoam > Constants
Density 1.0477e-003 lbm in⁻³

TABLE 37
lifoam > Isotropic Elasticity

Temperature F	Young's Modulus psi	Poisson's Ratio	Bulk Modulus psi	Shear Modulus psi
	203	3.e-002	71.986	98.544

VITA

Richard George Duff was born in Missouri in . After completing his degree at Metro Academic and Classical High School in St. Louis Missouri in 1997 he entered University of Missouri at Rolla, receiving the degree of Bachelor in Science of Petroleum Engineering in 2002. In 2003 he entered the graduate school at University of Missouri at Rolla completing a Masters in Science of Petroleum Engineering in 2004. During his stay at the University he worked in the Rock Mechanics and Explosives Research Center and completed his thesis titled “Characterization of a Horizontal Hydraulic Fracture in the Warner Sandstone of Nevada, Missouri” In 2004 Richard joined the graduate program at Louisiana State University in Baton Rouge Louisiana. In 2007 he joined Chevron USA as a full time employee while continuing to pursue academics after two years at ExxonMobil. Richard has been a featured speaker at several professional organization meetings including the American Association of Drilling Engineers, the Institute of Electrical and Electronics Engineers, the International Association of Drilling Contractors, the Society of Petroleum Engineers, and the International Association of Directional Drillers including topic such as distributed drilling measurement, drilling efficiency and optimization, and drilling bottom hole assembly design. Experience and scholarly pursuit has lead him to complete this dissertation “An Experimental and Computational Investigation of Rotating Flexible Shaft System Dynamics in Rotary Drilling Assemblies for Down Hole Drilling Vibration Mitigation“.